ARO 25614.1-EG-CF

(2)

NON-LINEAR VIBRATIONS, STABILITY, AND DYNAMICS OF STRUCTURES AND MECHANISMS

June 1-3, 1988

Abstracts

Sponsored by
Army Research Office

Donaldson Brown Continuing Education Center
Virginia Polytechnic Institute and State University

Chairmen: A. H. Nayfeh and D. T. Mook
Department of Engineering
Science and Mechanics
Virginia Polytechnic Institute
and State University
Blacksburg, VA 24061

UNCLASSIFIED MASTER COPY - FOR REPRODUCTION PURPOSES

SECURITY CLASSIFICATION OF THIS PAGE

REPORT DOCUMENTATION PAGE

1a. REPORT SECURITY CLASSIFICATION Unclassified	1b. RESTRICTIVE MARKINGS
2a. SECURITY CLASSIFICATION AUTHORITY	3. DISTRIBUTION / AVAILABILITY OF REPORT Approved for public release; distribution unlimited.
2b. DECLASSIFICATION / DOWNGRADING SCHEDULE	
4. PERFORMING ORGANIZATION REPORT NUMBER(S)	5. MONITORING ORGANIZATION REPORT NUMBER(S) ARO 25614.1-EG-CF
6a. NAME OF PERFORMING ORGANIZATION Va Polytechnic Inst & State U 6b. OFFICE SYMBOL (If applicable)	7a. NAME OF MONITORING ORGANIZATION U. S. Army Research Office
6c. ADDRESS (City, State, and ZIP Code) Blacksburg, VA 24061	7b. ADDRESS (City, State, and ZIP Code) P. O. Box 12211 Research Triangle Park, NC 27709-2211
8a. NAME OF FUNDING / SPONSORING ORGANIZATION U. S. Army Research Office 8b. OFFICE SYMBOL (If applicable)	9. PROCUREMENT INSTRUMENT IDENTIFICATION NUMBER DAAL03-88-G-0013
8c. ADDRESS (City, State, and ZIP Code) P. O. Box 12211 Research Triangle Park, NC 27709-2211	10. SOURCE OF FUNDING NUMBERS PROGRAM ELEMENT NO. / PROJECT NO. / TASK NO. / WORK UNIT ACCESSION NO.

11. TITLE (Include Security Classification)

Non-Linear Vibrations, Stability, and Dynamics of Structures and Mechanisms

12. PERSONAL AUTHOR(S)
A. H. Nayfeh and D. T. Mook

13a. TYPE OF REPORT	13b. TIME COVERED	14. DATE OF REPORT (Year, Month, Day)	15. PAGE COUNT
Final	FROM 5/1/88 TO 5/31/89	August 1989	

16. SUPPLEMENTARY NOTATION
The view, opinions and/or findings contained in this report are those of the author(s) and should not be construed as an official Department of the Army position, policy, or decision, unless so designated by other documentation.

17. COSATI CODES		
FIELD	GROUP	SUB-GROUP

18. SUBJECT TERMS (Continue on reverse if necessary and identify by block number)
Nonlinear Vibrations, Structures, Mechanical Systems, Chaotic Motions, Nonlinear Dynamics, Rotor Blades, Multibody Dynamics

19. ABSTRACT (Continue on reverse if necessary and identify by block number)

The conference was held as scheduled. Abstracts of the papers presented at the conference are contained in a report distributed by the Virginia Polytechnic Institute and State University.

20. DISTRIBUTION / AVAILABILITY OF ABSTRACT ☐ UNCLASSIFIED/UNLIMITED ☐ SAME AS RPT. ☐ DTIC USERS	21. ABSTRACT SECURITY CLASSIFICATION Unclassified
22a. NAME OF RESPONSIBLE INDIVIDUAL	22b. TELEPHONE (Include Area Code) / 22c. OFFICE SYMBOL

DD FORM 1473, 84 MAR 83 APR edition may be used until exhausted. All other editions are obsolete.

SECURITY CLASSIFICATION OF THIS PAGE
UNCLASSIFIED

NON-LINEAR VIBRATIONS, STABILITY, AND DYNAMICS OF STRUCTURES AND MECHANISMS

June 1-3, 1988

Abstracts

Sponsored by
Army Research Office

Donaldson Brown Continuing Education Center
Virginia Polytechnic Institute and State University

Chairmen: A. H. Nayfeh and D. T. Mook
Department of Engineering
Science and Mechanics
Virginia Polytechnic Institute
and State University
Blacksburg, VA 24061

Reception and Registration at CEC — Tuesday, 1900-2100, May 31

Session 1: Chaotic Motions — Wednesday, AM, June 1
Chairman: R. Miller, Air Force Office of Scientific Research

0800 OPENING REMARKS, A. H. Nayfeh and D. T. Mook, Virginia Polytechnic Institute and State University

WELCOME, P. Torgersen, Interim President and Dean, College of Engineering, Virginia Polytechnic Institute and State University

0830 "CHAOTIC OSCILLATIONS IN MECHANICAL SYSTEMS", E. H. Dowell, Duke University

0900 "INTERPOLATED MAPPING TECHNIQUES", B. H. Tongue, Georgia Institute of Technology

0915 "ON UNDERSTANDING CHAOS IN NONLINEAR OSCILLATORS HAVING A SINGLE EQUILIBRIUM POSITION", W. Szemplinska-Stupnicka and P. Niezgodski, Polish Academy of Sciences, Warsaw, Poland

0930 "BIFURCATIONS IN A FORCED SOFTENING DUFFING OSCILLATOR", A. H. Nayfeh and N. E. Sanchez, Virginia Polytechnic Institute and State University

0945 "EXTENSIONS AND NEW APPLICATIONS OF MELNIKOV'S METHOD FOR PREDICTING THE ONSET OF CHAOS", S. W. Shaw, Michigan State University

1000 "SUPPRESSION OF CHAOS BY NONLINEAR DAMPING", I. G. Tadjbakhsh and G. L. Anderson, Rensselaer Polytechnic Institute and U. S. Army Research Office

1015 Coffee Break

Session 2: Chaotic Motions — Wednesday, AM, June 1
Chairman: G. Anderson, U. S. Army Research Office

1045 "SYMMETRY BREAKING BIFURCATIONS IN MECHANICAL SYSTEMS AND IN SURFACE WAVES", P. R. Sethna, University of Minnesota

1115 "ASYMPTOTIC TECHNIQUES AND CHAOS IN WEAKLY NONLINEAR FORCED MECHANICAL SYSTEMS", A. K. Bajaj, Purdue University

1130 "NONLINEAR NONPLANAR PARAMETRIC RESPONSES OF AN INEXTENSIONAL BEAM", A. H. Nayfeh and P. F. Pai, Virginia Polytechnic Institute and State University

1145 "MODAL INTERACTION IN THE RESPONSE OF SHELLS TO A SUBHARMONIC EXCITATION", A. H. Nayfeh, R. A. Raouf, and J. F. Nayfeh, Virginia Polytechnic Institute and State University

1200 "THE EVALUATION OF THE REGION OF CHAOTIC MOTION IN CURVED STRUCTURES", C. F. Ng, NASA Langley Research Center

1215 "PARAMETER IDENTIFICATION IN CHAOTIC DYNAMIC SYSTEMS", D. J. Mook and P-H. Tong, State University of New York at Buffalo

1230 Lunch at CEC

Session 3: Nonstationary and Random Vibrations **Wednesday, PM, June 1**
Chairman: M. P. Singh, Virginia Polytechnic Institute and State University

1330 **"NONLINEAR NONSTATIONARY PROCESSES"**, R. M. Evan-Iwanowski and G. L. Ostiguy, University of Central Florida and Ecole Polytechnique, Montreal, Canada

1400 **"RESPONSE OF A SINGLE-DEGREE-OF-FREEDOM SYSTEM TO A NONSTATIONARY PARAMETRIC EXCITATION - THEORY AND EXPERIMENT"**, A. H. Nayfeh and H. L. Neal, Virginia Polytechnic Institute and State University

1415 **"ON THE PROBABILITY DENSITY FUNCTION OF THE RESPONSE OF NARROW-BAND EXCITED NONLINEAR OSCILLATIONS"**, Q. Liu and H. G. Davies, University of New Brunswick, Canada

1430 **"WIDE BAND RANDOM EXCITATION OF A THREE-DEGREE-OF-FREEDOM SYSTEM WITH PRINCIPAL INTERNAL RESONANCES"**, R. A. Ibrahim and W. Li, Wayne State University

1445 **"A GENERALIZED METHOD OF AVERAGING FOR DETERMINING THE RESPONSE OF NONLINEAR SYSTEMS TO RANDOM EXCITATIONS"**, A. H. Nayfeh and S. J. Serhan, Virginia Polytechnic Institute and State University

1500 **"DYNAMIC SNAP-BUCKLING UNDER STOCHASTIC LOADS"**, S. T. Ariaratnam and W-C. Xie, University of Waterloo, Canada

1515 **"A NEW APPROACH TO STOCHASTIC FLAP-LAG STABILITY OF A ROTOR BLADE IN HOVER"**, N. S. Namachchivaya and J. Prussing, University of Illinois at Urbana-Champaign

1530 **Coffee Break**

Session 4: Nonlinear Vibration Control **Wednesday, PM, June 1**
Chairman: E. H. Dowell, Duke University

1600 **"NONLINEAR OSCILLATIONS OF LARGE SYSTEMS WITH LOCALIZED NONLINEARITIES"**, P. Hagedorn, Technische Hochschule, Darmstadt, FRG

1630 **"ON THE ADAPTIVE CONTROL OF DYNAMIC SYSTEMS WITH FLEXIBLE STRUCTURES"**, R. L. Kosut, Integrated Systems, Inc., Santa Clara, CA

1645 **"ON THE STABILIZATION OF TETHERED SATELLITE SYSTEMS"**, E. H. Abed and D. -C. Liaw, University of Maryland

1700 **"A MATHEMATICAL FORMULATION AND CONTROL EXPRESSIONS FOR COMPLIANT CONTROL OF CONSTRAINED ROBOT MANIPULATORS"**, C. S. Yoon and F. M. A. Salam, Michigan State University

1715 **"FLEXIBLE ROBOT MODELS WITH REVOLUTE AND PRISMATIC JOINTS - HANDLING OF CLOSED LOOPS"**, M. Riemer and J. Wauer, Universitat Karlsruhe, FRG

1730 **"STABILITY OF FLEXIBLE MULTIBODY SYSTEMS DYNAMICS IN THE PRESENCE OF CLOSED LOOPS"**, F. M. L. Amirouche, University of Illinois at Chicago

1930 **Dinner at CEC**

Session 5: Experiments in Nonlinear Dynamics **Thursday, AM, June 2**
Chairman: R. Evan-Iwanowski, University of Central Florida

0830 "FRACTALS AND CHAOS IN ELASTIC SYSTEMS", F. C. Moon, Cornell University

0900 "NONLINEAR OSCILLATION OF A FLEXIBLE CANTILEVER: EXPERIMENTAL RESULTS", A. G. Haddow and S. M. Hasan, Michigan State University

0915 "NONLINEAR RESONANCES AND CHAOS IN A PARAMETRICALLY EXCITED FLEXIBLE BEAMS", T. D. Burton, Washington State University

0930 "THE NONLINEAR RESPONSE OF A SLENDER BEAM CARRYING A LUMPED MASS TO A PRINCIPAL PARAMETRIC EXCITATION", L. D. Zavodney and A. H. Nayfeh, Ohio State University and Virginia Polytechnic Institute and State University

0945 "THEORETICAL AND EXPERIMENTAL INVESTIGATION OF COMPLICATED RESPONSES OF A TWO-DEGREE-OF-FREEDOM STRUCTURE", A. H. Nayfeh, B. Balachandran, M. A. Colbert, and M. A. Nayfeh, Virginia Polytechnic Institute and State University

1000 **Coffee Break**

Session 6: Nonlinear Analysis of Beams and Rotor Blades **Thursday, AM, June 2**
Chairman: R. A. Wehage, US Army Tank-Automotive Command, Warren, MI

1030 "NONLINEAR OSCILLATIONS IN A ROTATING SHAFT SYSTEM", T. Yamamoto and Y. Ishida, Meijo University and Nagoya University, Japan

1045 "NONLINEAR EFFECTS IN THE STATIC AND DYNAMIC BEHAVIOR OF BEAMS AND ROTOR BLADES", D. H. Hodges, M. R. M. Crespo da Silva, and D. A. Peters, Georgia Institute of Technology and Rensselaer Polytechnic Institute

1100 "NONLINEAR FLEXURAL-FLEXURAL-TORSIONAL EXTENSIONAL DYNAMICS OF BEAMS: FORMULATION AND RESPONSE", M. R. M. Crespo da Silva, Rensselaer Polytechnic Institute

1115 "NONLINEAR MODAL COUPLING IN THE RESPONSE OF INEXTENSIONAL BEAMS", M. R. M. Crespo da Silva and C. L. Zaretzky, Rensselaer Polytechnic Institute

1130 "MODAL INTERACTIONS IN THE RESPONSE OF BEAMS TO A HARMONIC EXCITATION", J. F. Nayfeh, A. H. Nayfeh and D. T. Mook, Virginia Polytechnic Institute and State University

1145 "ANALYSIS AND DESIGN SENSITIVITY CALCULATION OF NONLINEAR FORCED VIBRATION OF STEPPED BEAMS", J. W. Hou, Y. X. Xue, C. Mei and C. Jackson, Old Dominion University

1200 "NON LINEAR OSCILLATIONS AND LIMIT CYCLES - A TIME FINITE ELEMENT APPROACH", M. Borri and P. Mantegazza, Georgia Institute of Technology

1215 "DYNAMICS OF BEAMS WITH TIP MASSES AND ATTACHED TO A MOVING BASE", S. Hanagud and S. Sarkar, Georgia Institute of Technology

1230 **Lunch at CEC**

Session 7: Nonlinear Analysis of Plates and Shells **Thursday, AM, June 2**
Chairman: D. Frederick, Virginia Polytechnic Institute and State University

1330 "NON-LINEAR OSCILLATIONS OF AN INEXTENSIBLE, AIR-INFLATED, CYLINDRICAL MEMBRANE", R. H. Plaut, Virginia Polytechnic Institute and State University

1345 "IMPACT OF SHELLS", C. R. Steele, Stanford University

1400 "DYNAMIC STABILITY OF AN ANNULAR SECTOR PLATE SUBJECTED TO INPLANE DYNAMIC MOMENTS", K. Takahashi, M. Hirakawa and Y. Natsuaki, Nagasaki University, Japan

1415 "NONLINEAR DYNAMIC STABILITY OF LAMINATED COMPOSITE SHEAR DEFORMABLE FLAT PANELS SUBJECTED TO IN-PLANE PERIODIC EDGE LOADS", L. Librescu and S. Thangjitham, Virginia Polytechnic Institute and State University

1430 "THE METHOD OF MULTIPLE SCALES FOR NONLINEAR RESONANCES IN THE FORCED RESPONSE OF ORTHOTROPIC RECTANGULAR PLATES", H. Eslami and O. A. Kandil, Embry-Riddle University and Old Dominion University

1445 "A FINITE ELEMENT METHOD FOR NONLINEAR PANEL FLUTTER OF COMPOSITE LAMINATES", C. Mei and C. E Gray, Jr., Old Dominion University and NASA Langley Research Center

1500 DYNAMIC STABILITY OF LAMINATED COMPOSITE SHELLS USING A SHEAR DEFORMATION THEORY", E. Yogeswaren and J. N. Reddy, Virginia Polytechnic Institute and State University

1515 **Coffee Break**

Session 8: Miscellaneous Topics in Nonlinear Dynamics **Thursday, PM, June 2**
Chairman: F. C. Moon, Cornell University

1545 "PLANAR RESPONSE OF ELASTIC CABLES TO A SUBHARMONIC OR SUPERHARMONIC EXCITATION", F. Benedettini and G. Rega, Universita dell Aquila, Italy

1600 "NONLINEAR OSCILLATIONS UNDER TWO-FREQUENCY PARAMETRIC EXCITATION", R. H. Plaut, J. J. Gentry, and D. T. Mook, Virginia Polytechnic Institute and State University

1615 "THE RESPONSE OF SEISMICALLY MOUNTED ROTOR SYSTEM WITH CUBIC NON-LINEARITIES", A. Ertas and E. K. Chew, Texas Tech University

1630 "QUENCHING OF SELF-EXCITED VIBRATIONS", K. R. Asfar, Jordan University of Science and Technology, Irbid, Jordan

1645 "EFFICIENT SOLUTION OF CONSTRAINED EQUATIONS OF MOTION BY RECURSIVE PROJECTION", R. A. Wehage, US Army Tank-Automotive Command, Warren, MI

1700 "GLOBALLY CONVERGENT NUMERICAL ALGORITHMS FOR NONLINEAR SYSTEMS OF EQUATIONS", L. T. Watson, Virginia Polytechnic Institute and State University

1900 **Banquet at Marriott Hotel**
"CHANGING PERCEPTION OF SCIENTISTS AND ENGINEERS IN SOCIETY", M. Salkind, Air Force Office of Scientific Research

Session 9: Multibody Dynamics — Friday, AM, June 3
Chairman: E. L. Marsh, National Science Foundation

0830 "SURVEY ON THE GENERATION AND SOLUTION OF MULTIBODY SYSTEM EQUATIONS", R. Schwertassek and C. Fuhrer, DFLVR and Technische Universitat Munchen, FRG

0900 "ON THE USE OF THE FINITE ELEMENT METHOD AND CLASSICAL APPROXIMATION TECHNIQUES IN THE NONLINEAR DYNAMICS OF MULTIBODY SYSTEMS", A. A. Shabana, University of Illinois at Chicago

0915 "COMPARATIVE STUDY OF METHODOLOGIES EMPLOYED IN CONSTRAINED MULTIBODY DYNAMICS", F. M. L. Amirouche, University of Illinois at Chicago

0930 "PRIMAL AND MIXED FORMS OF HAMILTON'S PRINCIPLE FOR CONSTRAINED RIGID AND FLEXIBLE DYNAMICAL SYSTEMS: NUMERICAL STUDIES", M. Borri, F. Mello, M. Iura and S. N. Atluri, Georgia Institute of Technology

0945 "ANALYSIS OF NONLINEARLY CONSTRAINED, NONHOLONOMIC MULTIBODY SYSTEMS", M. Xu, C. Liu, and R. C. Huston, Chongqing University, China, University of Cincinnati

1000 Coffee Break

Session 10: Multibody Dynamics — Friday, AM, June 3
Chairman: R. C. Huston, University of Cincinnati

1030 "NONLINEAR ANALYSIS OF LOSS OF STABILITY OF PERIODIC SOLUTIONS WITH AN APPLICATION TO ROBOTIC MOTIONS", E. Lindtner, A. Steindl, H. Troger, Technische Universitat, Vienna, Austria

1100 "SYSTEMATIC REDUCTION OF MULTIBODY EQUATIONS OF MOTION TO A MINIMAL SET", P. E. Nikravesh, University of Arizona

1115 "USE OF LINEAR AND NONLINEAR STRUCTURAL THEORIES IN FLEXIBLE MULTIBODY DYNAMICS", R. R. Ryan and H. H. Yoo, University of Michigan

1130 "NONLINEAR LARGE ROTATIONAL STRUCTURAL DYNAMICS", M. Iura and S. N. Atluri, Georgia Institute of Technology

1145 "DYNAMICS AND BIFURCATIONS OF ELASTIC SPACE STRUCTURES", M. Levi, Boston University

1200 Lunch at CEC

Session 11: Friction and Damping — Friday, PM, June 3
Chairman: T. L. Herdman, Virginia Polytechnic Institute and State University

1300 "THE EFFECT OF SOFTENING OF THE SUPPORTS ON THE STABILITY AND DYNAMICS OF STRUCTURES", M. A. Souza, Pontificia Universidade Catolica do Rio de Janeiro, Brasil

1315 "JOINT DAMPING AND JOINT NONLINEARITY EFFECTS IN DYNAMICS OF SPACE STRUCTURES", M. Bowden and J. Dugundji, Massachusetts Institute of Technology

1330 "EFFECTS OF VELOCITY-DEPENDENT FRICTION ON PERFORMANCE OF A RESILIENT-FRICTION BASE ISOLATOR, L. Su, G. Ahmadi and I. G. Tadjbakhsh, Clarkson University, Rensselaer Polytechnic Institute

1345 "NONLINEAR DYNAMIC RESPONSE OF FRACTIONALLY DAMPED STRUCTURAL SYSTEMS", J. Padovan, University of Akron

1400 "PERIODIC RESPONSE OF A CLASS OR HYSTERETIC OSCILLATORS", D. Capecchi and F. Vestroni, Universita' dell' Aquila, Italy

1415 "DYNAMICS OF NONLINEAR AUTOMOBILE SHOCK-ABSORBERS", J. Wallaschek, Technische Hochschule, Darmstadt, FRG

SESSION 1

CHAOTIC MOTIONS

WEDNESDAY - 0800 - 1015

June 1, 1988

CHAOTIC OSCILLATIONS IN MECHANICAL SYSTEMS

Earl H. Dowell
Duke University

ABSTRACT

Chaotic oscillations have now been observed in nonlinear mechanical systems by analytical, numerical and experimental methods. Nevertheless a more fundamental understanding of why and when such oscillations occur is of great importance. This goal will be pursued here by considering the relationship between chaos induced by forced oscillations vs self-excited oscillations, the relationship of indeterminancy of the final equilibrium state in the initial value problem to chaos in the sustained oscillation problem, comparison of theory to physical experiment, necessary and sufficient conditions for chaos to occur, and the question of convergence of systems of modal ordinary differential equations which derive from partial differential equations.

Acknowledgement: This work was supported in part by the Army Research Office, Contract DAAL03-87K0023, and the National Science Foundation, Grant MSM-8504105. Drs. Gary Anderson and Elbert Marsh are the program directors. This paper is a chapter from a forthcoming book, "Nonlinear Aeroelasticity," to be published by Springer-Verlag in 1988. The co-authors are Earl H. Dowell and Marat Ilgamov.

INTERPOLATED MAPPING TECHNIQUES*

Benson H. Tongue

The George W. Woodruff
School of Mechanical Engineering
Georgia Institute of Technology
Atlanta, GA 30332

Introduction. In order to completely characterize the response of nonlinear systems, it is often necessary to calculate time responses for many different initial conditions. This is due to the well known fact that nonlinear systems often support several distinct steady state solutions depending upon the particular initial conditions used [1]. In addition, one often wishes to determine the system response under a variety of system parameter values. Unfortunately, exploring a system's responses in this way is extremely time consuming due to the extremely large number of possible trajectories that have to be simulated.

In an attempt to alleviate this problem, Hsu and co-workers [2-7] introduced two new methods of analysis. The central idea, common to both techniques, is to treat phase space not as a continuum, but as a finite set of discrete states. The way in which this is done is to divide phase space into a rectangular array of "cells". In the Simple Cell approach, the center of each cell is used as the initial condition for every state that lies within that particular cell. The cell that this trajectory terminates in is recorded as the target cell for all points lying within the original cell. In this way the continuous system is reduced to that of a discrete mapping The difficulty arises from the fact that continuous trajectories cannot be generated due to the step discontinuities that occur at the beginning of each mapping. This introduces a distortion into the phase flow that effectively eliminates the possibility of accurately determining long term trajectories or local stability characteristics.

The second approach, Generalized Cell Mapping, constructs a probabilistic characterization of the phase flow by utilizing several trajectories in each cell and determining what fraction of these end in particular target cells. Based on the distribution of these target cells, a probabilistic mapping is constructed which allows one to determine steady state responses via Markov chain theory. This technique also is hampered by the impossibility of determining continuous trajectories for a given system.

The topic of the present work is an approach (Interpolated Mapping) that allows an accurate global determination of a system's dynamical responses without the restrictions that have hampered previous methods [8-11]. The notable feature of this methodology is that instead of viewing phase space as a discrete array that maps onto itself under the system's dynamics, the notion of a continuous phase space is retained. The continuous deformation of state space under the action of the governing dynamical equations is approximated from a knowledge of the exact response of a finite number of points. This information is then used along with an interpolation procedure to generate complete trajectories for any given initial conditions within the confines of the original array.

In the simplest application of the method, the points are arranged within a rectangular

* This work was supported by the National Science Foundation, Grant No. MSM-8451186.

grid. Trajectories are computed for all of the points for a fixed time duration, Δ. If the system is periodically forced, the natural value for Δ will be the fundamental period of the excitation. The terminal position of each trajectory is then recorded. This information forms the basis of a discrete mapping for the system from t_0 to $t_0 + \Delta$.

Figure 1 illustrates how an initial point, A, maps to the new position, B. To begin the iteration procedure, the relative position of a trajectory's initial position is determined with respect to the four array elements forming the vertices of a rectangle about this point (C_{11}, C_{12}, C_{21} and C_{22} in Figure 1a). The location of this point after another Δ increment of time is found by interpolating between the final locations of the trajectories emanating from the C_{ij}'s. The relative position of the point A to its surrounding array is shown in Figure 1a. It is displaced a distance x_{1_R} to the right from the leftmost array element and a distance x_{2_V} up from the lowermost array element. One mapping later, the relative positions have changed to those shown in Figure 1b. The new position of the discrete trajectory is given by the intersection of the two line segments (a,b) – (e,f) and (c,d) – (g,h). Extending the trajectory simply involves a repeated application of the interpolation technique.

It is important to observe that the individual segments of a given total trajectory are unique to that particular trajectory and will not occur in any other trajectory. Thus, even though a finite number of array elements is used initially, an infinite number of trajectories can be generated, not just a finite number of cell to cell mappings, as is the case for other existing mapping methods. Since no overt discretization is imposed on the possible states of the system, arbitrarily long trajectories can be computed. The ability to generate a continuum of trajectories allows the technique to efficiently be used in bifurcation studies and in determinations of a system's basins of attraction.

Because previously examined methods of iterative mapping enforced a step discontinuity in the state of the systems at each mapping interval, errors in the system response were made unavoidable. The present technique avoids this difficulty. Thus one is free to investigate relative stability, generate Lyapunov exponents, etc., at a very low cost and with a very high degree of accuracy. As an example, the basins of attraction and associated attractors for the equations

$$\dot{x}_1 = x_2$$

$$\dot{x}_2 = -.02x_2 - .25x_1 - x_1^3 + 8.5\cos(t)$$

are shown in Figures 2 (exact calculation) and 3 (Interpolated Mapping). Note that the two cases are almost indistinguishable.

The potential impact of these techniques is sizable. Until now, global nonlinear analyses have been largely confined to single degree of freedom systems because of excessive computer time requirements. For example, the calculation of the basins of attraction for a simple nonlinear pendulum can require literally hours of time on a supercomputer. Interpolated Mapping allows the same calculations to be done in just minutes of run time on a minicomputer. The implication is that one can do all of the currently performed analyses in a greatly accelerated fashion or, more importantly, attempt complicated, multi-degree of freedom analyses for the first time. The talk will focus on different types of interpolation strategies, dynamical limitations and future applications of the method.

REFERENCES

[1] Nayfeh, A. H. and Mook, D. T., *Nonlinear Oscillations*, New York: Wiley Interscience

[2] Hsu C. S., 1980, "A Theory of Cell-to-Cell Mapping Dynamical Systems," *ASME Journal of Applied Mechanics*, **47**, December, 931

[3] Hsu, C.S., and Guttalu, R.S., 1980, "An Unraveling Algorithm for Global Analysis of Dynamical Systems: An Application of Cell-to-Cell Mappings," *ASME Journal of Applied Mechanics*, **47**, December, 940

[4] Hsu C. S., Guttalu, R. S. and Zhu, W. H., 1982, "A Method of Analyzing Generalized Cell Mappings," *ASME Journal of Applied Mechanics*, **49**, December, 885

[5] Hsu, C.S., 1982, "A Probabilistic Theory of Nonlinear Dynamical Systems Based on the Cell Space Concept," *ASME Journal of Applied Mechanics*, **49**, December, 895

[6] Hsu, C.S. and Kim, M.C., 1985, "Statistics of Strange Attractors by Generalized Cell Mapping," *Journal of Statistical Physics* , **38**, 735

[7] Hsu, C.S. and Chiu, H.M., 1987, "Global Analysis of a System with Multiple Responses Including a Strange Attractor," *Journal of Sound and Vibration*, **114**, No. 2, April, 203

[8] Tongue, B.H., 1987 "On the Global Analysis of Nonlinear Systems Through Interpolated Cell Mapping," *Physica* **28D**, No. 3, October, 401

[9] Tongue, B. H., "Interpolated Cell Mapping of Dynamical Systems," to appear in the *ASME Journal of Applied Mechanics*, 1988

[10] Tongue, B. H. and Gu, K., "A Theoretical Basis for Interpolated Cell Mapping," to appear in the *SIAM Journal on Applied Mathematics*, October 1988

[11] Tongue, B. H., "A Higher Order Method of Interpolated Cell Mapping," to appear in the *Journal of Sound and Vibration*, 1988

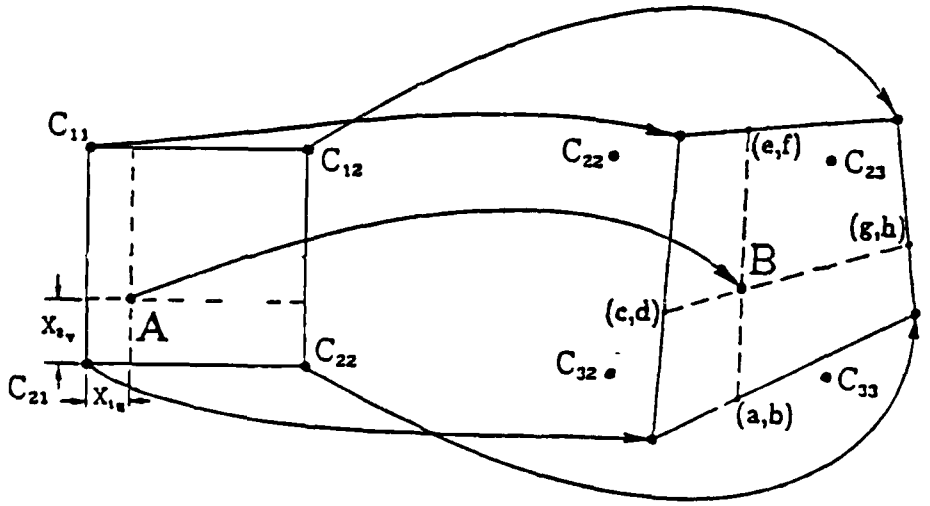

FIGURE 1

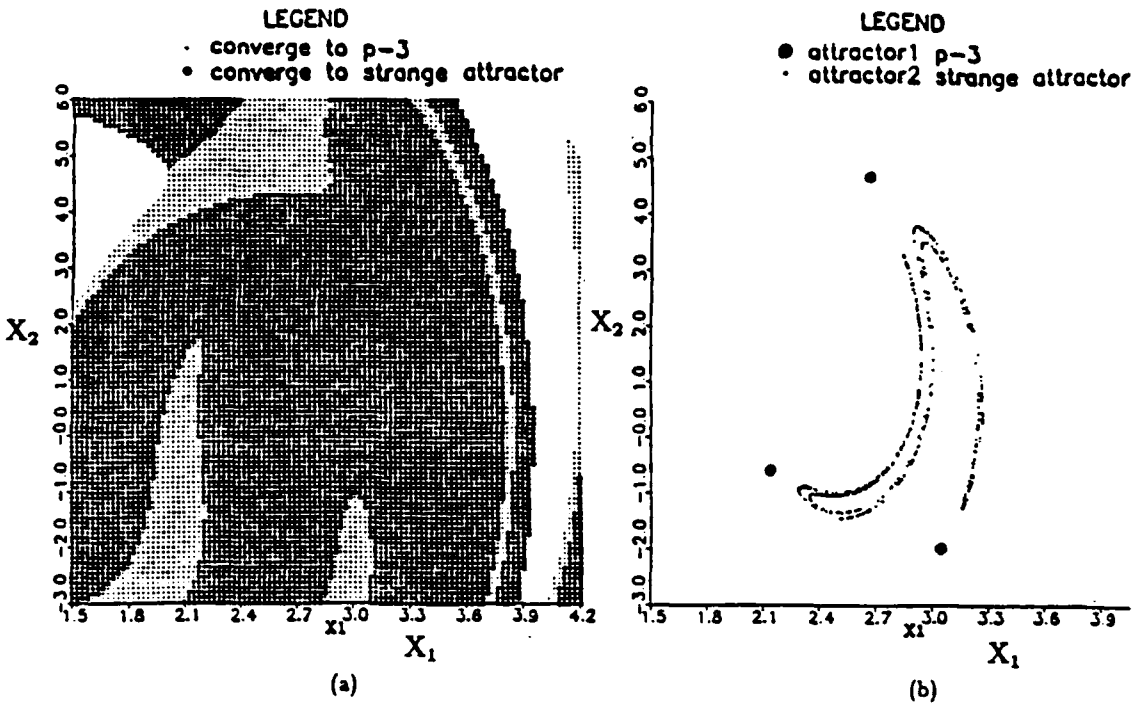

FIGURE 2

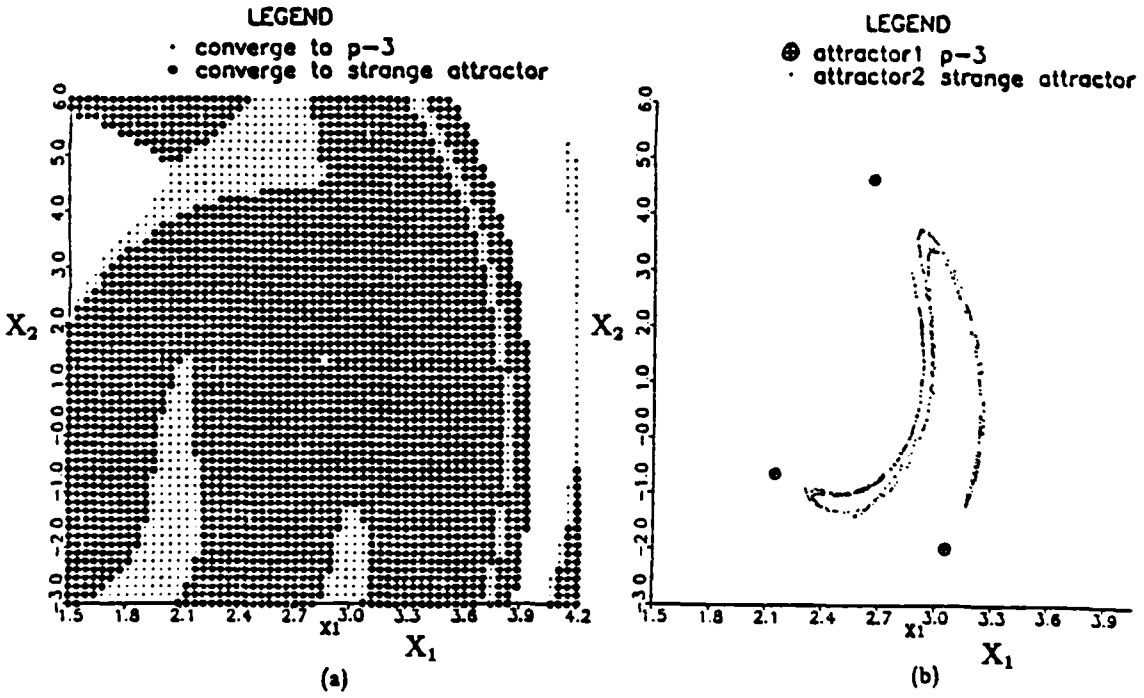

FIGURE 3

On Understanding Chaos in Nonlinear Oscillators Having a Single Equilibrium Position

W. Szemplinska-Stupnicka* and P. Niezgodzki
Institute of Fundamental Technological Research
PAS, Swietokrzyska 21, 00-049 Warsaw, Poland.

Introduction

This paper is concerned with the chaotic response of a single-degree-of-freedom system governed by the following equation of motion

$$\ddot{x} + \omega_0^2 x + h\dot{x} + \alpha_1 x^2 + \alpha_2 x^3 = P\cos\nu t, \quad \tau = \frac{2\pi}{\nu} \tag{1}$$

where $h > 0$ and the coefficients of the quadratic and cubic nonlinear terms, α_1 and α_2, satisfy the condition that $x = 0$ is the unique stable rest position at $P = 0$. Equations of this type arise in the analysis of large-amplitude vibrations of flexible structures when a single-mode solution is assumed. The behavior of the system is studied extensively by approximate analytical methods.

Since the year 1979, however, when a distinctly new type of steady-state solution known as chaotic motion was obtained by computer simulation, it became clear that our knowledge about the system behavior is far from complete. While chaotic motion in systems having two stable equlibrium positions (two-well potential system) can be intuitively explained by some physical arguments, the arguments fail in the system for which $x = 0$ is the only stable rest point.

In the present paper some attempts are made to provide a physical interpretation of chaotic motion in this class of systems by using arguments and mathematical tools based on the approximate theory. This became possible because of observations made by numerous authors that zones of chaotic motions separate two different types of periodic responses. Usually qT-periodic and T-periodic solutions are involved.

Computer-Simulation Results and the Concepts of the "Filtered" Chaotic Component of Motion

A typical example is sketched in Fig. 1. The frequency spectrum of $x(t)$ in Fig. 1a corresponds to a subultraharmonic resonance, and the qT periodic components are denoted by dashed lines. The solution can be approximately described as

$$x(t) = x(t + qT) = \sum_{n=0,1,2\ldots} A_n\cos(n\nu t + \phi_n) + \sum_{p=1,2,3\ldots} A_p\cos(\frac{p}{q}\nu t + \phi_p) \tag{2}$$

* Currently Visiting Professor, Department of Engineering Science and Mechanics, Virginia Polytechnic Institute and State University, Blacksburg, VA 24061.

where the first term contains harmonic components with period T, and the second comprises the harmonic components of period qT. On varying the frequency ν we arrive at the stability limit of this type of solution, and eventually to the T-periodic solution shown in Fig. 1c. If the forcing parameter P is sufficiently small, the decay of the qT-periodic component occurs at certain $\nu=\nu_j$, and hence only the transient motion and the associated jump phenomena are observed. At higher values of P, however, the decay of the qT-periodic component is preceded by a zone of chaotic motion. The most essential observation that comes from the frequency spectrum of the chaotic solution (Fig. 1b) is that continuous segments of the spectrum spread only around those harmonic components, which are due to decay. Because only the continous portion of the frequency spectrum contributes to the chaotic motion, a conclusion was drawn that the time histories of the individual chaotic components of the response might give insight into the nature of the response.

To make such an analysis possible, a numerical technique was developed to obtain the "filtered" response $\bar{x}(t)$, i.e., the component of the complete signal $x(t)$, that corresponds to the individual continuous segment of the frequency spectrum, denoted by $\Delta\nu$ in Fig. 1b.

An analysis of many samples of $\bar{x}(t)$ clearly indicated that it can be approximated by a single-harmonic component with the amplitude fluctuating randomly with time and the frequency being close to the middle frequency, but depending on the amplitude: [Fig. 2 and 3]

$$\bar{x}(t) = a(t)\cos[\bar{\omega}(a)t + \phi] \tag{3}$$

This brings an appealing idea that the "chaotic component" of motion here can be interpreted as a sort of "free-vibration" motion.

Secondary Resonances-Theoretical Analysis of the Stability Limits

In the approximate study of secondary resonances we start with the general solution of the linear, undamped system, Eqs. (1) for $f(t) = h = 0$:

$$x^{(0)}(t) = a\cos(\omega_0 t + \phi) + A_f\cos\nu t, \quad A_f = \frac{P}{\omega_0^2 - \nu^2} \tag{4}$$

where a, ϕ are arbitrary constants depending on initial conditions, and ν being far from ω_0.

If the damping terms is included, the free- vibration component decays with time. Where the complete nonlinear Eq. (1) is considered, however, it may happen that the "free-vibration" term is sustained, giving rise to the first approximate stable solution

$$x(t) = a\cos(\omega t + \phi) + A_f\cos(\nu t + u), \tag{5}$$

$$\frac{da}{dt} = \frac{d\phi}{dt} = 0, \quad a \neq 0 \tag{6}$$

The necessary condition for such a solution, and hence for the secondary resonance, to exist is that the frequencies be commensurable:

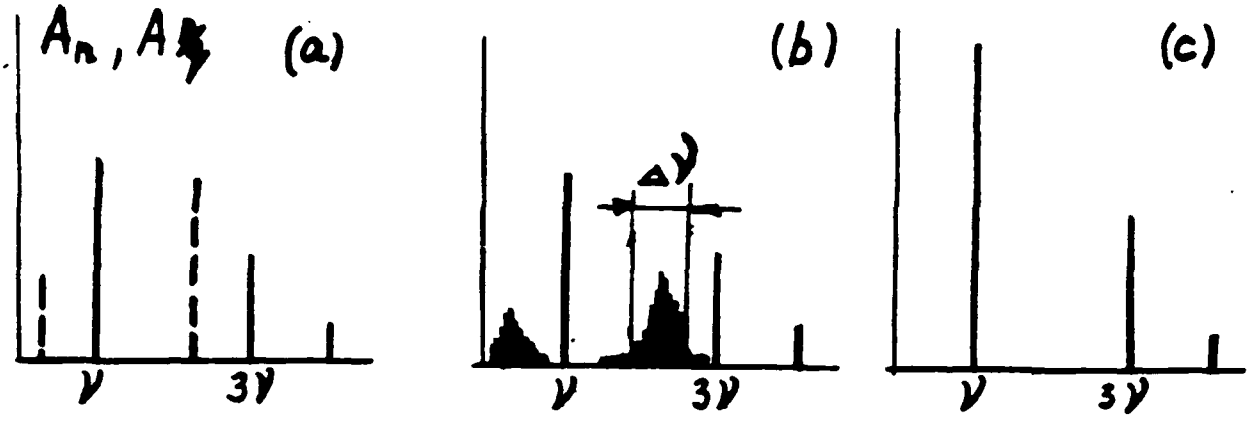

Figure 1.

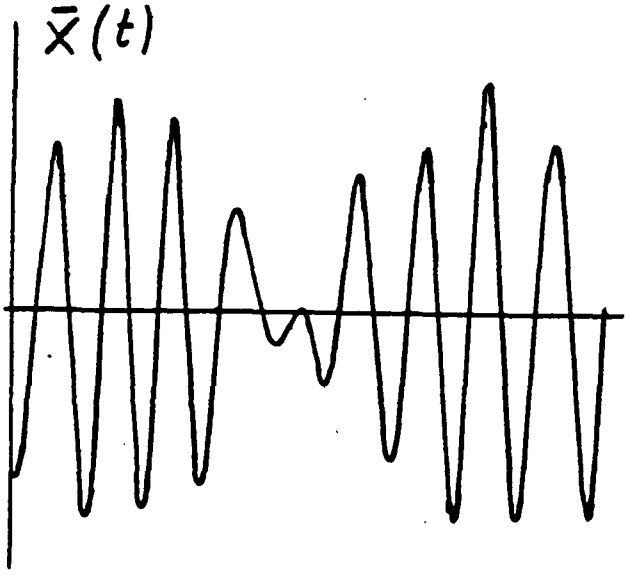

Figure 2. Example I.

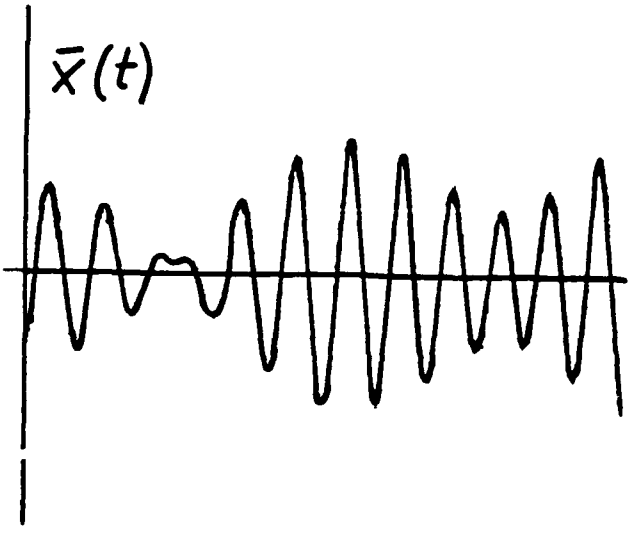

Figure 3. Example II.

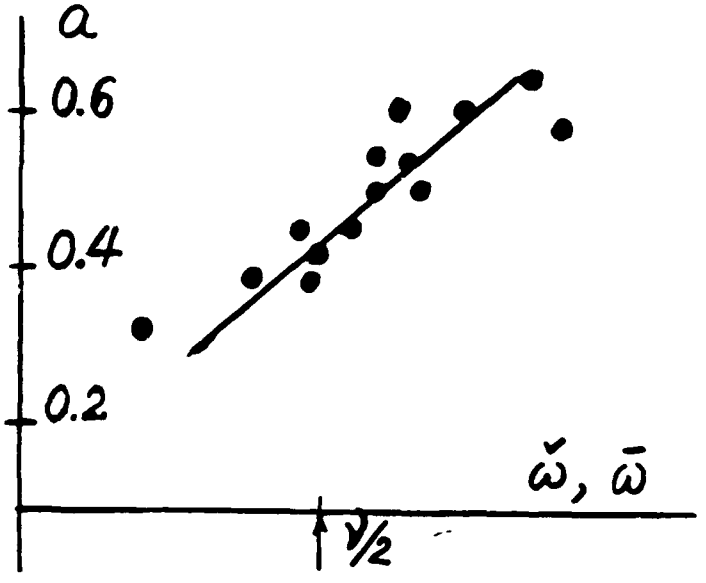

Figure 4. Example I.

$$\omega = \frac{p}{q}\nu,\ p, q = 1, 2, 3 \ldots\ p \neq q \tag{7}$$

and hence the steady-state solution (5) be qT-periodic. The loss of stability of the solution can be interpreted as the loss of the frequency entrainment (6).

The approximate methods lead immediately to the conclusion that the free-vibration component decays at the stability limit, $a \to 0$ as $t \to \infty$. The time history of the filtered response, however, suggests another type of instability, the instability for which the motion exhibits random-like fluctuation of the amplitude a in a certain zone of ν.

To verify this idea we have to compare the frequency-amplitude relationships obtained from the filtered response with the theoretical ones. To find the theoretical $\omega = \omega(a)$ at the stability limit we rewrite Eq. (5) in a more general form:

$$x(t) = z(t) + x_f(t), \text{ where } x_f(t) = \sum_{n=0,1,2\ldots} A_n \cos(n\nu t + \phi_n) \tag{9}$$

and insert it into Eq. (1).
$z(\alpha)$:

$$\ddot{z} + h\dot{z} + z\left[\omega_0^2 + 2\alpha_1\left(A_0 + \sum_{n=1,2\ldots} A_n\cos\theta_n\right) + 3\alpha_2\left(\frac{1}{2}\sum A_n^2 + \sum \frac{1}{2} A_n^2\cos 2\theta_n\right.\right.$$

$$\left.\left. + \sum A_n A_m \cos\theta_n \cos\theta_m\right)\right] + z^2\left[\alpha_1 + 3\alpha_2\left(A_0 + \sum A_n\cos\theta_n\right)\right] + \alpha_2 z^3 = F(\nu t)$$

where $\theta_n = n\nu t + \phi_n$, $n = 1,2\ldots$ and $F(\nu t)$ stands for all time-dependent terms. Eventually neglecting all time-dependent terms, we find that the "free-vibration" components of motion $z(t)$ is governed by equation

$$\ddot{z} + h\dot{z} + z\Omega^2 + z^2(\alpha_1 + 3\alpha_2 A_0) + \alpha_2 z^3 = 0 \tag{10}$$

$$\Omega^2 = \omega_0^2 + 2\alpha_1 A_0 + \frac{3}{2}\alpha_2 \sum_{n=1,2\ldots} A_n^2 \tag{11}$$

where $A_1 - A_n$ are the amplitudes of the forced term at the stability limit.

On the assumption of the simple-harmonic solution for $z(t)$ the theoretical first approximation to the amplitude-frequency relation is

$$\hat{\omega}^2(\alpha) = \omega_0^2 + 2\alpha_1 A_0 + \frac{3}{2}\alpha_2 \sum_{n=1,2\ldots} A_n^2 + \frac{3}{4}\alpha_2 \hat{a}^2 \tag{12}$$

Example 1

$\omega_0^2 = 0.38$, $\alpha_1 = 1.07$, $\alpha_2 = 1$, $P = 0.16$, $h = 0.05$, $\nu = 1.04$

The chaotic zone occurs in the neighborhood of the stability limit of the 1/2 subharmonic resonance

$$x(t) = x(t + 2\pi) = A_{1/2}\cos\left(\frac{\nu}{2}t + \phi_{1/2}\right) + A_0 + A_1\cos(\nu t + \phi_1)$$

with the continuous frequency spectrum around $\nu/2$. At the stability limit $A_{0\ell} = -0.276$, $A_{1\ell} = 0.24$. Equation ( ) yields $\Omega^2 = 0.1056$ and

$$\hat{\omega}(a) = 0.1056 + 3/4\ a^2$$

The theoretical $\hat{\omega} = \hat{\omega}(a)$ is represented in Fig. 4 by the solid line. Results obtained by an analysis of the filtered response $\bar{x}(t)$ are represented by the dots.

Example II

$$\omega_0^2 = 0, \quad \alpha_1 = 0, \quad \alpha_2 = 1.0, \quad P = 12.0, \quad h = 0.1, \quad \nu = 0.99.$$

The chaotic zone considered here occurs close to the stability limit of the 7/3 ultraharmonic resonance

$$x(t) = x(t + 3\tau) \approx \sum_{n=1,3,5} A_n \cos(\nu t + \phi_n) + \sum_{p=1,7} A_{p/3} \cos(p/3\nu t + \phi)$$

At the stability limit: $A_1 = 1.67$, $A_3 = 1.29$, $A_5 = 0.27$, yields

$$\Omega = \sqrt{\frac{3}{2} \sum_{n=1,2,3} A_n^2} = 2.60$$

The filtered response $x(t)$ in Fig. 3 corresponds to a narrow band of $\Delta\nu$ in the neighborhood of $7/3\nu$ so that the changes of $\bar{\omega}$ with the amplitude can hardly be observed. The averaged frequency was obtained as

$$\bar{\omega} \approx 2{,}50$$

Conclusions

The major point in the study of the nature of chaos is an observation and analysis of the "filtered response", i.e., the component of the complete chaotic response, which corresponds to an individual narrow-band continuous segment of the frequency spectrum. Because the filtered response $\bar{x}(t)$ shows a pattern similar to a single harmonic function of time with randomly varying amplitude and amplitude-dependent frequency, the idea of considering it to be a sort of "free-vibration" was developed. The theoretical explanation of this phenomenon was found by considering the concept of the stability limit of the secondary resonances in the light of the approximate theory.

Comparisons of the properties of the filtered response with those obtained by the first approximate theoretical analysis shows surprisingly good agreement.

References

1. Y. Ueda, Randomly transitional phenomena in the systems governed by Duffing's equation, J. Stat. Phys. 20, 1981-156 (1979).

2. Y. Ueda, Explosions of strange attractors exhibited by Duffing equation, Ann. N. Y. Acad. Sci. 357, 422-433 (1980.

3. W. Szemplinska-Stupnicka and J. Bajkowski, The ½ subharmonic resonance and its transition to chaotic motion in a non-linear oscillator, Int. J. Non-Lin. Mech. 21, 401-418, (1986).

4. W. Szemplinska-Stupnicka, Secondary resonances and approximate models of routes to chaotic motion in non-linear oscillators, J. Sound and Vib. 113, 155-172 (1987).

5. W. Szemplinska-Stupnicka, Bifurcations of harmonic solution leading to chaotic motion in the softening type Duffing's oscillator, Int.J. Non-Lin. Mech. 23 (1988).

6. G. M. Zaslavskii and B. V. Chirikov, Stochastic instability of nonlinear oscillations, Sov. Phys. Uspekti 14, 549-672 (1972).

Bifurcations in a Forced Softening Duffing Oscillator

A. H. Nayfeh and N. E. Sanchez
Department of Engineering Science and Mechanics
Virginia Polytechnic Institute and State University
Blacksburg, VA 24061

Abstract

The response of a damped Duffing oscillator of the softening type to a harmonic force is analyzed in a two parameter space including the frequency and amplitude of excitation. An approximate procedure to generate the bifurcation diagram in the parameter space of interest is developed by obtaining perturbation solutions in the neighborhood of the nonlinear resonances of the system and, through Floquet analysis, determining the bifurcation locus of these solutions. The results obtained are evaluated by comparing them with analog simulations, which show escape from the potential well among other behaviors.

1. Introduction

Interest in the Duffing oscillator with softening nonlinearity lies in the variety of physical phenomena that it models (e.g. , the rolling motion of a ship [1]) and the fact that it is isomorphic to other systems of importance in physics and engineering (e.g., Josephson junction oscillators and Foucault's pendulum). Particularly interesting is the response of the Duffing oscillator in the presence of harmonic forcing and damping, which has been found [2-4] to exhibit, among other features, hysteretic and chaotic behavior. Thus, we considered this latter system governed by a nondimensional differential equation of the form

$$\ddot{x} + 2\mu\dot{x} + x - \alpha x^3 = f\cos\Omega t \qquad \mu, \alpha > 0 \quad f\in F \quad \Omega\in W \quad F,W\subseteq\mathbb{R}^1 \tag{1}$$

where F and W represent appropriate domains to analyze the dependence of the solution on the parameters f and Ω, which can be alternatively changed. Our aim was to identify the regions of the parameter space $\mathbb{P} = F \times W$ where bifurcations occur by using approximate analytical techniques and simple numerics. Additionally, we carried out detailed analog simulations on a system governed by (1).

Figure 1 shows the potential well and the phase diagram of the Hamiltonian system associated with (1) when $\mu = 0.2$ and $\alpha = 1$. It is evident that under some conditions the system can escape from the potential well. We are especially interested in this event due to the catastrophic implications that it could carry in a physical system, e.g., the capsizing of a vessel. To determine the dependence of $x(f,\Omega)$ on the parameters, in Section 2 we develop an approximate solution using perturbation techniques. The stability of this solution is then determined using Floquet theory, which signals the location of bifurcation points. By sequentially applying this procedure, we generate a bifurcation diagram in the parameter space $\mathbb{P}$ for the T-periodic approximate solution. In Section 3 we present the results of analog simulations and compare these observations with the calculated solutions of Section 2.

2. Perturbation Solution

An approximate analytical solution of (1) may be obtained by assuming that the coefficients μ, α, and f are small. This smallness can be characterized using a single coefficient ε, where $\varepsilon << 1$, as scaling factor. Thus, we rewrite (1) as

$$\ddot{x} + x = \varepsilon(-2\mu\dot{x} + \alpha x^3 + f\cos\Omega t) \qquad \mu, \alpha > 0 \quad f\in F \quad \Omega\in W \quad F,W\subseteq\mathbb{R}^1 \tag{2}$$

A second-order straightforward expansion [5] of the type

$$x(t;\varepsilon) = x_0(t) + \varepsilon x_1(t) + \varepsilon^2 x_2(t)... \tag{3}$$

quickly identifies resonances in (2) occurring when $\Omega \simeq 1$, $\Omega \simeq 1/3$, $\Omega \simeq 3$, which render (3) nonuniform and consequently inappropriate. We determine a uniform second-order approximate solution for the primary resonance ($\Omega \simeq 1$) by applying the method of multiple scales, as presented by Nayfeh [5]. The subharmonic ($\Omega \simeq 3$) , and superharmonic ($\Omega \simeq 1/3$) resonances were found to produce considerably smaller amplitudes of response than the latter, so they were excluded from the frequency interval considered.

2.1 Multiple-Scales Solution for Primary Resonance

In this case the proximity of Ω to unity can be expressed as

$$\Omega^2 = 1 + \varepsilon\sigma \tag{4}$$

where σ is a detuning parameter. The natural frequency of the linear oscillator in (2) can be written in terms of Ω using (4), resulting in the following form:

$$\ddot{x} + \Omega^2 x = \varepsilon(\sigma x + \alpha x^3 - 2\mu\dot{x} + f\cos\Omega t) \tag{5}$$

We let

$$x(t;\varepsilon) = x_0(T_0, T_1, T_2) + \varepsilon x_1(T_0, T_1, T_2) + \varepsilon^2 x_2(T_0, T_1, T_2) + \ldots \tag{6}$$

where $T_0 = t$, $T_1 = \varepsilon t$, and $T_2 = \varepsilon^2 t$. Substituting (6) into (5) and equating coefficients of like powers of ε, we obtain

$$D_0^2 x_0 + \Omega^2 x_0 = 0 \tag{7}$$

$$D_0^2 x_1 + \Omega^2 x_1 = -2D_0 D_1 x_0 + \sigma x_0 - 2\mu D_0 x_0 + \alpha x_0^3 + f\cos\Omega t \tag{8}$$

$$D_0^2 x_2 + \Omega^2 x_2 = -2D_0 D_2 x_0 - 2D_0 D_1 x_1 - D_1^2 x_0 - 2\mu D_0 x_1 - 2\mu D_1 x_0 + \sigma x_1 + 3\alpha x_0^2 x_1 \tag{9}$$

The solution of (7) can be written as

$$x_0 = a\cos(\Omega t + \beta) \tag{10}$$

Eliminating secular terms from (8) and (9), we find that

$$x(t) = a\cos(\Omega t + \beta) - \varepsilon\frac{\alpha a^3}{32\Omega^2}\cos(3\Omega t + 3\beta) + \ldots \tag{11}$$

where a and β are given by

$$\dot{a} = -\varepsilon\mu a - \varepsilon^2\frac{3\alpha\mu}{8\Omega^2}a^3 + \varepsilon^2\frac{\mu f}{4\Omega^2}\cos\beta - (\varepsilon\frac{f}{2\Omega} + \varepsilon^2\frac{\sigma f}{8\Omega^3} + \varepsilon^2\frac{g\alpha f}{32\Omega^3}a^2)\sin\beta \tag{12}$$

$$a\dot{\beta} = -(\varepsilon\frac{\sigma}{2\Omega} + \varepsilon^2\frac{\mu^2}{2\Omega} + \varepsilon^2\frac{\sigma^2}{8\Omega^3})a - (\varepsilon\frac{3\alpha}{8\Omega} + \varepsilon^2\frac{3\alpha\sigma}{16\Omega^3})a^3 - \varepsilon^2\frac{15\alpha^2}{256\Omega^3}a^5$$
$$-(\varepsilon\frac{f}{2\Omega} + \varepsilon^2\frac{\sigma f}{8\Omega^3} + \varepsilon^2\frac{3\alpha f}{32\Omega^3}a^2)\cos\beta - \varepsilon^2\frac{\mu f}{4\Omega^2}\sin\beta \tag{13}$$

For steady-state periodic responses $\dot{a} = 0$ and $\dot{\beta} = 0$ so that (12) and (13) become a set of algebraic equations and can be solved numerically to determine a and β.

2.2 Stability Analysis

To ascertain the stability of the approximate solution (11), we examine the time evolution of the orbit after the application of an infinitesimal disturbance of arbitrary type $\xi(t)$ in the form

$$\hat{x}(t) = x(t) + \xi(t) \tag{14}$$

Substituting $\hat{x}(t)$ into (2) and keeping only linear terms in $\xi(t)$, we obtain

$$\ddot{\xi}(t) + 2\varepsilon\mu\dot{\xi}(t) + (1 - 3\varepsilon\alpha x^2(t))\xi(t) = 0 \tag{15}$$

which is a linear ordinary-differential equation with periodic coefficients having the period $T = 2\pi/\Omega$. The existence of nontrivial solutions can be shown via Floquet's theorem [5], which calls for solutions of the form

$$\xi(t + T) = \lambda\xi(t) \tag{16}$$

where λ is an eigenvalue (also called Floquet multiplier) of the monodromy matrix C associated with a fundamental matrix solution $\Phi(t)$ of (15) through the relation

$$\Phi(t + T) = \Phi(t)C \tag{17}$$

In the case $t = 0$, $\Phi(0) = I$, we have $C(t) = \Phi(T)$, which can be computed numerically by integrating (15) in $[0,T]$ subject to the initial conditions ($\xi(0) = 1.0, \dot{\xi}(0) = 0.$) and ($\xi(0) = 0., \dot{\xi}(0) = 1.0$), for each set of parameters (f,Ω). The periodic coefficient x(t) of (15) is evaluated using (11). The solution of x(t) is stable provided that $\xi(t)$ does not grow with t. This requires that $|\lambda| \leq 1$. Additionally, the manner in which λ

leaves the unit circle defines the bifurcation that occurs [6]. Determination of the stability of the periodic orbit (11) or its Poincare map, when a parameter is varied, can be accomplished by characterizing its codimension one bifurcations from the information provided by the Floquet multipliers λ. For the dissipative one-degree-of-freedom system described by (2), there are two types of bifurcations to be considered: period-doubling (or flip) and saddle-node (or tangent), which occur when λ goes through -1 or +1 respectively [6].

2.3 Bifurcation of Symmetric Solutions

The preceding procedure allows us to predict instabilities in the T-periodic solutions of (2) when either f or Ω is being changed. Period doubling has been found not to take place when the inversion symmetry of the system is shared by the solution (2). This implies that the symmetry of the solution must be broken before undergoing the bifurcation [3]. Since (11) satisfies $x(t + T/2) = -x(t)$ (i.e., it is symmetric), we can only observe saddle-node bifurcations of this orbit, which induce either symmetry breaking, or tangent instability depending on the region of the parameter space where the changes occur. Floquet analysis was performed on the multiple-scales approximation (11) for values of Ω in the interval $W = [0.4,1.0]$ and $F = [0.2,0.6]$ for $\mu = 0.2$ and $\alpha = 1.0$. The results are shown in Figure 2, where inserts (a), (b), and (c) correspond to the stable orbits found in the regions A, B, and C of the parameter space $\mathbb{P}$. These regions can be defined as follows:

$$A = \{ (f,\Omega)\in\mathbb{P} \mid \ x(t)\to X_1,\ as\ t\to\infty\ \ (x(0),\dot{x}(0))\in\Psi_1 \} \qquad \mathbb{P} = F\times W \tag{18}$$

where X_1 is the invariant set representing the large attractor and Ψ_1 is its basin of attraction. A similar definition holds for B referring to its invariant set X_2 and its basin of attraction Ψ_2. Consequently, C has an invariant set $X_1 \cup X_2$ and a basin of attraction $\Psi_1 \cap \Psi_2$. The large attractor in insert (a) is then stable in regions A and C. On the other hand, the small attractor in insert (b) is stable in regions B and C. Therefore, we observe bistability in C, where the two attractors coexist. Domains of stable solutions are, in this case , separated by lines of saddle-node bifurcations which indicate the loss of the T-periodic solution as either of the two parameters undergoes a change across the line. Attractor (a) loses stability across the solid line, while attractor (b) is lost when the parameters are changed across the dashed line. At very low forcing levels no bifurcation occurs and the two attractors merge into one. The direction in which the bifurcation lines are active is marked by arrows.

2.3 Bifurcation of Asymmetric Solutions

In order to predict period-doubling starting with a symmetric orbit we have to go to the second instability. This can be achieved by modifying the form of the solution (11), to allow for the appearance of even harmonics. A solution of the form

$$\tilde{x}(t) = \sum_{k=0}^{3} A_k \cos(k\Omega t + k\beta) \tag{19}$$

can be used. The method of harmonic balance is appropriate to determine the values of the constants A_k and β that satisfy (1). Substituting (19) into (1) and equating the coefficients of each of the three harmonics and constant term, we find

$$-\alpha A_0^3 - \frac{3}{2}\alpha(A_0A_1^2 + A_0A_2^2 + A_0A_3^2 + \frac{1}{2}A_1^2A_2 + A_1A_2A_3) + A_0 = 0 \tag{20}$$

$$-3\alpha(A_0^2A_1 + A_0A_1A_2 + A_0A_2A_3 + \frac{1}{4}A_1^3 + \frac{1}{4}A_1^2A_3 + \frac{1}{2}A_1A_2^2 + \frac{1}{2}A_1A_3^2 + \frac{1}{4}A_2^2A_3)$$

$$-f\cos(\beta) - A_1\Omega^2 + A_1 = 0 \tag{21}$$

$$-3\alpha(A_0^2A_2 + \frac{1}{2}A_0A_1^2 + A_0A_1A_3 + \frac{1}{2}A_1^2A_2 + \frac{1}{2}A_1A_2A_3 + \frac{1}{4}A_2^3 + \frac{1}{2}A_2A_3^2)$$

$$-4\Omega^2A_2 + A_2 = 0 \tag{22}$$

$$f\sin(\beta) + 2\mu\Omega A_1 = 0 \tag{23}$$

$$-3\alpha(A_0^2A_3 + A_0A_1A_2 + \frac{1}{4}A_1^3 + \frac{1}{2}A_1^2A_3 + \frac{1}{4}A_1A_2^2 + \frac{1}{2}A_2^2A_3 + \frac{1}{4}A_3^3) - 9\Omega^2A_3 + A_3 = 0 \tag{24}$$

This set of equations can be solved numerically to determine the A_k and β coefficients for any given set of parameters $(f,\Omega)\in \mathbb{P}$. The stability of (19) in the parameter space $\mathbb{P}$ can be settled again following the procedure described in 2.2, but replacing x(t) by $\bar{x}$ in (15). The results are summarized in Figure 3, which shows this time the occurrence of period-doubling bifurcations (solid curve) and, as before, the tangent instabilities (dashed). The circles mark the results obtained in section 2.3 for the symmetric orbit.

3. Analog Simulation

As a means to verify the behavior predicted in the previous sections, we used an analog computer to model the system described by (1). The results obtained are summarized in Figure 4, where we can observe the characteristic Y-shaped zones [7] encountered in many phase-locking systems and obtained previously from the T-periodic solution (Figure 3). However, this time we can get a complete picture of the events taking place after the T-periodic solution loses stability. The region marked B lies below the arm of the Y with negative slope, that we denote by y_1. Tangent instabilities take place when any of the parameters crosses y_1, and the future fate of the system is determined by the attracting set existing in the subset of the parameter space where it lands. When the system is initially at B and crosses y_1 into A, we observe the small orbit becoming unstable and the system hopping to the large attractor, which is the attracting set in this region. On the other hand, if y_1 is crossed into D, where

$$D = \{ (f,\Omega)\in\mathbb{P} \mid \ x(t)\to\infty, as\ \ t\to\infty \ \ (x(0),\dot{x}(0))\in\mathbb{R}^1 \} \qquad \mathbb{P} = F\times W \tag{25}$$

the solution becomes unbounded, since infinity is the only attracting set with nonzero basin.

The size of the domain A has not changed considerably. Two coalescent curves y_2 and y_3 lie on the side of the Y with positive slope, where y_2 marks the locus of the period doubling bifurcations observed in the oscilloscope and confirmed by the appearance of half-frequency components in the frequency content of a FFT(Fast Fourier Transform) of the solution. The symmetry breaking precursor was observed but the bifurcation line was not included to avoid obscuring the diagram. Shortly after the first period-doubling occurs, across y_2, what is believed to be a period-doubling sequence takes place. Only a few period multiplications can be observed before the broad-band spectrum appears in the FFT, indicating the presence of a chaotic attractor. When either of the parameters crosses the y_3 curve, the existing chaotic attractor vanishes, causing the system to jump to one of the attractors in the new domain. In this case the jump could be to the small attractor if the crossing goes into B, or to infinity if it goes into D. The last curve bordering domain A is y_4, which represents the locus of tangent instabilities causing the large attractor to jump to the small attractor.

Because of the inversion symmetry of (1), between y_2 and y_3 in Figure 4, x(t) and -x(t) are solutions; thus, two asymmetric attractors coexist and undergo a period-doubling sequence to chaos. Finally, we note that below $\Omega = 0.3$ we observe a small Y notch replicating in small scale all the behavior previously described, but this time located in the superharmonic frequency range where the system (1) has another resonance. Figure 5 shows data points (stars) obtained from the analog simulations for comparison with the predictions from section 2. Although the computed diagram only indicates the occurrence of saddle-node and period-doubling bifurcations on the arms of the Y, the fact that no other attractor is present in D should hint the possibility of escape.

Acknowledgement

This work was supported by the United States Office of Naval Research under grant # N00014-83-K-0184 NR 4322753 and the Air Force Office of Scientific Research under grant # AF0SR-86-0090.

References

1. A. H. Nayfeh and A. A. Khdeir, Nonlinear rolling of ships in regular beam seas. Intl. Shipbldg. prog. 33, 40 (1986)

2. B. A. Huberman and J. P. Crutchfield, Chaotic states of anharmonic systems in periodic fields. Phys. Rev. Lett. 43, 1743 (1979)

3. R. Raty, J. Von Boehm, and H. M. Isomäki, Absence of inversion symmetric limit cycles of even periods and the chaotic motion of Duffing's oscillator. Phys. Lett. 103A , 289 (1984)

4. S. N. Rasband, Marginal stability boundaries for some driven, damped, non-linear oscillators. Intl. J. Non-Linear Mech. 22, 477 (1987)

5. A. H. Nayfeh, Introduction to Perturbation Techniques, Wiley, New York (1981)

6. G. Ioos and D. D. Joseph, Elementary Stability and Bifurcation Theory, Springer-Verlag, New York (1981)

7. N. B. Abraham, J. P. Gollup, and H. L. Swinney, Testing nonlinear dynamics. Physica 11d, 252 (1983).

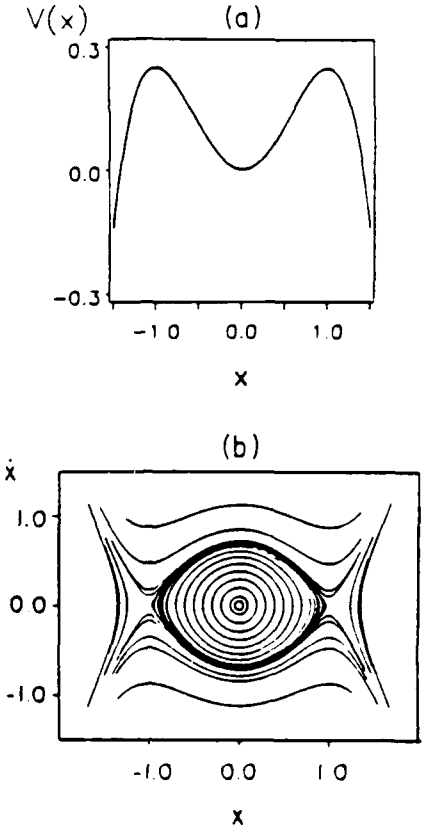

Figure 1 (a) Potential well $V(x) = \frac{1}{2}x^2 - \frac{1}{4}x^4$, (b) Phase diagram of oscillator $\ddot{x} + x - x^3 = 0$.

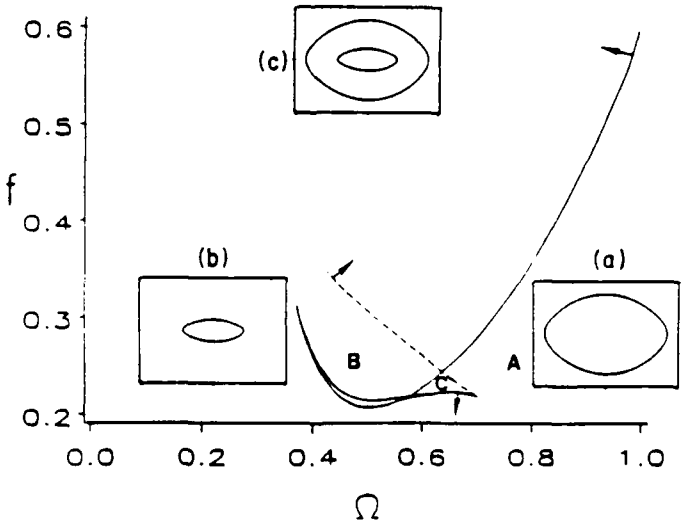

Figure 2 Bifurcation diagram of the approximate T-periodic multiple scales solution for $\mu = 0.2$, $\alpha = 1.0$. All curves represent represent saddle-node bifurcations. Inserts show existing attractors in A,B, and C. Arrows point the direction in which the bifurcations are active.

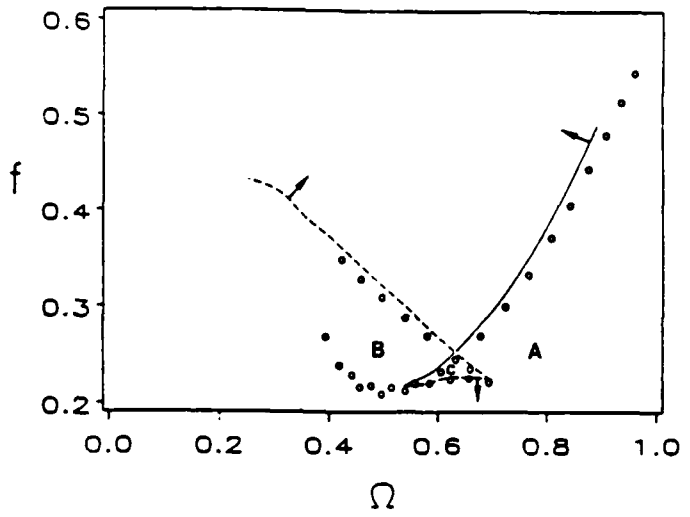

Figure 3 bifurcation diagram of the approximate T-periodic solution for $\mu = 0.2$, $\alpha = 1.0$. Harmonic balance results are shown in solid (period doubling) and dashed (saddle-node) curves. Circles show the multiple scales results.

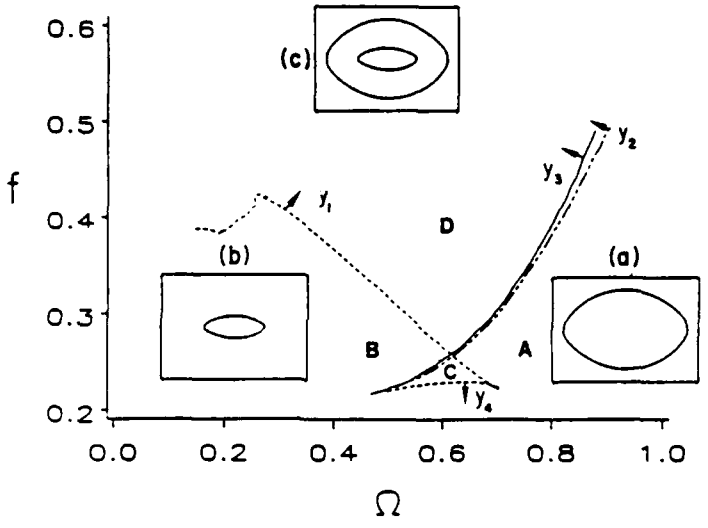

Figure 4 Bifurcation diagram from analog simulations

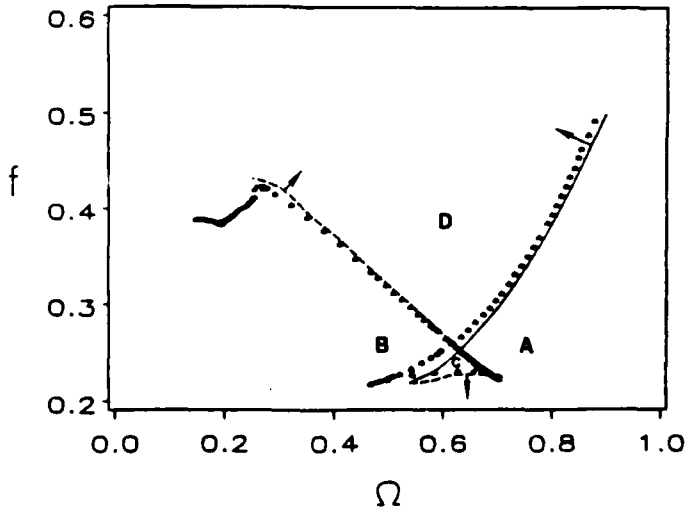

Figure 5 Predicted bifurcations; Period doubling (solid), saddle-node (dashed). Observed bifurcations in analog simulation (stars)

EXTENSIONS AND NEW APPLICATIONS OF MELNIKOV'S METHOD FOR PREDICTING THE ONSET OF CHAOS*

Steven W. Shaw
Department of Mechanical Engineering
Michigan State University
East Lansing, MI 48824

Melnikov's method [1] is one of very few methods which can provide necessary conditions for the existence of chaotic motions explicitly in terms of the system parameters. It is an asymptotic method which is capable of detecting the existence of transverse homoclinic points, which in turn guarantees the existence of horseshoes via the Smale-Birkhoff homoclinic theorem [2]. Horseshoes represent an unstable type of chaos which may be transient in nature, but they are often a precursor to the onset of sustained chaotic dynamics [3]. This analytical tool has been widely applied to single degree of freedom systems with periodic excitation (see [3-7] for example) and to conservative systems with more than one degree of freedom, [8-10]. Recent work has extended the method to include a wider range of applications including:

i) systems with small amplitude multi-frequency inputs
ii) systems with large amplitude, low frequency inputs
iii) certain dissipative multi-degree of freedom systems
iv) systems of type iii) with inputs of types i) or ii).

These extensions are due primarily to Wiggins and are outlined in his forthcoming book [10].

In this presentation we will review the usual, planar Melnikov method and will then proceed to discuss specific examples of physical systems which are amenable to the extended methods. These will include the forced, damped spherical pendulum, a buckled beam with low amplitude, multi-frequency inputs, and the simple planar pendulum with large amplitude, low-frequency excitation. The results will indicate the nature of the chaotic motions which are expected to occur in each situation.

*Supported in part by NSF and DARPA.

REFERENCES

1. V.K. Melnikov, "On the stability of the center for time periodic perturbations," Trans. Moscow Math. Soc. 12, 1-57, 1963.

2. J. Guckenheimer and P. Holmes, Nonlinear Oscillations, Dynamical Systems and Bifurcations of Vector Fields, Applied Mathematical Sciences #42, Springer Verlag, 1983.

3. F. Moon, J. Cusumano and P. Holmes, "Evidence for Homoclinic Orbits as a Precursor to Chaos in a Magnetic Pendulum," Physica 24D, 383-390, 1987.

4. F.M.A. Salam and S. Sastry, "Dynamics of the Forced Josephson Junction Circuit: The Regions of Chaos," IEEE Transactions on Circuits and Systems CAS-32, No. 8, 784-796, 1985.

5. S.W. Shaw and R.H. Rand, "The transition to chaos in a simple mechanical system," submitted.

6. P. Holmes, "A Nonlinear Oscillator with a Strange Attractor," Philosophical Transactions of the Royal Society A292, 419-448, 1979.

7. B.P. Koch and R.W. Leven, "Subharmonic and homoclinic bifurcations in a parametrically forced pendulum," Physica 16D, 1-13, 1985.

8. P. Holmes and J. Marsden, "Horseshoes in perturbations of Hamiltonians with two degrees of freedom," Communications in Mathematical Physics 82, 523-544, 1982.

9. F.M.A. Salam. Marsden, J. and P.P. Varaiya, "Chaos and Arnold Diffusion in Dynamical Systems," IEEE Transactions on Circuits and Systems CAS 30 (9), 697-708, 1983.

10. P. Holmes and J. Marsden, "Horseshoes and Arnold diffusion for Hamiltonian systems on Lie groups," Indiana U. Math. J. 32, 273-310, 1983.

11. S. Wiggins, Global Bifurcations and Chaos-Analytical Methods, Springer Verlag, to appear.

SUPPRESSION OF CHAOS BY NONLINEAR DAMPING

Iradj G. Tadjbakhsh
Rensselaer Polytechnic Institute, Troy, New York
Gary L. Anderson
U.S. Army Research Office, Durham, North Carolina

Introduction

This paper describes a new method of achieving vibration reduction of beams by means of damping of their axial displacements. Axial displacements are of a smaller order of magnitude than the flexural deflections. These displacements can be mechanically magnified in order to produce appreciable axial damping that will inhibit vibrations. The result is a dynamical system whose damping coefficient increases quadratically with the amplitude of oscillations.

The problem of nonlinear vibrations of rods and beams also has a long history. An account of its development is given in Nayfeh and Mook [1] where it is pointed out that the model that forms the basis of most nonlinear studies takes into account the nonlinear effect due to variation of the axial force. Crespo da Silva and Glynn [2] using variational approach showed that a consistent third order model has nonlinear contributions from inertia and flexure as well. In this paper a consistent third order model forms the basis of our study which however, is derived from Newton's laws of motion and agrees with Crespo da Silva's and Glynn's result.

Equations of Motion

The basic system that is considered consists of a simply supported beam that is axially damped. As shown in Figure 1, axial displacements of the beam caused by transverse oscillations is resisted by a dashpot (C) or another means of energy absorption such as friction. A rack-and-pinion element (M) can suitably magnify axial displacements to appreciable levels as necessary. Letting s denote the arc length along the beam and u(s,t) and v(s,t) the time dependent planar components of displacements in the x and y directions we have

$$(1+u_s)^2 + v_s^2 = 1 \tag{1}$$

where subscripts denote differentiation.

The axial force T acting on the end s = L of the beam also determined to second order of nonlinearity becomes

$$T_L = C(u_t)_{s=L}, \tag{2}$$

where C denotes the product of the damping coefficient of the dashpot and the factor magnifying axial motions. Now the axial displacement of the beam at its end s = L can be shown from (1) to be given by

$$u(L,t) = \frac{1}{2} \int_0^L (v_s)^2 \, ds. \tag{3}$$

When (3) is inserted into (2), the results is found to be

$$T_L = C \int_0^L v_s \, v_{st} \, ds. \tag{4}$$

From the equation of motion in the x-direction

$$[T\,(1+u_s) - N\,v_s]_s = m\,u_{tt}, \tag{5}$$

where $T = T(s,t)$ is the axial force at an arbitrary point s along the center line of the beam, and from the equation of dynamic angular equilibrium

$$N = -M_s \equiv -EI\,[(1+v_s^2/2)\,v_{ss}]_s \tag{6}$$

one can determine that

$$T = -\frac{m}{2} \int_L^{s_1} [\int_0^s (v_s^2)_{tt} \, ds_0] ds_1 - EI\, v_s\, v_{sss} + T_L \tag{7}$$

Here m is the mass per unit length of the beam, M is the bending moment and the boundary conditions $u(0,t) = 0$ and $M(L,t) = 0$ have been assumed. Substitution of (7) into the y-component of equation of motion

$$[Tv_s + (1+u_s)N]_s + f = mv_{tt} \tag{8}$$

yields

$$mv_{tt} + EI\,\{v_{ssss} + [v_s(v_s v_{ss})_s]_s\} + \frac{m}{2}\{v_s \int_L^s [\int_0^{s_1} (v_s^2)_{tt} \, ds_0] ds_1\}_s$$

$$- (T_L\, v_s)_s = f \tag{9}$$

where f(s,t) is the applied force in the y-direction.

Primary Resonance

The boundary conditions are assumed to be

$$v = v_{ss} = 0 \text{ at } s = 0,L. \tag{10}$$

In order to evaluate the effect of non-linear damping as represented by the term $(T_L v_s)_s$ in (9), specifically,

$$(T_L v_s)_s = (C v_s \int_0^L v_s v_{st}\, dx)_s, \tag{11}$$

the response of the beam to a first mode harmonic force of frequency Ω is considered. Similarly for the response we assume a first mode of variable amplitude. Then

$$f = \varepsilon^{3/2} F\cos\Omega t \sin\frac{\pi s}{L} \quad , \quad v = \varepsilon^{1/2} LA(t)\sin\frac{\pi s}{L} \tag{12}$$

where ε is a dimensionless small parameter that is introduced for the purpose of the perturbation analysis that will follow. Substitution into (9) and using Galerkin procedure brings about

$$\ddot{A} + A + \varepsilon\,\delta\,A^3 + \varepsilon\,\beta\,A(A^2)^{\cdot\cdot} + \varepsilon\alpha A^2\dot{A} = \varepsilon k \cos\nu\tau \ , \ (\dot{} = \frac{d}{d\tau}) \tag{13}$$

where δ and β are constants

$$\delta = \frac{\pi^2}{2} \quad , \quad \beta = \frac{\pi^4}{12} - \frac{3\pi^2}{32} \tag{14}$$

and the remaining quantities are defined by

$$\alpha = \frac{C\pi^4}{2mL\omega} \ , \quad \nu = \frac{\Omega}{\omega} \ , \quad \omega^2 = \frac{EI\pi^2}{mL^4} \ , \quad k = \frac{F}{mL\omega^2} \ , \quad \tau = \omega t \tag{15}$$

Using the method of multiple scales [1] a solution is sought in the form

$$A(t,\varepsilon) = A_o\,(T_o,T_1) + \varepsilon A_1\,(T_o,T_1) + \ldots \tag{16}$$

where $T_o = \tau$ and $T_1 = \varepsilon\tau$. For A_o one may assume a harmonic solution of slowly varying amplitude and phase, i.e.,

$$A_o = a(T_1)\cos\psi \quad , \quad \psi = T_o + \theta(T_1) \tag{17}$$

Fig. 3 shows the comparison of results obtained from a Runge-Kutta based numerical evaluation of (13) and (16) with the approximate result obtained on the basis of multiple scale analysis. The numerical evaluations are for the five points depicted with a (*) and which correspond to

the values $\nu = 0.8$, 0.9, 1.0, 1.1 and 1.2. The agreement is satisfactory for $\varepsilon = 0.01$ and $k = \alpha = 10$.

To study the characteristics of the undamped motion Poincare' map of the scaled velocity $\dot{A}/|\dot{A}_{max}|$ and the scaled displacement $A/|A_{max}|$ were plotted. This map is the two dimensional projection of the three dimensional phase diagram $(A, \dot{A}, \tau)$ onto the plane of $(A, \dot{A})$ which is sampled at regular time intervals. At resonance $\nu=1$ sampling was done at $T(2\pi)$ with T an integer in the interval $50 \leq T \leq 1050$. Strictly periodic motion of one period will be represented by a single point on the Poincare' map. Closed cycles represent recurrent variable motions. More complex motions occupy regions that can be characterized by means of fractals. All of these types of motions were observed for the undamped nonlinear motion. Generally more complex types of motions occurred as the amplitude of the forcing term was increased. This is observed in the sequence of Poincare maps shown in Figures 4-5.

The effect of the increase of nonlinear damping (increasing α) on the system is a gradual coalesence or shrinking of points and orbits in the Poincare' map toward more compact figures and eventually a single point representing periodic motion completely in phase with the applied force. For $\varepsilon = 1$, $k = 2.0$, $\nu = 1.0$, the progress toward a single periodic solution was observed as damping parameter α was increased in steps from $\alpha = 0.0$ to $\alpha = 0.1$. A single steady state periodic solution was observed for $\alpha = 1.0$ with $A_{max} = 0.9200$ and $\dot{A}_{max} = 0.0504$. Fig. 6 is a typical stage in this suppression process.

Acknowledgement

The authors wish to acknowledge useful discussions with M. Shahinpoor and M.R.M. Crespo da Silva. Contributions of B.C. Lin and Y. Su, graduate students at RPI, who performed the numerical computations are also acknowledged. The work of I.G. Tadjbakhsh was supported partially through a grant by the National Center for Earthquake Engineering Resarch at SUNY, Buffalo.

References

1. A.H. NAYFEH and T.D. MOOK 1979 Non-Linear Oscillations. New York: John Wiley and Sons.

2. M.R.M. CRESPO DA SILVA and C.C. GLYNN 1979 Journal of Structural Mechanics 6, 437-461. Non-linear Flexural Flexural-torsional dynamics of inextensional beams I, Equations of motion, II, Forced motions.

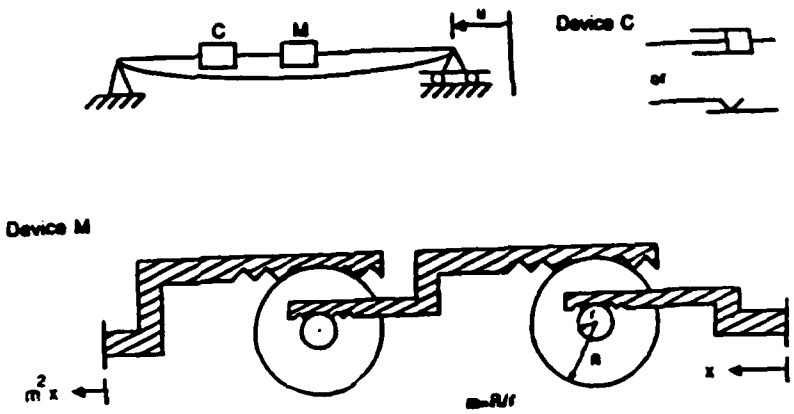

Figure 1. Schematic of axial damping of a vibrating beam

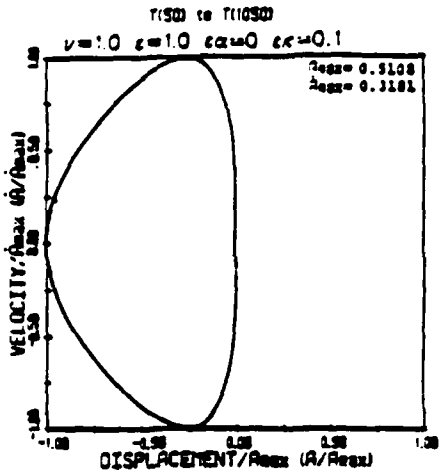

Figure 4. Poincare' map of a variable recurrent vibration

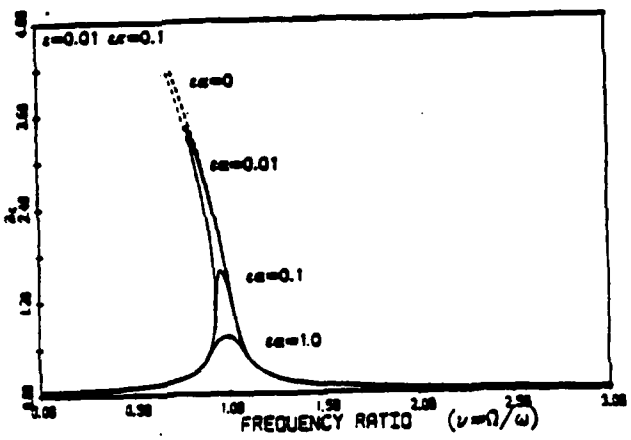

Figure 2. Effect of nonlinear damping on the steady-state amplitude

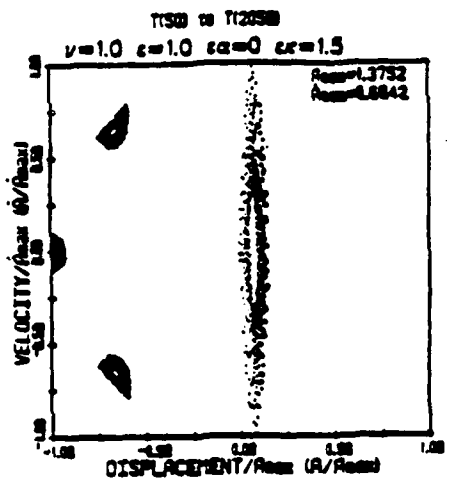

Figure 5. Poincare' map of a recurrent vibrations with several periods

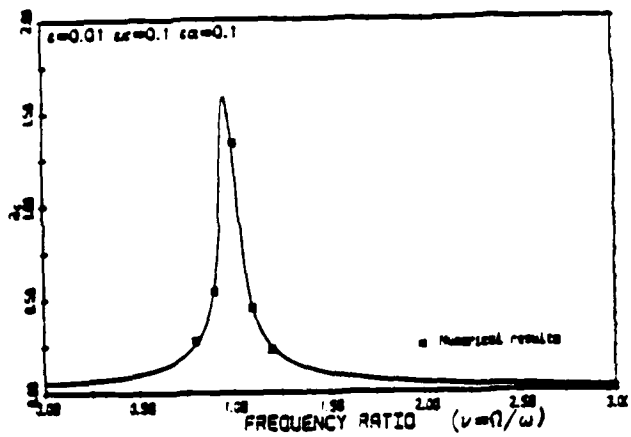

Figure 3. Comparison of exact numerical and approximate results for the steady-state amplitude

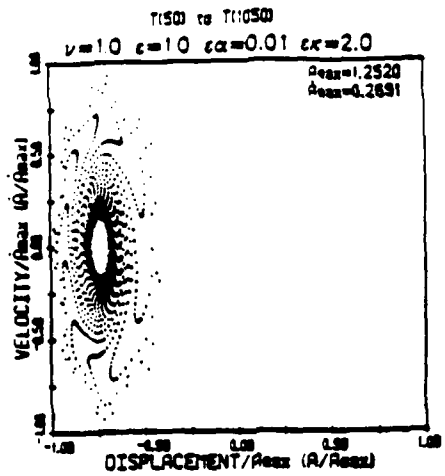

Figure 6. Effect of damping on the trajectories of motion in Poincare map

SESSION 2

CHAOTIC MOTIONS

WEDNESDAY - 1045 - 1230

June 1, 1988

ABSTRACT

Symmetry Breaking Bifurcations in Mechanical Systems and in surface Waves

P.R. Sethna

This study is concerned with symmetry breaking bifurcations in nonlinear dynamical systems with D_4 symmetry when two of the linear natural frequencies are nearly equal. The analysis can be shown to apply to a class of dynamical systems including vibrations of nearly square plates. Detailed results will be given in the case of surface waves in a nearly square container. The analysis shows that the periodic and quasi-periiodic standing, as well as travelling wave phenomena , occur. For certain critical values of the parameters, the system also exhibits chaotic phenomena. The theoretical results are verified with the aid of experiments. A video tape of some of the phenomena will be shown.

ASYMPTOTIC TECHNIQUES AND CHAOS IN WEAKLY NONLINEAR FORCED MECHANICAL SYSTEMS

by
A. K. Bajaj
School of Mechanical Engineering
Purdue University
West Lafayette, IN 47907

In many recent investigations into the dynamic behavior of multi-degree-of-freedom weakly nonlinear and harmonically excited systems it has been observed that the amplitude equations obtained via an asymptotic analysis can possess complex responses. These are in addition to the various steady state constant solutions which give rise to the phenomena of multiple periodic solutions, pump response etc. The complex dynamic behavior usually arises when a stable constant solution loses stability by Hopf bifurcation and the amplitude equations have a limit cycle solution. Changes in system parameters such as the excitation frequency, the damping and the amplitude of external forcing may lead to the limit cycle solution undergoing a cascade of period-doubling bifurcations which culminate in chaotic solutions. The theorems for the method of averaging then imply that for a small enough ϵ the original system has motion on an integral manifold. The solution can be physically interpreted as an amplitude modulated motion. The exact nature of the modulations in the motion is not predicted.

In the present work, fundamentals of the asymptotic methods are carefully reviewed and then some particular systems are studied with a view to exploring the range of applicability of the asymptotic analysis and the correspondence between the solutions of the averaged equations and those of the original system. The solutions of the original system equations are investigated for $\epsilon = 0.1$ by using longtime integration and Poincare section of the steady state motion. For moderate damping when the averaged equations have only stable limit cycle solutions over the interval in frequency, the Poincare section of the original equations consists of a set of points dense in a closed curve. The motion is thus almost periodic with noncommensurate frequencies. With variation in frequency, this motion undergoes a series of changes from almost periodic to phase-locked and phase-locked to almost periodic. Poincare sections clearly reveal that the periodic solutions of the system bifurcate into motion on a 2-torus. A decrease in damping results in the 2-torus becoming unstable via a torus-doubling. For small enough damping there is a cascade of torus-doublings leading ultimately to the destruction of the torus. The predictions of asymptotic analysis are qualitatively verified for parameter values at which the averaged systems possess hyperbolic solutions.

NONLINEAR NONPLANAR PARAMETRIC RESPONSES OF AN INEXTENSIONAL BEAM

Ali H. Nayfeh and Perngjin F. Pai
Department of Engineering Science and Mechanics
Virginia Polytechnic Institute and State University
Blacksburg, Virginia 24061

Abstract

The nonlinear integro-differential equations of motion for an inextensional beam are used to investigate the planar and nonplanar responses of a fixed-free beam to a principal parametric excitation. The beam is assumed to undergo flexure about two principal axes and torsion. The equations contain cubic nonlinearities due to curvature and inertia. Two uniform beams with rectangular cross sections are considered: one has an aspect ratio near unity, and the other has an aspect ratio near 6.27. In both cases, the beam possesses a one-to-one internal resonance with one of the natural flexural frequencies in one plane being approximately equal to one of the natural flexural frequencies in the second plane. A combination of the Galerkin procedure and the method of multiple scales is used to construct a first-order uniform expansion for the interaction of the two resonant modes, yielding four first-order nonlinear ordinary-differential equations governing the amplitudes and phases of the modes of vibration. The results show that the nonlinear inertia terms produce a softening effect and play a significant role in the planar responses of high-frequency modes. On the other hand, the nonlinear geometric terms produce a hardening effect and dominate the planar responses of low-frequency modes and nonplanar responses for all modes. If the nonlinear geometric terms were not included in the governing equations, then nonplanar responses would not be predicted. For some range of parameters, Hopf bifurcations exist and the response consists of amplitude- and phase-modulated or chaotic motions.

1. Introduction

A widely studied phenomenon is the response of axially driven rods. The axial load produces a parametric excitation, which results in time-dependent coefficients in the governing equations and boundary conditions. An important property of such systems is that a small excitation can produce a large response when the excitation frequency is not close to any of the natural frequencies of the system [1]. And, owing to certain nonlinear terms, the parametrically excited planar motions may in turn excite a mode which does not lie in the original plane. These phenomena are not disclosed by a linear approximation to these systems.

By taking into account the nonlinear inertia terms and considering linear curvature in the differential equations of motion, Haight and King [2] obtained the planar frequency-response curves of a parametrically excited rod by means of an averaging method. They also identified unstable regions in the planar response curves, which correspond to a plane shift to stable motions in the other principal plane. They did not find nonplanar motions. In this paper, we extend the analysis of Haight and King by including the nonlinear terms arising from the curvature and determine the nonplanar motions and their stability.

Most of the studies of the nonlinear dynamics of beams are based either on differential equations valid for systems in which torsional effects are neglected or on equations obtained by linearizing the beam's curvature. Only nonlinear inertia and stretching terms are commonly considered. Crespo da Silva and Glynn [3] showed that the generally neglected nonlinear terms arising from the curvature are the same order as the nonlinear terms due to inertia. To investigate large amplitude whirling motions of a simply supported beam constrained to have a fixed length, Ho, Scott and Eisley [4] neglected the longitudinal inertia and Poisson effects but accounted for large deformations through the use of Green's strain measure in the longitudinal direction. They showed that the nonlinear terms are cubic. They found both steady whirling motions and whirling motions of the beating type for some parameters.

2. Equations and Method of Solution

The equations governing the parametric vibration of the system shown in Fig.1 are

$$\ddot{v} + c\dot{v} + \beta_y v^{iv} = (1-\beta_y)[w''\int_1^s v''w''ds - w'''\int_0^s v''w'ds]'$$

$$-\frac{(1-\beta_y)^2}{\beta_y}[w''\int_0^s\int_1^s v''w''dsds]'' - \beta_y[v'(v'v'' + w'w'')']'$$

$$-\frac{1}{2}\{v'\int_1^s[\int_0^s(v'^2 + w'^2)ds]\dot{}ds\}' - [v''(s-1) + v']B\Omega^2\cos(\Omega t) \quad (1)$$

$$\ddot{w} + c\dot{w} + w^{iv} = -(1-\beta_y)[v''\int_1^s v''w''ds - v'''\int_0^s w''v'ds]'$$

$$-\frac{(1-\beta_y)^2}{\beta_y}[v''\int_0^s\int_1^s v''w''dsds]'' - [w'(v'v'' + w'w'')']'$$

$$-\frac{1}{2}[w'\int_1^s[\int_0^s(v'^2 + w'^2)ds]\dot{}ds]' - [w''(s-1) + w']B\Omega^2\cos(\Omega t) \quad (2)$$

and the boundary conditions are

$$v = w = v' = w' = 0 \quad \text{at } s = 0 \quad (3a)$$

$$v'' = w'' = v''' = w''' = 0 \quad \text{at } s = 1 \quad (3b)$$

To investigate the behavior of the beam to a principal parametric excitation in the presence of a one-to-one autoparametric resonance, we introduce two detuning parameters σ and δ_2, defined by

$$\Omega = 2\omega_{2n}(1 + \varepsilon^2\sigma) \text{ and } (h/\hat{b})^2 = 1 + \delta_0 + \varepsilon^2\delta_2 \quad (4)$$

and let $\omega_{1m} = \omega_{2n}$. By using the Galerkin procedure and the method of multiple scales, we obtain the first-order uniform expansion

$$v(s,t) = \varepsilon F_m(s)a_1(\varepsilon^2 t)\cos(\frac{1}{2}\Omega t - \gamma_1) + \ldots \quad (5a)$$

$$w(s,t) = \varepsilon F_n(s)a_2(\varepsilon^2 t)\cos(\frac{1}{2}\Omega t - \gamma_2) + \ldots \quad (5b)$$

where the equations governing the amplitudes and phases are

$$2\omega_{1m}a_1' + [R_1 + R_2a_2^2\sin 2(\gamma_1 - \gamma_2) + R_3\sin 2\gamma_1]a_1 = 0 \quad (6)$$

$$[2\omega_{1m}\gamma_1' - R_4 - R_5a_1^2 + R_6a_2^2 + R_2a_2^2\cos 2(\gamma_1 - \gamma_2) + R_3\cos 2\gamma_1]a_1 = 0 \quad (7)$$

$$2\omega_{2n}a_2' + [E_1 + E_2a_1^2\sin 2(\gamma_1 - \gamma_2) + E_3\sin 2\gamma_2]a_2 = 0 \quad (8)$$

$$[2\omega_{2n}\gamma_2' - E_4 - E_5a_2^2 - E_6a_1^2 - E_2a_1^2\cos 2(\gamma_1 - \gamma_2) + E_3\cos 2\gamma_2]a_2 = 0 \quad (9)$$

Here, the R_i and E_i are constants obtained by using numerical integration methods.

3. Numerical Results

Case 1: Near Square Cross Section

In this case, $\delta_0 = 0.0$ and $\beta_y = 0.7692$. We let $\mu = 0.05$ and $b = 0.03$. Figure 2 shows the re-

sponse curves of the first mode. It is well known that, for planar responses, if only in-plane disturbances are considered then the upper branch of a_2 will be stable [1]. But due to the disturbances in the y-direction , this branch is unstable. It follows from Eqs.(6) and (7) that

$$\sin 2\gamma_1 = \frac{-\mu}{2\omega_{1m}\alpha_7 b} \quad \text{and} \quad \sin 2\gamma_2 = \frac{-\mu}{2\omega_{2n}\beta_7 b}$$

So, if $\mu = 0$, then the phase angles $\gamma_1 = \gamma_2 = -90°$ for the upper branches, and $\gamma_1 = \gamma_2 = 0°$ for the lower branches. But the damping changes slightly the phase angles. If we increase μ, the upper and lower branches will move closer to each other. At some critical value of μ, these two will merge. If we increase b, the separation between these two branches will increase. We note from Fig. 2 that the planar solution in the stiff direction (i.e., z direction) is always unstable and hence the planar response is always in the weak direction (i.e., y direction). It follows from Eqs. (6)-(9) that the effective nonlinear spring coefficients α_e and β_e in the y and z directions are

$$\alpha_e = (1 + \delta_0)\alpha_4 - \frac{2}{3}\alpha_5\omega_{1m}^2 \text{ and } \beta_e = \beta_4 - \frac{2}{3}\beta_5\omega_{2n}^2$$

Since α_4, α_5, β_4, andβ_5 are positive, the nonlinear geometric terms $(1 + \delta_0)\alpha_4$ and β_4 are of the hardening type, whereas the nonlinear inertia terms $2/3\alpha_5\omega_{1m}^2$ and $2/3\beta_5\omega_{2n}^2$ are of the softening type. Hence, the overall type of the effective nonlinearity in the y(z) direction depends on the relative magnitudes of $\alpha_4(\beta_4)$ and $\alpha_5(\beta_5)$ and the mode shape. For the lower modes, Fig. 2 shows that the planar response curves are bent to the right, which implies that the nonlinear geometric terms dominate the response because they have a hardening effect. Neglecting the nonlinear geometric terms (i.e., letting $\alpha_i = \beta_i = 0$ for i = 1, 2, 3, and 4), we obtain the response curves shown in Fig. 3. Comparing Figures 2 and 3 shows that neglecting the geometric nonlinearity yields frequency curves that are even qualitatively wrong. The nonlinearity changes from a hardening to a softening type. Moreover, nonplanar responses cannot be predicted without including the geometric nonlinearity.

Figure 4 shows the response curves of the second mode. We note that for the upper branches of planar motions $\gamma_1 = \gamma_2 \simeq 0°$, and for the lower branches $\gamma_1 = \gamma_2 \simeq -90°$. These phase angles are different from those found in the response of the first mode (Figure 2). Owing to disturbances in the z-direction, the planar motion in the y-direction is unstable along the branch AB. Similarly, the planar motion in the z-direction becomes unstable along the branch CD due to disturbances in the y-direction. Another point is that the planar response curves are bent to the left, which means that the overall effective nonlinearity is of the softening type and hence the nonlinear inertia terms dominate the response.

Next, we return to Figures 2 and 4 to discuss the nonplanar response curves of the first two modes. As σ decreases from a value larger than that corresponding to the point B of Fig. 2, the nonplanar fixed point loses stability with a complex conjugate pair of eigenvalues moving into the right-half plane. This corresponds to the extensively studied Hopf bifurcation. Based on the Hopf bifurcation theorem, one expects amplitude- and phase-modulated motions for values of σ near B. We note that the phase angles of nonplanar responses are not constant, but the difference between γ_1 and γ_2 is always 90°. Furthermore, all the nonplanar response curves are bent to the right even for the second mode. This is not unexpected because as discussed earlier the nonlinear geometric terms control the nonplanar motion. For the first mode, the nonlinear geometric terms have a hardening effect, and hence the amplitudes of nonplanar motion are smaller than those of planar motion. On the other hand, for the second mode, the nonlinear geometric terms overcome the inertia terms and produce nonplanar motions that are larger than the planar motions.

If we increase the absolute value of δ_2 (i.e., increase the deviation of the cross section from a square), the planar response curves of the y-direction motion move away from those of the z-direction motion. Figures 5 and 6 show the response curves for the first two modes. Because of out-of-plane disburbances, the planar response is unstable along the branch AB of Fig. 5, which also shows the nonplanar response of the first mode. Here we have a Hopf bifurcation at point C. Using a Runge-Kutta routine to integrate Eqs. (6)-(9) for σ = - 0.0353 along the branch AC for a long period of time, we obtain the amplitude-modulation behavior shown in Fig. 7. The phase difference is not equal to 180° . Figure 8 shows the projection of the attractor on the $a_2 - a_1$ plane. Since the amplitude and phases are not constant but periodic with a period that is larger than that corresponding to free oscillations, the resulting motion is nonperiodic having two periods (i.e.,

motion on a torus). The spectrum of a_1 in Fig. 9 shows that the fundamental dimensionless frequency of the attractor is approximately 0.154 and hence its dimensionless period is approximately 6.5. This motion can be better visualized by plotting the motion of the tip-end of the beam, as shown in Fig. 10. This figure shows that the elliptical route keeps changing the lengths of axes and direction, and it also shows the twisting motion. Because of the nonlinear terms, the inertia force in the y-direction is not proportional to v(s,t) and the inertia force in the z-direction is not proportional to w(s,t), and hence the resultant inertia force is not parallel to the total displacement in the y-z plane and it induces a twisting moment on the beam. This is a whirling motion of the beating type. Increasing σ further to 0.07627 produces a period-doubling bifurcation of the attractor as shown in Figs. 11 and 12. Increasing σ further produces a bifurcation of this attractor to a fixed point, yielding a periodic rather than an aperiodic nonplanar motion. Thus, the response is a steady whirling motion.

Figure 6 shows also the nonplanar response of the second mode. We note that the Hopf bifurcation points E and F are adjacent to stable and unstable branches. It is found that the motion is chaotic. In Figs. 5 and 6, the nonplanar response curves always bifurcate from the planar response curves at frequencies higher than the natural frequency. The reason is that the motion in the y-direction has the same mode shape as that in the z-direction motion but it has a smaller linear natural freqyency; that is, it belongs to a lower-energy motion.

Case 2: Rectangular Cross Section

In this case, $\delta_0 = -0.9745$ (i.e., $\hat{b}/h \simeq 6.2673$) and $\beta_y = 0.3944$, and we let $\mu = 0.05$ and $b = 0.03$. For this beam, $\omega_{21} = \omega_{12}$. We investigate the possibility of nonplanar vibrations comprised of the first mode in the z-direction and the second mode in the y-direction. We find that there are two branches of nonplanar response curves: the left branch of the nonplanar response curve bifurcates from the stable branch of the planar response curve for the motion in the y-direction and, in that interval, the planar motion in the y-direction is unstable with respect to z-direction disturbances; the right branch of the nonplanar response curve bifurcates from the unstable branch of the planar response curve for the motion in the z-direction and, in this interval, both the planar motion in the y-direction and the nonplanar motion are stable, but the nonplanar motion belongs to a higher energy motion because its amplitudes are larger than those of the planar motion.

Acknowledgement

This work was supported by the Air Force Office of Scientific Research under Grant Nos. AFOSR-86-0090 and F49620-87-C-0088.

References

1. A. H. Nayfeh and D. T. Mook, *Nonlinear Oscillations,* Wiley-Interscience, New York, 1979.
2. E. C. Haight and W. W. King, "Stability of Parametrically Excited Vibrations of an Elastic Rod," *Dev. Theor. Appl. Mech.*, Vol. 5, 1971, pp. 677-714.
3. M. R. M. Crespo da Silva and C. C. Glynn, "Nonlinear Flexural-Flexural-Torsional Dynamics of Inextensional Beams--- I. Equations of Motion," *J. Struct. Mech.*, 6(4), 1978, pp. 437-448.
4. C.-H. Ho, R. A. Scott, and J. G. Eisley, "Nonplanar, Nonlinear Oscillations of a Beam---I. Forced Motions," *Int. J. Nonlinear Mechanics,* Vol. 10, 1975, pp. 113-127.

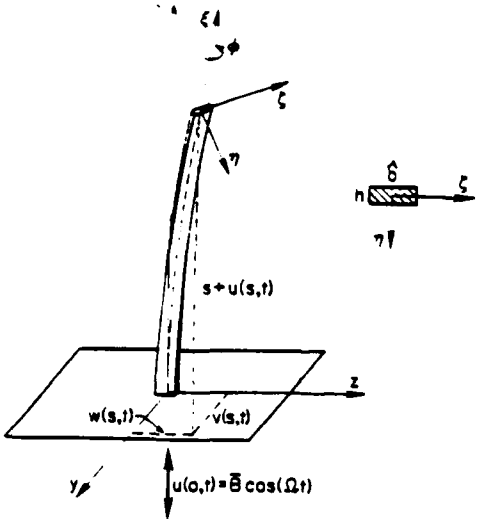

Figure 1. Coordinate systems : x-y-z = the inertial reference frame; $\xi - \eta - \zeta$ = the principal axes of the beam's cross section at position s.

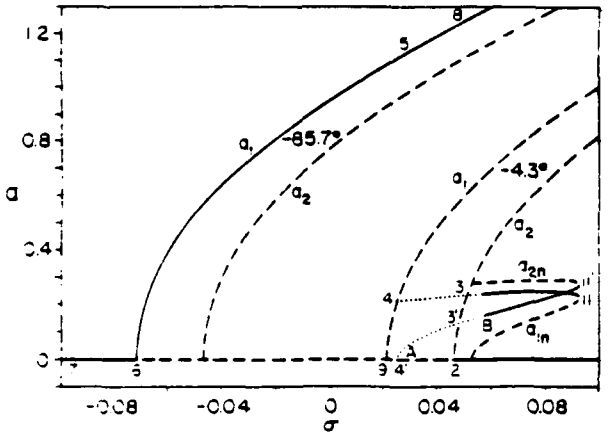

Figure 2. Response curves of the first mode for a beam with an aspect ratio $\hat{b}/h \simeq 1.0$: mode (1,1) , $\omega_{11} = \omega_{21}$, $\delta_0 = 0.0$, $\delta_2 = -0.05$, $\mu = 0.05$, $b = 0.03$, $\beta_y = 0.7692$; a_1 , a_2 = planar response amplitudes; a_{1n} , a_{2n} = nonplanar response amplitudes; (____) stable, (----) unstable with at least one eigenvalue being positive, (....) unstable with the real part of a complex pair of eigenvalues being positive.

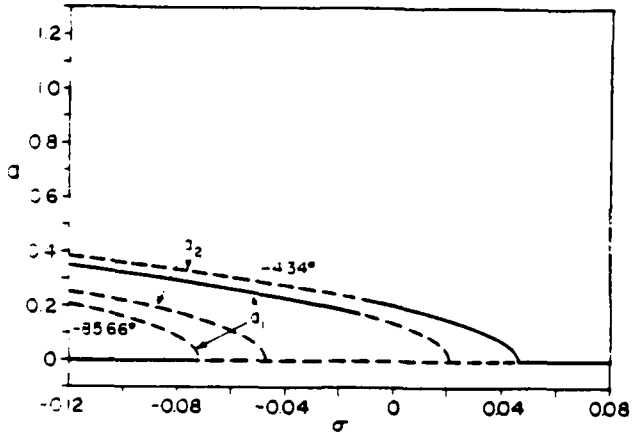

Figure 3. Response curves of the first mode in the absence of the nonlinear geometric terms, for a beam with an aspect ratio $\hat{b}/h \simeq 1.0$: mode (1,1) , $\omega_{11} = \omega_{21}$, $\delta_0 = 0.0$, $\delta_2 = -0.05$, $\mu = 0.05$, $b = 0.03$, $\beta_y = 0.7692$.

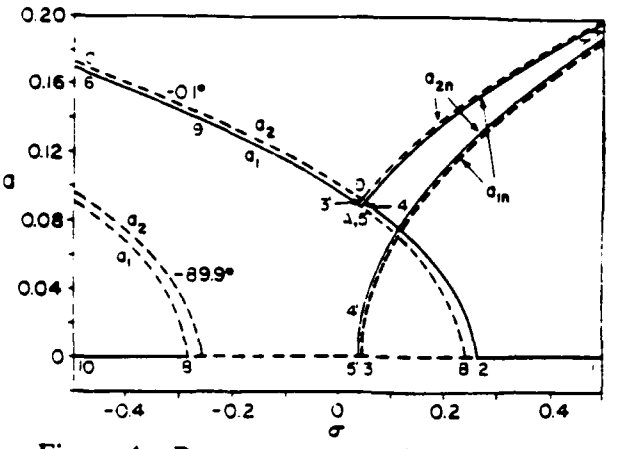

Figure 4. Response curves of the second mode for a beam with an aspect ratio $\hat{b}/h \simeq 1.0$: mode (2,2) , $\omega_{12} = \omega_{22}$, $\delta_0 = 0.0$, $\delta_2 = -0.05$, $\mu = 0.05$, $b = 0.03$, $\beta_y = 0.7692$.

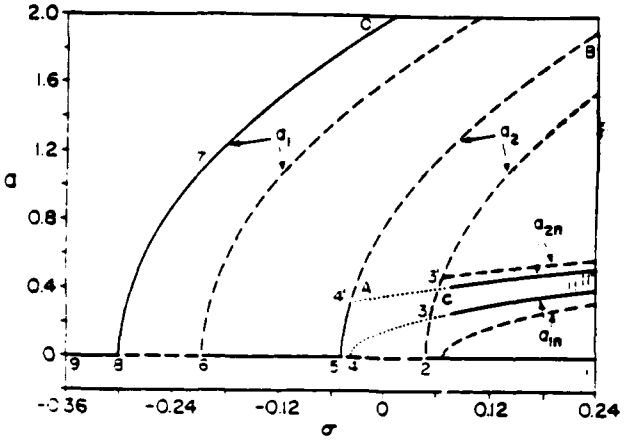

Figure 5. Response curves of the first mode for a beam with an aspect ratio $\hat{b}/h \simeq 1.0$: mode (1,1) $\omega_{11} = \omega_{21}$, $\delta_0 = 0.0$, $\delta_2 = -0.5$, $\mu = 0.05$, $b = 0.03$, $\beta_y = 0.7692$.

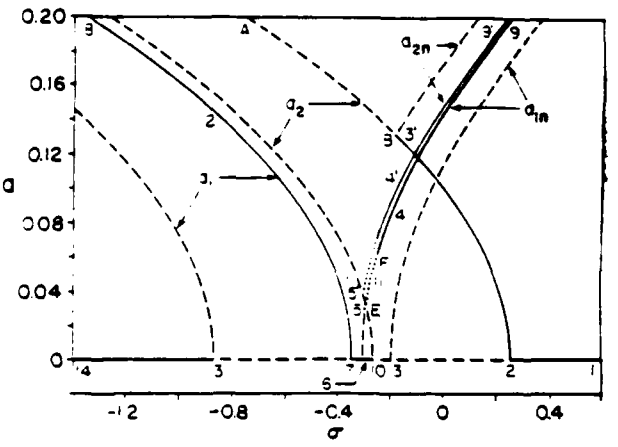

Figure 6. Response curves of the second mode for a beam with an aspect ratio $\hat{b}/h \simeq 1.0$: mode (2,2) , $\omega_{12} = \omega_{22}$, $\delta_0 = 0.0$, $\delta_2 = -1.2$, $\mu = 0.05$, $b = 0.03$, $\beta_y = 0.7692$.

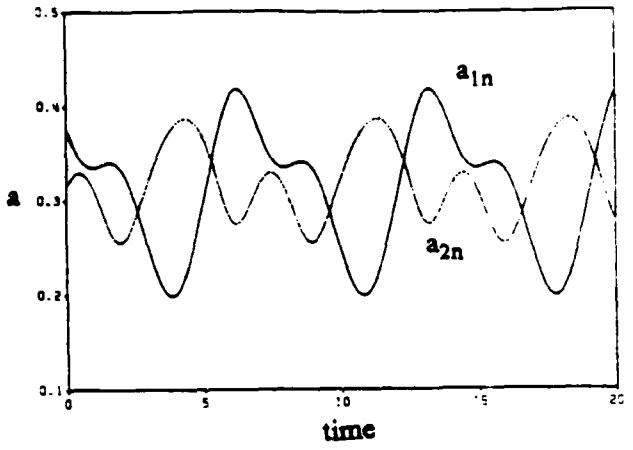

Figure 7. The long-time history of the amplitudes for the case of an amplitude- and phase-modulated motion : $\hat{b}/h \simeq 1.0$, mode (1,1) , $\omega_{11} = \omega_{21}$, $\delta_0 = 0.0$, $\delta_2 = -0.5$, $\mu = 0.05$, $b = 0.03$, $\beta_y = 0.7692$, $\sigma = -0.0353$.

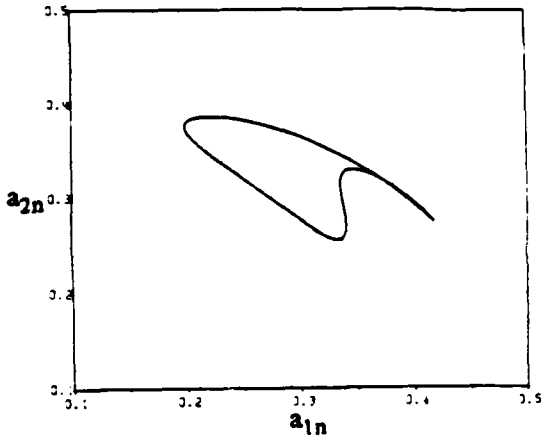

Figure 8. A projection of the trajectory onto the $a_1 - a_2$ plane : $\hat{b}/h \simeq 1.0$, mode (1,1) , $\omega_{11} = \omega_{21}$, $\delta_0 = 0.0$, $\delta_2 = -0.5$, $\mu = 0.05$, $b = 0.03$, $\beta_y = 0.7692$, $\sigma = -0.0353$.

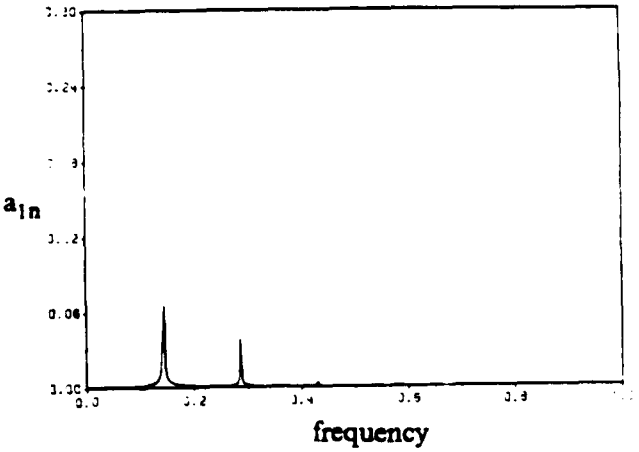

Figure 9. The Fourier harmonic analysis of a_1: $\hat{b}/h \simeq 1.0$, mode (1,1) , $\omega_{11} = \omega_{21}$, $\delta_0 = 0.0$, $\delta_2 = -0.5$, $\mu = 0.05$, $b = 0.03$, $\beta_y = 0.7692$, $\sigma = -0.0353$.

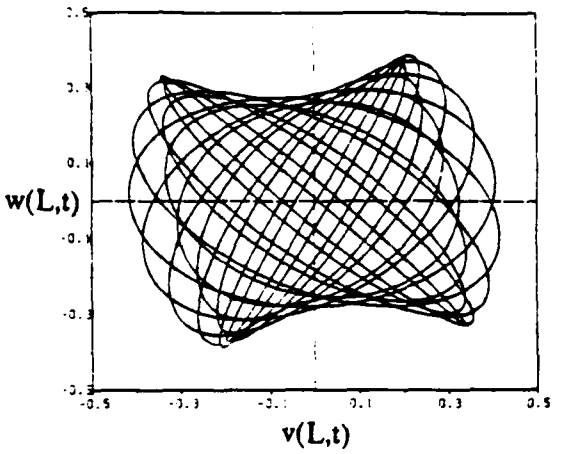

Figure 10. The path of the tip-end of the beam for the case of an amplitude- and phase-modulated motion : $\hat{b}/h \simeq 1.0$, mode (1,1) , $\omega_{11} = \omega_{21}$, $\delta_0 = 0.0$, $\delta_2 = -0.5$, $\mu = 0.05$, $b = 0.03$, $\beta_y = 0.7692$, $\sigma = -0.0353$, $\varepsilon = 0.5$.

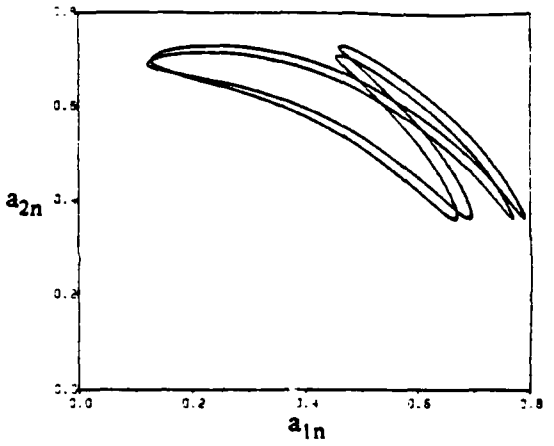

Figure 11. A projection of the trajectory onto the $a_1 - a_2$ plane : $\hat{b}/h \simeq 1.0$, mode (1,1) , $\omega_{11} = \omega_{21}$, $\delta_0 = 0.0$, $\delta_2 = -0.5$, $\mu = 0.05$, $b = 0.03$, $\beta_y = 0.7692$, $\sigma = 0.07627$.

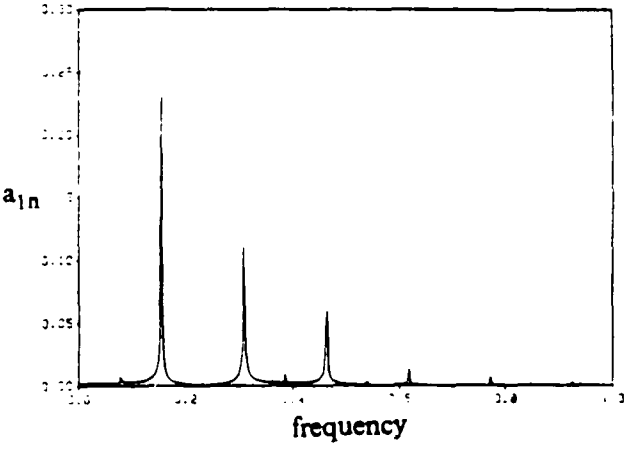

Figure 12. The Fourier harmonic analysis of a_1: $\hat{b}/h \simeq 1.0$, mode (1,1) , $\omega_{11} = \omega_{21}$, $\delta_0 = 0.0$, $\delta_2 = -0.5$, $\mu = 0.05$, $b = 0.03$, $\beta_y = 0.7692$, $\sigma = 0.07627$.

Nonlinear Response of Infinitly Long Circular Cylindrical Shells to Subharmonic Radial Loads

by
Ali H. Nayfeh, Raouf A. Raouf, and Jamal F. Nayfeh
Department of Engineering Science and Mechanics
Virginia Polytechnic Institute and State University
Blacksburg, VA 24061

To second-order, the equations of motion of an infinitely long circular cylindrical shell in dimensionless form are (Goodier and McIvor, 1964; Nayfeh and Raouf, 1987; and Raouf, 1985)

$$\ddot{w} + \alpha^2(w^{iv} + 2w'' + w) - \psi' + w = w''(\psi' - w) - \dot{\psi}^2 + \psi'^2 - 2w\psi' + w'\psi'' - \frac{1}{2}w'^2 + \frac{a(1-\nu^2)}{Eh}P(1 + \psi' - w) \tag{1}$$

and

$$\ddot{\psi} - \psi'' + w' = w'w'' - 2w'\psi' + 2\dot{w}\dot{\psi} + \frac{a(1-\nu^2)}{Eh}w'P \tag{2}$$

where the overdot indicates the partial derivative with respect to t, the prime indicates the partial derivative with respect to θ, w and ψ are the dimensionless radial and tangential displacements, respectively, and P is the applied pressure load. Here, $\alpha^2 = h^2/12a^2$, where h and a are the thickness and initial radius of the shell, respectively.

We use the method of multiple scales (Nayfeh, 1973, 1981) to determine a second-order uniform expansion of the solution of Eqs. (1) and (2) for small but finite amplitudes when P is given by

$$\frac{a(1-\nu^2)}{Eh}P = \varepsilon F\cos\Omega t \tag{3}$$

when $\Omega \approx 2\omega_o$ and $\omega_o \approx 2\omega_f$, where ω_o and ω_f are the linear natural frequencies of the breathing and flexural modes, respectively. Here, ε is a small dimensionless quantity. Thus, we assume that

$$w(\theta,t;\varepsilon) = \varepsilon w_1(\theta,T_o,T_1) + \varepsilon^2 w_2(\theta,T_o,T_1) + \ldots \tag{4}$$

$$\psi(\theta,t;\varepsilon) = \varepsilon\psi_1(\theta,T_o,T_1) + \varepsilon^2\psi_2(\theta,T_o,T_1) + \ldots \tag{5}$$

where $T_o = t$, a fast scale characterizing motions with the natural and excitation frequencies, and $T_1 = \varepsilon t$, a slow scale characterizing the modulation of the amplitudes and phases of the modes with damping, nonlinearity, and any possible resonances.

The evolution equations are (Nayfeh, Raouf and Nayfeh, 1988)

$$p_1' + \nu_2 q_1 + \mu_o p_1 + 2\Lambda_1(p_2q_2 + p_3q_3) + fq_1 = 0 \tag{6}$$

$$q_1' - \nu_2 p_1 + \mu_o q_1 - \Lambda_1(p_2^2 + p_3^2 - q_2^2 - q_3^2) + fp_1 = 0 \tag{7}$$

$$p_2' + \nu_1 q_2 + \mu_n p_2 + \Lambda_2(q_1 p_2 - q_2 p_1) = 0 \tag{8}$$

$$q_2' - \nu_1 p_2 + \mu_n q_2 - \Lambda_2(p_1 p_2 + q_1 q_2) = 0 \tag{9}$$

$$p_3' + \nu_1 q_3 + \mu_n p_3 + \Lambda_2(q_1 p_3 - q_3 p_1) = 0 \tag{10}$$

$$q_3' - \nu_1 p_3 + \mu_n q_3 - \Lambda_2(p_1 p_3 + q_1 q_3) = 0 \tag{11}$$

where μ_o and μ_n are modal damping coefficients,

$$\nu_1 = \frac{1}{2}\sigma_1 + \frac{1}{4}\sigma_2, \quad \nu_2 = \frac{1}{2}\sigma_2 \tag{12a}$$

$$\Omega = 2\omega_o + \varepsilon\sigma_2, \quad \omega_o = 2\omega_n + \varepsilon\sigma_1 \tag{12b}$$

The steady-state solutions of (6)-(11) correspond to $p_i' = q_i' = 0$. There are two possibilities. Either

$$a_o = a_n = b_n = 0 \tag{13}$$

or

$$a_o = a_o^* = \Lambda_2^{-1}\left[\mu_n^2 + \frac{1}{4}\left(\frac{1}{2}\sigma_2 + \sigma_1\right)^2\right]^{1/2} \tag{14}$$

$$a_n^2 + b_n^2 = -\chi_1 \pm \left(\frac{f^2 a_o^2}{\Lambda_1^2} - \chi_2^2\right)^{1/2} \tag{15}$$

where

$$a_o^2 = p_1^2 + q_1^2, \quad a_n^2 = p_2^2 + q_2^2, \quad b_n^2 = p_3^2 + q_3^2 \tag{16}$$

$$\chi_1 = \left[4\mu_o\mu_n - \sigma_2\left(\frac{1}{2}\sigma_2 + \sigma_1\right)\right]/4\Lambda_1\Lambda_2 \tag{17}$$

$$\chi_2 = \left[\mu_o(\sigma_2 + 2\sigma_1) + 2\sigma_2\mu_n\right]/4\Lambda_1\Lambda_2 \tag{18}$$

We study the flow governed by the autonomous evolution equations (6)-(11) rather than the original equations of motion. Thus, a fixed point of the flow corresponds to a periodic solution of Eqs. (1) and (2). The detuning parameter $\sigma_2 = \sigma_2(f/\Lambda_2)^{-1/2}$ is used as a bifurcation parameter, all others being held fixed.

In Fig. 1, we show a typical response curve. This figure shows two phenomena, typical of nonlinear systems, the saturation and jump phenomena (Nayfeh and Mook, 1979). As the amplitude f of the excitation increases from zero, only the trivial fixed point attractors exist, until a threshold is reached at $f = f_2$. The trivial solution is no longer stable and a jump phenomenon occurs. As f increases the

amplitude of the excited breathing mode saturates at a constant level and the extra input energy is spilled over into the flexural mode, which responds with a large amplitude wrinkling of the shell. At $f = f_3$, the fixed point attractors lose stability through a Hopf bifurcation.

Upon decreasing f, the amplitude of the flexural mode decreases and the amplitude of the breathing mode remains constant, until $f = f_1$ is reached. The critical value $f = f_1$ corresponds to a collision between the unstable and stable fixed points causing a jump to the trivial response. The flow undergoes a fold bifurcation.

Next we study the flow as $\hat{\sigma}_2$ changes. We take $\alpha^2 = 2.0918\times10^{-4}$, which yields $\omega_0 \approx 2\omega_6$ and $\hat{\sigma}_1 = \sigma_1(f/\Lambda_2)^{-\frac{1}{2}} = -0.73$. Moreover, we let $\hat{\mu}_{0,6} = \mu_{0,6}(f/\Lambda_2)^{-\frac{1}{2}} = 0.02$.

For $2.0353 < \hat{\sigma}_2 < -1.9987$, the flow asymptotically approaches a hyperbolic fixed point as $t \to \infty$ and the response of Eqs. (1) and (2) is either trivial or periodic. The behavior of the flow within the above interval is summarized in Fig. 2. Here, we make the following observations:

1. All periodic orbits are born symmetric and lose stability through a cyclic-fold bifurcation. Figure 3 shows a typical projection of attractor III and its power spectral density (PSD).
2. Deformation of attractors:
   All attractors undergo deformation as $\hat{\sigma}_2$ changes. Interesting behaviors are observed in the following attractors:

   a) Attractor IV starts at $\hat{\sigma}_2 = -1.8200$ as a symmetric one but loses its symmetry just before collision with a repeller.

   b) Attractor IX is born at $\hat{\sigma}_2 = 1.9953$ as a symmetric one, loses symmetry but regains it before collision.

   c) Attractor X is born at $\hat{\sigma}_2 = 1.9953$ as a symmetric one. It goes into a period-three motion, becomes asymmetric, and then regains its symmetry before collision as shown in Figs. 4(a-d), respectively.

3. The evolution equations (6)-(11) exhibit a symmetry apparent in the projections of the phase trajectories (Fig. 3). The flow is invariant under the transformation

$$T: \begin{Bmatrix} p_1 \\ q_1 \\ p_2 \\ q_2 \end{Bmatrix} \to \begin{bmatrix} -1 & 0 & 0 & 0 \\ 0 & -1 & 0 & 0 \\ 0 & 0 & 0 & 1 \\ 0 & 0 & -1 & 0 \end{bmatrix} \begin{Bmatrix} p_1 \\ q_1 \\ p_2 \\ q_2 \end{Bmatrix} \qquad (19)$$

4. At $\hat{\sigma}_2 = -1.55$ (chaotic region), the Lyapunov exponents are 0.566, 0.000, -0.057, -0.624 and the dimension is $d_f \approx 3.8$.

ACKNOWLEDGEMENT

This work was supported by the National Science Foundation under Grant # MSM-8521748 and the Air Force Office of Scientific Research under Grant # AFOSR-86-0090.

REFERENCES

1. Nayfeh, A. H., 1973, Perturbation Methods, Wiley-Interscience New York.

2. Nayfeh, A. H. and Mook, D. T., 1979, Nonlinear Oscillations, Wiley-Intersicence.

3. Nayfeh, A. H., 1981, Introduction to Perturbation Techniques, Wiley-Interscience, New York.

4. Nayfeh, A. H. and Raouf, R. A., 1987a, "Nonlinear Forced Response of Infinitely Long Circular Cylindrical Shells," ASME Journal of Applied Mechanics, Vol. 109, pp. 571-577.

5. Nayfeh, A. H. and Raouf, R. A., 1987b, "Nonlinear Oscillation of Circular Cylindrical Shells," International Journal of Solids and Structures, Vol. 23, pp. 1625-1638.

6. Raouf, R. A., 1985 "Nonlinear Forced Response of Circular Cylindrical Shells," Thesis, Department of Engineering Science and Mechanics, Virginia Polytechnic Institute and State University, Blacksburg, VA.

7. Nayfeh, A. H., Raouf, R. A., and Nayfeh, J. F., 1988 "Nonlinear Response of Long Circular Cylindrical Shells to Subharmonic Radial Loads," ASME Journal of Applied Mechanics, submitted for publication.

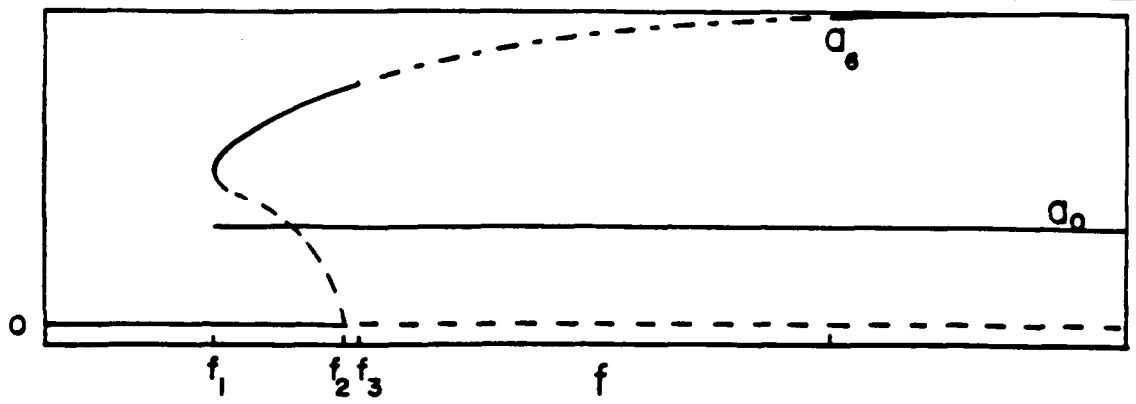

FIG·1 TYPICAL RESPONSE AMPLITUDE

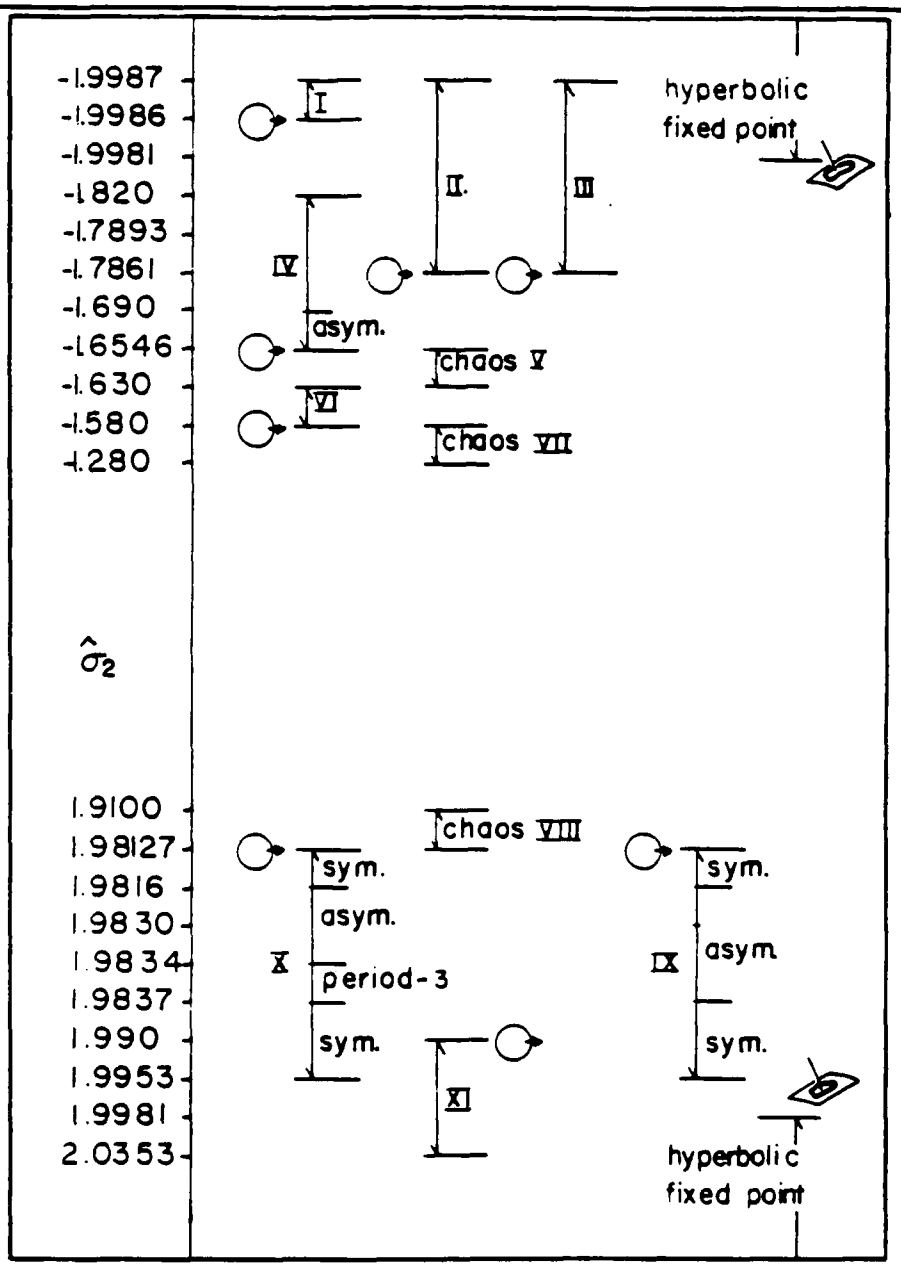

FIG 2

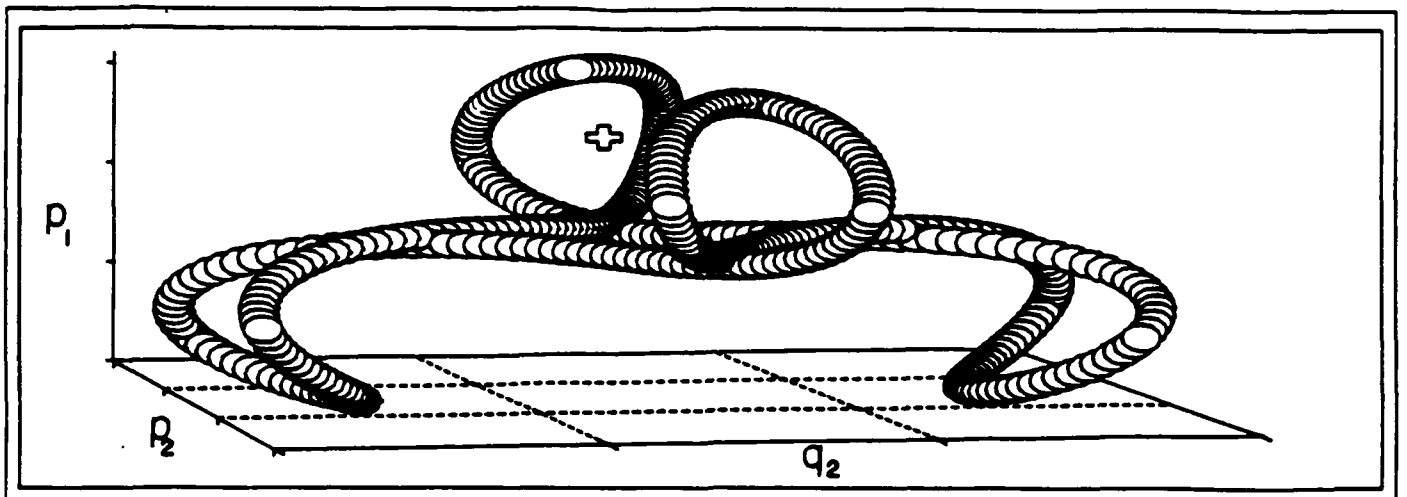

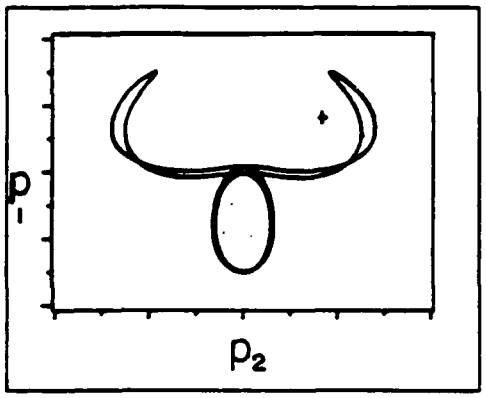

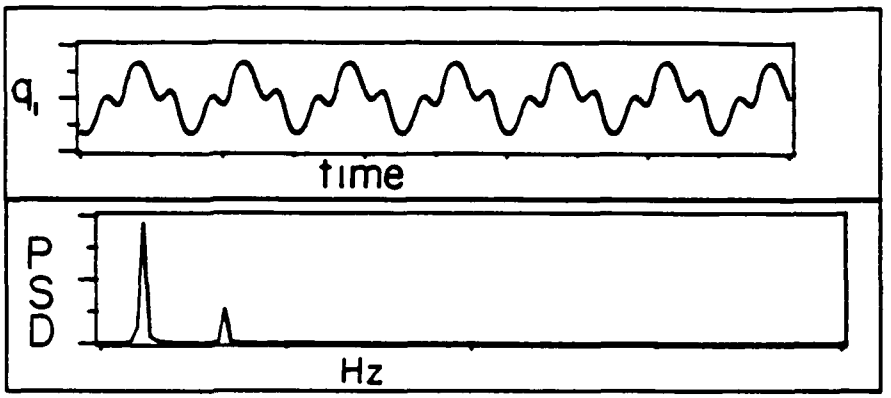

FIG 3 $\hat{\sigma}_2 = -1.82$

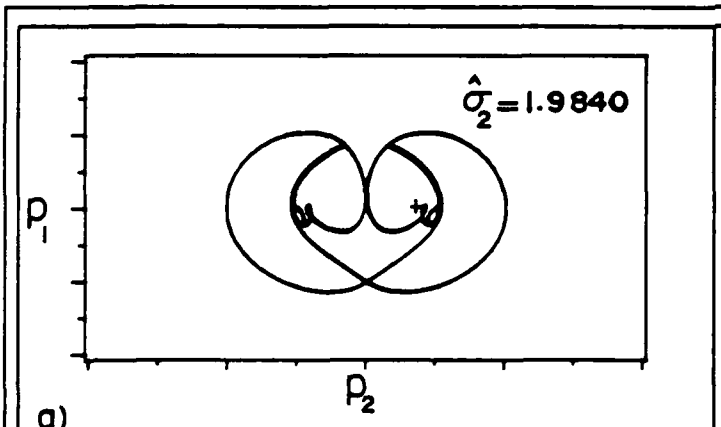

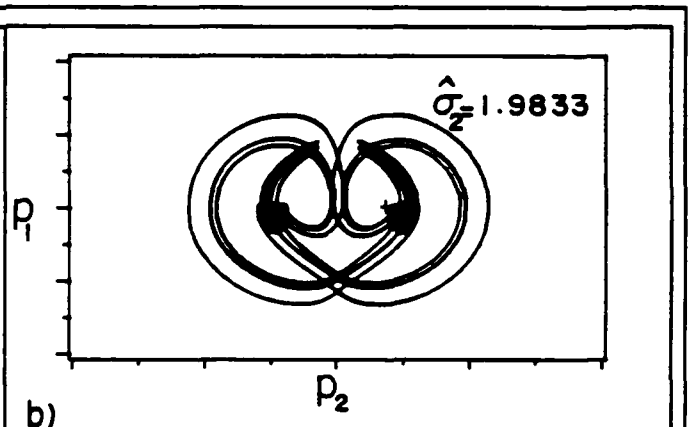

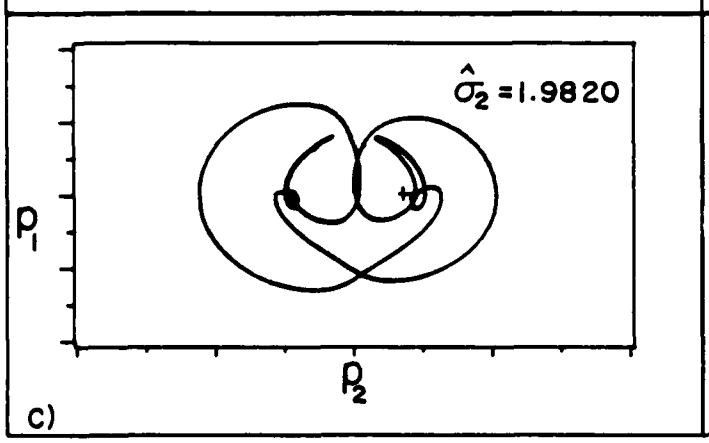

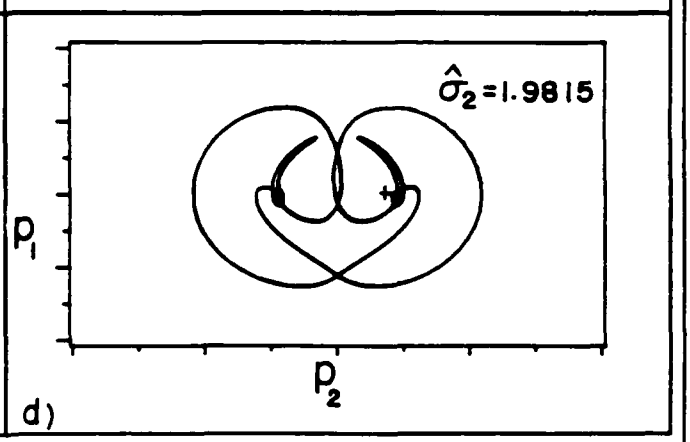

FIG 4 DEFORMATION OF ATTRACTOR X

THE EVALUATION OF THE REGION OF CHAOTIC MOTION IN CURVED STRUCTURES

By

Chung Fai Ng
Resident Research Associate
Structural Acoustics Branch
NASA Langley Research Center
Hampton, VA 23665-5225

For Presentation at
the Second Conference on Non-Linear, Stability,
and Dynamics of Structures and Mechanisms
June 1-3, 1988
Blacksburg, Virginia

Curved structures such as postbuckled beams, plates and cylindrical plates are known to have softening spring behavior. In some cases, as the effects of softening increase, the effective stiffness is reduced to zero and instability starts. The dynamic instabilities of a beam or plate was studied by representing the deformation shapes by one to three terms of shape function and analyzing the resulting coupled nonlinear equations of motion using Runge-Kunta Techniques. It is found that the dynamic instability under sinusoidal excitation takes the form of a non-periodic chaotic motion. Typically, in a buckled plate, the chaotic motion starts when the r.m.s. displacement reaches 35% of the buckled value and under sinusoidal excitation at 80% of the linear natural frequency. However, the chaotic motion stops when the excitation is increased beyond a certain level and periodic motion resumes. This motion is shown in figure 1 as an oscillatory motion from C to C' passes through the region of negative stiffness (between A & B) and its mean position is at zero, which is an unstable static position. Also, the oscillatory motion exhibits hardening spring behavior, like that of a flat plate, showing that the effects of softening due to curvature are less significant when the dynamic amplitude is large. This can be seen from the fact that a flat and a buckled plate have similar magnitude of stiffness for large displacement (from figure 1). In summary, a curved plate starting with a softening spring system with mean position at the statically stable position ends eventually with a hardening spring dynamic system with

mean at a statically unstable position. The transitional region between the two systems being the region of chaotic motion. In this paper, emphases are on the evaluation of the lower and upper boundaries of the chaotic region rather than the characteristics of the chaotic motions itself. Effects of imperfections and the presence of antisymmetric (2,1) mode and higher symmetric mode (3,1) on the starting point of chaotic motion are studied and approximate analytical formulae are derived. Comparisons are made with experiments on buckled beams and plates using excitation frequencies from 5 Hz to twice the fundamental frequency.

The results are very useful for prediction of sinusoidal and random responses of curved plates.

FIG. 1

FORCE VS DISPLACEMENT
FOR FLAT AND BUCKLED PLATES

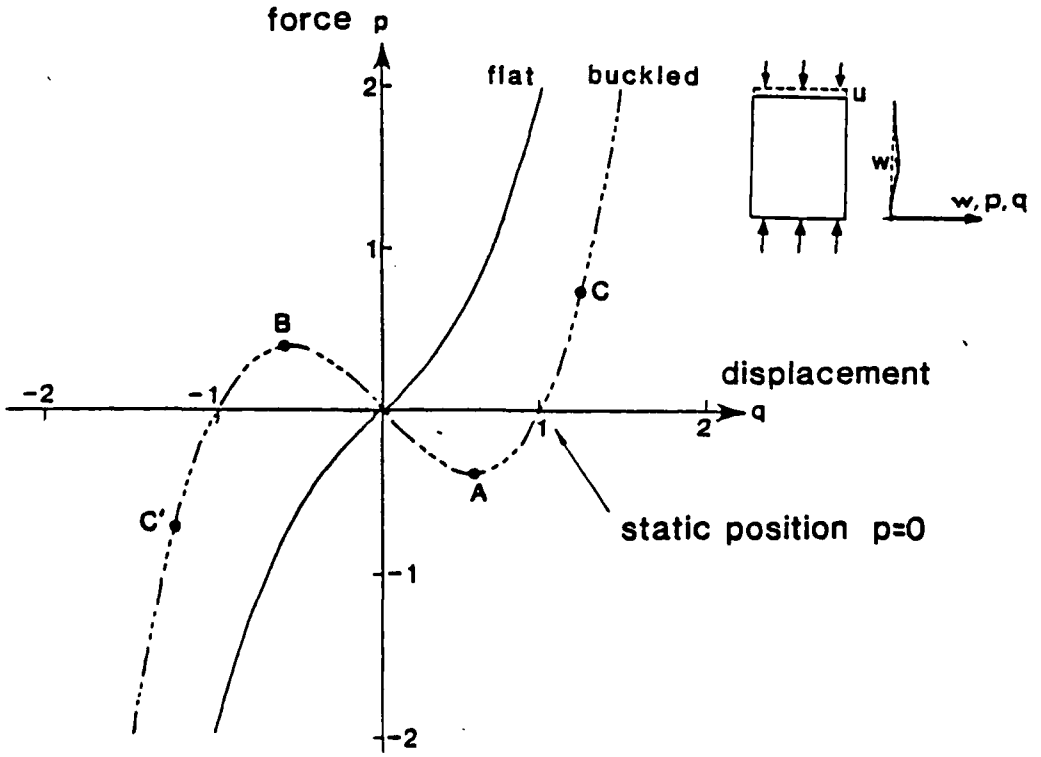

Parameter Identification In Chaotic Dynamic Systems

by

D. Joseph Mook*
Pao-Hong Tong†
Department of Mechanical and Aerospace Engineering
State University of New York at Buffalo
Buffalo, New York 14260

Abstract

The study of chaotic dynamic systems continues to generate considerable interest in the mathematics and mechanics research communities. The research work to date has consisted largely of investigating the properties and solutions of mathematical models which exhibit chaos, of building simple physical systems which demonstrate chaotic motion, and of investigating the possibility of the existence of chaos in various physical systems. There remains a critical issue which must be addressed before many of these results may be incorporated into engineering analysis and design, which is, how does one obtain an accurate mathematical model for an actual system known to be chaotic?

Some efforts have recently been made to apply existing well-known parameter identification techniques to the problem of identifying unknown parameters in a chaotic dynamic system model. These efforts have been largely unsuccessful, indicating a need for new methods to identify chaotic systems. This motivation led to the present study.

In this paper, we present a method for estimating the parameters in a chaotic dynamic system model from discrete measurements of the system's output. The method works well on the example problems considered. The effects of measurement noise and frequency are discussed, and ideas which may be useful in choosing model terms for a chaotic system are presented.

---

* Assistant Professor
† Graduate Assistant

SESSION 3

NONSTATIONARY AND RANDOM VIBRATIONS

WEDNESDAY - 1330 - 1530

June 1, 1988

NONLINEAR NONSTATIONARY PROCESSES

R. M. Evan-Iwanowski* and G. L. Ostiguy**

ABSTRACT: The objective of this write-up is (i) to present new and refined results on the nonstationary (NS) manifestations of mechanical systems: the Duffing oscillator, relaxation vibrations, and dynamic stability which indicate the departures from the corresponding stationary (ST) responses, or result in specifically NS behavior; (ii) to identify the factors and the aspects which affect the NS responses; and (iii) to delineate the NS unsolved problems related to the systems in (i). This work is viewed as a contribution for further theoretical developments and for applications in technology.

I. INTRODUCTION.

Physical world as perceived by the Systems Dynamics (SD) is nonlinear (NL), nonstationary (NS)[1], and random (stochastic)[2]. The mathematical models (ordinary differential equations (ODEs or simply DEs) in our case), which represent this world contain nonlinear terms and nonstationary components.

In recent years, the unprecedented achievements were registered in ST SD. Quantitative and qualitative - geometrical or topological methods - were used leading to these achievements. The developments in NS systems showed relatively little activities. The main reason is that, in spite of the NS manifestations being obvious, they are complex and difficult to track. Clearly, the ST systems constitute a point of departure for the NS systems, and at the same time, the NS systems should contain the ST systems as a special or limiting case.

It has been established that in some cases even small changes of the control variables or initial conditions may result in considerable changes in the dynamic responses. It is thus expected that the NS modes may alter substantially the ST responses.

In the studies in the ST SD, primary attention is focused on the three classes of the most common[3] single degree of freedom (1DF) systems:
(1) Duffing oscillators, (2) Relaxation oscillations, and (3) Parametric systems related to dynamic stability. Similar methodology has been followed in the studies of NS systems.

---

*Visiting Professor, University of Central Florida, Orlando, FL 32816

**Professor, Ecole Polytechnique, Montreal, Quebec H3C3A7.

[1]NS systems contain some time dependent components or control variables.

[2]Not treated in this write-up.

[3]Many physical, engineering, and scientific manifestations are modeled by these equations.

This write-up concerns itself with a special NS modes, viz., transitions through resonances (TtRs)-time varying frequencies and/or amplitudes of the external excitations (ee).

The studies in TtR fall into two categories[4]: (1) when the time varying parameters are arbitrary, explicit functions of time with extended ranges of their variations, so-called robust TtR, and (2) when these parameters are considered to vary very slowly, i.e., they are close to the ST values or they ever need be defined as explicit functions of time, and they are referred to as evolving TtR.

2. DEVELOPMENTS AND DELINEATION OF TtR PROBLEMS

The early NS developments were related to the robust NS systems and were presented in a paper [1] and two monographs [2] and [3], where the asymptotic methods of Krylov-Bugolyubov have been extended to include NS processes, the KBM method. Numerous illustrations of applications of special functions and KBM methods to the technological problems were presented [3], [4].

A formal extension of the KBM method to the multiple degrees of freedom systems to include combination resonances has been presented in [5] and applied to a set of problems exhibiting these type of resonances, especially in the area of dynamic stability [6].

The main factors which affect the TtR responses are the values and directions of the sweep rates α_ν and α_B, in linear TtR of the frequency $\nu = \nu_0 + \alpha_\nu t$ and the amplitude of $B = B_0 + \alpha_B t$ of the ee, α and γ in cyclic TtR: $\nu = \nu_0 + \gamma \mathrm{Sin}\alpha t$. Other time forms of the TtR are in use: logarithmic, powers of t and exponential.

Other factors affecting the NS responses are: initial conditions (IC) either ON the stationary curve (SC) or NOT-ON SC, damping parameter, modes of oscillations, static loads, spatial boundary conditions, static loads.

Duffing Oscillator. $\ddot{x} + \omega^2 x + \zeta\dot{x} + \mu x^3 = B(t)\cos\theta(t)$. Amplitude-frequency plots (a, ν) in linear TtR, are presented in Fig. 1, originating on SC and NOT ON SC. It is seen from Fig. 1 that such TtR curves eliminate fold discontinuity, and they jump or drop in a cascading wavy form, terminating with dying out high frequency oscillations at the junction with the SC curve.

The evolving TtR was used, among other means, in [7] to predict the incipient jump. It is remarked there that such prediction has little practical consequence, because it is too close to the actual ST jump frequency. 'Injecting', however, an NS (TtR) mode ON the NS drop response, a stable plateau is reached which may delay the drop process Fig. 2. Complete explanation of the elimination of the discontinuities in robust TtR responses is lacking.

Another only partly answered practical question is related to the determination of α corresponding to a given maximum of the TtR amplitude.

---

[4] Deeper reasons may be identified for the existence of these categories.

The cyclic TtR may be successfully used in dynamic controls by applying alternately sweeps α and $-\alpha$ to move a point from the position A to the position B Fig. 3 (schematic).

The effects of the NS damping coefficient $\zeta(t)$ and the effects of the ee amplitude B(t) are shown in Fig. 4.

There is an inherent difficulty in defining the NS phase-planes. This is so because of the inherent existing asynchroneity in the NS responses, due to time variations of the phase shift ϕ [12].

While for some cases, the NS response amplitude variations exhibit a considerable amount of wavyness, the corresponding TtR ϕ plots exhibit a smooth behavior Fig. 5. It may thus be advantageous in some cases, particularly in applications, to track the TtR manifestations using ϕ rather than a. Recently obtained partial results by Kitis and Evan-Iwanowski on the NS chaotic responses of a Duffing-Hayashi oscillator offer quite revealing observations Figs. 6, 7, 8. For $\alpha_{\phi} = 10^{-2}$ for the first 90 sec the NS chaotic response coincides with the ST; then they diverge. However, the NS response remains chaotic till it shows a quasi-periodic character Fig. 7. The same picture is seen from Fig. 8 for $\alpha_{B} = 10^{-2}$ the divergence appears at 30 sec, and the structured, quasi-periodic motion appears at 22 sec. Thus, the NS modes quench the ST chaotic motion for sufficiently fast TtR.

Further studies of these points may be related to Fig. 9, showing a number of different ST responses of the Duffing-Hayashi oscillator in (ζ, B) plane [15]. Each of these responses could be cast in NS modes. The early studies on the evolving TtR in Duffing oscillator are found in [8] in undamped linear Duffing equation and in [9] for the same equation with damping. By an appropriate selection of the time scales, key equations were obtained connecting the amplitudes in the first approximation. This method was also used in [10] for damped, nonlinear Duffing oscillator to establish a sense in which NS response approaches the ST jumps. Lately, in [11] the work in [10] has been extended for the effects of the initial conditions NOT ON the STC.

Relaxation Systems. $\ddot{x} + \omega^2 x - \varepsilon(1 - x^2)\dot{x} = B(t) \cos \theta(t)$. In evolving TtR interesting results have been obtained at Northwestern University [12], presenting evolving Hopf bifurcation, memory effect, resonance, and nerve accommodation. Currently, Tran and Evan-Iwanowski are working on these problems Fig. 10, 11. Needless-to-say that this area demands further intensive studies.

Dynamic Stability. $\ddot{x} + \Omega^2[1 - 2\mu \cos \theta(t)]\, x + \zeta\dot{x} + \mu x^3 = 0$. Dynamic Stability problems (or parametrically excited systems) find wide and essential applications in structures of rockets, aircraft, tall antennas, rotatory machinery, ect. These structures are often subjected to the TtR modes. For these reasons, they recently received attention of a number of researches [5], [6], [13, [14] pertaining to linear or nearly linear and cyclic TtR. These results present some specifically NS manifestations which indicate a need for further studies. These are: (1) penetration (delayed NS responses) Fig. 12, whereby the TtR responses initiated outside of the stable branch penetrate (delay) into the instability region (IR) and then jump catastrophically on the stable branch; (2) The NS drag-in and out, initially stable configuration outside of the IR is rendered

unstable when subjected to TtR mode and vice versa. This manifestation depends on damping, IC rate of TtR, the mode, static load, Figs. 13-17; clearly this TtR behavior presents considerable concern for an analyst-designer; (3) Three nonoverlapping categories of the TtR C1, C2 and C3 are shown in Figs. 18, 19. This manifestation may have some effect on the random vibration methodology when α is random; (4) the most striking behavior is observed in cyclic TtR, ($\nu(t) = \nu_o + \gamma \sin \alpha t$ in dynamic stability problems Figs. 20, 21. These are: (a) for some TtR parameters γ and α, the response is centered about the mean value (whether they are periodic or chaotic is not yet resolved) Fig. 20; (b) for some γ and α, they drop rapidly to static equilibrium Fig. 21, thus offering an effective means of stabilization; (c) they wander up and down, which may for suitable selection of α and/or γ be used for a programmed motion Fig. 22.

Interesting results were obtained on a slender column subjected to two-harmonic excitations with the frequencies ν_1, and ν_2. Firstly, the analysis indicates that the system is always divergent. However, the experiments showed that for $|\nu_1 - \nu_2| \doteq 1$ Hz, the column exhibited an "unordered" motion Fig. 23.

Experimental Work. Experimental work is essential in ascertaining validity of some predicted phenomena or uncovering some new ones. For instance, the experimental works established first the existence of chaotic motions, and explained mathematically later. Experimental works conducted at Syracuse University and later carried out at Ecole Polytechnique, Montreal, particularly in parametric stationary and nonstationary modes, show very good agreement with analytical results. This fact reinforces the effectiveness of the perturbation methods and computer schemes used.

CONCLUSIONS.

An obvious conclusion is that the NS processes, in our case the TtRs affect almost all manifestations of the ST SD. A global menu thus for the future work in this field is: (i) to apply NS processes to the well-established bifunction theories and the conjectures as well, (ii) to proceed to study NS attractors including strange attractors (chaos). The NS processes in the evolving formulations found already their applications in dynamics, nuclear physics*, chemistry, medicine, biology, etc. The robust formulations of the NS processes are indispensable in analysis and design in structural engineering, especially in dynamic stability (parametric ee.)

The NS processes constitute an indispensible component of the basic SD studies. They also constitute an indispensible input to the technological (engineering) point of view: They may be utilized for gaining mechanical advantages in design and may serve to establish design criteria, i.e., in the determination of the parameter ranges within which the predicted responses are secured. The lack of the detailed knowledge of these manifestations may result in dire technical consequences.

(2AE14N202TXY)

---

*Communication from Professor G. Höher, Inst. Nuclear Physics, Karlsruhe.

REFERENCES:

1. Lewis, F.M. (1932). Trans. ASME, 54, 253-261.219. 2. Mitropolsky, Y.A. (1965). Davey, New York. vii,137,162,219. 3. Goloskokow, E.G. and Fillipow, A.P.(1971). - Verlag. Berlin. 4. Evan-Iwanowski,R.M.(1969). Appl. Mech. Rev.,22,213-219. 5. Evan-Iwanowski, R.M. (1976). Elsevier, New York. vii, 219,260,267,268,402,417,418. 6. Ostiguy, G.L. (1976). - Ph.D. Dissertation, Syracuse University. 7. Thompson, J.M.T. and Stewart, H.B.(1986), J. Wiley and Sons, New York, N.Y. p.11, 129-131. 8. Kevorkian, J.(1971). SIAMJ. Appl. Math.20, pp.364-373. 9. Ablowitz, M.J., Funk B.A. and Newell, A.C.(1973). Stud.Appl.Math.,52, pp. 51-74. 10. Collinge I.R. and Ockendon,J.R.(1979). SIAMJ.Appl.Math.,37, pp.350-357. 11. Johnson D.A. (1986), private communication from Dr. Ockendon. 12. Communication from Professor Erneux, Northwestern University. 13. Ostiguy, G.L. and Evan-Iwanowski, R.M.(1982), ASME Journal of Mechanical Design, 104, pp.417-425. 14. Bluteau, C.(1984). Ecole Polytechnique, Montreal. 15. Ueda Y. (1980), Holmes, P.J.(ed.). SIAMJ. Phila. 311-322.

FIGURES:

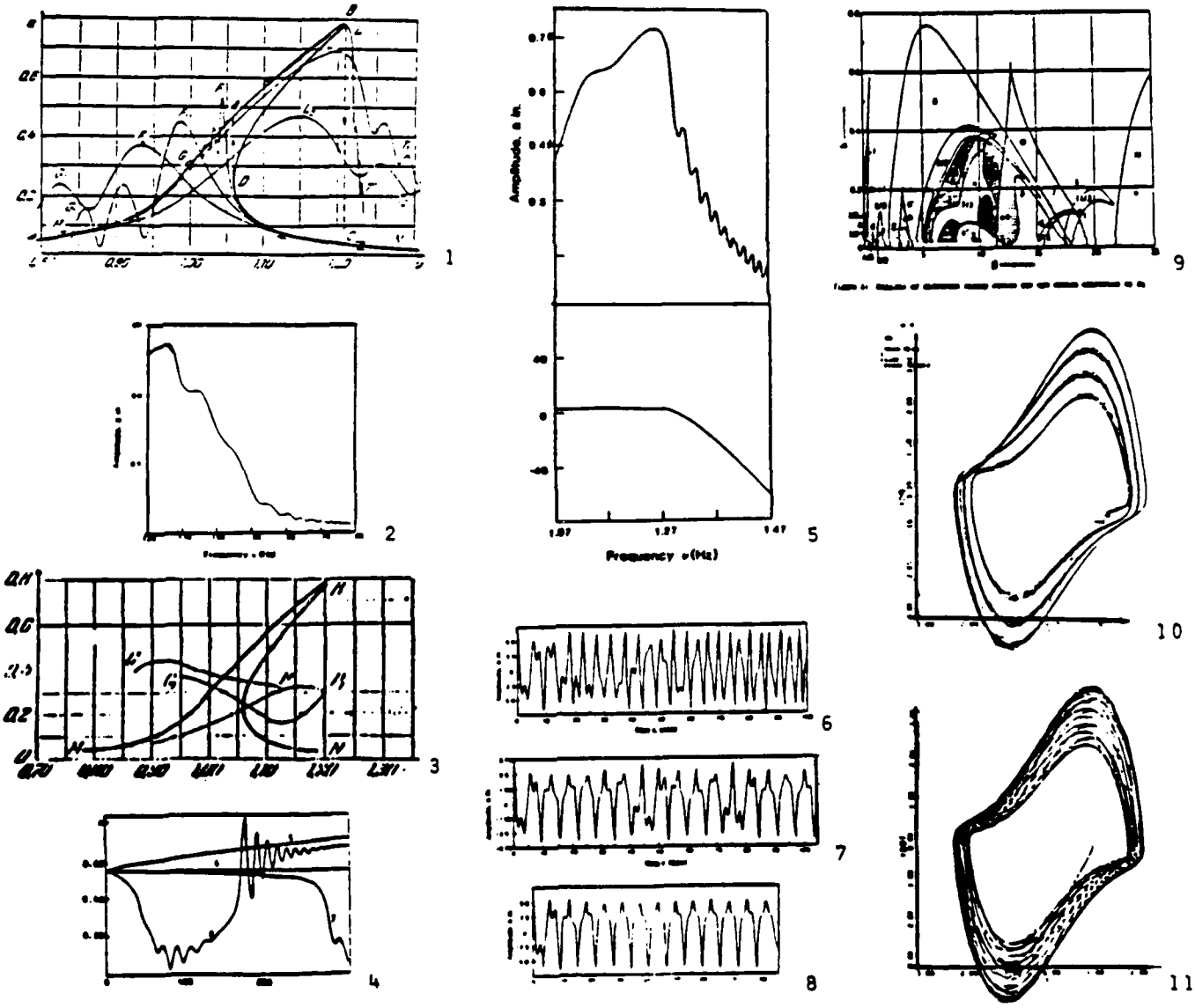

Figs. 1-9. Duffing Oscillator

Figs. 10,11. Relaxation Oscillation

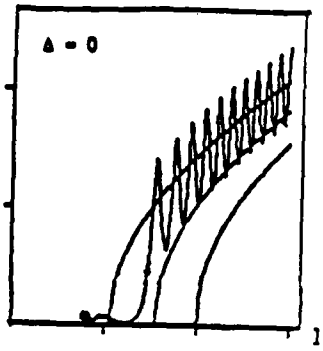

12

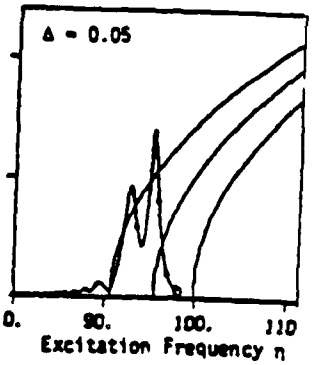

16

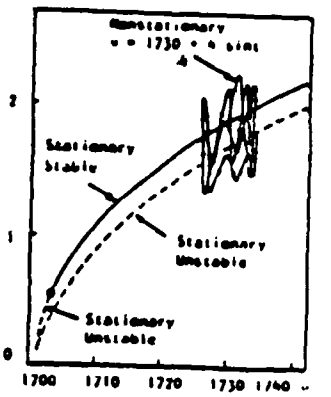

20

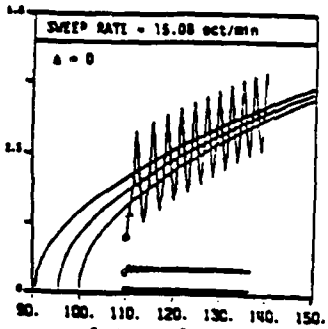

13

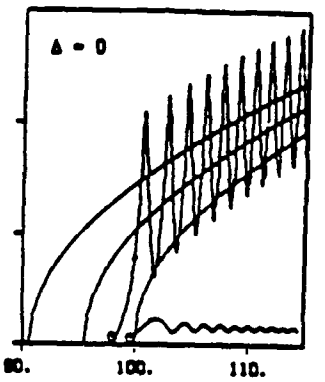

17

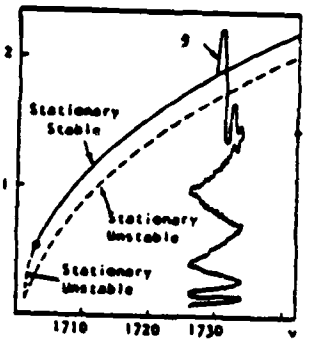

21

Fig. 5.15. Combination Resonance $\nu = 2\omega_2 + \omega_3$. Table 5.4.

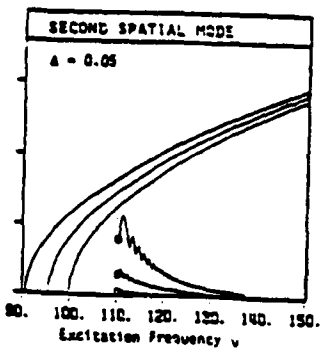

14

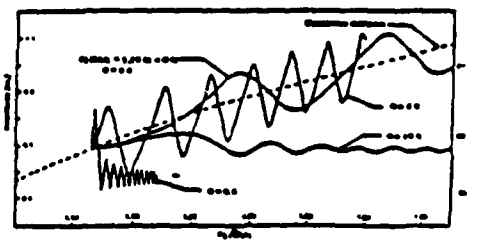

18

Fig. 3.2. Transition through resonance: effect of transition rate on resonance response.

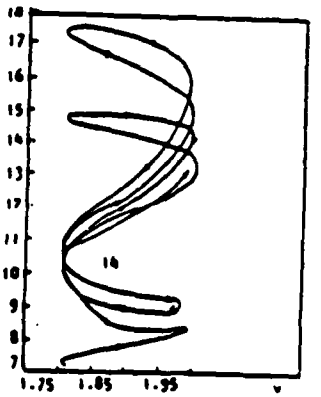

22

Fig. 4.10. Nonstationary Response. Table 4.1.

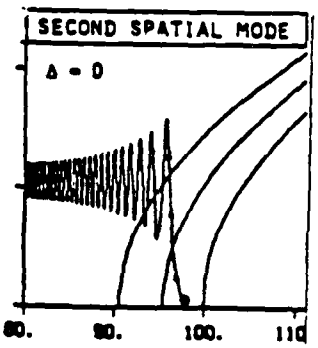

15

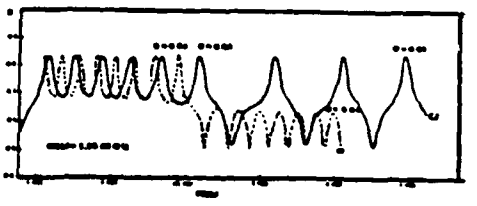

19

Fig. 3.4. ($\omega = \nu/2$) Parametric resonance: nonstationary response. Note the almost coincidence of two TtR responses (CR).

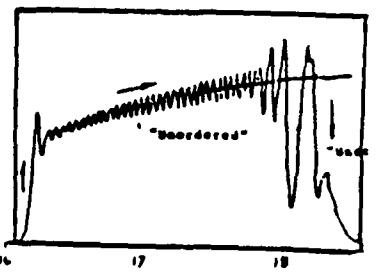

23

Figs. 12-23. Dynamic Stability

RESPONSE OF A SINGLE-DEGREE-OF-FREEDOM SYSTEM TO A NONSTATIONARY PARAMETRIC EXCITATION - THEORY AND EXPERIMENT

A. H. Nayfeh and H. L. Neal
Department of Engineering Science and Mechanics
Virginia Polytechnic Institute and State University
Blacksburg, VA 24061

In this paper, we examine the nonstationary response of a one-degree-of-freedom nonlinear system to a nonperiodic principal parametric excitation with varying frequency. We use the method of multiple scales to determine two ordinary differential equations governing the amplitude and phase of the nonstationary response. From these equations, we obtain the stationary responses and their stability. Next, the modulation equations are integrated on a digital computer using several different sweep rates and initial conditions. Then, we simulate the original differential equation on an analog computer using several sets of values for the parameters in the governing equation. Finally, we use a mechanical model to qualitatively verify the results.

The governing equations for the system under study are

$$\ddot{u} + \omega_0^2 u + 2\varepsilon\mu\dot{u} + \varepsilon\alpha u^3 + 2\varepsilon f\, u\, \cos\theta = 0 \tag{1}$$

$$\dot{\theta} = \Omega = 2\omega_0 + \varepsilon\sigma \tag{2}$$

Here, ω_0 is the natural frequency, μ is the damping coefficient, α is the coefficient of the cubic nonlinearity, f is a measure of the excitation amplitude, and the dots denote derivatives with respect to time. The parameter ε, which is much less than one, serves as a bookkeeping device in the method of multiple scales analysis. The excitation is nonperiodic because its frequency varies linearly with time. The frequency is varied by varying the detuning parameter, σ, according to

$$\sigma = \sigma_0 + r\varepsilon t \tag{3}$$

where r is the sweep rate. Because of the parametric excitation, we must include nonlinear terms in the governing equation. Otherwise, an analysis of the equation would predict a trivial response up to a critical value of excitation and an infinite response thereafter. The nonlinear terms can result from many sources, including large rotations of structural elements, nonlinear material behavior, or inertia from distributed or concentrated masses. An example of a nonlinear system with parametric excitation is a ship excited by a head or follower sea. A simpler example is an axially-excited beam with a concentrated mass at one end.

The response of such systems is nonstationary--it has changing amplitude and phase--due to the nonperiodic excitation. We examine the response when the excitation frequency is varied near the principal parametric resonant frequency. The situation where the excitation frequency is swept through the principal parametric resonant frequency is usually referred to as passage through resonance. Passage through resonance could occur, for example, when a motor that operates beyond the principal parametric resonant frequency is started up or shut down.

Using the method of multiple scales, we find that the nonstationary response of the system is given by

$$u = a\, \cos\left(\frac{1}{2}\Omega t - \gamma\right) + \ldots \tag{4}$$

$$a' = -\mu a - \frac{fa}{2\omega_0}\sin\gamma \tag{5}$$

$$\gamma' = \sigma - \frac{3\alpha}{4\omega_0} a^2 - \frac{f}{\omega_0} \cos \gamma \tag{6}$$

where the primes indicate derivatives with respect to the slow time scale $T_1 = \varepsilon t$.

We find the stationary responses to periodic excitations by setting σ = constant and $a' = \gamma' = 0$. There are three stationary solutions. The trivial solution a = 0, which exists for all values of σ, and it is stable as long as

$$f^2 < \omega_0^2(\sigma^2 + 4\mu^2) \tag{7}$$

There are two nontrivial stationary solutions; the larger solution is always stable, and the smaller solution is always unstable. The three solutions are shown in the $a - \sigma$ plane in Figure 1. The solid branches represent stable solutions whereas the broken lines represent unstable solutions.

Next, we digitally integrate the modulation equations for the nonstationary amplitude and phase. Integrating Eqs. (5) and (6) will give incorrect results when a is trivial, because we divided by a in deriving them. So we use their equivalent Cartesian form. Near-trivial initial conditions with magnitudes around 0.01 to 0.001 are used for the digital integration. These initial conditions, which represent the small disturbances from rest that act on the system, are used since using exactly trivial initial conditions would require very small integration steps to get equivalent results. The results (Figure 2) show five phenomena in which the nonstationary response differs from the stationary response. First, on forward sweeps the trivial response penetrates into the region where the stationary trivial response is unstable (Figure 2a). Second, the response amplitude grows and oscillates about the stable nontrivial stationary solution (Figure 2a). Third, the nonstationary response converges to the stable stationary response (Figure 2a). Fourth, on reverse sweeps, the nontrivial response lingers into the region where only the stationary trivial response exits (Figure 2b). Fifth, on reverse sweeps, the response rebounds to small amplitudes several times after initially becoming trivial (Figure 2b). These nonstationary phenomena are quantitatively changed by changing the sweep rate or the near-trivial initial conditions. We note that time increases from left to right in Figure 2a and from right to left in Figure 2b.

We also digitally integrate the original differential equation. With the same sweep rate and similar initial conditions, this integration agrees well with the integration of the modulation equations for small values of ε except for a small shifting of the solutions with respect to one another. This shift results from approximations involved in using the method of multiple scales and from using different measures of amplitude in the two integrations. The close agreement is shown in Figure 3.

Next, the original governing equation is simulated on an analog computer. Eight different sets of the parameters ω_0, μ, α, f, and ε are used in the simulations so that the effect of each parameter can be examined. Near-trivial initial conditions are again used as noise in the analog computer prevents the use of exactly trivial initial conditions. The results agree qualitatively with the digital integration results, and the five nonstationary phenomena are found to be affected by the values of the parameters ω_0, μ, α, f, and ε . Sample forward and a reverse sweeps are shown in Figures 4a and 4b, respectively.

Finally, a mechanical model governed by a differential equation somewhat more complex than the one studied here is used to qualitatively verify the previous results. Sweeps with four positive and five negative sweep rates are conducted, and the five nonstationary phenomena are again observed. The amplitude traces for a forward and reverse sweep are shown in Figures 5a and 5b, respectively.

Acknowledgement

This work was supported by the Office of Naval Research under Grant # N00014-83-K-0184, NR 4322753 and the Office of Scientific Research under Grant # AFOSR-86-0090.

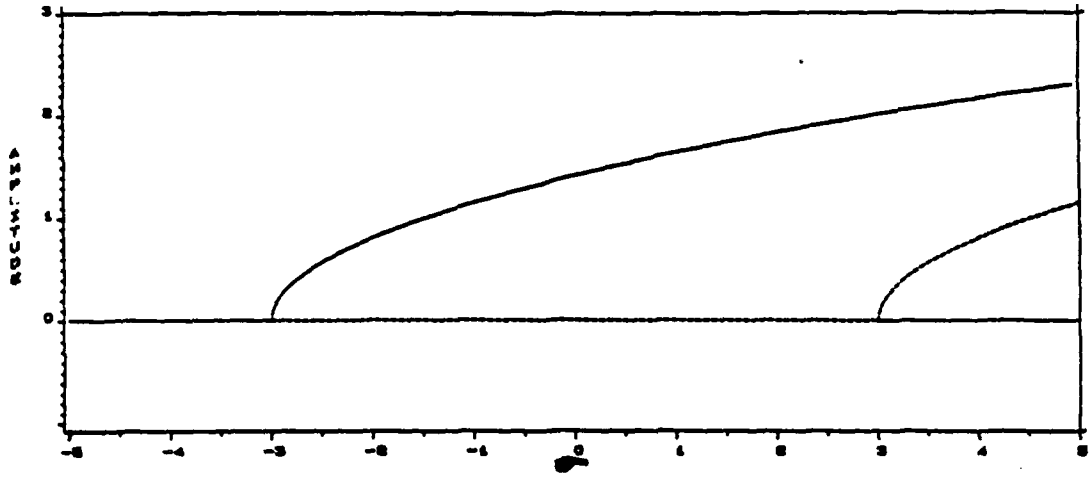

Figure 1. Stationary response curves. ———— stable
------- unstable

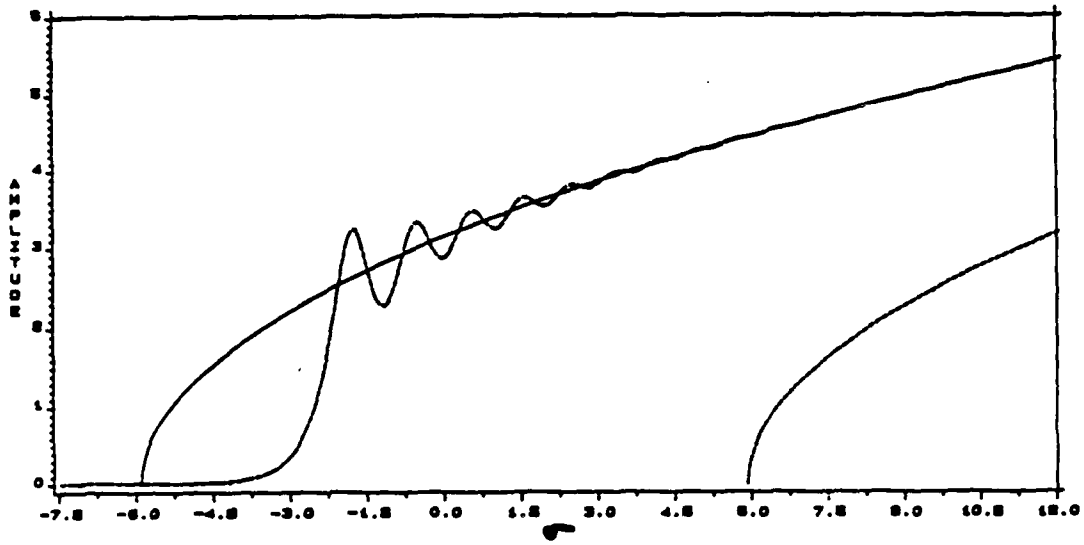

Figure 2a. Forward sweep with r = 1.0. ———— stationary-stable
-------- stationary-unstable —— - —nonstationary

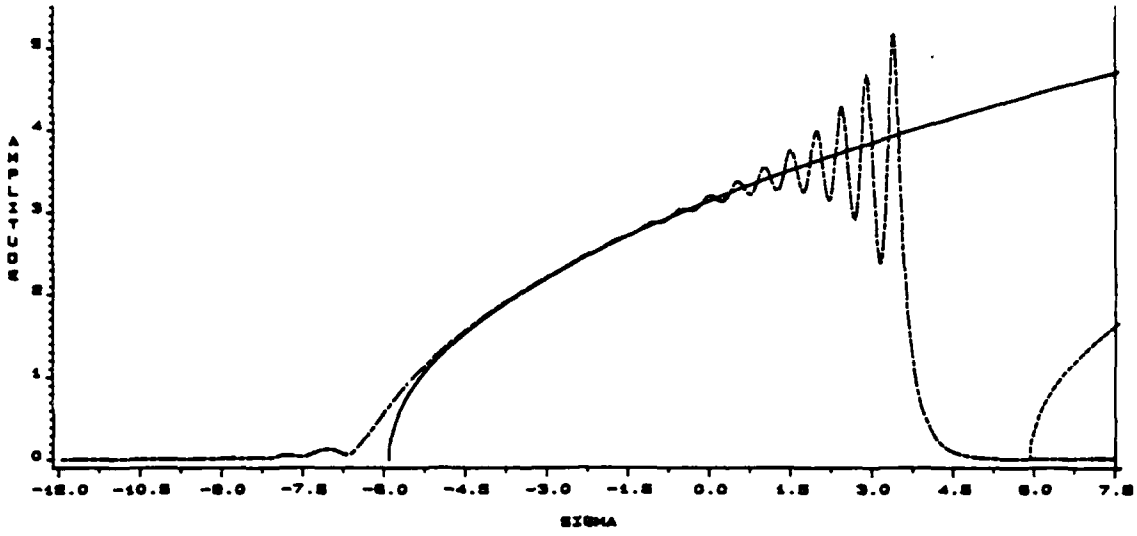

Figure 2b. Reverse sweep with r = -0.5. ———— stationary-stable
— - - - -stationary-unstable —— - ——nonstationary

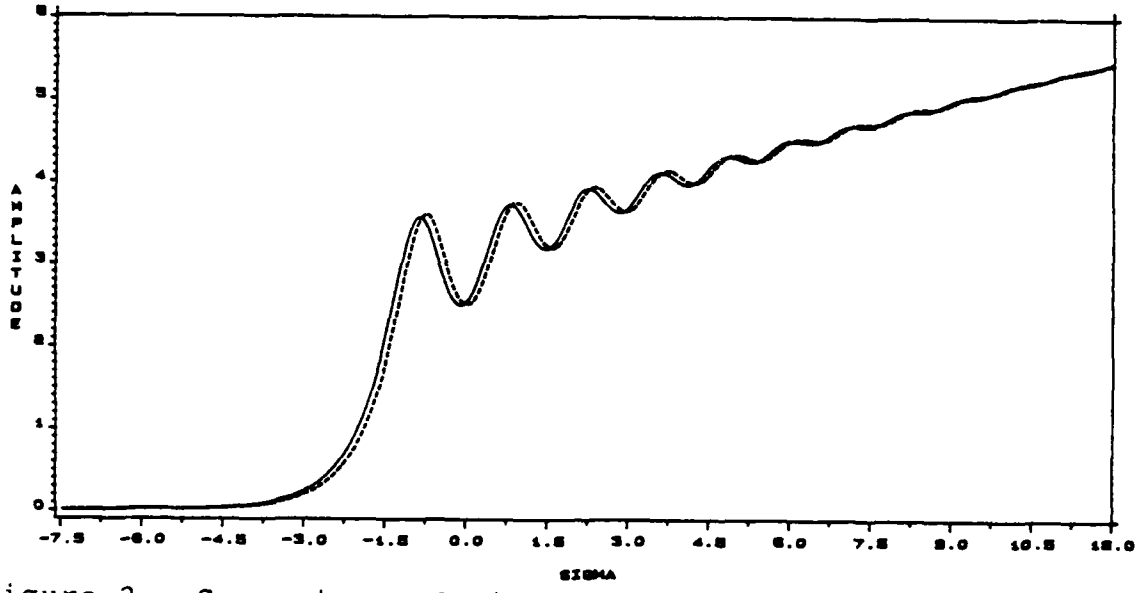

Figure 3. Comparison of digital integrations.———— method-of-multiple-scales — — — — original-differential-equation

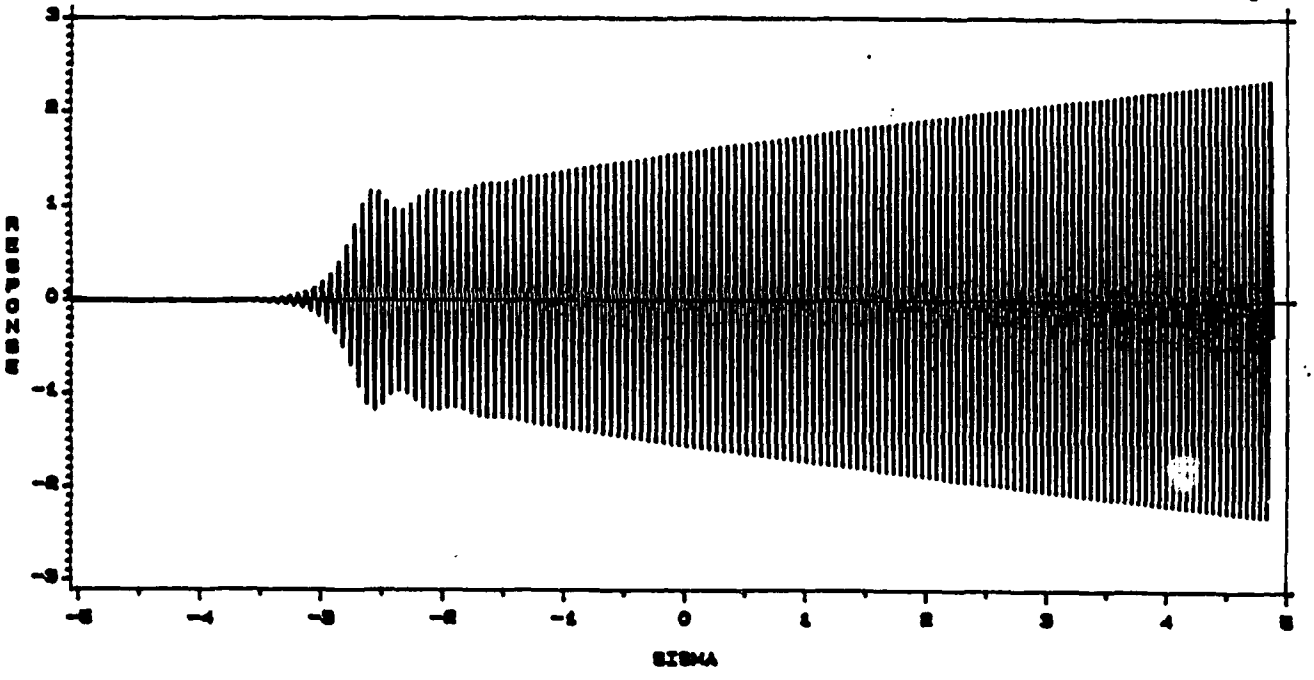

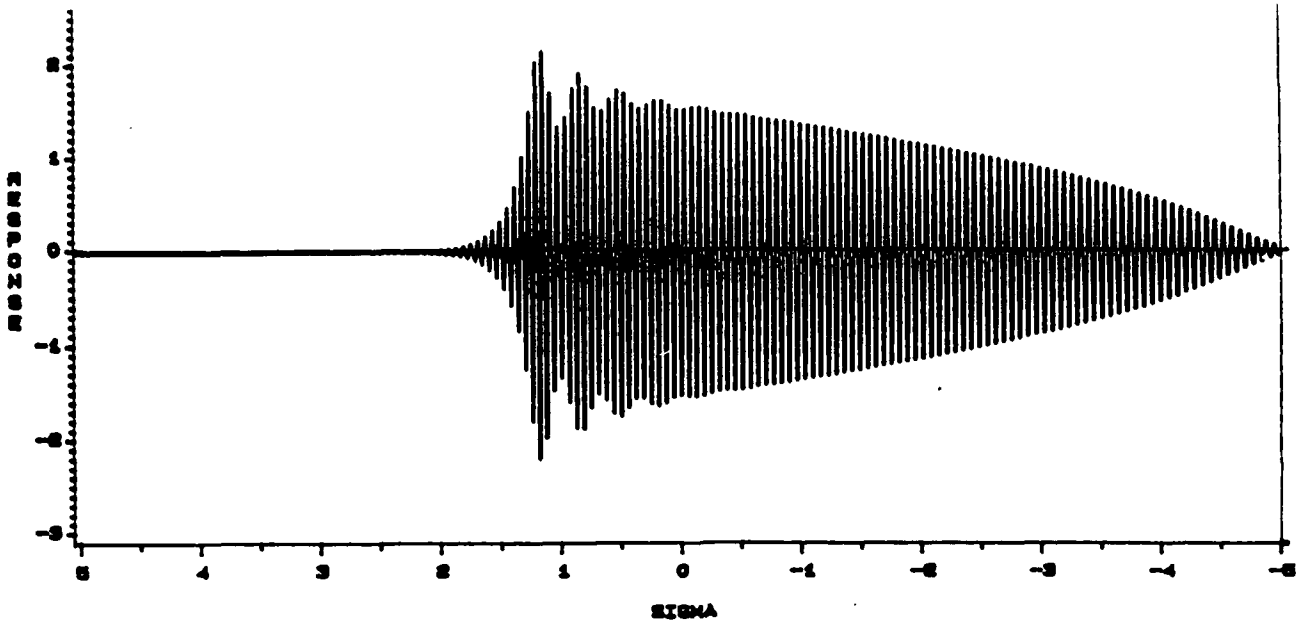

Figure 4b. Reverse sweep with r =-0.2 on analog computer.

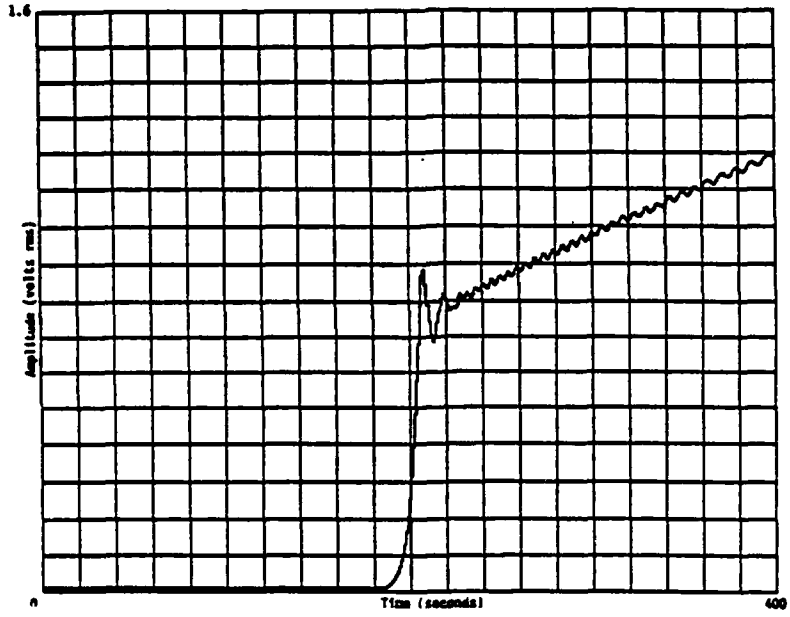

Figure 5a. Forward sweep using mechanical model.

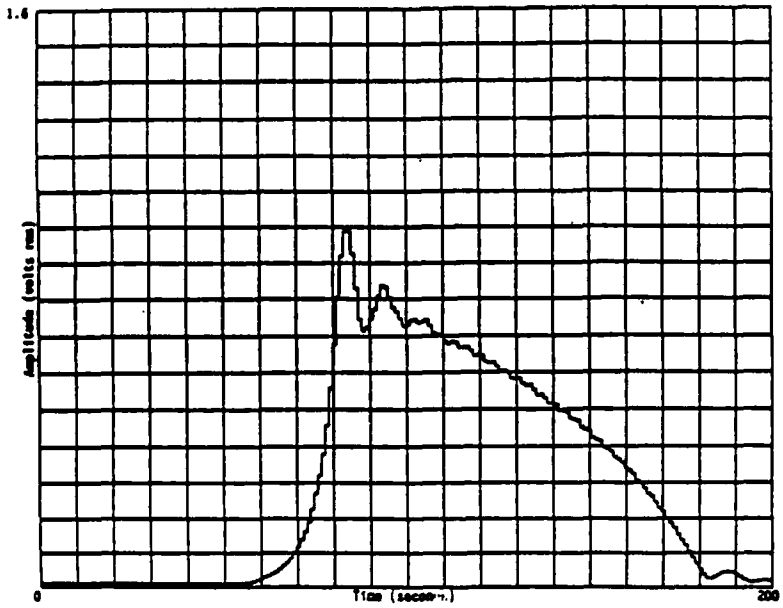

Figure 5b. Reverse sweep using mechanical model

ON THE PROBABILITY DENSITY FUNCTION OF THE RESPONSE OF NARROW-BAND EXCITED NONLINEAR OSCILLATORS

Qiang Liu and Huw G. Davies
Department of Mechanical Engineering
University of New Brunswick
P.O. Box 4400
Fredericton, New Brunswick, Canada E3B 5A3

Abstract

The probability density function (pdf) for the envelope of the response of a nonlinear oscillator driven by random narrow band noise is discussed. The nonlinearity treated involves general cubic terms and includes the Duffing and van der Poll oscillators as special cases. The input excitation envelope is Rayleigh distributed. The response envelope pdf is obtained for the limiting case of small excitation bandwidth. It includes cases of multiple valued response (Duffing) and limit cycles (van der Poll).

The research was supported by the Natural Sciences and Engineering Research Council of Canada.

Introduction

We consider in this paper the response of a nonlinear oscillator described by the equation

$$\ddot{y} + \beta\dot{y} + \omega_o^2 y + g(y,\dot{y}) = f \qquad (1)$$

where $f(t)$ is a narrow band random excitation, and $g(y,\dot{y})$ is a general cubic nonlinearity.

$$g(y,\dot{y}) = \mu_1\dot{y}y^2 + \mu_2\dot{y}^2y + \mu_3\dot{y}^3 + \mu_4 y^3 \ . \qquad (2)$$

The excitation is described by

$$f = F_s \sin\omega_f t + F_c \cos\omega_f t \qquad (3)$$

$$\dot{F}_c = (\frac{\gamma}{2})^{\frac{1}{2}} w_c - \frac{\gamma}{2} F_c \qquad (4)$$

$$\dot{F}_s = (\frac{\gamma}{2})^{\frac{1}{2}} w_s - \frac{\gamma}{2} F_s \qquad (5)$$

where w_c and w_s are independent gaussian white noise sources with spectrum level S_o. f has bandwidth γ at excitation frequency ω_f.

Now if f in (1) is white noise the stationary two dimensional pdf $p(y,\dot{y})$ can be obtained for certain forms of $g(y,\dot{y})$. In the present narrow band case, although the Fokker Planck equation for the four dimensional pdf $p(y,\dot{y},F_c,F_s)$ is easily obtained, we are not aware of solutions of this equation for any form of $g(y,\dot{y})$. In what follows, we first obtain the time dependent envelope equations corresponding to equations (1), (4) and (5) using the approach of Rajan and Davies [1]. A simplified form of these envelope equations is then used to find the pdf $p(\sigma, \sigma_f)$ where σ and σ_f are the response and excitation envelopes, respectively. Numerical simulations are used to corroborate the analytic work.

Envelope equations

We start by making the exact transformation (see, for example, Roberts and Spanos [2])

$$y = x \cos \omega_f t + z \sin \omega_f t \tag{6}$$

$$\dot{y} = -\omega_f x \sin \omega_f t + \omega_f z \cos \omega_f t \tag{7}$$

Equations (6) and (7) are substituted into (1), (7) being used to evaluate $\ddot{y}$, and two separate equations obtained for $\dot{x}$ and $\dot{z}$. These equations are averaged (over one period $2\pi/\omega_f$) as in [2] and then squared and combined with (4) and (5) as in [1]. After some algebra one finds the results

$$\dot{\sigma}^2 = -\beta_e \sigma^2 + P/2\omega_f \tag{8}$$

$$\dot{P} = -(\gamma + \beta_e) P/2 + \delta_e Q + \sigma_f^2/\omega_f \tag{9}$$

$$\dot{Q} = -(\gamma + \beta_e) Q/2 - \delta_e P \tag{10}$$

where $\sigma^2 = (x^2 + z^2)/2$ (11)

$$\sigma_f^2 = (F_c^2 + F_s^2)/2 \tag{12}$$

$$P = F_c z - F_s x \tag{13}$$

$$Q = F_c x + F_s z \tag{14}$$

$$\beta_e = \beta + \mu_1 \sigma^2/2 + 3\mu_3 \omega_f^2 \sigma^2/2 \tag{15}$$

$$\delta_e = (\omega_f^2 - \omega_o^2 - \mu_2 \omega_f^2 \sigma^2/2 - 3\mu_4 \sigma^2/2)/2\omega_f \tag{16}$$

It is clear that the multiple time scale approach of Nayfeh and Mook [3] instead of the averaging of [2] will yield the same results. β_e and δ_e represent equivalent damping and frequency difference, respectively. The equations (8) to (16) reduce to those of [1] for the case $\mu_1 = \mu_2 = \mu_3 = 0$.

Equations (8) to (10) describe a third order system for output σ^2 with slowly varying random input σ_f^2. We are still dealing with

a four dimensional pdf, and again have not found a solution. Instead we approximate (8) to (10) for the case of very small γ. The response envelop can exhibit multiple values, and a jump phenomenon from one pseudo stable level to another. Except for transients associated with the jumps, however, we are dealing with a slowly varying process that can be described by just the particular integral component of (8) to (10). In combining (8) to (10) we are thus justified in assuming, for example, that $\dot{\sigma}^2 = \sigma^2\, 0(\gamma)$, so that second and third order derivatives and products of first and higher derivatives may be neglected. The resulting first order equation from (8) to (10) is

$$A_1\dot{\sigma}^2 + \beta_e A_2\sigma^2 = (\dot{\sigma}_f^2 + (\gamma + \beta_e)\,\sigma_f^2/2)/2\omega_f^2 \tag{17}$$

where

$$A_1(\sigma^2,\sigma_f^2) = \delta_e^2 + 5\,\beta_e^2/4 + 3\beta_e D_1\,\sigma^2/2$$

$$- \beta_e^2 D_2\sigma^2/(2\delta_e) + D_2\sigma_f^2/(2\omega_f^2\delta_e)$$

$$\beta_e A_2(\sigma^2) = \beta_e\,(\delta_e^2 + \beta_e^2/4 + \gamma\beta_e/2)$$

$$D_2 = \dot{\delta}_e/\dot{\sigma}^2 \quad , \quad D_1 = \dot{\beta}_e/\dot{\sigma}^2$$

In order to describe the excitation we return to (4) and (5) and use the stochastic averaging method of [2]. Average values of $w_c F_c$ and $w_s F_s$ are approximated by mean and fluctuating parts. We thus obtain

$$\dot{\sigma}_F^2 = \gamma(2\pi S_o - \sigma_F^2) + (4\pi\gamma S_o\,\sigma_F^2)^{1/2}\; G(t) \tag{18}$$

where $\sigma_F^2 = 2\sigma_f^2$ and $G(t)$ is unit amplitude white noise. We note that the pdf $p(\sigma_F^2)$ obtained from (18) is exponential, so that $p(\sigma_F)$ is Rayleigh as expected. Finally we combine (17) and (18) to give

$$\dot{\sigma}^2 = f_1(\sigma^2,\, \sigma_F^2) + (4\pi S_o\gamma\sigma_F^2)^{1/2}\, G(t)/(4\omega_f^2 A_1) \tag{19}$$

where

$$f_1 = \frac{-A_2\beta_e\sigma^2}{A_1} + \frac{\pi S_o\gamma}{2\omega_f^2 A_1} + \frac{(\beta_e-\gamma)\sigma_F^2}{8\omega_f^2 A_1}\,.$$

Equations (18) and (19) are two nonlinear state equations for the excitation and response envelopes with unit amplitude white noise as the basic input.

Probability density function

The stationary form of the Fokker Planck equation for $p(\sigma^2,\sigma_F^2)$ is easily written. We assume that for small γ p can be written $p = p_o + \gamma p_1 + 0(\gamma^2)$. To zero order γ the Fokker Planck equation reduces to

$$\frac{\partial}{\partial \sigma^2} \{f_1(\sigma^2,\sigma_F^2), p_o(\sigma^2,\sigma_F^2)\} = 0 \ . \tag{20}$$

We write $p_o(\sigma^2,\sigma_F^2) = p(\sigma_F^2)\ p_o(\sigma^2|\sigma_F^2)$. The appropriate solution of (20) is

$$p_o(\sigma^2|\sigma_F^2) = (\text{constant})\ \ \delta(f_1(\sigma^2, \sigma_F^2)) \tag{21}$$

The required pdf can then be obtained in the form

$$p_o(\sigma^2) = (\text{constant}) \int_o^\infty \exp\left(-\frac{\sigma_F^2}{2\pi So}\right)\ \delta\left\{\frac{\beta_e}{A_1}(-A_2\sigma^2 + \sigma_F^2/8\omega_f^2)\right\} d\sigma_F^2 \tag{22}$$

For the Duffing case, which is compared with numerical simulation in the next section, integration of (22) yields (transforming $p_c(\sigma^2)$ to $p_o(\sigma)$)

$$p_o(\sigma) = (\text{constant})\ \sigma\left|\delta_e(\delta_e - 3\mu_4\ \sigma^2/2\omega_f) + 5\beta^2/4\right|$$

$$* \exp\left(-\frac{4\omega_f^2}{\pi S_o}(\delta_e^2 + \beta^2/4)^2\ \sigma^2\right) \ . \tag{23}$$

This form reduces to the correct Rayleigh distribution in the linear case $\mu_4 = 0$. The form (23) however, shows two local maxima (a bimodal distribution) in cases where the response envelope is multivalued.

For the van der Poll case, with $\mu_2 = \mu_3 = \mu_4 = 0$ and $\mu_1 = -\beta$, we have $\beta_e = \beta(1 - \sigma^2/2)$. The pdf (22) in this case exhibits a delta function at the limit cycle $\sigma^2 = 2$.

Numerical simulation

Numerical results are shown in the figures for the Duffing oscillator. Figures 1A and 1B show the time histories of the response envelope; 1A is obtained from a direct integration of (1) to (5), 1B shows that the approximate equations (18) and (19) are adequate for this very low γ. Figures 2A,B,C are the pdf $p(\sigma)$; 2A obtained from the time history 1A, 2B from 1B, and 2C from the analytic result (23). The multivalued nature of the response shows up clearly in the time histories and the pdf.

References

1. S. Rajan and H.G. Davies, J. Sound Vibn. accepted for publication (1987).

2. J.B. Roberts and P.D. Spanos, Int. J. Nonlin. Mech. 21 (1986).

3. A.H. Nayfeh and D.T. Mook, Nonlinear Oscillations, Wiley (1979).

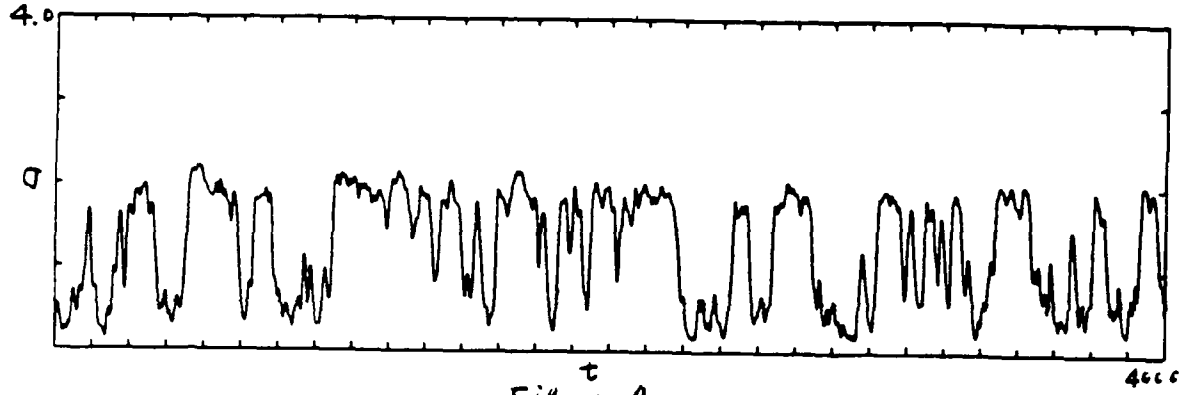

Fig. 1.A.

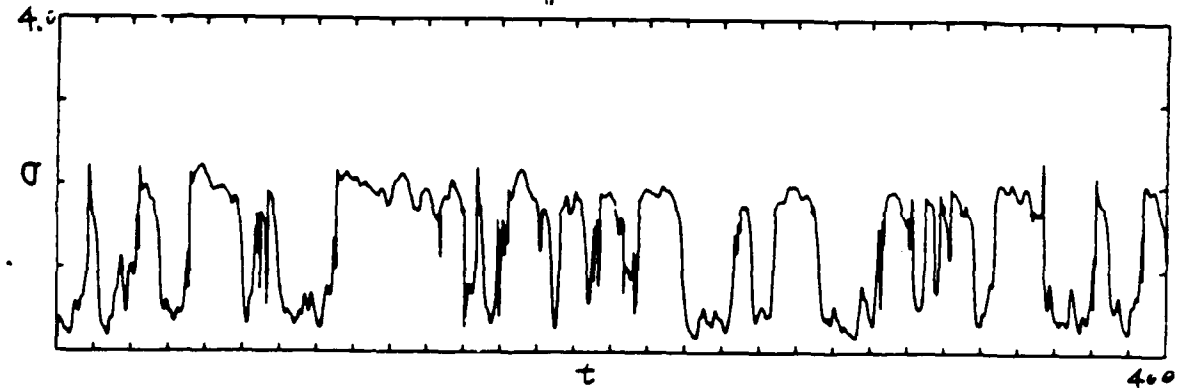

Fig. 1.B.

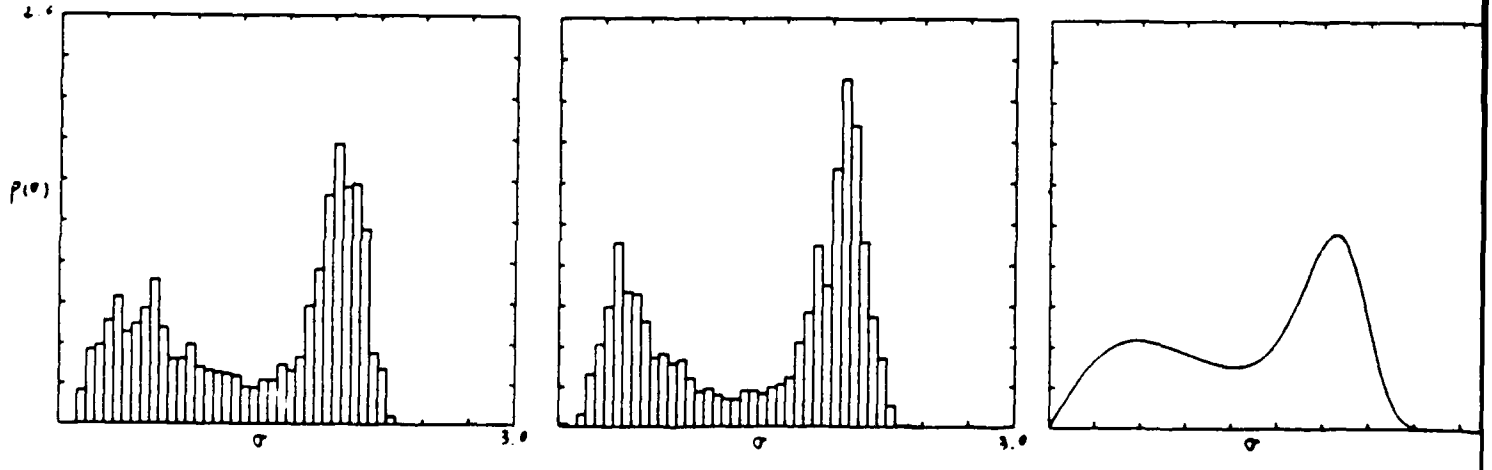

WIDE BAND RANDOM EXCITATION OF A THREE-DEGREE-OF-FREEDOM SYSTEM WITH PRINCIPAL INTERNAL RESONANCES

R. A. Ibrahim and W. Li
Wayne State University
Department of Mechanical Engineering
Detroit, MI 48098

Introduction

This investigation is a continuation of previous work [1,2] on the random excitation of a three-degree-of-freedom structural model whose normal coordinates are nonlinearly coupled. The modal coupling is due to inertia quadratic nonlinearity and results in four different internal resonance conditions. One of these conditions involves the nonlinear interaction of three modes, while the other three give rise to autoparametric interaction between two modes. The three internal resonance conditions are of principal type, ($\omega_i = 2\omega_j$, where ω_i and ω_j are two normal mode frequencies of the system), and have different degrees of response dynamic characteristics. The random response corresponding to the three cases is determined by using the Fokker-Planck equation approach to generate a general differential equation for the response joint moments. This equation is found to constitute an infinite coupled set of differential equations which are closed via a non-Gaussian closure scheme. The closure scheme is based on the properties of higher order response cumulants. The analytical derivations of the equations of motion in the Markov vector form and the response moment equations are performed by using the computer manipulation software MACSYMA.

The linear modal analysis of the system reveals four possible internal conditions. These are:

i. $\omega_3 = \omega_1 + \omega_2$

ii. $\omega_2 = 2\,\omega_1$

iii. $\omega_2 = 2\,\omega_1$

iv. $\omega_2 = 2\,\omega_1$

The system response corresponding to combination internal resonance (i) is determined in references [1,2] by using Gaussian and non-Gaussian closure schemes. The Gaussian closure solution predicts nonlinear interaction between second and third modes at the internal detuning parameter $r=\omega_3/(\omega_1+\omega_2)$

= 1.18. This unexpected result is scrutinized and it is found that at r = 1.18 the second and third modes are in exact internal tuning, i.e. $\omega_3=2\omega_2$. The non-Gaussian closure, on the other hand, successfully predicts nonlinear three-mode interaction in the neighborhood of r=1.0. The autoparametric interaction occurs among the three modes in such a way that the mean square response of the first two modes are always greater than the linear solution, while it is less for the third mode. A new feature of considerable interest is the contrast in the form of the mean square response curves above the exact detuning ratio r>1.0 for a certain combination of system parameters and excitation level. This is indicated by multiple solutions over a finite portion of internal detuning parameter. The well known saturation phenomenon [3] which usually occurs in deterministic systems with quadratic nonlinearity is not predicted because the excitation is random and includes a wide range of frequencies which always excite the system modes.

The present analysis is extended to analyze the system response in the vicinity the three principal internal resonance conditions (ii) through (iv). This means that the analysis is restricted to autoparametric interaction between two normal modes in a three-degree-of-freedom system. If Gaussian closure is applied one should generate 14 differential equations in the first and second order response moments. On the other hand, if non-Gaussian closure is used one should generate 69 moment equations in the first through fourth order moments. The solutions of these two sets of moment equations are obtained for each principal internal resonance condition.

First and Second Modes Interaction: $\omega_2 = 2\omega_1$

The Gaussian closure solution predicts both stationary and nonstationary responses depending on the value of the internal detuning parameter $r = \omega_2/\omega_1$. The response is stationary when r is well remote from the exact internal tuning r=2. The non-Gaussian closure solution yields a stationary response for all value of r. The time history records display the interaction in a form of energy exchange between the two modes during the transient period. The basic characteristics of the mean square responses occur in such way that the motion of the first mode acts as a vibration absorber to the second mode. It is observed that the nonlinear interaction takes place over a narrow band of internal detuning parameter r. Contrary to the first case of combination internal resonance the nonlinear interaction is less sensitive to the external excitation level. In other words, the interaction is only manifested under relatively higher excitation spectral density level, $D/2\zeta_2$

First and Third Modes Interaction: $\omega_3 = 2\omega_1$

Unlike the previous case, the Gaussian closure fails to predict any nonlinear interaction and all solutions are identical to the linear response for all possible values of system parameters, excitation spectral density levels and initial conditions. The Gaussian closure scheme, on the other hand, gives results which are different from the linear response and involve nonlinear interaction only for excitation spectral density $D/2\zeta_3$ level greater than 40. Below that level the response is completely linear.

Second and Third Modes Interaction: $\omega_3 = 2\omega_2$

In the neighborhood of the exact internal resonance the Gaussian closure scheme gives a quasi-stationary response. The nonlinear interaction is found

to take place over a small range of $r = 2 \pm O(\varepsilon)$. The non-Gaussian closure solution shows fluctuations in a form of energy exchange between the two modes during the transient period. These fluctuations are completely vanished during the steady state response. The steady state is also determined by setting the right-hand sides of the closed 69 equations. The resulting nonlinear algebraic equations are solved numerically by using the IMSL subroutine ZSPOW. The results are determined as function of the internal detuning parameter r and it is found that the region of autoparametric interaction becomes more wider as the nonlinear coupling parameter increases.

Conclusions

The random response of a three-degree-of-freedom structural model is determined in the neighborhood of three different principal internal resonance conditions. The response statistics are sensitive to small levels of the excitation spectral density when the third normal mode frequency is twice the second normal mode frequency. However, the autoparametric interaction is only sensitive to a relatively high excitation level when the first and second or the first and third modes are internally tuned. The stochastic interaction of the three cases is characterized by irregular energy exchange between the interacted modes.

Acknowledgment

This research is supported by a grant from the Air Force Office of Scientific Research under grant no. AFOSR 85-0008. Dr. Anthony K. Amos is the program manager.

References

1. Ibrahim, R. A. and Hedayati, Z., "Stochastic Modal Interaction in Linear and Nonlinear Aeroelastic Structures," Probabilistic Engineering Mechanics 1(4), pp. 182-191, 1986.

2. Ibrahim, R. A. and Li, W., "Structural Modal Interaction with Combination Internal Resonance under Wide Band Random Excitation," Journal of Sound and Vibration 123(2), 1988.

3. Nayfeh, A. H. and Mook, D. T., Nonlinear Oscillations, Wiley-Interscience, New York, 1979.

A GENERALIZED METHOD OF AVERAGING FOR DETERMINING THE RESPONSE OF NONLINEAR SYSTEMS TO RANDOM EXCITATIONS

by
Ali H. Nayfeh and Samir J. Serhan
Department of Engineering Science and Mechanics
Virginia Polytechnic Institute and State University
Blacksburg, VA 24061

In this paper a generalized method of equivalent linearization is developed for the determination of the response of systems with cubic nonlinearities to random excitations. The method explains some observed nonlinear phenomena such as non-Gaussian responses, broadening effects, and shift of the resonant frequency. The method is illustrated by studying the response of the Duffing oscillator to a Gaussian white noise.

Problem Formulation

We consider a second-order nonlinear system with stochastic excitation described by the equation

$$\ddot{u} + \omega_o^2 u + 2\varepsilon\mu\dot{u} + \varepsilon\alpha u^3 = F(t) \tag{1}$$

where ω_o is the linear natural frequency, μ and α are constants, ε is a small but finite constant, and F is a zero-mean Gaussian random excitation with a white power spectral density S_o of $O(\varepsilon)$.

The method of equivalent linearization is based on replacing the nonlinear equation (1) by an equivalent linear equation whose solution furnishes an approximate solution to Eq. (1); that is,

$$\ddot{u} + \omega_e^2 u + \mu_e \dot{u} = F(t) \tag{2}$$

The equivalent stiffness ω_e^2 and damping μ_e parameters can be determined by minimizing the mean-square value of the difference between Eqs. (1) and (2). Equation (2) shows a linear relation between the statistics of the excitation and those of the response. The equivalent linear model given by Eq. (2) fails to account for many of the phenomena peculiar to nonlinear systems. These include non-Gaussian responses, multi-valued responses, jumps, modal frequency shifts, broadening effects, superharmonic, subharmonic, ultrasubharmonic and combination resonances, period-multiplying bifurcations and chaos. The proposed method accounts for some of these phenomena.

In investigating the response of panels to acoustic loading, test results (1,5,6) demonstrated the broadening of the response curves and the increase of the resonant frequency of the fundamental mode at high noise levels. To explain these phenomena, Mei and Prasad (2) had to include nonlinear damping terms in Eq. (1). Using the proposed method, we can explain the experimental observations without the resort to nonlinear damping.

Proposed Method

The random excitation in Eq. (1) is divided into two uncorrelated parts as $F = f_1 + f_2$. The first part is f_1 whose spectral density is around ω_o. The second part is f_2 whose spectral density is away from ω_o. Moreover, we express the solution of Eq. (1) as

$$u = x + v \tag{3}$$

where

$$\ddot{x} + \omega_o^2 x + 2\varepsilon\mu\dot{x} = f_2(t) \tag{4}$$

Substituting Eqs. (3) into Eq. (1) and using Eq. (4), we obtain the following equation governing v:

$$\ddot{v} + \omega_o^2 v + 2\varepsilon\mu\dot{v} + 3\varepsilon\alpha x^2 v + 3\varepsilon\alpha x v^2 + \varepsilon\alpha v^3 + \varepsilon\alpha x^3 = f_1(t) \tag{5}$$

Next, we replace Eq. (5) with the equivalent linear equation

$$\ddot{v} + \omega_e^2 v + 2\varepsilon\mu\dot{v} = g(t) \tag{6}$$

where

$$\omega_e^2 = \omega_o^2 + \langle 3\varepsilon\alpha x^2 v^2 + 3\varepsilon\alpha x v^3 + \varepsilon\alpha v^4 \rangle / \langle v^2 \rangle \tag{7}$$

$$g = f_1 - \varepsilon\alpha x^3 \tag{8}$$

The presence of $\varepsilon\alpha x^3$ in the excitation g provides the non-Gaussian feature of the nonlinear response u. The term $\langle x^2 v^2 \rangle$ accounts for both an increase in the linear frequency and ultrasubharmonics, the term $\langle xv^3 \rangle$ accounts for the subharmonic of order one-third, and the term x^3 in g accounts for the superharmonic resonance and all combination resonances. If we neglect the subharmonic and ultrasubharmonic resonances, Eq. (7) becomes

$$\omega_e^2 = \omega_o^2 + 3\varepsilon\alpha\langle x^2 \rangle + \varepsilon\alpha\langle v^4 \rangle / \langle v^2 \rangle \tag{9}$$

If we assume that v is psuedo-sinusoidal, then $\langle v^4 \rangle = \frac{3}{2} \langle v^2 \rangle^2$ and Eq. (9) becomes

$$\omega_e^2 = \omega_o^2 + 3\varepsilon\alpha\langle x^2 \rangle + \frac{3}{2}\varepsilon\alpha\langle v^2 \rangle \tag{10}$$

Using Eq. (4), the mean-square value of x can be written as

$$\langle x^2 \rangle = \frac{S_o}{4\omega_o^2\omega_d}\left[\ln \frac{(\omega_1+\omega_d)^2+\varepsilon^2\mu^2}{(\omega_1-\omega_d)^2+\varepsilon^2\mu^2} - \ln \frac{(\omega_c-\omega_d)^2+\varepsilon^2\mu^2}{(\omega_2-\omega_d)^2+\varepsilon^2\mu^2} + \ln \frac{(\omega_c+\omega_d)^2+\varepsilon^2\mu^2}{(\omega_2+\omega_d)^2+\varepsilon^2\mu^2}\right]$$

$$+ \frac{S_o}{2\varepsilon\mu\omega_o^2}\left[\tan^{-1}\frac{\omega_1-\omega_d}{\varepsilon\mu} + \tan^{-1}\frac{\omega_1+\omega_d}{\varepsilon\mu} + \tan^{-1}\frac{\omega_c-\omega_d}{\varepsilon\mu} + \tan^{-1}\frac{\omega_c+\omega_d}{\varepsilon\mu}\right.$$

$$\left. - \tan^{-1}\frac{\omega_2+\omega_d}{\varepsilon\mu}\right] \qquad (11)$$

where ω_c is the cutoff frequency and

$$\omega_1 = \omega_o - \frac{1}{2}\beta,\ \omega_2 = \omega_o + \frac{1}{2}\beta, \quad \text{and} \quad \omega_d = (\omega_o^2 - \varepsilon^2\mu^2)^{\frac{1}{2}} \qquad (12)$$

Here, β is the bandwidth of the narrow-band process f_1.

As a result, the nonlinear equation (1) is replaced by two equivalent linear equations (4) and (5) and the mean-square response has the form

$$\langle u^2 \rangle = \frac{\pi S_o[2\varepsilon\mu(\omega_e^2+\beta^2)+\beta(\omega_o^2+4\varepsilon^2\mu^2)]}{2\varepsilon\mu\omega_o^2\beta\omega_e^2[(\omega_o^2-\omega_e^2)^2+(2\varepsilon\mu+\beta)(2\varepsilon\mu\omega_o^2+\beta\omega_e^2)]} + \frac{\varepsilon\pi\alpha S x^3(\omega_e^2)}{2\mu\omega_e^2} \qquad (13)$$

where ω_e^2 is given by Eq. (7) and

$$S_{x^3}(\omega_e^2) = 9\langle x^2 \rangle S_x(\omega_e^2) + 6\int_{-\infty}^{\infty}\int_{-\infty}^{\infty} S_x(r_1)S_x(r_2)S_x(\omega_e^2 - r_1 - r_2)dr_1dr_2 \qquad (14)$$

Here, $S_x(\omega)$ is the output spectral density of the linear response x in Eq. (4)

$$S_x(\omega) = \frac{S_{f2}(\omega)}{(\omega_o^2-\omega^2)^2+4\varepsilon^2\mu^2\omega^2} \qquad (15)$$

Conclusions

A method is presented for determining the response of nonlinear systems to random excitations. The original nonlinear governing equation is replaced by two equivalent linear equations. The method provides some means to describe the non-Gaussian feature of the nonlinear response and preserves its wide-band character. The interaction and feedback between the nonlinearity and excitation creates nonlinear resonances. These lead to a linear shift in the frequency and an adjustment of the strength of the primary excitation. The former is responsible for the increase in the modal frequency and the latter contributes to the experimentally observed broadening of the response curves.

Acknowledgement

This work was supported by the Air Force Office of Scientific Research under Grant # AFOSR-86-0090 and Grant # F49620-87-C-0088.

References

1. C. MEI and K. R. WENTZ May 1982 23rd Structures, Structural Dynamics and Materials Conference, New Orleans, LA 514-520. Analytical and experimental nonlinear response of rectangular panels to acoustic excitation.

2. C. MEI and C. B. PRASAD 1986 27th Structures, Structural Dynamics and Materials Conference 644-653. Effects of nonlinear damping on random response of beams to acoustic loading.

3. A. H. NAYFEH 1973 Perturbation Methods. New York: Wiley.

4. A. H. NAYFEH 1981 Introduction to Perturbation Techniques. New York: Wiley.

5. J. SOOVERE 1981 J. Aircraft 19, 304-310. Sonic fatigue testing of an advanced composite aileron.

6. R. G. WHITE Oct. 1978 Composites 251-258. Comparison of the statistical properties of the aluminum alloy and CFRP plates to acoustic excitation.

DYNAMIC SNAP-BUCKLING UNDER STOCHASTIC LOADS

S. T. Ariaratnam and Wei-Chau Xie,
Solid Mechanics Division,
Faculty of Engineering,
University of Waterloo,
Waterloo, Ontario, Canada, N2L 3G1.

ABSTRACT

In shallow curved structures such as arches and shells under symmetrically distributed loads, usually only the symmetric mode of deformation is excited. However, due to the inherent nonlinear coupling, the antisymmetric mode can also be excited under certain conditions and become unstable leading to snap-buckling of the structure.

We consider the plane motion of a simply supported shallow arch of uniform cross-section whose axis in the unloaded configuration has a form $w_0(x)$, on which the dynamic deflection $w(x,t)$ is superposed. There is a lateral loading $p(x,t)$ as shown in Figure 1. The problem to be considered here is that of a low, half-sine, pinned arch loaded stochastically by a half-sine spatially distributed load. The initial shape is taken in the form

$$w_0(x) = q_0 \sin\frac{\pi x}{L},$$

where q_0 is the initial rise parameter. The expression for the loading, directed upward, is given by

$$p(x,t) = -P(t)\sin\frac{\pi x}{L},$$

where $P(t)$ is a random process with mean value $E[P(t)] = P_0 \geq 0$. The dynamic deflection may be represented approximately by

$$w(x,t) = q_1 \sin\frac{\pi x}{L} + q_2 \sin\frac{2\pi x}{L},$$

where q_1, q_2 are the amplitudes of the symmetric and the antisymmetric modes. Then, the equations of motion are given by

$$\mu\ddot{q}_1+\beta\dot{q}_1+\left(\frac{\pi}{L}\right)^4\left[EIq_1-\frac{EA}{4}(q_0+q_1)(q_1^2+4q_2^2+2q_0q_1)\right]=-P(t),$$
$$\mu\ddot{q}_2+\beta\dot{q}_2+\left(\frac{\pi}{L}\right)^4\left[16EIq_2+EAq_2(q_1^2+4q_2^2+2q_0q_1)\right]=0, \tag{1}$$

where μ is the mass per unit length, β is the viscous damping coefficient per unit length, EA and EI denote, respectively, the axial and the flexural stiffness of the arch rib.

If $E[P(t)]=P_0\neq 0$, we take $P(t)=P_0+\xi(t)$, where $\xi(t)$ is a zero mean, wide-band process which can be approximated by a Gaussian white noise, i.e.

$$E[\xi(t)]=0, \quad \text{and} \quad E[\xi(t)\xi(t+\tau)]=\kappa\delta(\tau),$$

where κ is the intensity of the load fluctuation, and $\delta(\tau)$ is the Dirac delta function.

It is known (Fung and Kaplan [1952]) that under a purely static load P_0, if the initial rise q_0 is such that $q_0/2\rho>\sqrt{5.5}$, snap-buckling into a non-symmetric mode can occur if $P>P_{cr}=2EI\rho(\pi/L)^4\left[q_0/2\rho+3(q_0^2/4\rho^2-4)^{1/2}\right]$, where $\rho=(I/A)^{1/2}$. The effect of a stochastic load on the stability of the structure when $q_0/2\rho>\sqrt{5.5}$ and $P_0<P_{cr}$ is considered in the following.

It is noted that only the symmetric mode is directly excited and the antisymmetric mode is at rest. Then the first of equations (1) becomes

$$\mu\ddot{q}_1+\beta\dot{q}_1+\left(\frac{\pi}{L}\right)^4\left[EIq_1+\frac{EA}{4}(q_0+q_1)(q_1^2+2q_0q_1)\right]=-[P_0+\xi(t)]. \tag{2}$$

Assuming $q_1=q_{1e}+X_1(t)$, where q_{1e} corresponds to the deflection due to the static load P_0 and $X_1(t)$ to the additional deflection due to the random load $\xi(t)$, the static deflection q_{1e} is given by

$$\frac{EA}{4}\left(\frac{\pi}{L}\right)^4\left[\rho^2q_{1e}+(q_0+q_{1e})(q_{1e}^2+2q_0q_{1e})\right]=-P_0. \tag{3}$$

Then, subtracting equation (3) from (2) leads to the equation for the deflection component corresponding to the fluctuational part of the load:

$$\mu\ddot{X}_1+\beta\dot{X}_1+\frac{EA}{4}\left(\frac{\pi}{L}\right)^4\left[(4\rho^2+2q_0^2+6q_0q_{1e}-3q_{1e}^2)X_1+(3q_0+q_{1e})X_1^2+X_1^3\right]=-\xi(t). \tag{4}$$

The stationary marginal probability density of the displacement process $X_1(t)$, obtained by solving the associated Fokker-Planck equation is

$$p(x_1)=C_0\exp\left(-\frac{\beta EA}{2\kappa}\left(\frac{\pi}{L}\right)^4\left[\frac{1}{2}(4\rho^2+2q_0^2+6q_0q_{1e}+3q_{1e}^2)x_1^2+(q_0+q_{1e})x_1^3+\frac{1}{4}x_1^4\right]\right), \tag{5}$$

where C_0 is the normalization constant.

To investigate the stability of both the excited mode and the rest mode described by equations (1), substituting the perturbed solution

$$q_1 = q_{1e} + X_1 + x_1, \quad q_2 = 0 + 0 + x_2, \tag{6}$$

into equations (1), neglecting all nonlinear terms and making use of equations (3), and (4) results in

$$\begin{aligned} &\mu\ddot{x}_1 - \beta x_1 + \frac{EA}{4}\left(\frac{\pi}{L}\right)^4 (1\rho^2 + 2q_0^2 + 6q_0 q_{1e} + 3q_{1e}^2) + 3(q_0 + q_{1e})X_1 + 3X_1^2]x_1 = 0, \\ &\mu\ddot{x}_2 + \beta\dot{x}_2 + EA\left(\frac{\pi}{L}\right)^4 [(16\rho^2 + q_{1e}^2 + 2q_0 q_{1e}) + 2(q_0 + q_{1e})X_1 + X_1^2]x_2 = 0. \end{aligned} \tag{7}$$

or

$$\ddot{x}_i + 2\zeta_i\omega_i\dot{x}_i + [\omega_i^2 + g_i(t)]x_i = 0, \quad i = 1,2, \tag{8}$$

where

$$\begin{aligned} &\zeta_i = \frac{\beta}{4\mu\omega_i}, \quad i = 1,2, \\ &\omega_1^2 = \frac{EA}{4\mu}\left(\frac{\pi}{L}\right)^4 (4\rho^2 + 2q_0^2 - 6q_0 q_{1e} + 3q_{1e}^2), \quad \omega_2^2 = \frac{EA}{\mu}\left(\frac{\pi}{L}\right)^4 (16\rho^2 + q_{1e}^2 + 2q_0 q_{1e}), \\ &g_1(t) = \frac{3EA}{4\mu}\left(\frac{\pi}{L}\right)^4 [2(q_0 + q_{1e})X_1 + X_1^2], \quad g_2(t) = \frac{EA}{\mu}\left(\frac{\pi}{L}\right)^4 [2(q_0 + q_{1e})X_1 + X_1^2]. \end{aligned} \tag{9}$$

Equations (8) are of the form

$$\ddot{x} + 2\zeta\omega\dot{x} + [\omega^2 + g(t)]x = 0, \tag{10}$$

where $g(t)$ is an ergodic random process. Since the probability density of the random process X_1, $p(x_1)$, is known, it is possible to find the probability density of the random process g_i. According to the multiplicative ergodic theorem of Oseledec [1968], equation (10) possesses two real Liapunov exponents λ_1, λ_2 ($\lambda_1 > \lambda_2$) defined by

$$\lambda_i(x_0) = \lim_{t\to\infty} \sup \frac{1}{t}\log\|x(t, x_{i0})\|, \quad i = 1,2, \tag{11}$$

for appropriate initial random variable x_{i0}.

If both λ_1, λ_2 are negative, the solutions are asymptotically stable with probability 1 (w.p.1). The solutions are unstable as soon as $\lambda_{max} = \lambda_1 = 0$. In general, the Liapunov exponents are difficult to evaluate even numerically. However, for equation (10), it is possible to obtain upper bounds to λ_{max} using a method due to Infante [1968] and its extension by Kozin and Wu [1973], from which sufficient conditions for asymptotic stable w.p.1 may be found.

As an example, we consider a steel arch of rectangular cross-section having the following parameters: density of material $= 7850\ kg\ m^{-3}$, Young's modulus $E = 0.2\times10^{12}\ N\ m^{-2}$, rectangular cross-section with height $= 0.03\ m$, width $= 0.02\ m$, length of span $L = 1\ m$, initial rise $q_0 = 0.07\ m$. Two values for the mean load P_0 are considered, namely $P_0 = 1\times10^4\ N$, $5\times10^4\ N$, corresponding to static deflection $q_{1e} = -0.3421\times10^{-3}\ m$, $-0.17581\times10^{-2}\ m$, respectively.

Sufficient a.s. asymptotic stability regions for both the vibrating mode and the rest mode are obtained by using the Schwarz inequality and an optimization method; the results are plotted in Figures 2 and 3.

For further details, reference may be made to Ariaratnam and Xie [1988]

ACKNOWLEDGEMENT

This research was supported by the National Sciences and Engineering Research Council of Canada through Grant No.A-1815.

REFERENCES

Ariaratnam, S.T. and Xie, W.-C., 1988, "Dynamic Snap-Buckling of Structures under Stochastic Loads", to appear in *Recent Progress in Stochastic Structural Dynamics*, S.T. Ariaratnam, G. Schueller and I. Elishakoff (Eds.), Elsevier, U.K.

Fung, Y.C. and Kaplan, A., 1952, "Buckling of Low Arches or Curved Beams of Small Curvature", *NACA Tech. Note* 2840.

Infante, E. F., 1968, "On the Stability of Some Linear Nonautonomous Random Systems", *J. Appl. Mech* , Vol.35, No.1, pp.7-12.

Kozin, F. and Wu, C.W., 1973, "On the Stability of Linear Stochastic Differential Equations", *J. Appl. Mech.*, Vol. 40, pp.87-92.

Oseledec, V.I., 1968, "A Multiplicative Ergodic Theorem, Liapunov Characteristic Numbers for Dynamical Systems", *Trudy Moskov. Mat. Obsc.*, Vol. 19, pp.179-210, (English Translation).

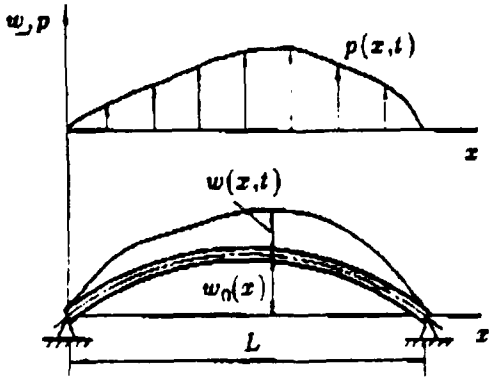

Fig.1 Two-Pinned Arch and Loading

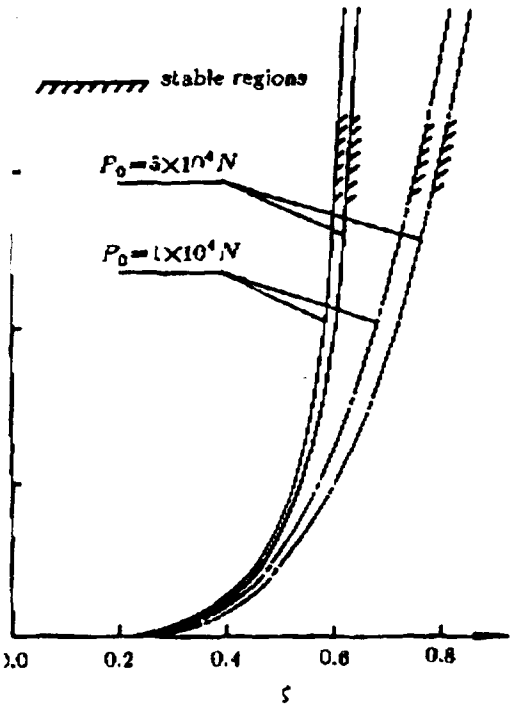

Regions of Almost-Sure Asymptotic Stability
(First Mode)

— Stability Boundary via Schwarz Inequality

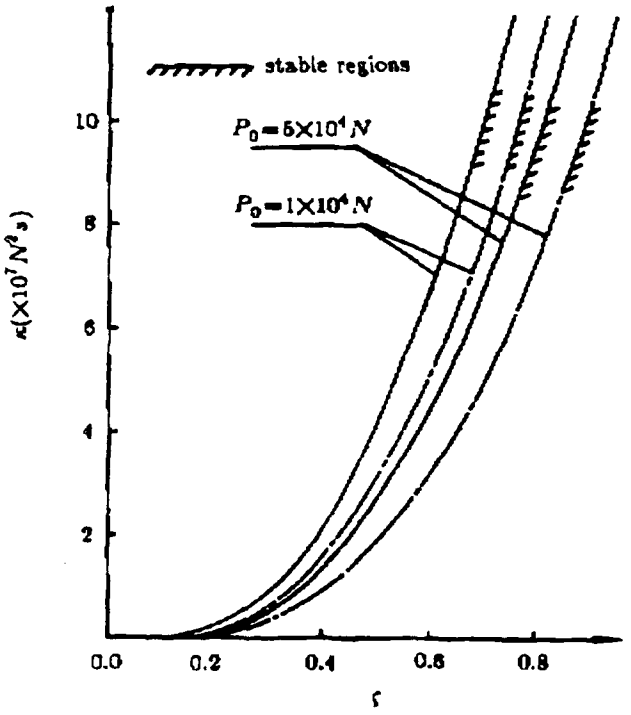

Fig.3 Regions of Almost-Sure Asymptotic Stabi
(Second Mode)

——— Stability Boundary via Schwarz Inequ

A NEW APPROACH TO

STOCHASTIC FLAP-LAG STABILITY

OF A ROTOR BLADE IN HOVER

by

N. Sri Namachchivaya

and

John Prussing

Department of Aeronautical and Astronautical Engineering
University of Illinois at Urbana-Champaign
104 South Mathews Avenue
Urbana, IL 61801

ABSTRACT

In recent years, considerable progress has been made towards understanding the dynamics of helicopter rotor blade systems in both hover and the forward flight conditions [1-4]. From an operational, as well as safety point of view, the most important problem is certainly the stability of the system. However, theoretical investigations on rotor blade stability published to date, with a few notable exceptions, have been restricted to deterministic analyses.

In the service life of a helicopter, numerous encounters with thunderstorm and clear-air turbulence can be expected. Furthermore, because of the very nature that lift is generated by blade rotation, some level of self-created turbulence is also unavoidable. Therefore, random turbulence in the atmosphere should be included in a realistic analysis. This has been done partially in, for example, References [5-7], where the vertical component of the turbulence velocity has been taken into consideration. The inclusion of random vertical inflow results in additional non-parametric excitation terms appearing on the right hand side of the equations. The objective was to calculate certain statistical properties of the structural response, including the spectral density, level crossing averages, and peak magnitude distribution.

It is well known, however, that stability of a dynamic system depends only on parametric excitations. The inclusion of vertical inflow in Refs. [5-7] does not change the stability analysis; that is, the stability analysis remains deterministic.

A preliminary analysis of the stochastic stability of flap-lag rotor blade motion was made in Ref. [8], in which the turbulence was modeled as white noise and the method of stochastic averaging was employed to determine first and second moment stability. Reference 8 is a continuation of the work

in Refs. [9-10]. Related analyses of rotor blade stochastic stability and response are given in Refs. [11-13].

In the present analysis the problem of Ref. 8 is approached from a different point of view, namely that in Refs. [14-15]. The flap-lag system is analyzed as having a single critical mode (lead-lag) and a highly damped mode (flap). Using the methods of Refs. [14-15] the nth mode stability can be analyzed with significantly less algebra than the mean-square (second moment) stability of Ref. 8.

The linearized equations of flap-lag motion in hover are given in terms of the flap angle β and the lead-lag angle ζ as [Ref. 8]

$$\begin{pmatrix} \delta\ddot{\beta} \\ \delta\ddot{\zeta} \end{pmatrix} + [\bar{C} + C_\nu]\begin{pmatrix} \delta\dot{\beta} \\ \delta\dot{\zeta} \end{pmatrix} + [\bar{K} + K_\nu]\begin{pmatrix} \delta\beta \\ \delta\zeta \end{pmatrix} = \begin{pmatrix} 0 \\ 0 \end{pmatrix} \qquad (1)$$

where

$$\bar{C} = \begin{bmatrix} h\,, & 2\bar{\beta} + h(\bar{\phi} - 2\bar{\theta}) \\ -2\bar{\beta} - h(2\bar{\phi} - \theta)\,, & h(\bar{\phi}\,\bar{\theta} + 2Cd_o/a) \end{bmatrix}$$

$$\bar{K} = \begin{bmatrix} P - h\theta_\beta\,, & Z - h\theta_\zeta \\ Z + h\bar{\phi}\theta_\beta + R\theta_\beta(\bar{\beta}-\beta_\infty)(\omega_\xi^2 - \omega_\beta^2)\,, & W + h\theta_\zeta\bar{\phi} \end{bmatrix}$$

represent the deterministic damping and stiffness, and

$$C_\nu = \nu \begin{bmatrix} 0\,, & 4h/3 \\ -8h/3\,, & 4h\bar{\theta}/3 \end{bmatrix} = \nu^* h \begin{bmatrix} 0 & 1 \\ -2 & \bar{\theta} \end{bmatrix}$$

$$K_\nu = \nu \begin{bmatrix} -8h\bar{\beta}/3\,, & 0 \\ 4h\theta_\beta\,, & 4h\theta_\zeta/3 \end{bmatrix} = \nu^* h \begin{bmatrix} -2\bar{\beta} & 0 \\ \theta_\beta & \theta_\zeta \end{bmatrix}$$

represent the stochastic contributions, where $\nu(t)$ represents the vertical turbulence component, and the other variables represent various system parameters (see Ref. 8).

Equation (1) can be written in first-order form as

$$\dot{\underline{x}} = A\,\underline{x} + \nu(t)\,B\,\underline{x} \tag{2}$$

The analysis of Eq. (2) becomes easier if it is brought to the simplest partially diagonal form that still retains real variables. To this end, consider a transformation $\underline{x} = T\underline{y}$, i.e., $\underline{y} = [\underline{u},\underline{v}]$

$$x_j = 2(c_j^1 u_1 + d_j^1 u_2) + 2(c_j^2 v_1 + d_j^2 v_2) \tag{3}$$

where superscripts 1 and 2 correspond to the eigenvectors of the critical and stable eigenvalues, respectively. Substituting Eq. (3) in Eq. (2) and premultiplying by the adjoint-eigenvectgor $\underline{b}$ yields

$$\dot{\underline{u}} = C_o\underline{u} + (K\underline{u} + M\underline{v})\,\nu(t) \tag{4a}$$

$$\dot{\underline{v}} = D_o\underline{v} + (N\underline{u} + L\underline{v})\,\nu(t) \tag{4b}$$

where

$$C_o = \begin{bmatrix} 0 & \omega_1 \\ -\omega_1 & 0 \end{bmatrix}, \quad \bar{C}_1 = \begin{bmatrix} \delta_1' & \omega_1' \\ -\omega_1 & \delta_1' \end{bmatrix}, \quad D_o = \begin{bmatrix} \delta_2 & \omega_1 \\ -\omega_2 & \delta_2 \end{bmatrix},$$

prime denotes the differentiation with respect to w_o,

For the stochastic problem, i.e., $\nu(t) \neq 0$, it has been shown by Sri Namachchivaya and Lin [15] that the stochastic terms of Eq. (4b) contribute to the drift and diffusion coefficients of Eq. (4a). Thus, utilizing the ideas from the deterministic and stochastic averaging theorems, as indicated in [15], the amplitude and phase converge weakly to a Markov diffusion process with infinitesimal generator L^o.

$$L^o f(a,\phi) = m_a(a)\,\frac{\partial}{\partial a}\,f(a,\phi) + m_\phi(a)\,\frac{\partial}{\partial \phi}\,f(a,\phi)$$

$$+ \frac{1}{2}[\sigma\sigma]_{aa}\frac{\partial^2 f}{\partial a^2}(a,\phi) + [\sigma\sigma]_{\phi\phi}\frac{\partial^2 f}{\partial \phi^2}(a,\phi) + [\sigma\sigma]_{a\phi}\frac{\partial^2 f}{\partial a\,\partial \phi}(a,\phi) \qquad (5)$$

Consider the Fokker-Planck equation associated with L^o. Integrating this equation over ϕ (assuming periodicity in ϕ) yields

$$\frac{\partial \bar{p}}{\partial t} = -\frac{\partial}{\partial a}\left[\left\{\bar{\alpha} + \frac{\gamma}{2}\right)a\right\}\bar{p}\right] + \frac{1}{2}\bar{\gamma}\frac{\partial}{\partial a^2}\left[a^2\,\bar{p}\right] \qquad (6)$$

where

$$\bar{\alpha} = \bar{\delta}'\eta + \frac{1}{8}\kappa_2 S_{\xi\xi}(2\omega_1) + \bar{\zeta}\,, \quad \gamma = \frac{1}{8}\left[2\kappa_1 S_{\xi\xi}(0) + \kappa_2 S_{\xi\xi}(2\omega_1)\right]$$

$$\bar{\zeta} = \frac{1}{8}\left[\kappa_3 \bar{S}_{\xi\xi}(\omega_1+\omega_2) + \kappa_4 \bar{S}_{\xi\xi}(\omega_1-\omega_2) - \kappa_5 \psi_{\xi\xi}(\omega_1+\omega_2)\right.$$

$$\left. + \kappa_6\,\bar{\psi}_{\xi\xi}(\omega_1-\omega_2)\right]$$

$$S_{\xi\xi}(\omega) = 2\int_0^\infty R_{\xi\xi}(\tau)\cos\omega\tau\,d\tau,\quad \bar{S}_{\xi\xi}(\omega) = 2\int_0^\infty e^{-\alpha_2\tau}R_{\xi\xi}(\tau)\cos\omega\tau\,d\tau\,,$$

$$\psi_{\xi\xi}(\omega) = 2\int_0^\infty R_{\xi\xi}(\tau)\sin\omega\tau\,d\tau,\quad \bar{\psi}_{\xi\xi}(\omega) = 2\int_0^\infty e^{-\alpha_2\tau}R_{\xi\xi}(\tau)\sin\omega\tau\,d\tau\,,$$

$$\bar{p}(a,t) = \frac{1}{2\pi}\int_0^{2\pi} p(a,\phi,t)\,d\phi$$

and κ_i, $i = 1,2,\ldots,6$ are defined in terms of coefficients of matrices K, M, N in [15]. The above equation is similar to that obtained in [14]. From Eq. (6), the stability condition for the nth moment of the linear system can be written as

$$16(\delta'\eta + \bar{\zeta}) + (n+2)\kappa_2 S_{\xi\xi}(2\omega_1) + 2n\,\kappa_1 S_{\xi\xi}(0) < 0 \qquad (7)$$

Equation (7) represents a significant simplification over the mean square stochastic stability analysis of Ref. 8. In addition, higher moment

stability can be assessed. The simplification occurs because there is a single critical mode. This allows a problem of smaller dimension to be analyzed.

REFERENCES

1. Sissingh, G. J., "Dynamics of Rotors Operating at High Advance Ratios," Journal American Helicopter Society, Vol. 13, No. 3, July 1968, pp. 56-63.

2. Sissingh, G. J. and Kuczynski, W. A., "Investigations on the Effect of Blade Torsion on the Dynamics of Flapping Motion, "Journal American Helicopter Society, Vol. 15, No. 2, April 1970, pp. 2-9.

3. Peters, D. A. and Hohenemser, K. H., "Application of Floquet Transition Matrix to Problems of Lifting Rotor Stability," 26th National Forum of the American Helicopter Society, Paper No. 412, Washington, DC, June 1970.

4. Peters, D. A., "Flap-Lag Stability of Helicopter Rotor Blades in Forward Flight," Journal of the American Helicopter Society, Vol. 20, No. 4, October 1975, pp. 2-13.

5. Gaonkar, G. H. and Hohenemser, K. H., "Stochastic Properties of Turbulence Excited Rotor Blade Vibrations," AIAA Journal, Vol. 9, No. 3, March 1971, pp. 419-424.

6. Wan, F.Y.M., "Nonstationary Response of Linear Time-Varying Dynamical Systems to Random Excitations," ASME Paper No. 73-APM-6, June 1973.

7. Gaonkar, G. H., "Peak Statistics and Narrow-Band Features of Coupled Torsion-Flapping Rotor Blade Vibrations to Turbulence," Journal of Sound and Vibration, Vol. 34, No. 1, 1974, pp. 35-52.

8. Prussing, J. E. and Lin, Y. K., "Rotor Blade Flap-Lag Stability in Turbulent Flows," Journal American Helicopter Society, Vol. 27, No. 2, April 1982, pp. 51-57.

9. Lin, Y. K., Fujimori, Y. and Ariaratnam, S. T., "Rotor Blade Stability in Turbulent Flows - Part I," AIAA Journal, Vol. 17, No. 6, June 1979, pp. 545-552.

10. Fujimori, Y., Lin, Y. K. and Ariaratnam, S. T., "Rotor Blade Stability in Turbulent Flows - Part II," AIAA Journal, Vol. 17, No. 7, July 1979, pp. 673-678.

11. Fuh, J. S., Hong, C-Y.R., Lin, Y. K. and Prussing, J. E., "Coupled Flap-Torsional Response of a Rotor Blade in Forward Flight Due to Atmospheric Turbulence Excitations," Journal of the American Helicopter Society, Vol. 28, No. 3, July 1983, pp. 3-12.

12. Prussing, J. E. and Lin, Y. K., "A Closed-Form Analysis of Rotor Blade Flap-Lag Stability in Hover and Low-Speed Forward Flight in Turbulent

Flow," Journal of the American Helicopter Society, Vol. 28, No. 3, July 1983, pp. 42-46.

13. Prussing, J. E., Lin, Y. K. and Shiau, T-N., "Rotor Blade Flap-Lag Stability and Response in Forward Flight in Turbulent Flow," Journal of the American Helicopter Society, Vol. 29, No. 4, October 1984, pp. 81-87.

14 Namachchivaya, N. Sri, "Hopf Bifurcations in the Presence of Both Parametric and External Stochastic Excitations," Journal of Applied Mechanics, to appear.

15. Namachchivaya, N. Sri and Lin, Y. K., "Application of Stochastic Averaging for Systems with High Damping," Journal of Probabilistic Engineering Mechanics, to appear.

SESSION 4

NONLINEAR VIBRATION CONTROL

WEDNESDAY - 1600 - 1930

June 1, 1988

NONLINEAR OSCILLATIONS OF LARGE SYSTEMS WITH LOCALIZED NONLINEARITIES

P. HAGEDORN
Institut für Mechanik, TH Darmstadt, Hochschulstraße 1, 6100 Darmstadt W.Germany

Abstract

Numerical simulations of the dynamics of large mechanical and electromechanical systems are becoming more and more common in the area of aerospace structures and in other fields. In many of these systems the nonlinearities are concentrated in a few elements only, the larger part of the system being linear. This class of systems forms the subject of the present paper.

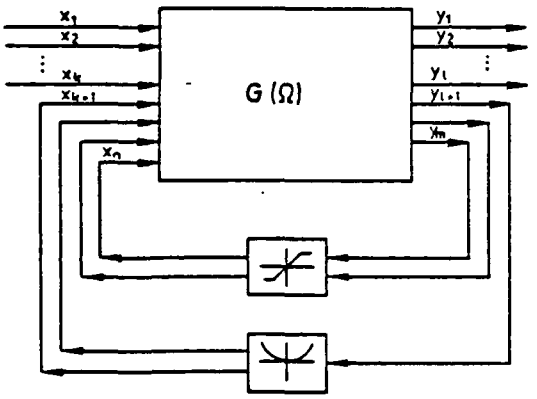

Fig.1: Complex system with linear and nonlinear subsystems

We consider a system according to Fig.1 composed of a large linear subsystem with input

$$x(t) = (x_1(t),\ x_2(t),\ \ldots,\ x_n(t))^T \tag{1}$$

and output

$$y(t) = (y_1(t),\ y_2(t),\ \ldots,\ y_m(t))^T \tag{2}$$

containing also several nonlinear elements. The dynamic behavior of the linear part can be described in the time domain as

$$y(t) = \int_0^t H(\tau)\ x(t-\tau)\ d\tau, \tag{3}$$

the m x n matrix H(t) being the impulse response matrix, i.e. the element

$h_{ij}(t)$ is the response of the output $y_i(t)$ to an input of the type $x_j(t) = \delta(t)$. For practical purposes the upper boundary in this integral can be substituted by a finite "decay time", depending on the damping present in the system.

In addition to the large linear subsystem, the system of Fig.1 contains also nonlinear elements or subsystems, through which some of the outputs, say y_{l+1}, y_{l+2}, ..., y_m are fed back to some of the inputs, for example x_{k+1}, x_{k+2}, ..., x_n. Only the inputs x_1, x_2, ..., x_k are then accessible and only these variables are inputs for the *complex system* (i.e. the composed system). The input-output relations between the x_1, x_2, ..., x_k and the y_1, y_2, ..., y_l in the complex system of Fig.1 are sought, that is, the outputs $y_1(t)$, $y_2(t)$, ..., $y_l(t)$ are to be obtained via numerical simulations from given inputs $x_1(t)$, $x_2(t)$, ..., $x_k(t)$. In the present paper we solve this problem using directly the transfer properties of the linear subsystem.

Suppose for a moment that the nonlinearities are such that the y_{l+1}, y_{l+2}, ..., y_m are simply functions of the values of the input variables x_{k+1}, x_{k+2}, ..., x_n taken at the same time, as would be the case for example for nonlinear springs with displacements and forces as inputs and outputs. Since the x_1, x_2, ...,x_k are given as time functions and the x_{k+1}, x_{k+2}, ...,x_n as functions of some of the y_1, y_2, ..., y_m, we can write

$$\mathbf{x}(t) = \mathbf{x}[\mathbf{y}(t), t]. \tag{4}$$

This notation does not reflect the fact that $\mathbf{x}$ does not depend on y_1, y_2, ..., y_l but has the advantage of being very simple. With (4) in (3) we now obtain the vector integral equation

$$\mathbf{y}(t) = \int_0^t \mathbf{H}(\tau)\, \mathbf{x}[\mathbf{y}(t-\tau),\ t-\tau]\, d\tau, \tag{5}$$

in which the time function $\mathbf{y}(t)$ is the unknown, while $\mathbf{x}(\mathbf{y},t)$ is given. This integral equation has to be solved numerically for $\mathbf{y}(t)$ in order to obtain the system response.

If the nonlinear elements are such that the x_{k+1}, x_{k+2}, ..., x_n are functions not only of the values of y_{l+1}, y_{l+2}, ..., y_m, but for example also of their derivatives, then (4) has to be substituted by

$$x(t) = x[y(t),\ \dot{y}(t),\ t]. \tag{6}$$

Similarly, higher order derivatives could also be included. The problem can however always be recast into the form (5), by introducing additional variables.

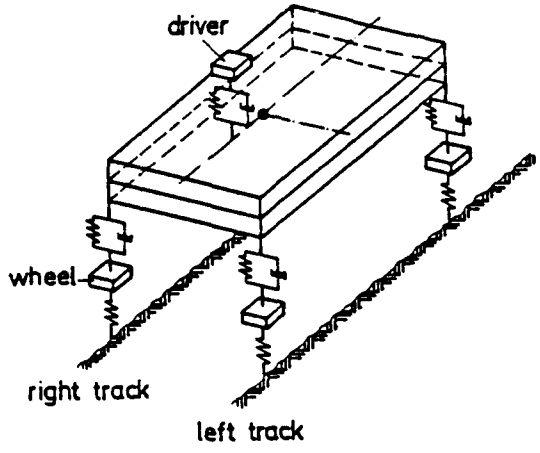

Fig.2: Simple model for the dynamics of a car

The integral equation (5) has been used successfully for numerical simulations in several cases by the author. A simple example is the simulation of passenger cars, mainly in studies of riding comfort. In this aspect of vehicle dynamics usually almost the whole system is to a large extent linear, the only essential nonlinearities being the dampers and the pneumatic tyres. The corresponding mechanical model of Fig.2 is obviously a dynamic system of the type depicted in Fig.1. Since this system is still relatively complicated, we discuss instead the simpler system of Fig.3, which contains most of the essential features of the original system. It is formed by two masses and three linear springs and dampers, all of which are supposed to be identical for greater simplicity. In addition, there is a nonlinear element connecting the two point masses, which for simplicity we assume to be a nonlinear spring with a piecewise constant stiffness, as shown in Fig.4. The external input into the system is by means of the displacement $s(t)$ of the point A. The linear subsystem has therefore two input variables, namely $v(t)$ and $f(t)$ (the force at the nonlinear damper) and two output variables $z_1(t)$, $z_2(t)$, i.e.

$$\mathbf{x} = (f,\ v)^T, \tag{7}$$

$$\mathbf{y} = (z_1,\ z_2)^T. \tag{8}$$

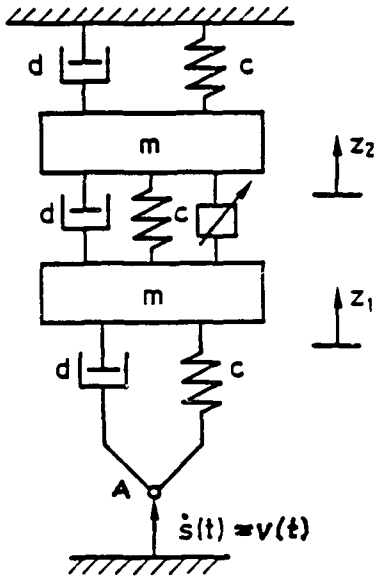

Fig.3: Nonlinear system with two degrees of freedom

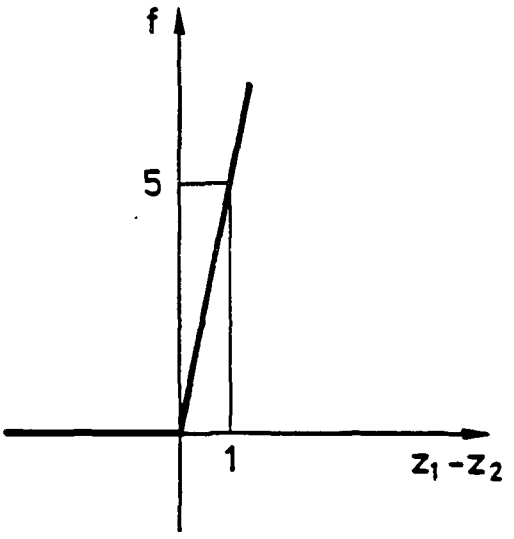

Fig.4: The characteristics of the nonlinear spring

The dynamics of the linear subsystem is obviously described by the equations of motion

$$m\ddot{z}_1 + c(2z_1 - z_2) + d(2\dot{z}_1 - \dot{z}_2) = - f(t) + c\int_0^t v(\bar{t})\, d\bar{t} + dv(t), \qquad (9)$$

$$m\ddot{z}_2 + c(2z_2 - z_1) + d(2\dot{z}_2 - \dot{z}_1) = f(t). \qquad (10)$$

The solution can be written in the form (5), with

$$h_{12}(t) = \frac{1}{6}\left\{4 - 3e^{-\delta t}\left[\cos \omega_1 t - \frac{\delta}{\omega_1} \sin \omega_1 t\right] - e^{-3\delta t}\left[\cos \omega_2 t - \frac{3\delta}{\omega_2} \sin \omega_2 t\right]\right\}, \qquad (11)$$

etc., where the abbreviations $\delta := d/2m$; $\omega_0^2 := c/m$; $\omega_1^2 := \omega_0^2 - \delta^2$; $\omega_2^2 := 3\omega_0^2 - 9\delta^2$ were used. As an example the system response is calculated for the function

$$s(t) = \begin{cases} \frac{h_0}{2}(1 - \cos \Omega t), & 0 \leq t \leq \frac{4\pi}{\Omega}, \\ 0, & t < 0,\ t > \frac{4\pi}{\Omega}. \end{cases} \qquad (12)$$

Fig.5 shows some numerical results obtained in this manner for $m = 1$, $d = 0.04$, $c = 1$, $\Omega = 1$, $h_0 = 1$. The integrations in (5) were performed with a simple first order numerical scheme for different values of Δt. These results are compared with a "numerically exact" solution of the differential equations, obtained via a fourth order Runge-Kutta method (with $\Delta t = 0.5$).

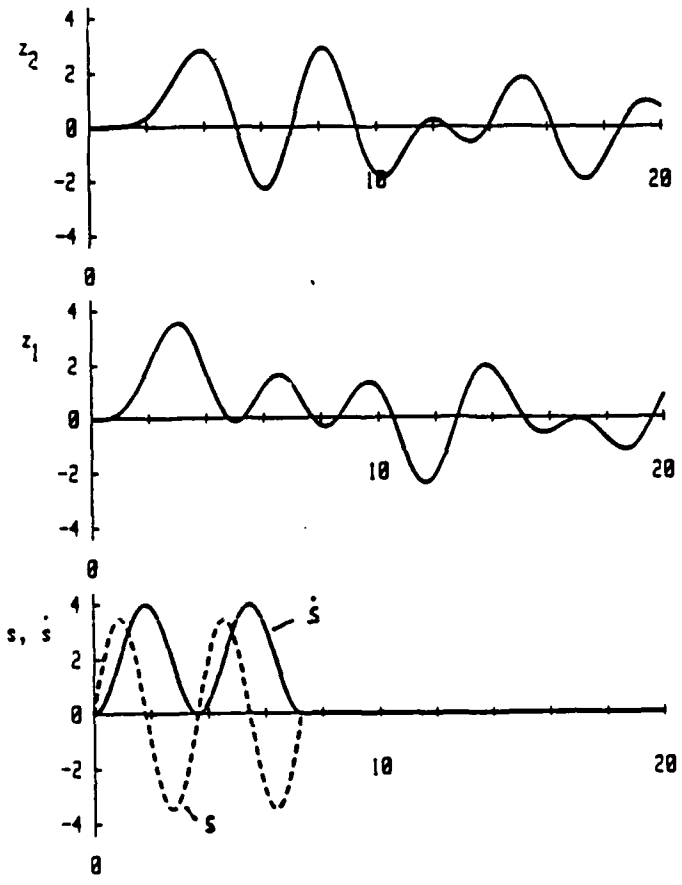

Fig.5: Numerical results

In the paper, additional numerical results are given and it is also shown how the idea of splitting up the complex system into linear and nonlinear subsystems can be used in the measurement of transfer properties.

On the Adaptive Control of Dynamic Systems with Flexible Structures

Robert L. Kosut

Integrated Systems,Inc., 2500 Mission College Blvd., Santa Clara, CA 95054
and
Information Systems Lab,Stanford University,Stanford,CA 94305

Abstract

The purpose of this talk is to present a practical method for analyzing the stability properties of adaptive control systems in general, and in particular, dynamic systems with flexible structures. The basis for the stability analysis is the application of the classical method of averaging for analyzing the behavior of ordinary differential equations with a small parameter. The theoretical analysis reveals comman properties of many adaptive algorithms, including causes of instability and the means to counteract them*. The limitations and practical use of the theory is discussed. The theory will be applied to both MRAC (Model Reference Adaptive Control) systems and to STR (Self Tuning Regulators). Specific applications will include: large flexible space structures, robotic systems, and disc drives.

*Theoretical background material may be found in *Stability of Adaptive Systems: Passivity and Averaging Analysis* (MIT Press, 1986) by B.D.C. Anderson, R.R. Bitmead, C.R. Johnson, Jr., P.V. Kokotovic, R.L. Kosut, I.M.Y. Mareels, L. Praly, and B.D. Riedle.

ON THE STABILIZATION OF TETHERED SATELLITE SYSTEMS†

E.H. Abed and D.-C. Liaw
Department of Electrical Engineering
and the Systems Research Center
University of Maryland, College Park, MD 20742 USA

Abstract

The nonlinear dynamic model of the shuttle/tethered satellite system (TSS) studied by Liaw and Abed [1] and the associated results are reviewed and extended in this talk. Recall [1]-[3] that the TSS consists of a shuttle and a satellite connected by a tether, in orbit around the Earth. In this work, issues of stability and stabilization in the station keeping and the deployment and retrieval processes are considered. Two approaches are used in the investigation. The first is based on a Liapunov function for the nonlinear model. The second method relies on Hopf bifurcation theory, as in [1]. Two other issues are briefly considered: the existence of an invariant manifold for the dynamics, and controllability of the TSS via tension control alone. In particular, it is observed that purely in-plane motion of the TSS corresponds to an invariant manifold of the dynamics. Moreover, the full nonlinear system is shown to be uncontrollable if the only available control is the tension in the tether. This fact is interesting in the light of the favorable stabilizability properties of the system.

The model of the TSS developed in [1] is a sixth order lumped parameter model, with state variables o (out of plane angle), θ (in plane angle), and ℓ (tether length), as well as their time derivatives ω_o, ω_θ and $\dot{\ell}$, respectively. The model is obtained using the system Lagrangian in [1] under the assumptions of a massless, rigid tether, a satellite of mass m very small compared to the shuttle mass m_s, no aerodynamic drag forces, and a circular orbit of the shuttle. The model is, in the notation of [1], as follows:

† Supported in part by the Air Force Office of Scientific Research under URI Grant AFOSR-87-0073, and by the NSF under Grants ECS-86-57561 and CDR-85-00108.

$$\dot{\phi} = \omega_\phi \tag{1}$$

$$\dot{\phi_\omega} = -\frac{2v}{\ell}\omega_\phi - \frac{1}{2}\sin(2\phi)(\omega_\theta + \Omega)^2 - \frac{\Omega^2 r_0}{\ell}\cos\theta\sin\phi(1 - \frac{r_0^3}{r_m^3}) \tag{2}$$

$$\dot{\theta} = \omega_\theta \tag{3}$$

$$\dot{\omega_\theta} = -\frac{2v}{\ell}(\omega_\theta + \Omega) + 2\tan\phi(\omega_\theta + \Omega)\omega_\phi - \frac{\Omega^2 r_0 \sin\theta}{\ell\cos\phi}(1 - \frac{r_0^3}{r_m^3}) \tag{4}$$

$$\dot{\ell} = v \tag{5}$$

$$\dot{v} = \ell\omega_\phi^2 + \ell\cos^2\phi(\omega_\theta + \Omega)^2 - \frac{\Omega^2 r_0^3 \ell}{r_m^3} + \Omega^2 r_0\cos\theta\cos\phi(1 - \frac{r_0^3}{r_m^3}) + \frac{T}{m} \tag{6}$$

In (1)-(6), r_0 is the constant radius of the shuttle orbit, Ω is the constant angular velocity of the shuttle in its orbit, and r_m denotes the varying radius of the satellite orbit, given by

$$r_m^2 = r_0^2 + \ell^2 + 2r_0\ell\cos\phi\cos\theta$$

and T denotes the tension in the tether.

It is shown in [1] that, at an equilibrium point, the system (1)-(6) nominally possesses two pairs of purely imaginary eigenvalues. One of these pairs may be stabilized by linear output feedback, while the other pair is uncontrollable. This motivates the use in [1] of results on stabilization of Hopf bifurcations [4] to yield a family of stabilizing tension control laws for station keeping. Liapunov functions for nonautonomous linearized systems associated with (1)-(6) are used in [1] to prove stability of deployment and instability of retrieval for constant angle deployment and retrieval strategies for which the system retains an equilibrium point.

The Liapunov function candidate for the system (1)-(6) is taken as the *total system energy*, the sum of the kinetic and potential energies (KE and PE, respectively), where

$$KE = \frac{1}{2}m_s\Omega^2 r_0^2 + \frac{1}{2}m[\dot{\ell}^2 + \ell^2\dot{\phi}^2 + \ell^2\cos^2\phi(\dot{\theta} + \Omega)^2 + \Omega^2 r_0^2 + 2\Omega r_0\dot{\ell}\cos\phi\sin\theta - 2\Omega r_0\ell\sin\phi\sin\theta\dot{\phi} + 2\Omega r_0\ell\cos\phi\cos\theta(\dot{\theta} + \Omega)],$$

$$PE = -\frac{GMm_s}{r_0} - \frac{GMm}{r_m}$$

This Liapunov function candidate is useful in deriving stabilizing tension control laws T in feedback form. This is most easily seen for the station keeping application studied in [1], wherein the TSS is to be stabilized about a fixed tether length.

Work is proceeding on the question of the quality of the total system energy as a Liapunov function for the system, in terms of the size of the predicted region of attraction. In addition, generalization of the results summarized above to allow for flexibility of the tether, nonzero tether mass, noncircular orbit, and appreciable satellite mass is in progress.

The existence of an invariant manifold for Eqs. (1)-(6) is easy to check. Note that if, in Eqs. (1), (2), at some instant of time $\phi = 0$, $\omega_\phi = 0$, then this holds for all subsequent times. Therefore the set $\phi = 0, \omega_\phi = 0$ is an invariant manifold of (1)-(6), regardless of the form of the tension control law T. The attractivity of this invariant manifold can only be determined from the nonlinear terms, since the Jacobian matrix of Eqs. (1), (2) with respect to ϕ, ω_ϕ has a pair of purely imaginary eigenvalues (a critical case). Moreover, the existence of this invariant manifold, regardless of the tension control law T, implies that the system (1)-(6) is uncontrollable.

References

[1] D.-C. Liaw and E.H. Abed, "Stability Analysis and Control of Tethered Satellites," *Proc. USAF/NASA Workshop on Model Determination for Large Space Systems*, Pasadena, CA, March 1988, in press.

[2] C.C. Rupp and J.H. Laue, "Shuttle/Tethered Satellite System," *The Journal of the Astronautical Sciences*, Vol. 26, No. 1, pp. 1-17, 1978.

[3] D.A. Arnold, "The Behavior of Long Tethers in Space," *The Journal of the Astronautical Sciences*, Vol. 35, No. 1, pp. 3-18, 1987.

[4] E.H. Abed and J.-H. Fu, "Local Feedback Stabilization and Bifurcation Control, I. Hopf Bifurcation," *Systems and Control Letters*, Vol. 7, pp. 11-17, 1986.

A MATHEMATICAL FORMULATION AND CONTROL EXPRESSIONS FOR COMPLIANT CONTROL OF CONSTRAINED ROBOT MANIPULATORS

Choong Sup Yoon and Fathi. M. A. Salam

Department of Electrical Engineering and Systems Science

Michigan State University

East Lansing, MI 48824

ABSTRACT

We formulate the compliant control problem mathematically employing the framework of constrained Hamiltonian systems. We then derive nonlinear control expressions for the force and the motion on the constraint surface. The derivations reveal conditions that define the class of constraint surfaces allowable in the formulations. Two examples are then given to illustrate the formulation and the methodology.

Introduction

Most robots are currently used for very limited tasks usually characterized by position-to-position movements, e.g., pick-and-place, spot welding and spray painting. Other essential but complicated tasks involve contact with the manipulator's environment, e.g., inserting a pin into a hole, assembling, plasma welding, contour following, deburring, grinding, etc., see [1,2]. Such contact usually results in the generation of external forces acting on the end effector of the manipulator. External contact forces such as the ones introduced by constraint surfaces always modify the dynamical behavior of a manipulator. Consequently, issues of appropriate modeling and of effective new control strategies arise.

Compliant control is concerned with the control of a robot manipulator in contact with its environment, see [3-4]. The end effector of the manipulator first converges to the constraint surface at a specified position generating a specified force upon contact. Then, the end effector moves along a desired path on the surface while maintaining a desired contact force profile (along this path). Thus, compliant motion calls for the input torque to achieve tracking for a specified path on the constraint surface, and with a specified contact force.

In principle, such tracking is possible because the constraint surface limits movement to a submanifold (on surface) and consequently frees some components of the input torque to control the contact force with the surface. However, the nonlinearity of the governing dynamics as well as the constraint equations potentially make the control process difficult if not impossible. The difficulty may translate mathematically to the presence of singularities at some points on the constraint surface or to the lack of well-posedness of the governing system of equations.

We choose to formulation the problem in joint space. An advantage of this choice is that the constraint now applies to the joint angles directly; consequently the constraint applies to the links of the manipulator and not merely to its end effector as it is the case in

the task space formulation. Another advantage is that once the class of allowable constraints is specified in the joint space, the simpler and direct use of the forward kinematic would provide the corresponding class of the allowable constraints surfaces in the joint space. We remark, however, that determining useful, in terms of applications, class of surfaces is a nontrivial research problem.

The control process we envision may take the following steps. The end effector is first steered to a point on the constraint surface using, e.g., the linear feedback control strategies reported in [5-7]. In addition, one must also guarantee that at the final (desired) position on the surface, a specified (normal) force is generated. Once the end effector is located at a specific position and with a specified force, one may then apply compliant control strategies to generate or to track a desired path with a desired contact force profile. Some results on compliant control have been reported in [3-4].

In this work, we propose a control strategy which consists of the sum of two nonlinear controls. One control restricts (the end effector of) the manipulator to the constraint surface; this control represents the force control part. The other control steers (the end effector of) the manipulator along a specified path on the constraint surface; this control represents the position control part. Then we show that these nonlinear controls can be supplied by the input torque vector at the joints. Specifically, we give an expression for the (physical) torque which would generate the desired nonlinear controls. (It is possible to include the dynamics of the actuators and consider the actuator voltages as the physical inputs) Further work need to exploit force and velocity feedback to achieve attractivity of the constraint surface in order for the formulation and the control to be robust.

We employ the geometric tools of symplectic Hamiltonian systems in setting up our framework. Although these tools have been used in [3], our emphasis is quite different: we assume that the amplitude (modulo a multiplicative constant) of the desired force is given as a function defined on the constraint surface; then we derive the control required to maintain that desired force. We also derive the second component of the control strategy which generates desired paths or trajectories on the constraint surface. The derivations require that the constraint surfaces satisfy conditions in terms of a matrix of Poisson brackets being nonsingular. These conditions in fact specify the class of constraint surfaces allowable in our formulation.

The formulation does not yet take advantage of feedback of error signals, with respect to a desired position, velocity or force. Moreover, while our analytical results are valuable on their own merits, we recognize that in application one has to take into account the effect of disturbances, unmodeled dynamics, and the dynamics of the material of the constraint surface itself. We hope to pursue these issues in future works to blend our theoretical derivations with practical applications. It should be recognized however that the theoretical framework provides guidance and deep insights into how to properly devise and apply the control strategies.

Summary of Results

The Hamiltonian of the overall constrained robot system (H_T) can be shown to be

$$H_T = H + \sum_{j=1}^{2m}(\lambda_j + \hat{u}_j)\Phi^j + \sum_{j=1}^{2n-2m}\tilde{u}_j\Psi^j, \tag{1}$$

where H is the free Hamiltonian, λ_j is a Lagrangian multiplier, Φ^j represents one of the set of equations that model constraint, and Ψ^j represents one of the corresponding set of orthogonal complement to the set of constraint equations. $\hat{u}$ represents the $2m$-dimensional force control input vector and $\tilde{u}$ represnts the $(2n-2m)$-dimensional compliant motion control input vector. These controls can be derived to equal ([8])

$$\hat{u} = C_{\Phi\Phi}^{-1}C_{H_\lambda,\Phi} \tag{2.i}$$

$$C_{\Phi\Phi} = [(\Phi^{ij})] = [\{\Phi^i , \Phi^j\}]$$

$$C_{H_{\lambda^*}\Phi} = [\{H_{\lambda^*},\Phi^1\},.....,\{H_{\lambda^*},\Phi^{2m}\}]^T$$

$$\tilde{u} = S_{\Psi\Psi}^{-T} S_{H\Psi} \tag{2.ii}$$

$$S_{\Psi\Psi} = [(\Psi^{ij})] = [\{\Psi^i,\Psi^j\}]$$

$$S_{H\Psi} = [\ \{\ H^* - H_T,\ \Psi^1\ \}\ ,.....,\ \{\ H^* - H_T,\ \Psi^{2n-2m}\ \}\ ]^T$$

The dynamic equations of the Hamiltonian H_T can be expressed as

$$\dot{q}^i = \frac{\partial H}{\partial p^i} + \sum_{j=1}^{2m}(\lambda_j + \hat{u}_j)\frac{\partial \Phi^j}{\partial p^i} + \sum_{j=1}^{2n-2m}\tilde{u}_j\frac{\partial \Psi^j}{\partial p^i} \qquad i=1,....,n \tag{3.i}$$

$$\dot{p}^i = -\frac{\partial H}{\partial q^i} - \sum_{j=1}^{2m}(\lambda_j + \hat{u}_j)\frac{\partial \Phi^j}{\partial q^i} - \sum_{j=1}^{2n-2m}\tilde{u}_j\frac{\partial \Psi^j}{\partial q^i} \qquad i=1,....,n \tag{3.ii}$$

The vector form of (3) can be written as

$$\dot{q} = \frac{\partial H}{\partial p} + A_1(\hat{u} + \lambda) + B_1\tilde{u} \tag{4.i}$$

$$\dot{p} = -\frac{\partial H}{\partial q} - A_2(\hat{u} + \lambda) - B_2\tilde{u} \tag{4.ii}$$

where

$$A_1 = \begin{bmatrix} \frac{\partial \Phi^1}{\partial p^1} & \cdots & \frac{\partial \Phi^{2m}}{\partial p^1} \\ \vdots & \cdots & \vdots \\ \frac{\partial \Phi^1}{\partial p^n} & \cdots & \frac{\partial \Phi^{2m}}{\partial p^n} \end{bmatrix} \qquad A_2 = \begin{bmatrix} \frac{\partial \Phi^1}{\partial q^1} & \cdots & \frac{\partial \Phi^{2m}}{\partial q^1} \\ \vdots & \cdots & \vdots \\ \frac{\partial \Phi^1}{\partial q^n} & \cdots & \frac{\partial \Phi^{2m}}{\partial q^n} \end{bmatrix} \tag{5.i}$$

$$B_1 = \begin{bmatrix} \frac{\partial \Psi^1}{\partial p^1} & \cdots & \frac{\partial \Psi^{2n-2m}}{\partial p^1} \\ \vdots & \cdots & \vdots \\ \frac{\partial \Psi^1}{\partial p^n} & \cdots & \frac{\partial \Psi^{2n-2m}}{\partial p^n} \end{bmatrix} \qquad b_2 = \begin{bmatrix} \frac{\partial \Psi^1}{\partial q^1} & \cdots & \frac{\partial \Psi^{2n-2m}}{\partial q^1} \\ \vdots & \cdots & \vdots \\ \frac{\partial \Psi^1}{\partial q^n} & \cdots & \frac{\partial \Psi^{2n-2m}}{\partial q^n} \end{bmatrix} \tag{5.ii}$$

The required torque input at the joints of the manipulators is given by

$$\tau = (-A_2 + \dot{M}(q)A_1 + M(q)\dot{A}_1)\hat{u} + M(q)A_1\dot{\hat{u}} + (-B_2 + \dot{M}(q)A_1 + M(q)\dot{B}_1)\tilde{u} + M(q)B_1\dot{\tilde{u}} \tag{6}$$

REFERENCES

[1] M.Brady et.al.(editor), "Robot Motion: Planning and Control," *MIT Press, 1982.*

[2] R.P.C.Paul, "Robot Manipulators: Mathematics, Programming, and Control," *MIT Press, 1981.*

[3] N. Harris McClamroch and Anthony M.Bloch, "Control of Constrained Hamiltonian Systems and Applications to Control of Constrained Robots," *Dynamical Systems Approaches to Nonlinear Problems in Systems and Circuits edited by F.M.A Salam and M.L. Levi, SIAM, 1988, pp. 394-403.*

[4] M.H.Raibert and J.J. Craig, "Hybrid Position/Force Control of Manipulators," *ASME J. of Dynamic, Systems, Measurement and Control, 102, 1981, 126-133.*

[5] M.Takegaki and S.Arimoto, "A New Feedback Method for Dynamic Control of Manipulators," *J. of Dynamic Systems, Measurement, and Control Vol.102 June 1981, pp. 119-125.*

[6] M.Takegaki and S.Arimoto, "Stability and Robustness of PID Feedback Control for Robot Manipulators of Sensory Capability," *Robotics Research, M.Brady and R.Paul (editors), MIT Press, 1984, 783-799.*

[7] F.M.A.Salam, "Velocity feedback Control and Dynamic Properties of Robot Manipulators, " *The 26th IEEE Conference on Decision and Control, Los Angeles, December 9-11, 1987.*

[8] C. S. Yoon and F. M. A. Salam, *"Compliant Control of Constrained Robot Manipulators: A Mathematical Formulation and Control Expressions," 27th IEEE Conference on Decision and Control, 1988, submitted.*

FLEXIBLE ROBOT MODELS WITH REVOLUTE AND PRISMATIC JOINTS - - HANDLING OF CLOSED LOOPS

Michael Riemer and Jörg Wauer
Institut für Technische Mechanik
Universität Karlsruhe
Kaiserstraße 12, D-7500 Karlsruhe 1, FRG

Synopsis. Supplementing recent investigations generating the equations of motion for flexible industrial robot models with revolute and prismatic joints here the treatment of closed loops is presented.

1. Introduction

In the dynamics of multibody systems with deformable components, structures with material boundary conditions, e.g., revolute joints, and tree structure, e.g., open chains, have been considered. Until quite recently, only a few contributions have taken into consideration the effects of non-material constraints, e.g., by means of prismatic joints /1/ and the handling of closed loops /2/, respectively. But these effects have been considered neither completely nor simultaneously. The first detailed investigations deriving the equations of motion for such non-material systems, but without closed loops, have been carried out in the recent past /3,4/. As a supplement, here the extension to closed loop systems will be discussed, namely, in the first part with an example of a simple one-body distributed parameter system and in the second part for a planar two-body system with beam-shaped structural members as a typical sub-class of general flexible non-material multibody systems involving closed loops. The results of /3,4/ and this short communication will be combined in a forthcoming paper /5/.

2. Axially moving string as a simple model

The simplest prototype for a non-material flexible system involving closed loops is represented in Figure 1. The string pre-stressed by an axial constant force H_0, performs an overall motion s(t) in the axial direction and superimposed small vibrations described by the vector field of displacements u. The motion is constrained by the material, moving support A and the non-material, locally fixed support C. For the co-ordinate system we choose the inertial frame $e_{\hat{k}}$ ($\hat{k}$=1,2) and the locally attached tangential unit base vectors e_k (k=1,2). They define the non-deformed reference configuration and the Lagrangian co-ordinate (LC) ξ^1 of the string.

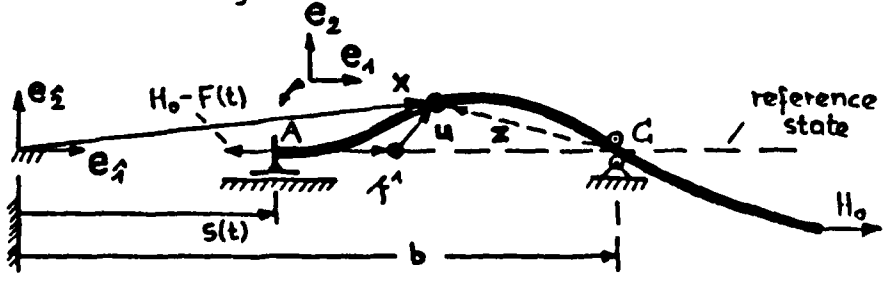

Figure 1

Here the transformation

$$e_k = a^{\hat{l}}_{\cdot k}\, e_{\hat{l}} \;, \quad (a^{\hat{l}}_{\cdot k}) = \begin{bmatrix} 1 & 0 \\ 0 & 1 \end{bmatrix} \tag{1}$$

between the reference frames is very simple, but an essential property holds, in general: Locally attached tangential base vectors (here e_k) are independent of the deformations of the body they belong to. Applying Kirchhoff-Hamilton's principle (KHP) /6/

$$\delta_\xi \int_{t_1}^{t_2} (T-V)\,dt + \int_{t_1}^{t_2} W_{virt}\, dt = 0 \tag{2}$$

the kinetic and potential energies T and V as well as the virtual work W_{virt} have to be established in advance. For a string their non-linear formulation is given in /7, eq.(9)/. In order to handle the problem in the sense of multibody systems, first of all we consider the underlying tree structure, which is obtained by removing support C. Then (2) yields by means of a classical mathematical procedure, the non-linear field equations /6/

$$-\mu u^{\hat{1}}_{\cdot,tt} + N_{\cdot,1} = 0\,, \quad N = EA\left(u^{\hat{1}}_{\cdot,1} + \frac{3}{2} u^{\hat{1}}_{\cdot,1} u^{\hat{1}}_{\cdot,1} + \frac{1}{2} u^{\hat{2}}_{\cdot,1} u^{\hat{2}}_{\cdot,1}\right),\ EA = \text{flexural stiffness},$$

$$-\mu u^{\hat{2}}_{\cdot,tt} + Q_{\cdot,1} = 0\,, \quad Q = EA\, u^{\hat{2}}_{\cdot,1} u^{\hat{2}}_{\cdot,1}\,, \quad \mu = \text{mass per length} \tag{3}$$

for the one-field problem with geometrical boundary conditions at $\xi^1=0$ (support A) and dynamical ones at the free end $\xi^1=1$. If s(t) is not prescribed, the equation for the overall motion is

$$S = F(t) - \mu \int_0^1 (\ddot{s} + u^{\hat{1}}_{\cdot,tt})\, d\xi^1 = 0 \tag{3a}$$

with the given force F(t). Now the above discussed tree structure (Fig. 1 without support C) is closed by adding the <u>non-material</u> support C at the position

$$r = r^{\hat{k}} e_{\hat{k}}, \quad (r^{\hat{k}}) = \begin{bmatrix} b \\ 0 \end{bmatrix} \tag{4}$$

in the inertial frame. Hence, the corresponding constraint equation for the string is

$$\begin{aligned} C &= x(\xi^1 = \xi_c(t), t) - r = 0 \quad \text{or} \\ C^{\hat{k}} &= x^{\hat{k}}(\xi^1 = \xi_c(t), t) - r^{\hat{k}} = 0, \ \hat{k} = 1,2 \end{aligned} \tag{5}$$

wherein

$$x = \left([s(t) + \xi^1 + u^1]\, a^{\hat{l}}_{\cdot 1} + u^2\, a^{\hat{l}}_{\cdot 2}\right) e_{\hat{l}} \tag{6}$$

is the position vector of an arbitrary material point ξ^1 in the deformed state $u = u^k e_k$ measured in the inertial frame $e_{\hat{k}}$. Therewith $(5)_2$ reads

$$\hat{k}=1:\ s(t) + \xi_c(t) + u^1(\xi_c, t) = b, \quad \hat{k}=2:\ u^2(\xi_c, t) = 0. \tag{7}$$

Undoubtedly $(7)_2$ is obvious looking at Figure 1, but only a formalism like (4), (5) and (6) can be used to establish algorithms for general multibody systems. $(7)_1$ determines the LC $\xi_c(t)$ of the actual material point (MP) at support C. The additive supplement to KHP (3) then is

$$\delta\chi = \delta_z \int_{t_1}^{t_2} \lambda_{\hat{k}}(t)\, C^{\hat{k}}\, dt, \tag{8}$$

with a minimal set of Lagrangian multipliers (LM's) $\lambda_{\hat{k}}$ depending on time t only. In $C^{\hat{k}}$, (5), it is essential that only the actual MP with the LC $\xi^1=\xi_c(t)$ is considered. This requires the variational operator δ_z in (8) instead of the classical one, δ_ξ. The relationship between the locally measured, non-material variation (z=const. in Fig. 1) δ_z at support C and the material one (ξ^1=const.) δ_ξ is given by the chain rule /7/

$$\delta_z[\,] = [\,]_{,1}\,\delta_z\xi_c + \delta_\xi[\,] \tag{9}$$

indicating the change of MP's at C by the convective part $[\,]_{,1}\delta_z\xi_c$. (8) can be evaluated in the form

$$\delta\chi = \int_{t_1}^{t_2} \lambda_{\hat{k}}(t)\,\delta_z C^{\hat{k}}\, dt = \int_{t_1}^{t_2} \left[\lambda_{\hat{1}}(\delta s+\delta_z\xi_c+\delta_z u^1|_{\xi_c}) + \lambda_{\hat{2}}\delta_z u^2|_{\xi_c}\right] dt, \tag{10}$$

wherein all variations are independent and also $(5)_2$ is taken into account. Because of support C, the integration in (2) over the interval [0,1] must be split into the two non-material intervals $[0,\xi_c(t))$ and $(\xi_c(t),1]$, which lead also to variations δ_z defined in (9). Following the arguments in /6/, together with (10), the new equations of motion for the closed-loop case can be derived: The <u>two</u> field equations (3) remain valid for the two fields left and right of C, respectively. The <u>four</u> material boundary conditions remain unchanged, too. The "open-chain" equation (3a) for the overall motion s(t) suffers a correction due to

$$S+\lambda_{\hat{1}}+[U]^+_-=0,\quad [U]^+_- = -\mu\left[\frac{(\dot{s}+u^1_{,t})^2}{1+u^1_{,1}}\right]^{\xi_c+0}_{\xi_c-0}. \tag{11}$$

Additionally the <u>four</u> non-material boundary conditions at C occur in the form

$$\begin{aligned} &\lambda_{\hat{1}} + [U+N]^+_- = 0, \quad \lambda_{\hat{2}} + [W+Q]^+_- = 0,\\ &[u^1]^+_- = 0, \quad [u^2]^+_- = 0, \quad [W]^+_- = -\mu\left[\frac{(\dot{s}+u^1_{,t})u^2_{,t}}{1+u^1_{,1}}\right]^{\xi_c+0}_{\xi_c-0} \end{aligned} \tag{12}$$

together with <u>three</u> equations for the constraints

$$C^{\hat{k}}=0, \quad \lambda_{\hat{1}} - [(W+Q)u^2_{,1} + (U+N)u^1_{,1}]^+_- = 0 \tag{13}$$

beeing in accordance with the number of additional unknowns $\lambda_{\hat{k}}(t)$ ($\hat{k}$=1,2) and $\xi_c(t)$. In order to discuss the method of "body-doubling" /8/, the system in Figure 1 must be divided into an open chain (system I: string plus support A only) and the doubled body (system II: string with support C only) having tree structure, too. Each of the bodies have half the original mass. To fit the two subsystems I,II it is necessary to match the node co-ordinates by means of their position vectors. Using the reference frames in Figure 1 for both I and II, we obtain

$$A^k = {}^{II}u^k(\xi^1=0,t)=0, \quad C^{\hat{1}} = s(t)+\xi_c+{}^{I}u^1(\xi_c,t)-b=0, \quad C^{\hat{2}} = {}^{I}u^2(\xi_c,t)=0, \qquad (14)$$

wherein $C^{\hat{k}}$=0 is identically the constraint equation (5), here for body I. Matching the MP's in the fields results in

$$f^k = {}^{I}u^k - {}^{II}u^k = 0, \quad k=1,2. \qquad (15)$$

In order to generate the supplements for the existing equations of motion (3),(3a), six LM's have to be introduced due to

$$\delta\chi = \int_{t_1}^{t_2} \left[\lambda_{\hat{k}}(t)\, C^{\hat{k}} + {}_A\lambda_k(t)\, A^k + \int_0^l {}_f\lambda_k(\xi^1,t)\, f^k\, d\xi^1\right] dt. \qquad (16)$$

Compared with (10), the method of "body-doubling" need more LM's and, hence, four additional equations. But the most important difference is the dependence of two of the position co-ordinate ξ^1, leading to considerable complications during the discretization procedure, which is usually used to obtain approximate solutions.

3. Two-body robot model (see /5/)

The considerations carried out in the last chapter will now be extended to a more practical system. It consists of two elastic bars I and J (see Figure 2). They perform a general overall motion $x(t)$ and $\varphi(t)$ together with a rotational and translational rigid body motion $\alpha(t)$ and $s(t)$ of the second component, J, relative to the other one, I. The relative motion is realized by the non-material revolute-prismatic joint G. Small plane elastic vibrations denoted by the vector fields of displacements ${}^{I}u, {}^{J}u$ and the scalar fields of bending angles ${}^{I}\vartheta, {}^{J}\vartheta$ are superimposed. In Timoshenko's beam theory $\mathbf{u}$ is independent of ϑ due to the shear deformation. The transformation between the reference frames can be performed analogously to (1) as well as the generation of the equations of motion for the underlying tree structure (after removing joint C). Closing the open chain by prescribing the path of C in the inertial frame along a smooth curve $\mathbf{r}$ result in constraint equations (similar to (4),(5)) with a minimal set of LM's. The associated supplement (similar to (8)) together with the operators of the tree structure lead to <u>five</u> integro-differential equations for the overall motion, <u>nine</u> partial differential equations for the deformations, <u>three</u> non-material boundary conditions at G, and <u>three</u> additional constraint equations. All equations are coupled to each other and contain non-classical terms. For details see reference /5/.

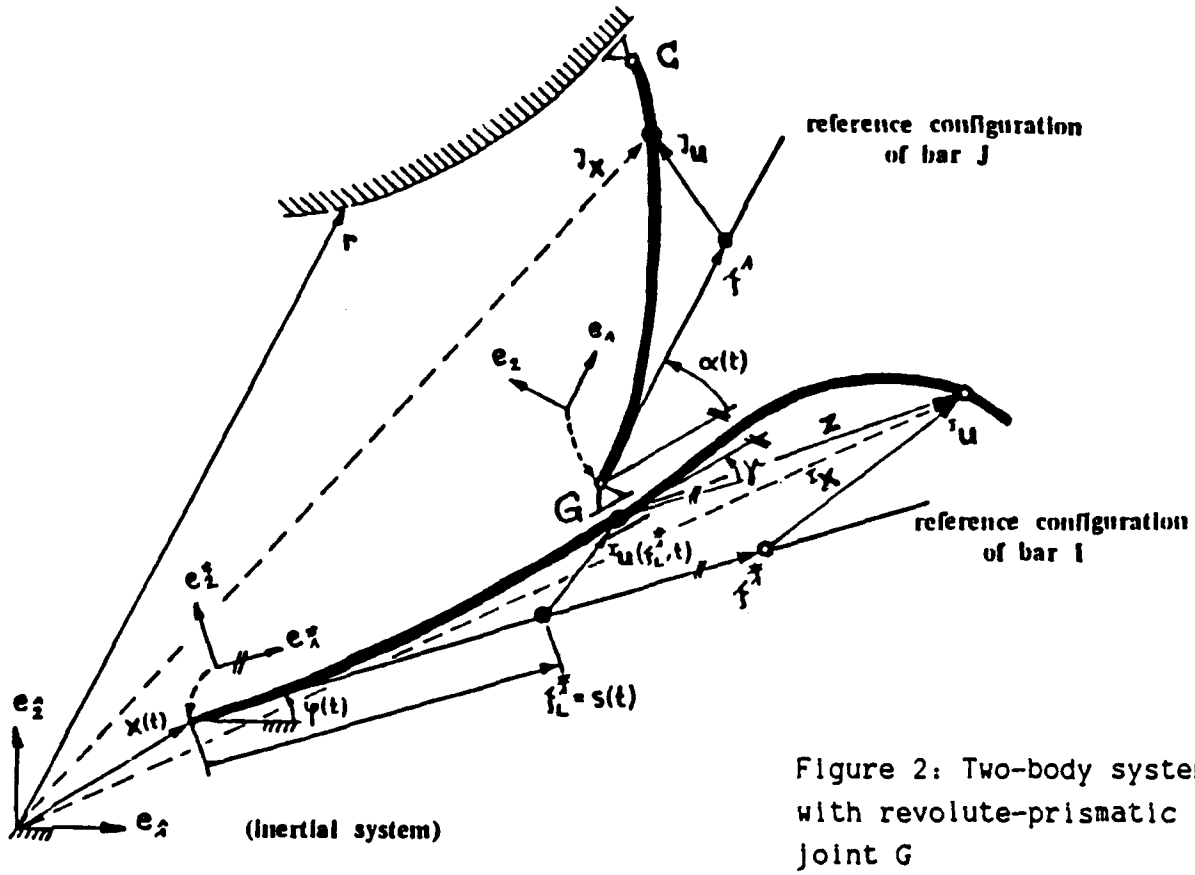

Figure 2: Two-body system with revolute-prismatic joint G

4. Conclusions

Extensions of flexible multibody systems with tree structure to such cases involving closed loops denote an important topic in the dynamics of robotics, for example. If the connecting joints belong to the group of so-called non-material constraints, e.g., a prismatic joint, not only the analytical description of the kinematics and the non-classical handling of variational and differential operators, but also the treatment of closed loops lead to considerable complications. The formalism presented here results in a minimal set of equations of motion, which can be reduced by direct variational approaches to ordinary differential equations. The method remains fundamentally unchanged when applied to spatial motions or three-dimensional components.

References

/1/ LILOV, L., WITTENBURG, J., Dynamics of Chains of Rigid Bodies and Elastic Rods with Revolute and Prismatic Joints, In Bianci/Schiehlen (eds.): Dynamics of Multibody Systems, Springer, 1986, p.141-152.

/2/ LILOV, L. K., Dynamics of Elastic Multibody Systems Involving Closed Loops, In Bianci/Schiehlen (eds.): Dynamics of Multibody Systems, Springer, 1986, p.129-140.

/3/ RIEMER, M., WAUER, J., Zur Behandlung von Schubgelenken in Mehrkörpersystemen mit verformbaren Teilstrukturen, ZAMM (1988), to appear.

/4/ RIEMER M., WAUER, J., Equations of Motion for Hybrid Industrial Robot Models with Revolute and Prismatic Joints, ICIAM-Conference Paris, 1987, unpublished.

/5/ RIEMER, M., WAUER, J., Equations of Motion for Flexible Multibody Systems with Revolute and Prismatic Joints, CISM-IFToMM-Conference, Udine, 1988, to appear.

/6/ RIEMER, M., Zur Theorie elastischer Kontinua mit nichtmateriellen Übergangsbedingungen, Dr.-Ing. Thesis, Univ. Karlsruhe, 1985.

/7/ RIEMER, M., Anwendung des Prinzips von Hamilton auf die mit konstanter Geschwindigkeit bewegte Saite, ZAMM (1986), p.T78-T80.

/8/ WOLZ, U., Dynamik von Mehrkörpersystemen - Theorie und symbolische Programmierung, Dr.-Ing. Thesis, Univ. Karlsruhe, Fortschr.-Ber. VDI-Z., R. 11, Nr. 75, 1985.

STABILITY OF FLEXIBLE MULTIBODY SYSTEMS DYNAMICS IN THE PRESENCE OF CLOSED LOOPS

Amirouche F.M.L
Assistant Professor
Dpt of Mechanical Engineering
University of Illinois at Chicago
Chicago Ill 60680

ABSTRACT

A common problem in the analysis of rigid and flexible constrained multibody dynamics arises when the Jacobian matrix becomes singular.This in fact result in some numerical instability in the integration of the governing equations of motion.

Usually when a multibody system is subjected to simple nonholomic and holonomic constraints of the form BY=G(where B denotes the Jacobian matrix ,Y the generalized speeds and G is a function of time t),it is customary to assume that B has full rank and its orthogonal complement array C in the constrained space exists.However in certain configuration the loop can go from 3D to 2D type of formation causing the Jacobian matrix to be singular.A common approach to insure stability of the system is to avoid the singularity position.This require more efforts than needed and doesn't guaranty the continuity of the system motion in the neighborhood of singular positions.

An algorithm based on the Pseudo-Uptriangular-Decomposition -Method(PUTD) introduced by Amirouche et al is used to detect when a particular constraint equation vanishes in the process of the uptriangulazation of the Jacobian matrix.This identification is essential as it permits one to compute the orthogonal complement array even when B changes rank.Two

methods are then introduced to insure the numerical stability of complex dynamical systems with variable closed-loops.

SESSION 5

EXPERIMENTS IN NONLINEAR DYNAMICS

THURSDAY - 0830 - 1000

June 2, 1988

FRACTALS AND CHAOS IN ELASTIC SYSTEMS

Lecture by

Francis C. Moon
Professor and Director
Sibley School of Mechanical
and Aerospace Engineering
Cornell University

ABSTRACT

In recent years new phenomena have been discovered in nonlinear dynamics, namely chaotic oscillations in deterministic systems. In this lecture physical examples will be discussed from mechanical, control, space structures and fluid-elastic systems. To describe this chaotic phenomena, new mathematical ideas have entered dynamics such as fractals. In this lecture I will illustrate how fractal concepts and Poincaré maps are used to describe strange attractors and other properties of chaotic systems such as basin boundaries. In particular, we show how to calculate the fractal dimension of a chaotic attractor from experimental data for nonlinear vibrations of an elastic beam and vibrations of fluid flow through a flexible tube. A discussion of new experimental techniques in nonlinear dynamics will be given. A demonstration of chaotic vibration will be performed.

Nonlinear Oscillation of a Flexible Cantilever: Experimental Results

Alan G. Haddow & Syed M. Hasan
Dept. of Mechanical Engineering
Michigan State University
East Lansing, Michigan

1. Introduction.

A collection of experimental results which describe the nonlinear oscillatory behavior of a flexible cantilever beam are presented. The approximate dimensions of the beam are 30" x 0.5" x 0.02" and it is forced through a sinusoidal base excitation in the axial direction. This is the "input" term. The response, or the "output" term, is measured by a strain-gage attached near the root of the cantilever. The following sections describe a number of the phenomena observed. The periodic or almost periodic responses occur for planar motion, whereas if non-planar motions arise, various forms of chaos result.

2. Linear Stability and Nontrivial Steady-States.

It is well documented that the dynamic stability of a beam excited by a sinusoidal displacement in the axial direction is given by a Strutt diagram. In the displacement-frequency parameter space there are wedge shaped boundaries which seperate the stable and the unstable regions. The nose of these regions occur at forcing frequencies that are equal to twice the linear natural frequencies of the system. They also occur at multiples and combinations of these natural frequencies. Figure 1 presents experimental data which define one of these regions. It is associated with the 4th natural frequency of the system. The excitation frequency is $\approx$ 92 Hz and for a set of parameters inside the unstable region, the model responds in the 4th mode. Linear theory predicts that this unstable response would grow exponentially. However, as the response grows the effects of non-linearities can not be ignored. This results in the beam attaining a steady-state. Keeping the magnitude of the base acceleration constant, it is possible to investigate the variation of the amplitude of this steady-state response as a function of the forcing frequency. Figure 2 presents such results. Note the large multi-valued region in which both trivial and nontrivial steady-state solutions are found.

3. Transient Chaos.

If the frequency is such that the response of the system is quite large, e.g. point A on Figure 2, then it is possible to observe transient chaos if the system is perturbed from its steady-state. For this value of force the response never remains chaotic, but always returns to either the trivial or the non-trivial, single mode, steady-state value. The basic form of the response while in this chaotic regime is similar to that given in Figure 4.

4. Steady-State and Intermittent Chaos.

Increasing the level of the force slightly (see Figure 1) results in the frequency response curve presented in Figure 3. If the frequency is decreased enough an out-of-plane mode is excited and a chaotic response results. The term steady-state chaos refers to the fact that the response remains chaotic for all time. A time trace of such a response is presented in Figure 4 along with its FFT. By altering only the initial conditions the stable, trivial solution can of course be attained. In addition it is possible to find multi-mode responses. Figure 5 shows such a case.

5. Extremely Low Subharmonic Response.

A time trace of the input and the output are presented in Figure 6 for a forcing frequency of ≈ 190 Hz. (Note the change in the time scales.) Initially the beam responds at the forcing frequency but as time progresses, the energy seems to cascade down through the modes. The authors believe this is a consequence of internal resonances. Eventually a very low frequency, steady-state response is attained.

6. Concluding Remarks

A selection of some experimental observations of the nonlinear behaviour of a cantilever beam have been presented. Work is in progress exploring a number of the phenomena in more detail, particularly the extremely low subharmonic response. This type of energy transfer to remote modes has received little attention in the past.

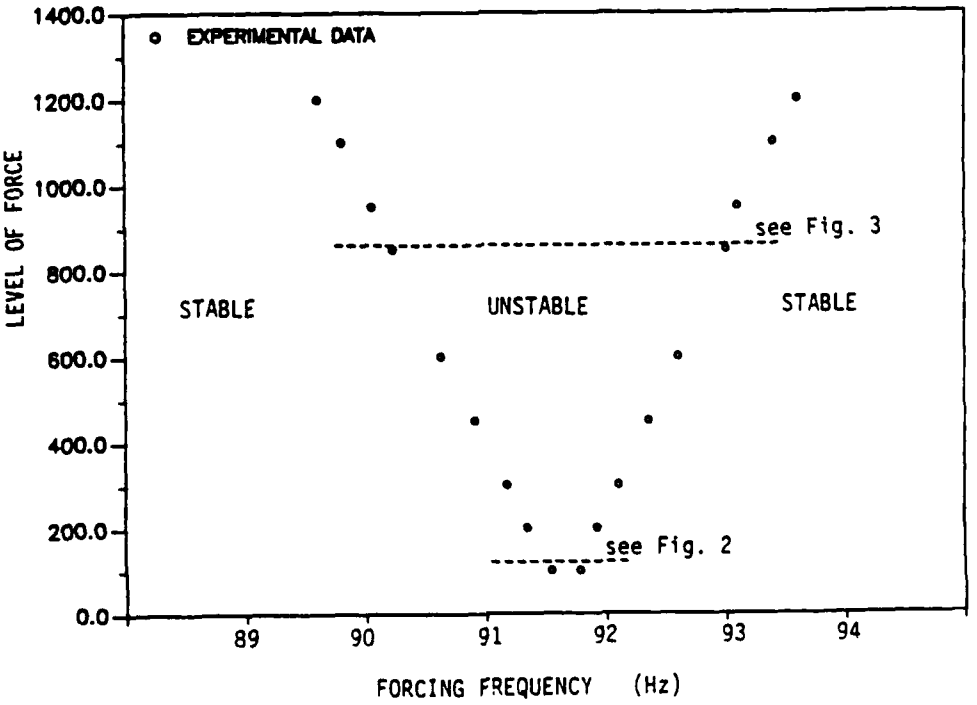

FIGURE 1. Stability diagram for the fourth mode.

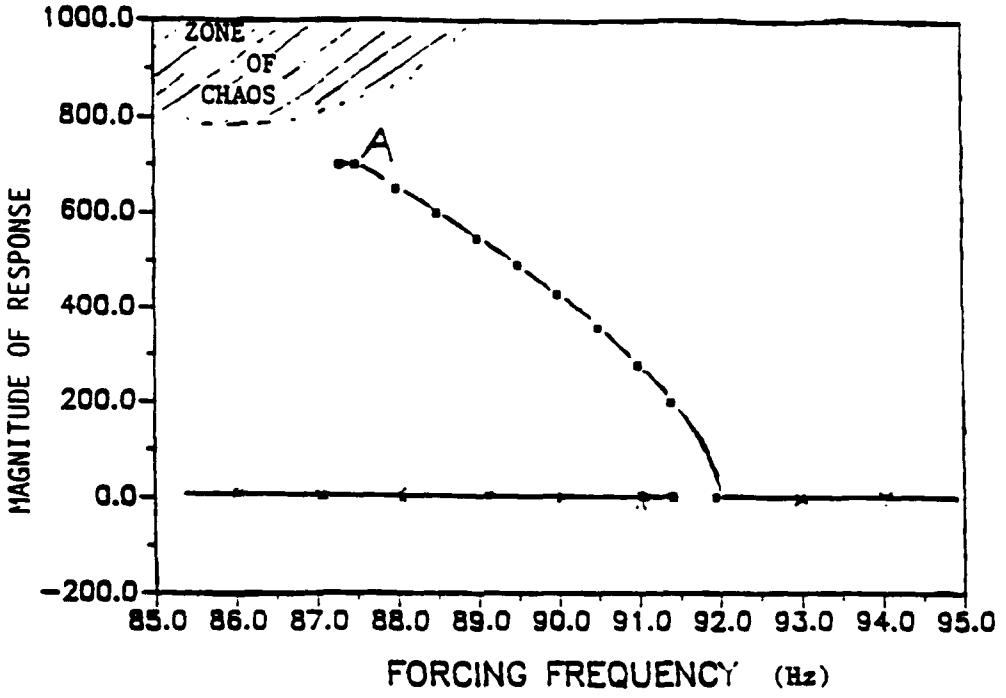

FIGURE 2. Steady-state parametric response. Level of force constant (see Fig. 1).

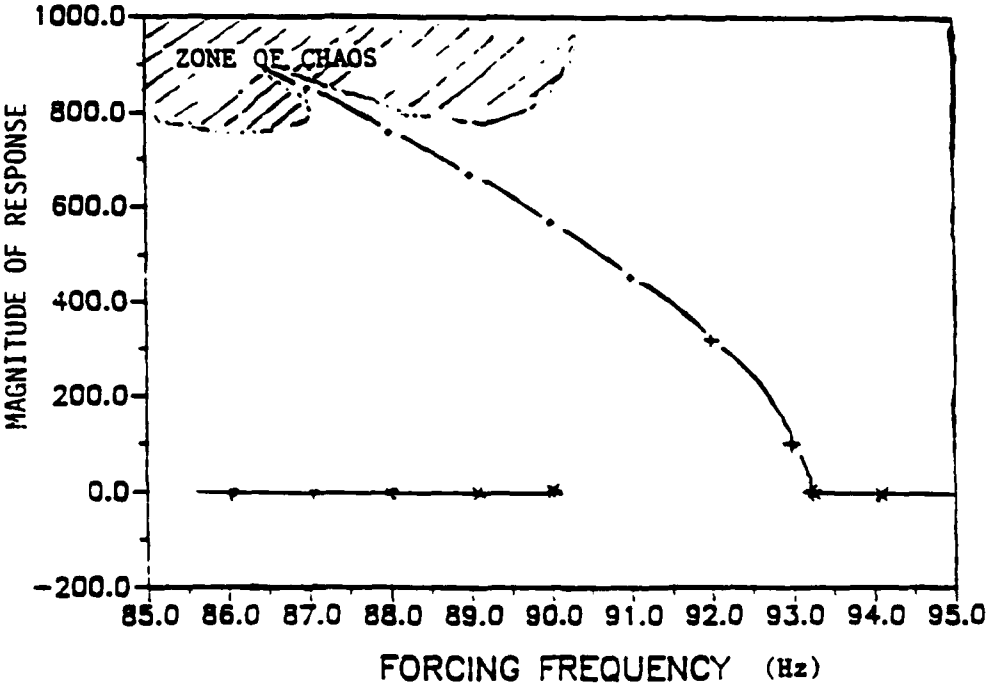

FIGURE 3. Steady-state parametric response. Level of force constant (see Fig. 1).

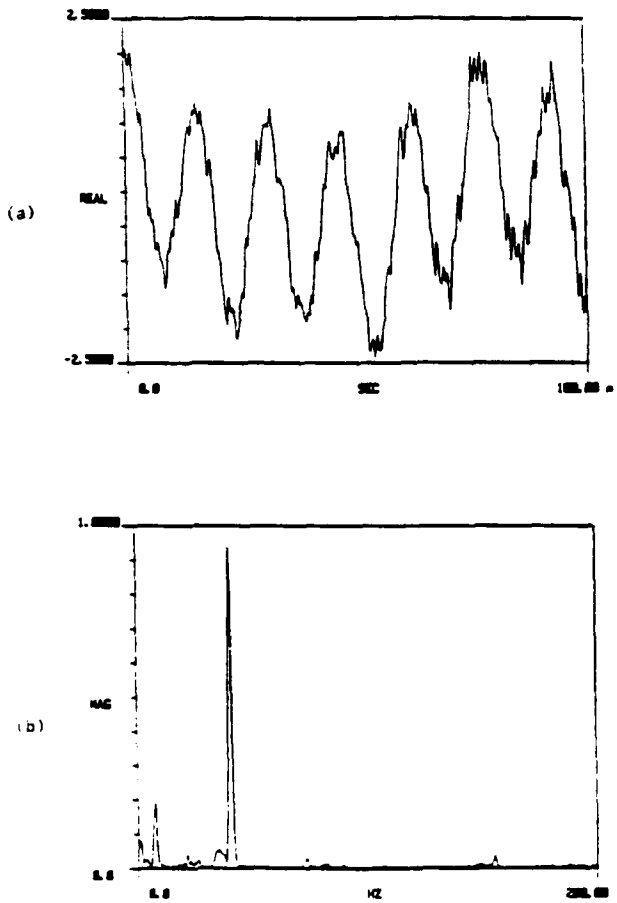

FIGURE 4. Chaotic response for a forcing frequency of 85.5 Hz. (a) Time trace of the output. (b) FFT of (a).

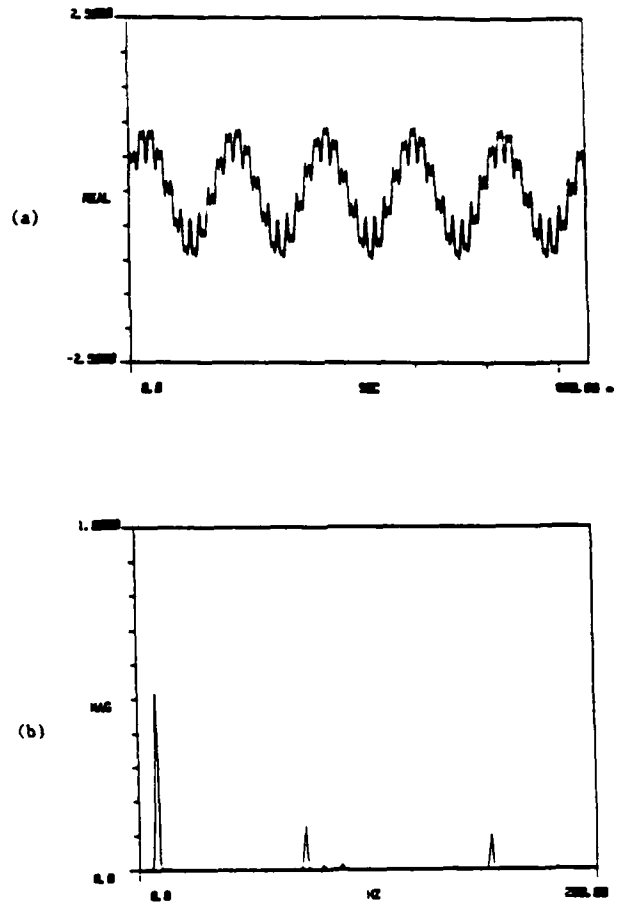

FIGURE 5. Combination of responses at a forcing frequency of 85.5 Hz. (a) Time trace of the output. (b) FFT of (a).

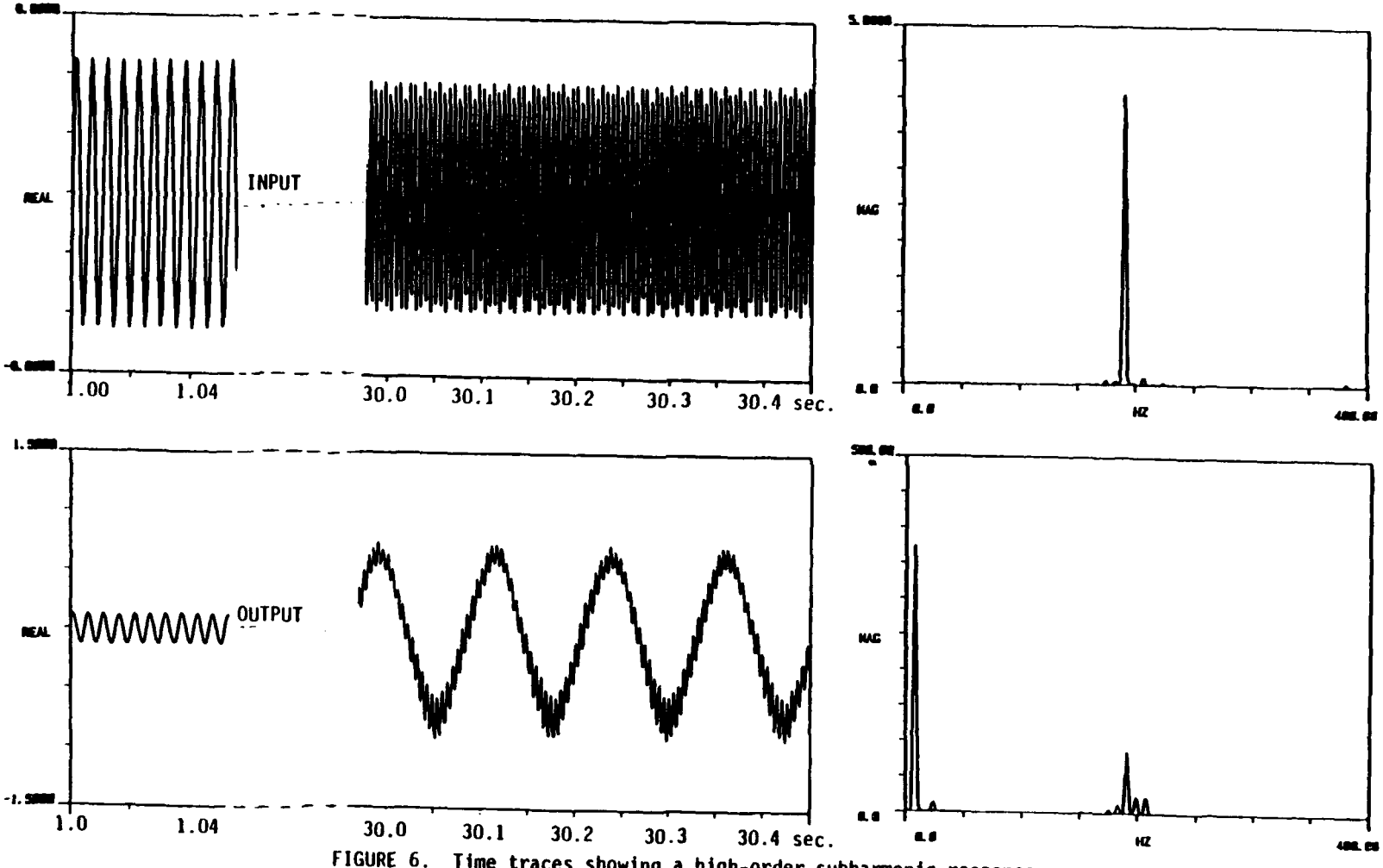

FIGURE 6. Time traces showing a high-order subharmonic response. (FFT's of the steady-state portions.)

NONLINEAR RESONANCES AND CHAOTIC MOTION IN A FLEXIBLE PARAMETRICALLY EXCITED BEAM

T.D. Burton and M. Kolowith
Department of Mechanical and Materials Engineering
Washington State University
Pullman, WA 99164-2920 USA

ABSTRACT

We present experimental and analytical results for a flexible, parametrically excited, vertically mounted beam. The exciting frequency Ω is near twice the fourth mode natural frequency ω_4. We have observed steady, periodic motions associated with the fourth mode principal parametric resonance and chaotic motions, both occurring in a narrow band near $\Omega = 2\omega_4$.

INTRODUCTION

A schematic of the experimental setup is shown in Figure 1. The test specimen, mounted as a vertical cantilever, is SAE 1094 steel of dimensions 35.625 in x 1 in x 1/32 in. The beam is very flexible in the "in-plane" direction and very stiff in the "out-of-plane" direction. The in-plane flexural stiffness EI = 76.29 lb-in^2 and the mass per unit length $\rho = 0.2388 \times 10^{-4}$ lb sec^2/in^2. The vibrational motion was monitored with a strain gage, which was mounted at X/L $\approx$ 0.2, near the first peak of the fourth mode shape. The harmonic base motion was monitored with an accelerometer. The five lowest natural frequencies of the beam, determined experimentally, are approximately 0.5 hz, 4.8 hz, 14.0 hz, 27.8 hz, and 46.0 hz, respectively.

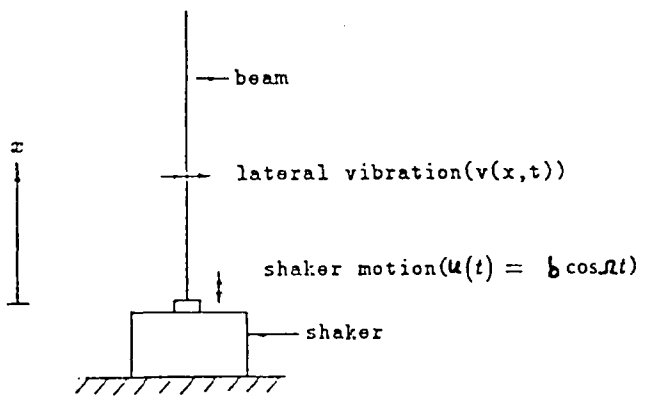

Figure 1. Schematic of experimental setup.

The objectives of the experiment were 1) to study the steady state, periodic motions of the nonlinear resonant response associated with the principal parametric resonance of the fourth mode ($\Omega \approx 2\omega_4$), 2) to study the chaotic motions which were observed to occur in this same frequency range, and 3) to study the connection between the two types of motion, particularly the transitions form periodic to chaotic motion and vice versa.

Moon [1] has studied experimentally the chaotic motions of a harmonically driven, magnetically buckled beam. We note three basic differences in our experimental conditions: 1) the beam is driven parametrically rather than directly, 2) the vertical configuration is statically stable; thus, multiple static equilibria are not present, and 3) the nonlinearities are a result of the geometry of large amplitude motion, rather than being due to an external

agent. Presented in the following sections are analytical and experimental results for the steady, periodic forth mode motion and experimental results which characterize the chaotic motion.

ANALYSIS AND EXPERIMENTAL RESULTS: PERIODIC MOTIONS

If the base excitation parameter $b\Omega^2$ is relatively small and if $\Omega \approx 2\omega_4$, the system exhibits planar, unimodal, periodic motions characteristic of a single degree of freedom, parametrically excited oscillator having a softening nonlinearity. The analysis of these motions is based on the following equation of undamped, large amplitude, planar motion, which was derived by Krishnamurthy [2], based on the previous analysis of Crespo da Silva and Glynn [3]:

$$\ddot{v} + v'''' + \left[v'(v'v'')'\right]' + \frac{1}{2}\left[v' \int_1^S \left[\int_0^{S_1} v'^2 dS_2\right]^{\cdot\cdot} dS_1\right]' = (u_0\Omega_0^2 \cos\Omega_0 T - g_0)[(1-S)v'' - v']. \tag{1}$$

Here dots are derivatives with respect to the dimensionless time $T = (EI/\rho L^4)^{\frac{1}{2}}t$, $v = V/L$, and $u_0 = b/L$.

In equation (1) the first of the nonlinear terms is a static, hardening nonlinarity arising from the potential energy stored in bending, while the second nonlinear term is softening and is a result of the kinetic energy of axial motion. As noted by Haight and King [4], the latter, inertial nonlinearity is the dominant nonlinear effect.

If one assumes the motion to be dominated by a single mode, $v(s,T) = \phi(S)z(\tau)$ where $\phi(S)$ is the linear mode four free vibration mode shape, equation (1) may be converted to following modal equation for the fourth mode:

$$\ddot{y} + y[1 + 2q\cos 2\bar{\Omega}\tau] + \alpha_1 y(y^2)^{\cdot} + \alpha_2 y^3 = 0. \tag{2}$$

Here $\bar{\Omega} = \Omega/2\omega_4$, dots are derivatives with respect to a new time $\tau = \delta^4 T, \delta = 10.99554\ldots$ is the fourth mode eigenvalue, $y = \delta z, q = .9512u_o\delta^2\bar{\Omega}^2, \alpha_1 = 14.05$ and $\alpha_2 = 1.09$. The maximum value of the dimensionless displacement y is of the order of 0.10.

The measured mode four frequency response for the case $q \cong 0.014$ is shown in Figure 2. In the range $55.12hz < \Omega < 55.88hz$, the null solution $v(s,T) = 0$ is unstable. Stable and unstable nonzero solutions arise via pitchfork bifurcations at $\Omega_2 = 55.88hz$ and $\Omega_1 = 55.12hz$, respectively. These solutions coalesce in a saddle node bifurcation at $\Omega_3 \cong 54.12hz$. Thus, one observes the jump phenomenon as Ω is decreased through Ω_3 and as Ω is increased through Ω_1.

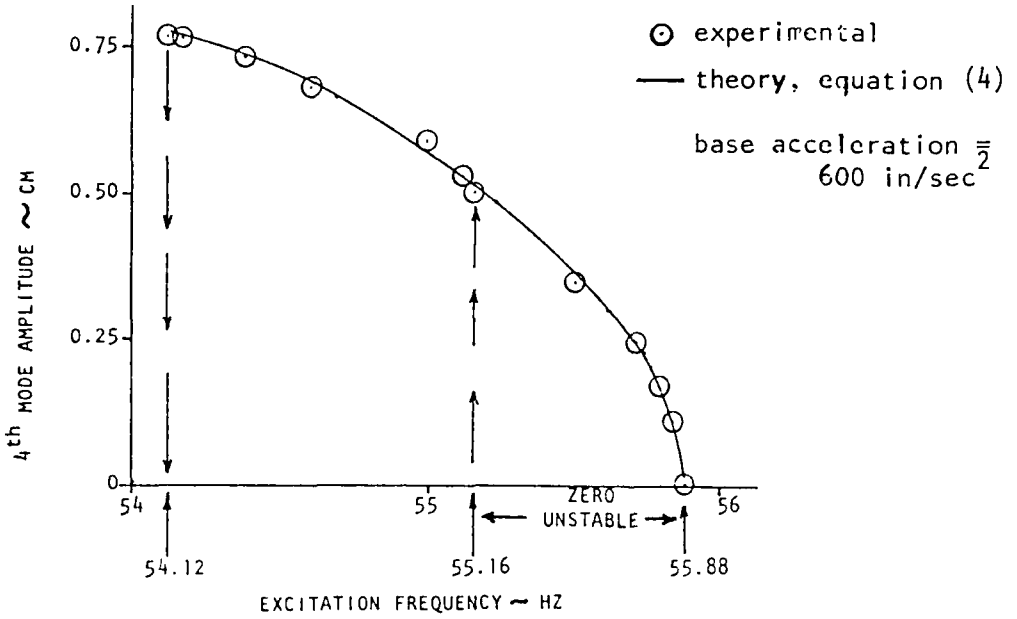

Figure 2. Frequency response, steady mode 4 motion.

In relating the experimental and analytical results, it is necessary to add some modal damping in equation (2). A nonlinear damping model was employed, so that the modal equation actually analyzed was

$$\ddot{y} + 2\zeta\dot{y}(1 + \mu y^2) + [1 + 2q\cos 2\bar{\Omega}\tau] + \alpha_1 y(y^2)^{\cdot\cdot} + \alpha_2 y^3 = 0 \tag{3}$$

The linear damping factor $\zeta = 0.002$ was measured form free vibration tests at small amplitude, while $\mu = 3500$ was determined so as to match the observed jump frequency Ω_3. (free vibration tests at large amplitude revealed an effective damping factor $\xi \cong 0.005$ at an amplitude of 0.75 cm, and this corresponds to $\mu \cong 2000$).

A harmonic balance (or first order multi-scale) analysis of equation (3), $y(\tau) = a\cos(\bar{\Omega}\tau + \phi)$ yields the following relation for the nonzero mode four steady state vibration amplitude a:

$$a^2 = \frac{\pm\left\{q^2 - \bar{\Omega}^2\left[2\xi\left(1 + \frac{\mu a^2}{4}\right)\right]^2\right\}^{\frac{1}{2}} + (1 - \bar{\Omega}^2)}{\alpha_1\bar{\Omega}^2 - \frac{3}{4}\alpha_3} \tag{4}$$

The comparison of experimental results and those given by equation (4) is shown in Figure 2. While both linear and nonlinear damping models provide good agreement for $\Omega \geq 54.4$hz, some nonlinear damping is clearly necessary if the bifurcation frequency Ω_3 is to be determined analytically.

It should be noted that numerical integration of equation (3) yields results which are virtually indistinguishable from those obtained from equation (4). This is because the steady state solutions to (3) are dominated by the fundamental harmonic (this is also true of the experimental results, as shown in Figure 3). This appears to occur because, for the case $\bar{\Omega} = 1, \alpha_2 = \xi = 0$, the exact periodic solution to equation (3) is simple harmonic, an unusual occurrence in nonlinear oscillators. We conclude that the steady state, periodic mode four motion is well predicted by the theory. Note, however, that the particular nonlinear damping model used is not necessarily physically motivated.

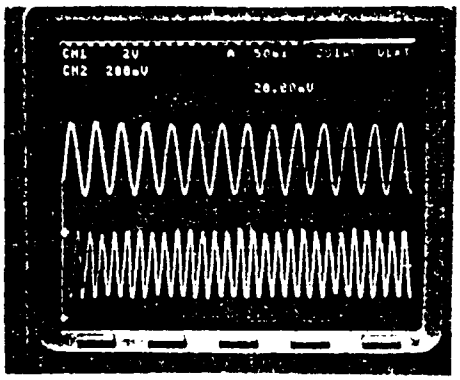

a) top: strain gage vs. time
bottom: base acceleration
vs. time

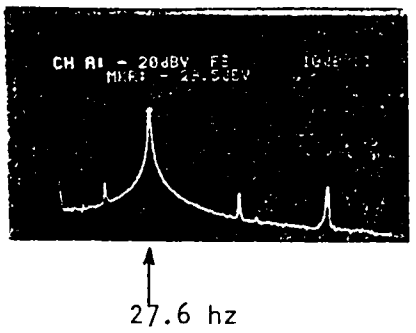

b) FFT of strain gage signal
(log scale)

Figure 3 Steady mode 4 response.

EXPERIMENTAL RESULTS: CHAOTIC MOTION

Chaotic motions were observed in certain regions of the parameter (b, Ω) space near $\Omega = 2\omega_4$. The strain gage output and frequency spectrum for a typical chaotic motion are shown in Figures 4(a) and 4(b) For reference, the frequency spectrum for a typical free oscillation, generating by striking the beam, is shown in 4(c). The chaotic response exhibits the characteristic irregularity in the time series and broadening in the spectrum. It is apparent that the lowest six or seven in-plane vibration modes are involved in the chaotic motion. Direct observation of the chaotic motion also indicates the lowest torsional mode to be present, accompanied by an out of plane displacement due to combined torsion and in-plane curvature.

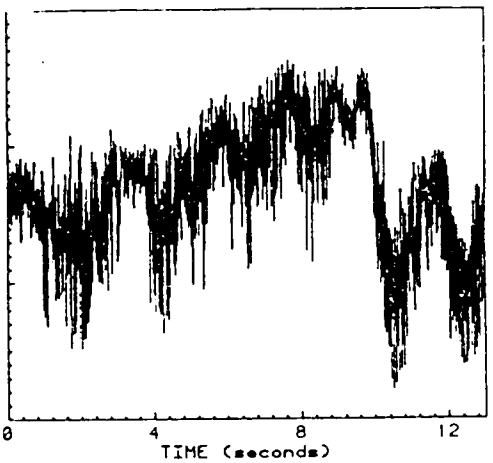

a) strain gage output
vs. time.

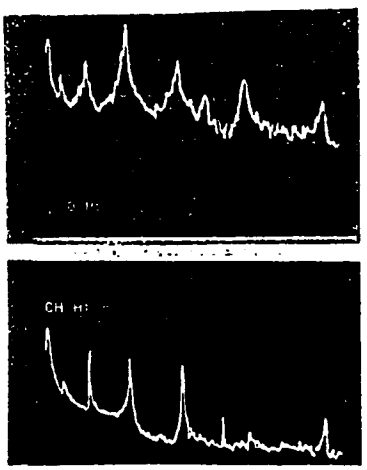

b) FFT of strain
gage output,
chaotic motion.

c) FFT of strain
gage output,
free oscillation.

Figure 4 Chaotic response.

Shown in Figure 5 are regions of the parameter plane (b, Ω) in which chaotic motions were observed. A stable chaotic motion was defined as one persisting for three minutes or longer (approximately 10,000 cycles of excitation). As Figure 5 shows, the minimum base excitation required to sustain chaotic motion occurs at $(\Omega/2\omega_4) \approx .985$, with a fairly sharp increase in required excitation level on either side of this frequency. In the "transition" regions the response was observed to cycle back and forth between chaotic and mode 4 motions, with more time spent in chaos as the base excitation was increased at fixed driving frequency. This may indicate a transition to chaotic motion via the intermittency route, in which, as the excitation level q is increased beyond

a critical value q_c, the fraction of time spent in chaos is proportional to $(q - q_c)^{1/2}$. We were unable to verify this conjecture quantitatively, however, as our exciter exhibited sufficient drift in excitation level over the long measurement times required (1-3 hours) that reliable determination of the fraction of time spent in chaos was not possible.

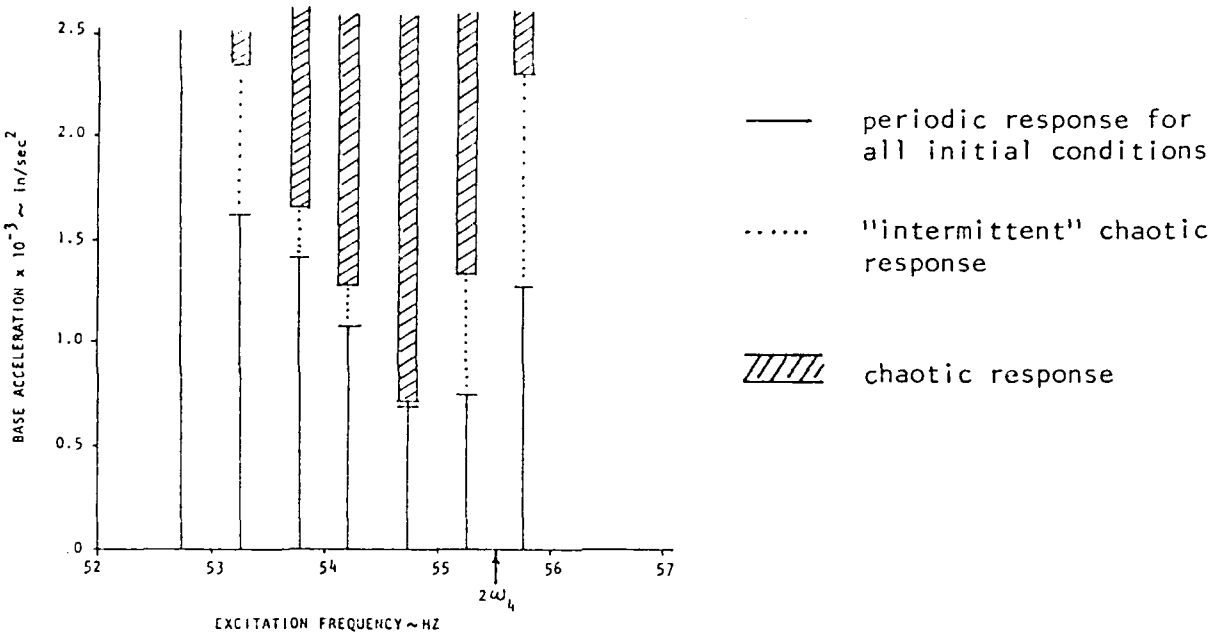

Figure 5. Regions of parameter plane for which chaotic motion occurs.

Numerical solutions of the single mode model, equation (3), did not exhibit chaotic behavior for any parameter values comparable to those of the experiments. Thus, an analysis of the loss of stability of the node 4 motion as a parameter is varied will require a multi-mode expansion of equation (1) and possibly the inclusion of torsion and out of plane motions as well. This is not surprising in view of the obvious participation of multiple modes in the chaotic response.

CONCLUDING REMARKS

The experimental and analytical results show the steady node 4 motions to be well described by a single mode model in which the kinetic energy of axial motion provides the dominant nonlinear effect. The chaotic motions observed at higher excitation levels will require a multi-mode model for their prediction. Furthermore, more precise measurements need to be made in order to characterize experimentally the transitions into/out of chaotic motion.

REFERENCES

1. Moon, F.C., Experiments on chaotic motion of a forced nonlinear oscillator: strange attractors, J. Appl. Mech, 47, 639-644 (1980).
2. Krishnamurthy, K., "Dynamics and control of flexible robotic manipulators," PhD thesis, Department of Mechanical Engineering, Washington State University (1986).
3. Crespo da Silva, M.R.M. and CC. Glynn, "Nonlinear flexural-flexural-torsional dynamics of inextensional beams. I. Equations of motion," J. Struct. Mech 6 (4), 437-448 (1978).
4. Haight, E.C. and W.W. King, "Stability of parametrically excited vibrations of an elastic rod," Proc. Southeastern Conf. Theor. Appl. Mech., 5th, Raleigh, NC (1969).

The Nonlinear Response of a Slender Beam Carrying a Lumped Mass to a Principal Parametric Excitation

by
Lawrence D. Zavodney
Department of Engineering Mechanics
The Ohio State University
Columbus, OH 43210
and
Ali H. Nayfeh
Department of Engineering Science and Mechanics
Virginia Polytechnic Institute and State University
Blacksburg, VA 24061

Many structural elements can be modelled as a slender continuous beam with concentrated masses located between the ends. When the support of a cantilevered beam undergoes motion, the beam is subject to vibration--either external or parametric, or both. Many researchers have investigated parametric resonances in structures; the text of Nayfeh and Mook [1] provides an extensive review of the literature. Schmidt and Tondl [2] also consider parametric resonances in their text. Haxton and Barr [3] studied a cantilever beam carrying a tip mass mounted onto another oscillating large mass; the system was considered an autoparametric vibration absorber. Sato, et al [4] analyzed the parametric response of a horizontal beam carrying a concentrated mass in a gravity field.

1. Derivation of the Nonlinear Differential Equation of Motion

The governing equation of motion of the beam shown in Figure 1 is derived using the Euler-Bernoulli theory. We assume that the effects of shearing deformation and rotatory inertia of the beam can be neglected. If the beam is kept relatively short (< 30 beam widths), the transverse vibration is purely in plane (if the lumped mass is symmetrical with the centerline), and if the excitation frequency is far below the first torsional mode, then we can safely neglect the torsional modes of the beam in the analysis. These assumptions are consistent with observations in the laboratory. Also, we do not observe any combination or internal resonances.

Keeping up to third-order terms, we obtain the governing equation:

$$EI(v_{ssss} + \frac{1}{2} v_{ssss}v_s^2 + 3v_s v_{ss} v_{sss} + v_{ss}^3) + (1 - \frac{1}{2} v_s^2 - \ldots)$$

$$\cdot [\rho + m\delta(s - d)]\ddot{v} - \frac{\partial}{\partial s}(Nv_s) + v_s v_{ss} \int_s^L [\rho + m\delta(\xi - d)]\ddot{v}d\xi$$

$$- \frac{\partial}{\partial s}\{J\delta(s - d)[\ddot{v}_s(1 + \frac{1}{2} v_s^2 + \ldots) + v_s \dot{v}_s^2]\}$$

$$+ (1 - \frac{1}{2} v_s^2 - \ldots)c\dot{v} + v_s v_{ss} \int_s^L c\dot{v}d\xi = 0 , \qquad (1)$$

where

$$N = \frac{1}{2}\rho\int_s^L\left[\int_0^\xi (v_\eta^2)_{tt}d\eta\right]d\xi - \frac{1}{2}m\int_s^L \delta(\xi - d)\left[\int_0^\xi (v_\eta^2)_{tt}d\eta\right]d\xi$$

$$+ m(\ddot{z} - g)\int_s^L \delta(\xi - d)d\xi + \rho L(1 - \frac{s}{L})(\ddot{z} - g) \ . \qquad (2)$$

2. Solution of the Linear Problem

The governing equation is nonlinear and does not admit a closed-form solution. Therefore, an approximate solution will be sought that satisfies both the equation and the boundary conditions. Since the boundary conditions are spatial and independent of time, we represent the solution of the nonlinear problem in the form

$$v(s,t) = \sum_n r\psi_n(s)G_n(t) \ , \qquad (3)$$

where r is a scaling factor, $\psi_n(s)$ is the shape function of the nth linear mode, and $G_n(t)$ is the time modulation of the nth mode and assumed to be harmonic. The undamped linear free vibration problem (without the rotatory effects of m) is governed by

$$EIv^{iv} + [\rho + m\delta(s - d)]\ddot{v} = 0 \ , \qquad (4)$$

Without loss of generality, we will solve explicitly for the first mode, with the understanding that the eigenfunction of the nth mode and its associated eigenvalue correspond to the nth characteristic.

The solution of (4) that satisfies the boundary conditions is

$$\psi(s) = C_1[(\sin\frac{k}{L}s - \sinh\frac{k}{L}s) - \Lambda(\cos\frac{k}{L}s - \cosh\frac{k}{L}s)]$$

$$+ C_1U(s - d)\{(h_1 - \Lambda h_2)[\sin\frac{k}{L}(s - d) - \sinh\frac{k}{L}(s - d)]$$

$$+ (h_3 - \Lambda h_4)[\cos\frac{k}{L}(s - d) - \cosh\frac{k}{L}(s - d)]\} \ , \qquad (5)$$

where the characteristic k is the nth root of the characteristic equation. The h_i in (5) are constants associated with k. Details of the derivation and solution are in reference [5].

3. Solution of the Nonlinear Differential Equation of Motion

Since we are analyzing the first mode, this continuous system can be discretized by Galerkin's method. When this procedure is applied to (1) for the case of a single mode, we obtain

$$G_{\tau\tau} + 2\varepsilon\zeta G_{\tau} + [1 - \varepsilon f \cos(\phi\tau)]G + \varepsilon\alpha G^3 + \varepsilon\kappa_1 G G_{\tau}^2$$

$$+ \varepsilon\kappa_2 G^2 G_{\tau\tau} - 2\varepsilon\zeta\nu G^2 G_{\tau} = 0 \ , \qquad (6)$$

where ζ, α, K_1, K_2, ν are constants, f is the amplitude of excitation, and ε is a dimensionless parameter. Equation (6) contains cubic nonlinearities and nonlinear damping, and hence it does not lend itself to a closed-form solution. It can be analyzed by a perturbation or a numerical technique.

A first-order uniform solution using the method of multiple scales [6,7] is found to be

$$G(\tau) = a\cos(\tfrac{1}{2}\phi\tau + \beta) + \varepsilon a\{\frac{f}{4\phi^2} + \frac{a^2}{32}(\frac{4\alpha}{\phi^2} - \kappa_1 - \kappa_2)\cos[3(\tfrac{1}{2}\phi\tau + \beta)]$$

$$+ \frac{\zeta\nu}{8\phi} a^2 \sin[3(\tfrac{1}{2}\phi\tau + \beta)]\} + \ldots \ . \qquad (7)$$

The frequency-response curve for a typical system is shown in Figure 2. The dashed curves represent unstable solutions. Figure 3, which corresponds to region II of Figure 2, shows that parametric vibrations exist only when the excitation amplitude exceeds a threshold value. When the frequency of the excitation is increased to region III, the frequency-response curve is multivalued, resulting in a subcritical instability. This is shown in Figure 4.

4. Results and Discussion of the Composite Beam Experiments

A symetrical 0-90-90-0° 4-ply graphite-epoxy composite plate 0.022 inches thick was fabricated and cut into strips one-half inch wide. The frequency-response curves of the composite beam for three levels of excitation amplitude are shown in Figure 5. We observe that the general behavior is as predicted by the theory. There is, however, a maximum frequency at which point further increases in the frequency cause a jump down to the lower branch. We also note the appearance of chaotic behavior for the largest amplitude response; it was preceded by a modulation in the amplitude. We observe a penetration of a stable trivial solution into what is typically the unstable region of parametric resonance. Inside this "unstable" region small disturbances decayed and large disturbances grew, but as the region was penetrated, the disturbances that decayed became smaller and smaller until the trivial solution became unstable to all disturbances. We also see the lower branch lifting off the frequency axis as the frequency is decreased from above. This behavior was not predicted and appears to be intensified due to the higher level and nonlinear nature of the damping present in the composite beam.

The nature of the parametric resonance for $\phi = 2.000$ and for a table acceleration level of 1.00 g is shown in Figure 6(a). When the excitation frequency is increased to $\phi = 2.013$ and the model is released from rest, the lower branch attracts the response, as shown in Figure

6(b). After the system achieved steady state, it was disturbed, and we note that the disturbance caused the system to jump up to the large amplitude response. Here the system modulates and does not achieve a constant steady-state amplitude.

5. Results and Discussion of the Metallic Beam Experiments

A flexible steel beam was fabricated, instrumented with a strain gage and fitted with a small mass. The frequency response curve is shown in Figure 7. We again note a penetration of a stable trivial solution into the region predicted to be unstable by the theory, and we note a modulation in the large steady-state amplitude just before it jumps down. The amplitude response for ϕ = 2.000 is shown in Figure 8. These results also show remarkable agreement with the theory (see Figure 3).

REFERENCES

1. Nayfeh, A. H. and Mook, D. T. (1979). Nonlinear Oscillations, Wiley-Interscience, New York.
2. Schmidt, G. and Tondl, Ales (1986). Non-Linear Vibrations, Akademie-Verlag, Berlin.
3. Haxton, R. S. and Barr, A. D. S. (1972). The autoparametric vibration absorber. Transactions of the ASME, Journal of Engineering for Industry, pp. 119-125.
4. Sato, K., Saito, H. and Otomi, K. (1978). The parametric response of a horizontal beam carrying a concentrated mass under gravity. Journal of Applied Mechanics, 45, 643-648.
5. Zavodney, L. D. (1987). A theoretical and experimental investigation of parametrically excited nonlinear mechanical systems. Ph.D. Dissertation, Virginia Polytechnic Institute and State University, Blacksburg, VA.
6. Nayfeh, A. H. (1973). Perturbation Methods, Wiley-Interscience, New York.
7. Nayfeh, A. H. (1981). Introduction to Perturbation Techniques, Wiley Interscience, New York.

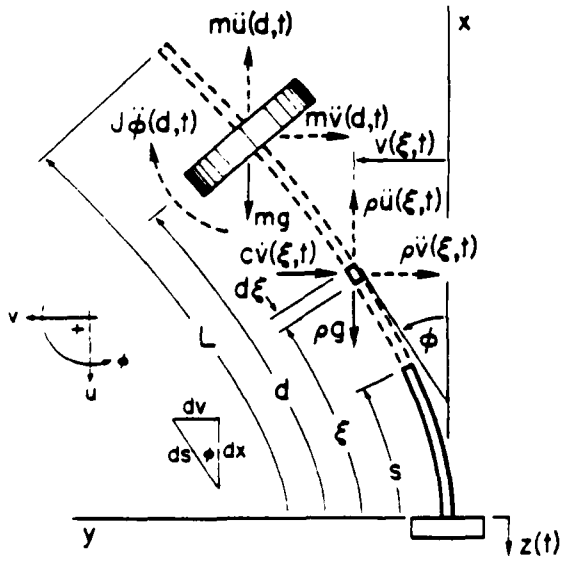

Figure 1. Cantilevered beam with a concentrated mass subjected to vertical base motion.

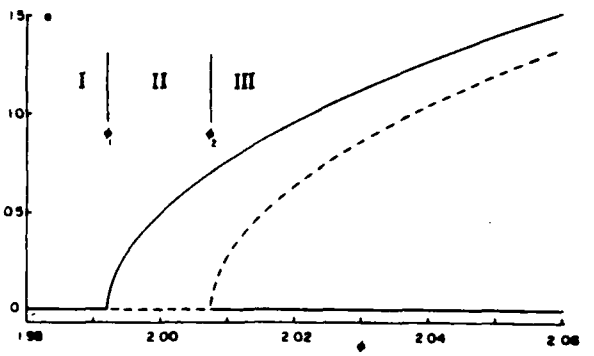

Figure 2. Theoretically determined frequency-response curve.

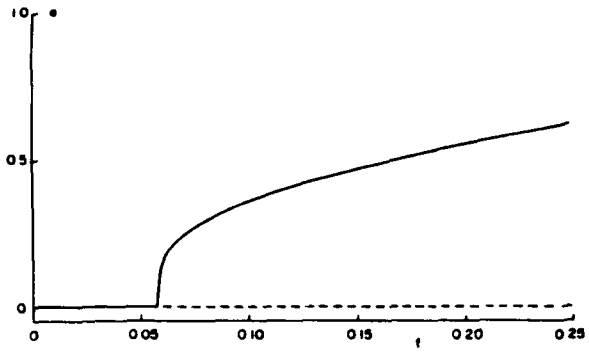

Figure 3. Theoretically determined variation of the steady-state amplitude a with the amplitude of excitation f in region II of Figure 2: $\epsilon = 2.000$.

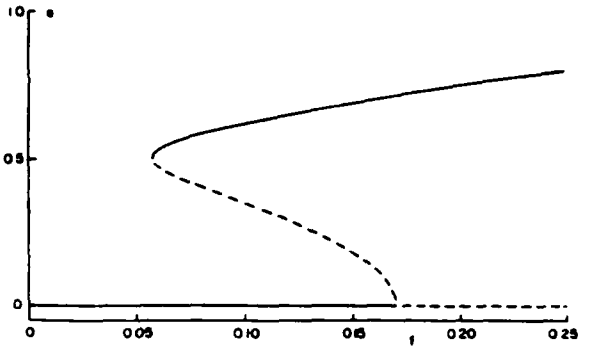

Figure 4. Theoretically determined variation of the steady-state amplitude a with the amplitude of excitation f in region III of Figure 2.

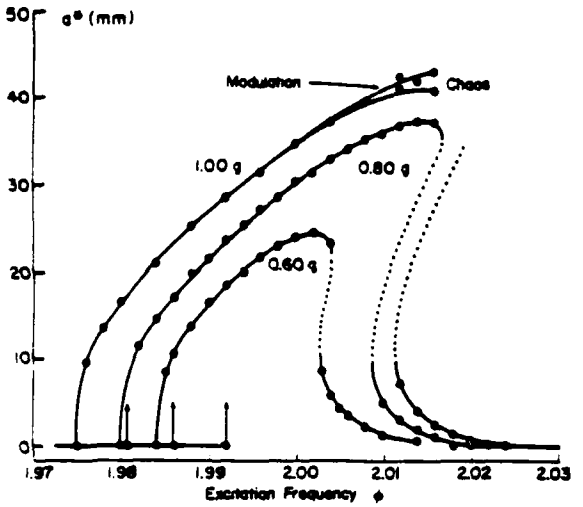

Figure 5. Frequency-response curves for three levels of excitation amplitude f of the composite beam. Note that chaotic behavior occurs at the largest amplitude of excitation.

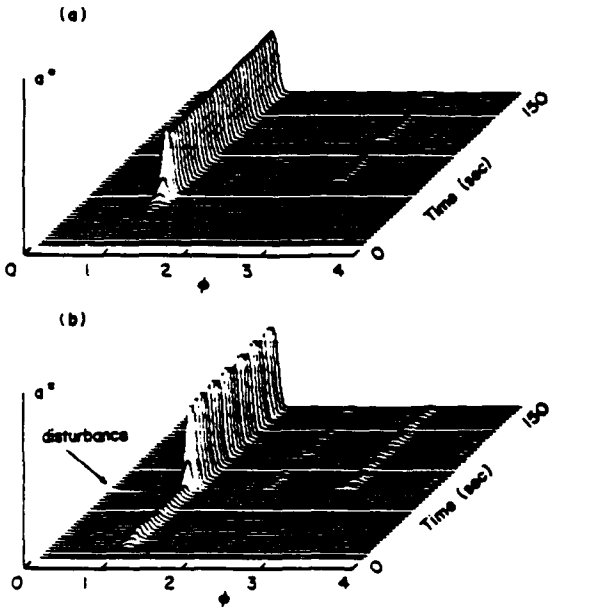

Figure 6. Spectral time history of the composite beam to a principal parametric excitation: (a) $\epsilon = 2.000$, (b) $\epsilon = 2.013$. Both responses start with the trivial solution. When $\epsilon = 2.013$ two solutions are possible.

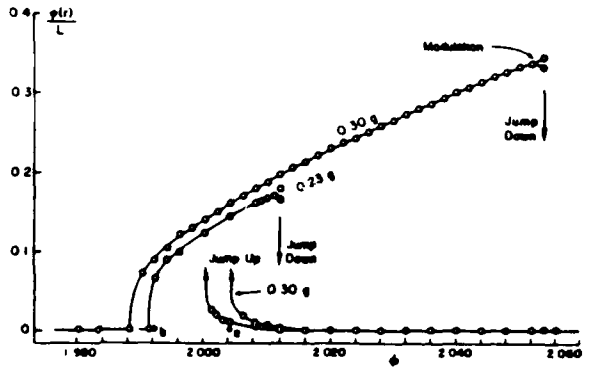

Figure 7. Frequency-response curves for the metallic beam for two acceleration levels.

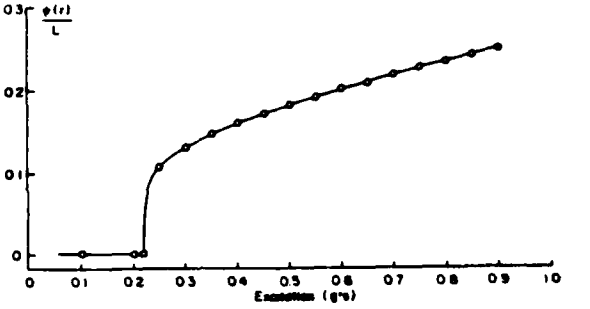

Figure 8. Variation of the amplitude a* with the excitation amplitude f of the metallic beam for $\epsilon = 2.000$.

THEORETICAL AND EXPERIMENTAL INVESTIGATION OF COMPLICATED RESPONSES OF A TWO-DEGREE-OF-FREEDOM STRUCTURE

A. H. Nayfeh, B. Balachandran, M. A. Colbert, and M. A. Nayfeh
Department of Engineering Science and Mechanics
Virginia Polytechnic Institute and State University
Blacksburg, VA 24061

An experimental study of the response of a two-degree-of-freedom structure with quadratic nonlinearities and a two-to-one internal resonance to a primary resonant excitation was conducted. The responses were analyzed using hardware and software developed for performing time-dependent modal decomposition. When the driving frequency is close to the higher frequency periodic and aperiodic responses were observed as predicted by theory. The experimentally observed frequency response of the system shows good qualitative agreement with the theoretical predictions.

We consider the response of internally coupled oscillators to harmonic excitations. If u_1 and u_2 are the generalized coordinates of the motion, then the governing equations are of the form

$$\ddot{u}_1 + \omega_1^2 u_1 + 2\mu_1\dot{u}_1 + \delta_1 u_1^2 + \delta_2 u_1 u_2 + \delta_3 u_2^2 + \delta_4 \dot{u}_1^2 + \delta_5 \dot{u}_1\dot{u}_2 + \delta_6 \dot{u}_2^2 + \delta_7 u_1\ddot{u}_1 + \delta_8 u_2\ddot{u}_1 + \delta_9 u_1\ddot{u}_2 + \delta_{10} u_2\ddot{u}_2 + (h_{11}u_1 + h_{12}u_2)\cos\Omega t = F\cos\Omega t , \tag{1}$$

$$\ddot{u}_2 + \omega_2^2 u_2 + 2\mu_2\dot{u}_2 + \alpha_1 u_1^2 + \alpha_2 u_1 u_2 + \alpha_3 u_2^2 + \alpha_4 \dot{u}_1^2 + \alpha_5 \dot{u}_1\dot{u}_2 + \alpha_6 \dot{u}_2^2 + \alpha_7 u_1\ddot{u}_1 + \alpha_8 u_2\ddot{u}_1 + \alpha_9 u_1\ddot{u}_2 + \alpha_{10} u_2\ddot{u}_2 + (h_{21}u_1 + h_{22}u_2)\cos\Omega t = G\cos\Omega t , \tag{2}$$

where the highest order of terms retained is quadratic. In these equations, ω_1 and ω_2 are the linear natural frequencies of the system, Ω is the excitation frequency, μ_1 and μ_2 are the modal dampings, and F, G, Ω, ω_n, δ_n, α_n and h_{mn} are constants.

Considering the case $\omega_2 = 2\omega_1 + \sigma_1$ and $\Omega = \omega_2 + \sigma_2$, where σ_1 and σ_2 are small detuning parameters, one finds that, to the first approximation, the response is [1]

$$u_1 = a_1\cos(\tfrac{1}{2}\Omega t - \tfrac{1}{2}\gamma_1 - \tfrac{1}{2}\gamma_2) + \ldots \tag{3}$$

$$u_2 = a_2\cos(\Omega t - \gamma_2) + \ldots \tag{4}$$

where the amplitudes a_n and β_n are governed by the following equations:

$$\dot{a}_1 = -\mu_1 a_1 - \Lambda_1 a_1 a_2 \sin\gamma_1 \tag{5}$$

$$\dot{a}_2 = -\mu_2 a_2 + \Lambda_2 a_1^2 \sin\gamma_1 + g \sin\gamma_2 \tag{6}$$

$$a_1\dot{\beta}_1 = \Lambda_1 a_1 a_2 \cos\gamma_1 \tag{7}$$

$$a_2\dot{\beta}_2 = \Lambda_2 a_1^2 \cos\gamma_1 - g \cos\gamma_2 \tag{8}$$

where

$$\gamma_1 = \sigma_1 t + \beta_2 - 2\beta_1 \quad \text{and} \quad \gamma_2 = \sigma_2 t - \beta_2 \tag{9}$$

and

$$4\omega_1\Lambda_1 = \delta_2 + \delta_5\omega_1\omega_2 - \delta_8\omega_1^2 - \delta_9\omega_2^2 , \tag{10}$$

$$4\omega_2\Lambda_2 = \alpha_1 - \alpha_4\omega_1^2 - \alpha_7\omega_1^2 . \tag{11}$$

Periodic solutions of equations (1) and (2) correspond to the fixed points of equations (5)-(9). They are obtained by setting $\dot{a}_1 = \dot{a}_2 = \dot{\gamma}_1 = \dot{\gamma}_2 = 0$. There are two possibilities. First,

$$a_1 = 0 \quad \text{and} \quad a_2 = \frac{g}{\sqrt{\sigma_2^2+\mu_2^2}}, \quad g = G/2\omega_2 \tag{12}$$

and, to the first approximation the response is

$$u_1 = 0 \quad \text{and} \quad u_2 = a_2\cos(\Omega t - \gamma_2) + \ldots \tag{13}$$

which is essentially the linear solution. Second,

$$a_1 = (\Lambda_1\Lambda_2)^{-\frac{1}{2}}\left[\chi_1 \pm (g\Lambda_1^2 - \chi_2^2)^{\frac{1}{2}}\right]^{\frac{1}{2}} \tag{14}$$

$$a_2 = a_{2s} = |\Lambda_1|^{-1}\left[\mu_1^2 + \frac{1}{4}(\sigma_1 + \sigma_2)^2\right]^{\frac{1}{2}} \tag{15}$$

where

$$\chi_1 = \frac{1}{2}\sigma_2(\sigma_1 + \sigma_2) - \mu_1\mu_2 , \tag{16}$$

$$\chi_2 = \sigma_2\mu_1 + \frac{1}{2}\mu_2(\sigma_1 + \sigma_2) , \tag{17}$$

and to the first approximation the response is given by equations (3) and (4), where a_1 and a_2 are defined in equations (14) and (15).

We note that not all fixed points are stable. They can lose stability in one of two ways

1) An eigenvalue crosses the imaginary axis into the right-half plane along the real axis

or

2) A pair of complex conjugate values crosses transversally into the right-half plane.

The former is associated with the jump phenomenon while the latter is associated with the Hopf bifurcation. Figure 1 shows frequency-response curves for the case $\Lambda_1 = 1.0$, $\Lambda_2 = 0.6$, $\mu_1 = \mu_2 = 0.02$, $\sigma_2 = 0.12$ and g = 0.1. The solid branches correspond to stable periodic motions, the dashed portions correspond to unstable fixed points with at least one eigenvalue being positive, and the dotted portion ($-0.047 \leq \sigma_1 \leq -0.0127$) corresponds to unstable fixed points with the real part of a complex conjugate pair of eigenvalues being positive. In the latter case, the amplitudes and phases are not constant but vary with time. The corresponding response is an amplitude- and phase-modulated or chaotic motion.

An experiment with a structure composed of two light beams and two concentrated masses, as in Figure 2, was conducted to observe the amplitude- and phase-modulated motions and to analyze them. The same model had been used by Nayfeh and Zavodney [2] to observe amplitude- and phase-modulated motions when the driving frequency is close to the lower natural frequency. The linear resonant frequencies of the structure were determined using a random excitation. The linear resonant natural frequencies were found to be $f_1 = 8.130$ Hz and $f_2 = 16.44$ Hz. Figure 2 shows also the associated mode shapes. Strain gages were used to measure the displacements of the beam ends. The frequency of excitation ranged from 15.5 Hz to 17.5 Hz and the signals from the strain gage were analyzed using an FFT analyzer, from which the amplitudes a_1^* and a_2^* were found; they are proportional to the modal amplitudes a_1 and a_2, respectively. The frequency response obtained from sweeping up and down the frequency range at a constant level of excitation is shown in Figure 3. The points where Hopf bifurcation was seen is also shown in the figure. It should be noted that this occurs only when $\sigma_1 > 0$ and $\sigma_2 < 0$. Comparing Figures 3 and 1 , one can see the qualitative agreement between theory and experiment.

To perform the time-dependent modal decomposition, we used the signal from the strain gage on the vertical beam. This signal was low-pass filtered ($f_c = 40$ Hz) and amplified and sent to an IBM PC which acquired data through an 8-bit analog-to-digital converter. A quartz clock was used to set the desired sampling rate. Using an FFT algorithm, we transformed the data from the time domain into the frequency domain, enabling us to do the subsequent digital filtering. The digital filtering separated the two modes. The separated frequency components were transformed back into the time domain using an inverse FFT (IFFT) algorithm. Using quadrature demodulation on the separated signals, we extracted the $a_i^*(t)$ and $\beta_i(t)$. The process was performed as follows.

To determine the amplitude $a(t)$ and phase $\beta(t)$ of the signal $a(t)\cos[\omega t + \beta(t)]$, we multiply it by $\sin\omega t$ and $\cos\omega t$ and express the resulting expressions as

$$a(t)\cos[\omega t + \beta(t)]\cos\omega t = \frac{1}{2}\, a(t)[\cos(2\omega t + \beta(t)) + \cos(\beta(t))] \qquad (18)$$

$$a(t)\cos[\omega t + \beta(t)]\sin\omega t = \frac{1}{2}\, a(t)[\sin(2\omega t + \beta(t)) - \sin(\beta(t))] \qquad (19)$$

Using a low-pass filter to eliminate the 2ω component, we obtain

$$p(t) = \frac{1}{2}\, a(t)\cos\beta(t) \text{ and } q(t) = -\frac{1}{2}\, a(t)\sin\beta(t), \qquad (20)$$

Then, we calculate $a(t)$ and $\beta(t)$ according to

$$a = 2\sqrt{p^2 + q^2},\ \beta = \tan^{-1} - \frac{q}{p} \qquad (21)$$

Using the aforementioned procedure, we analyzed the strain gage signal. In the region of stable periodic motions, we found a point attractor, which showed up as a point in the $a_1^* - a_2^*$ phase plane. In the region of amplitude- and phase-modulated motions, a limit cycle was seen in the projection of the attractor onto the $a_1^* - a_2^*$ phase plane. Figure 4 shows the strain gage signal, the separated modal components, the amplitudes $a_1^*(t)$ and $a_2^*(t)$, and the limit cycle in the $a_1^* - a_2^*$ plane.

References

1. A. H. Nayfeh, "Application of the method of multiple scales to nonlinearly coupled oscillators" Chapter for the Lasers, Molecules and Methods, a Volume in the Advances in Chemical Physics Series, (1987).

2. A. H. Nayfeh and L. D. Zavodney, "Experimental observation of amplitude- and phase-modulated responses of two internally coupled oscillators to a harmonic excitation," accepted for publication, Journal of Applied Mechanics, 1988.

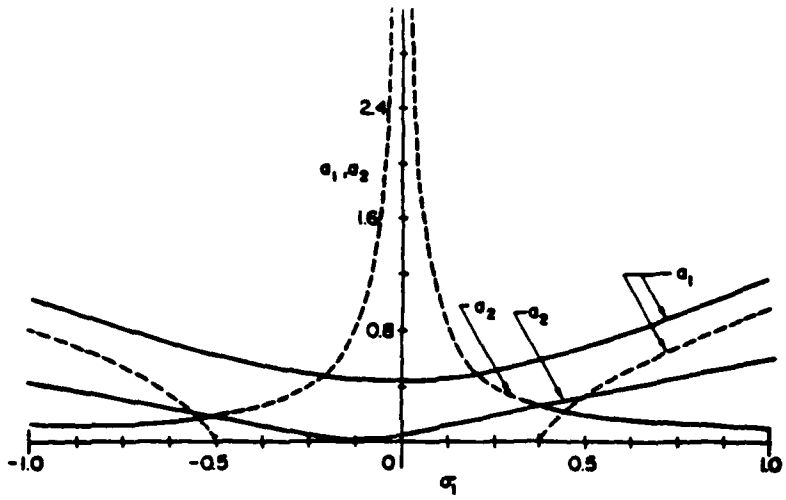

Figure 1. Theoretically predicted frequency-response curves for the case $\Lambda_1 = 1.0$, $\Lambda_2 = 0.5$, $\mu_1 = \mu_2 = 0.02$, $\sigma_2 = 0.12$, $g = 0.1$.

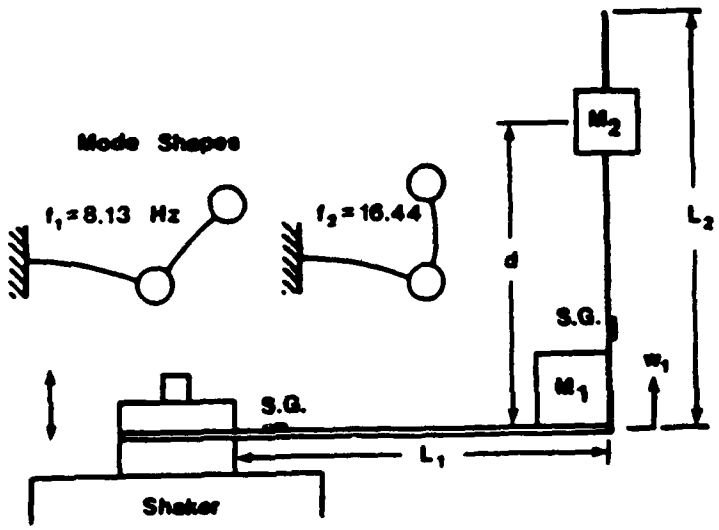

Figure 2. Two-degree-of-freedom model tuned for a 2:1 internal resonance and accompanying linear mode shapes. Beam 1: 1.676 mm x 12.827 mm x 154.51 mm, $\rho_1 = 0.162$ g/mm, $m_1 = 33.1$g; Beam 2: 0.559mm x 12.802 mm x 152.40 mm, $\rho_2 = 0.0496$g/mm, $m_2 = 40.0$g; d = 90.525 mm.

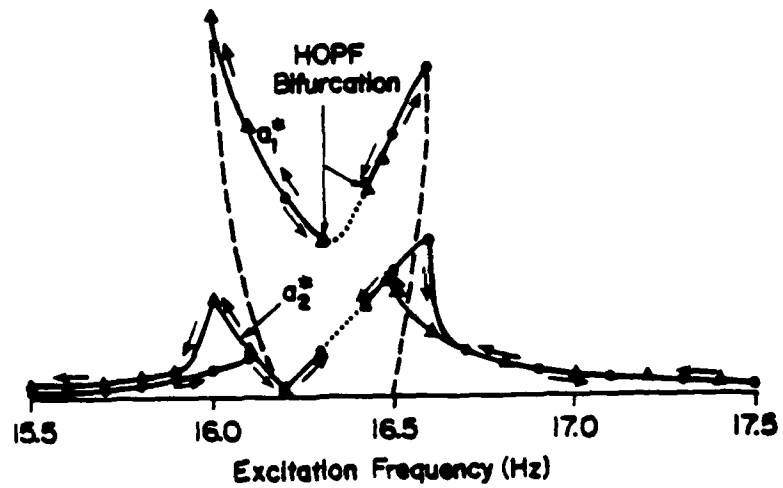

Figure 3. Experimentally obtained frequency-response curves when the excitation frequency Ω is close to the higher natural frequency $f_2 = 16.44$ Hz.

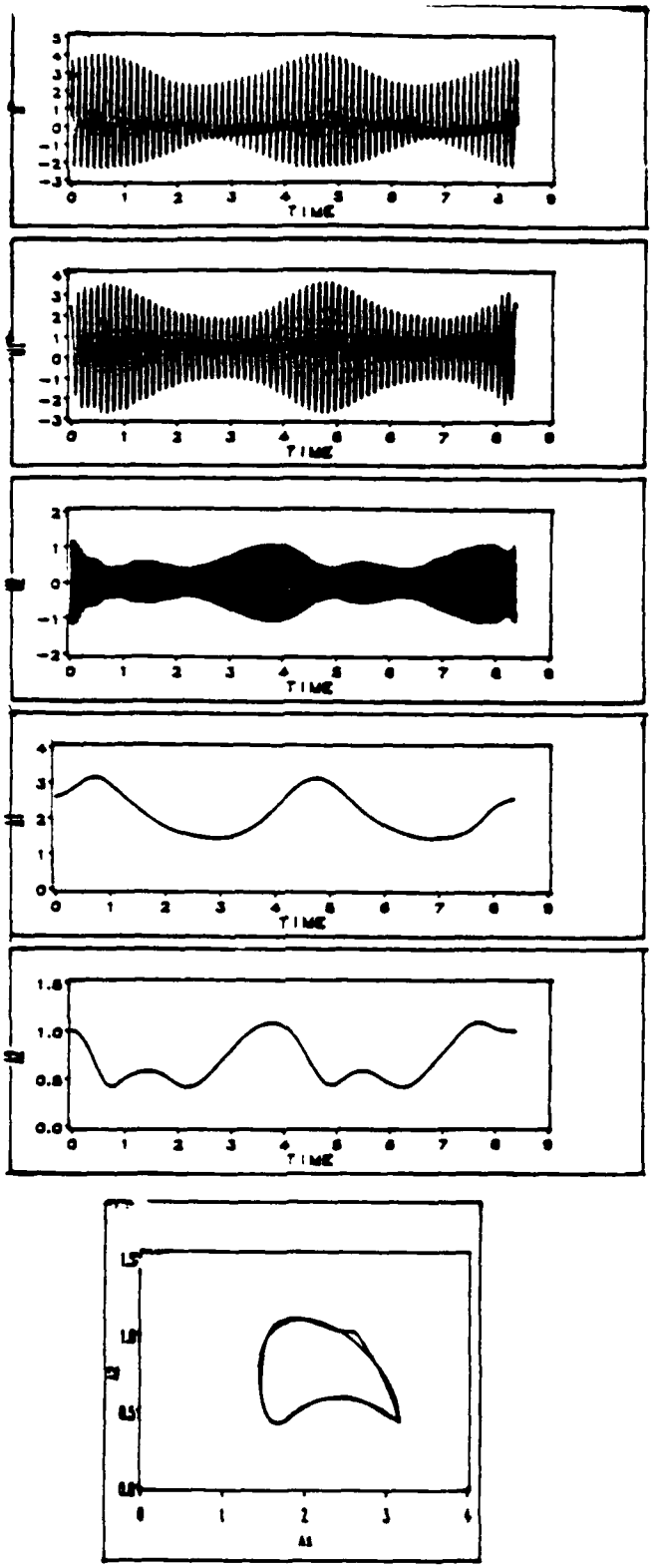

Figure 4. (a) Long-time history of the displacement of mass M_2.
(b) Long-time history of the modal components of the displacement of mass M_2.
(c) Long-time history of the modal amplitudes $a_1^*(t)$, $a_2^*(t)$.
(d) Amplitudes phase plane.

SESSION 6

NONLINEAR ANALYSIS OF BEAMS AND ROTOR BLADES

THURSDAY - 1030 - 1230

June 2, 1988

Nonlinear Oscillations in a Rotating Shaft System

Toshio Yamamoto* and Yukio Ishida**
* Professor,Dept.of Sci. and Tech., Meijo Univ., Shiogamaguchi, Tenpaku-ku, Nagoya,468, Japan.
** Associate Professor,School of Eng.,Nagoya Univ. Furo-cho, Chikusa-ku, Nagoya, 464, Japan.

1. Introduction

When a rotating shaft is supported by ball bearings, there appear nonlinear spring characteristics in restoring forces due to clearance in bearngs. Consequently, many kinds of nonlinear forced oscillations may occur. But, based on the results of the experiments we have conducted,some of these often appear with large amplitude and others are not observed[1]-[4]. Lateral vibrations of a shaft become a whirling motion due to a gyroscopic moment, and nonlinear oscillations have unique characteristics which are not observed in rectilinear systems. This paper will show that the adoption of polar coordinates helps to clarify such properties and predict the occurrence of oscillations.

2. Equations of Motion and Nonlinear Spring Characteristics

2.1 Equations of motion We consider a four-degree-of-freedom (FDOF) system where a rotor is mounted on an elastic shaft. A rectangular coordinate system O-xyz (z-axis coincides with a bearing center line) is considered, and the deflection and inclination of the rotor are expressed by $r(x,y)$ and $\theta(\theta_x,\theta_y)$. Let the rotor mass be m, the polar and diametral moments of inertia be I_p and I, the static and dynamic unbalance of the rotor be e and τ, the angle between these unbalances be β, the spring constants be α, γ, δ, the angular velocity of the shaft be ω, and the damping coefficients be $c_{ij}(i,j=1,2)$. By adopting the quantity $e_0=mg/\alpha$ as a representative value, we define the following dimensionless quantities:

$$\left.\begin{aligned} &x'=x/e_0,\quad y'=y/e_0,\quad \theta_x'=\theta_x/(e_0\sqrt{m/I}),\quad \theta_y'=\theta_y/(e_0\sqrt{m/I}),\quad t'=t\sqrt{\alpha/m},\\ &i_p=I_p/I,\quad \omega'=\omega\sqrt{m/\alpha},\quad \gamma'=\gamma\sqrt{m/I}/\alpha,\quad \delta'=m\delta/(\alpha I),\quad c_{11}'=c_{11}/\sqrt{m\alpha},\\ &c_{12}'=c_{12}/\sqrt{\alpha I},\quad c_{22}'=c_{22}\sqrt{m/\alpha}/I,\quad e'=e/e_0,\quad \tau'=\tau/(e_0\sqrt{m/I}) \end{aligned}\right\} \quad (1)$$

The equations of motion are expressed as follows:

$$\left.\begin{aligned} &\ddot{x}+c_{11}\dot{x}+c_{12}\dot{\theta}_x+x+\gamma\theta_x+N_x = e\omega^2\cos\omega t\\ &\ddot{y}+c_{11}\dot{y}+c_{12}\dot{\theta}_y+y+\gamma\theta_y+N_y = e\omega^2\sin\omega t\\ &\ddot{\theta}_x+i_p\omega\dot{\theta}_y+c_{12}\dot{x}+c_{22}\dot{\theta}_x+\gamma x+\delta\theta_x+N_{\theta x} = (i_p-1)\tau\omega^2\cos(\omega t+\beta_1)\\ &\ddot{\theta}_y-i_p\omega\dot{\theta}_x+c_{12}\dot{y}+c_{22}\dot{\theta}_y+\gamma y+\delta\theta_y+N_{\theta y} = (i_p-1)\tau\omega^2\sin(\omega t+\beta_1) \end{aligned}\right\} \quad (2)$$

where the primes are omitted, and nonlinear terms are expressed by N_x, N_y, $N_{\theta x}$, $N_{\theta y}$.

In order to explain the physical meanings and how to analyze phenomena, we use the following two-degree-of-freedom (TDOF) system.

$$\left.\begin{aligned} &\ddot{\theta}_x+i_p\omega\dot{\theta}_y+c\dot{\theta}_x+\theta_x+N_{\theta x} = (1-i_p)\tau\omega^2\cos\omega t\\ &\ddot{\theta}_y-i_p\omega\dot{\theta}_x+c\dot{\theta}_y+\theta_y+N_{\theta y} = (1-i_p)\tau\omega^2\sin\omega t \end{aligned}\right\} \quad (3)$$

For the dimensionless quantities in Eq.(3), some modifications are necessary in their definition.

2.2 Nonlinear terms The nonlinear terms are derived from the potential energy V. In the TDOF system, the energy V is expressed as follows when up to the third order terms are considered in restoring forces.

$$\begin{aligned} V = {} & (\theta_x^2+\theta_y^2)/2+(\varepsilon_{30}\theta_x^3+\varepsilon_{21}\theta_x^2\theta_y+\varepsilon_{12}\theta_x\theta_y^2+\varepsilon_{03}\theta_y^3)\\ & +(\beta_{40}\theta_x^4+\beta_{31}\theta_x^3\theta_y+\beta_{22}\theta_x^2\theta_y^2+\beta_{13}\theta_x\theta_y^3+\beta_{04}\theta_y^4) \end{aligned} \quad (4)$$

The restoring forces are obtained from this by $\theta_x + N_{\theta x} = \partial V/\partial\theta_x$ and $\theta_y + N_{\theta y} = \partial V/\partial\theta_y$.

As the shaft moves in a whirling mode, it is considered that the polar coordinates is more suitable to explain the phenomena. By the transformation $\theta_x = \theta\cos\phi$, $\theta_y = \theta\sin\phi$, Eq(4) is expressed by the polar coordinates as follows:

$$\begin{aligned} V &= (1/2)\theta^2 + (\varepsilon_c^{(1)}\cos\phi + \varepsilon_s^{(1)}\sin\phi + \varepsilon_c^{(3)}\cos 3\phi + \varepsilon_s^{(3)}\sin 3\phi)\theta^3 \\ &\quad + (\beta^{(0)} + \beta_c^{(2)}\cos 2\phi + \beta_s^{(2)}\sin 2\phi + \beta_c^{(4)}\cos 4\phi + \beta_s^{(4)}\sin 4\phi)\theta^4 \\ &= (1/2)\theta^2 + \{\varepsilon^{(1)}\cos(\phi-\phi_1) + \varepsilon^{(3)}\cos 3(\phi-\phi_3)\}\theta^3 \\ &\quad + \{\beta^{(0)} + \beta^{(2)}\cos 2(\phi-\phi_2) + \beta^{(4)}\cos 4(\phi-\phi_4)\}\theta^4 \end{aligned} \tag{5}$$

The following relations holds between these coefficients

$$\left.\begin{aligned} &\varepsilon_c^{(1)} = (3\varepsilon_{30} + \varepsilon_{12})/4, \quad \varepsilon_s^{(1)} = (\varepsilon_{21} + 3\varepsilon_{03})/4, \quad \varepsilon_c^{(3)} = (\varepsilon_{30} - \varepsilon_{12})/4, \quad \varepsilon_s^{(3)} = \\ &(\varepsilon_{21} - \varepsilon_{03})/4, \quad \beta^{(0)} = (3\beta_{40} + \beta_{22} + 3\beta_{04})/8, \quad \beta_c^{(2)} = (\beta_{40} - \beta_{04})/2, \\ &\beta_s^{(2)} = (\beta_{31} + \beta_{13})/4, \quad \beta_c^{(4)} = (\beta_{40} - \beta_{22} + \beta_{04})/8, \quad \beta_s^{(4)} = (\beta_{31} - \beta_{13})/8. \end{aligned}\right\} \tag{6}$$

The coefficients $\varepsilon^{(1)}, \ldots$, and $\phi_1, \ldots$, are obtained by the relation $\varepsilon^{(1)} = \sqrt{\varepsilon_c^{(1)2} + \varepsilon_s^{(1)2}}$, $\phi_1 = \tan^{-1}(\varepsilon_s^{(1)}/\varepsilon_c^{(1)}), \ldots$. The coefficients $\varepsilon_c^{(i)}$ and $\varepsilon_s^{(i)}$ (i=1,3) belong to the unsymmetrical nonlinear spring characteristics and $\beta_c^{(i)}$ and $\beta_s^{(i)}$ (i=0,2,4) belong to symmetrical ones.

Figure 1(a) shows a distribution of potential energy V. The shape of V for a nonlinear system deviates irregularly from that for a linear system whose potential energy is $V_0 = (\theta_x^2 + \theta_y^2)/2$. But this nonlinear spring characteristic can be classified into regular components if we represent it by polar coordinates. Figures 1(b)-(f) shows cross sections of surface V with a plane parallel to the $\theta_x\theta_y$-plane, in the cases that one of $\varepsilon^{(1)}$, $\varepsilon^{(3)}$, $\beta^{(0)}$, $\beta^{(2)}$, and $\beta^{(4)}$ exists, respectively. It is seen that $\varepsilon_c^{(n)}$, $\beta_s^{(n)}$, etc. are coefficients of terms which vary their magnitude n times while the angle ϕ changes its value from 0 to 2π. We designate these nonlinear components by the notation $N(n)$ in this paper.

In the case of FDOF system, the potential energy is expressed by

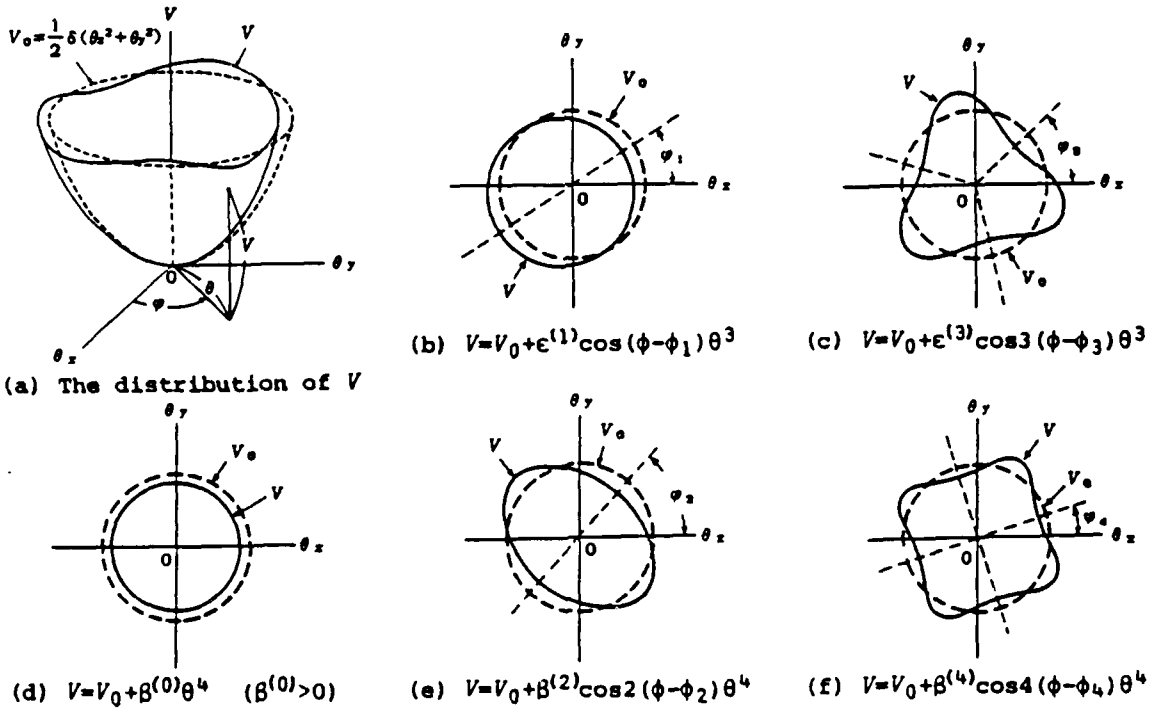

(a) The distribution of V

(b) $V = V_0 + \varepsilon^{(1)}\cos(\phi-\phi_1)\theta^3$

(c) $V = V_0 + \varepsilon^{(3)}\cos 3(\phi-\phi_3)\theta^3$

(d) $V = V_0 + \beta^{(0)}\theta^4$ $(\beta^{(0)} > 0)$

(e) $V = V_0 + \beta^{(2)}\cos 2(\phi-\phi_2)\theta^4$

(f) $V = V_0 + \beta^{(4)}\cos 4(\phi-\phi_4)\theta^4$

Fig.1 Nonlinear components and the potential energy distribution

$$V=\frac{1}{2}(x^2+y^2)+\gamma(x\theta_x+y\theta_y)+\frac{\delta}{2}(\theta_x^2+\theta_y^2)+\sum_{\substack{a,b,c,d=1\\(a+b+c+d=3)}}^{3}\varepsilon_{abcd}x^a y^b\theta_x^c\theta_y^d+\sum_{\substack{a,b,c,d=1\\(a+b+c+d=4)}}^{4}\beta_{abcd}x^a y^b\theta_x^c\theta_y^d \quad (7)$$

Restoring forces are derived by differentiating this energy by x, y, θ_x, and θ_y, respectively. By the transformation $x=r\cos\phi_r$, $y=r\sin\phi_r$, $\theta_x=\theta\cos\phi_\theta$, and $\theta=\theta\sin\phi_\theta$, this potential energy is transformed into the polar coordinate system $(r, \phi_r, \theta, \phi_\theta)$. We show the obtained equation partially as follows.

$$\begin{aligned}V=&\{r^2/2+\gamma r\theta\cos(\phi_r-\phi_\theta)+\delta\theta^2/2\}\\&+\{(\varepsilon_{30c}^{(1)}\cos\phi_r+\varepsilon_{30s}^{(1)}\sin\phi_r)r^3+\ldots\}\\&+[\beta_{40}^{(0)}r^4+\{\beta_{31c}^{(0)}\cos(\phi_r-\phi_\theta)+\beta_{31s}^{(0)}\sin(\phi_r-\phi_\theta)\}r^3\theta+\ldots]\end{aligned} \quad (8)$$

In this equation, the angles which are not contained in Eq(5) appear. For example, the angle $(\phi_r-\phi_\theta)$ is constant during the whirling motion, and therefore the terms containing $(\phi_r-\phi_\theta)$ is a component expressed by $N(0)$. Similar to Eq.(6), the relations $\varepsilon_{30c}^{(1)}=(3\varepsilon_{3000}+\varepsilon_{1200})/4$, ... holds among these coefficients.

2.3 Frequency equation and resonance points Let the natural frequency be p. The frequency equation of FDOF system is obtained from Eq.(2) as follows.

$$(1-p^2)(\delta+i_p\omega p-p^2)-\gamma^2=0 \quad (9)$$

This equation has four roots $p_1\sim p_4$. These frequencies are shown in Fig.2 as a function of ω. In a FDOF system with square and cubic nonlinearity, subharmonic (Sub-H) oscillations and summed-and-differential harmonic (S-and-D-H) oscillations listed in Table 1 have the possibility to occur theoretically. We designate the former by the symbol $[\omega=mp_i]$ and the latter by the symbol $[\omega=mp_i+np_j]$. These symbols express relations which hold at the resonance points. These resonance points are given by the cross points in Fig.2.

The frequency equation of TDOF system of Eq(3) is given by

$$1+i_p\omega p-p^2=0 \quad (10)$$

which has two roots $p_f(>0)$ and $p_b(<0)$.

3. Resonance Curves of the Subharmonic Oscillation $[+(1/2)\omega]$

As a representative example, we select the Sub-H oscillation of order 1/2 with a mode of forward precession. First, we discuss a TDOF system in order to present an outline of analysis. In the neighborhood of the rotating speed $\omega=\omega_0$ where the relation $\omega=2p_f$ holds, the Sub-H oscillation with frequency $(1/2)\omega$ appears in addition to the harmonic component with frequency ω. When these two components exist, higher order components with magnitude of $O(\varepsilon)$ appear due to the nonlinearity. [The symbol $O(\varepsilon)$ means that the quantity has the same magnitude as the small parameter ε.] These higher order components represent small deviation of the orbit. Therefore, we suppose an approximate solution as follows:

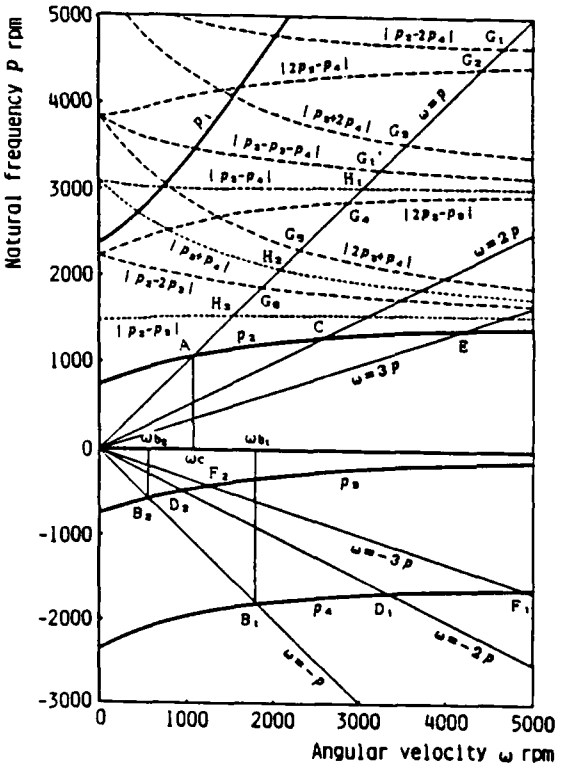

Fig.2 $p-\omega$ diagram

$$\left.\begin{aligned}\theta_x &= R\cos\theta_f + P\cos(\omega t+\beta) + \varepsilon(a\cos\theta_f + b\sin\theta_f)\\ \theta_y &= R\sin\theta_f + P\sin(\omega t+\beta) + \varepsilon(a'\sin\theta_f + b'\cos\theta_f)\end{aligned}\right\} \quad (11)$$

where $\theta_f = (1/2\cdot\omega t + \delta_\psi)$. By inserting this solution into Eq(3), and using a method of harmonic balance, we get the following equations.

$$\left.\begin{aligned}(1-i_\rho)\omega\dot{R} &= -c(1/2)\omega R - 2(\varepsilon_c^{(1)}\sin 2\delta_f - \varepsilon_s^{(1)}\cos 2\delta_f)RP\\ (1-i_\rho)\omega R\dot{\delta}_f &= G_1 R - 2(\varepsilon_c^{(1)}\cos 2\delta_f + \varepsilon_s^{(1)}\sin 2\delta_f)RP + 4\beta^{(0)}(R^2+2P^2)R\end{aligned}\right\} \quad (12)$$

Where, $G_1 = 1+i_\rho\omega(\omega/2)-(\omega/2)^2$. The harmonic solution are given in the accuracy of $O(\varepsilon)$ as $P=(1-i_\rho)\tau\omega^2/\{1-(1-i_\rho)\omega^2\}$, $\beta=\pi$. From Eq.(12), we get the following equations which give the stationary solutions R_0, δ_0.

$$\left.\begin{aligned}&R_0 = 0 \qquad\qquad (a)\\ &\{G_1 + 4\beta^{(0)}(R_0^2+2P^2)\}^2 + c^2(\omega/2)^2 = 4\varepsilon^{(1)2}P^2 \qquad (b)\end{aligned}\right\} \quad (13)$$

We can investigate the stability of these solutions by the same method used in the literature[5]. Resonance curves are shown in Fig.3, where full lines and dotted lines represent stable and unstable solutions, respectively. From Eq.(13), we see that only the components N(0) and N(1) have influence on this oscillation. Figure 3(a) shows that N(0) (that is, the coefficient $\beta^{(0)}$) determines the inclination of the resonance curve, and Fig.3(b) shows that N(1) (that is, the coefficients $\varepsilon_c^{(1)}$ and $\varepsilon_s^{(1)}$) determine the intensity of the oscillation.

In FDOF system, the same kind of subharmonic oscillation appears at the point C in Fig.2, where the relation $\omega = 2p_2$ or $p_2=(1/2)\omega$ holds. The way of the theoretical analysis is almost the same as that mentioned above, althogh its calculation is more complex and abundant. The equation corresponding to Eq.(13b) is given by the following equation.

$$[\{(\omega/2)^2 - p_2^2\} - \{A(N(0))R_2^2 + B(N(0),F)\} + C^2\omega^2 = D(N(1),F) \quad (14)$$

In this equation, A(N(0)) means a constant containing the coefficients $\beta_{40}^{(0)}$, $\beta_{31c}^{(0)}$, ..., B(N(0),F) is a constant containing $\beta_{40}^{(0)}$ $\beta_{31c}^{(0)}$, ... and the amplitude F_i of harmonic solutions, C is a constant relating to damping, and D(N(1),F) is a constant containing $\varepsilon_{30c}^{(1)}$, ... and F_i. By comparing Eq.(13) and Eq.(14), it is concluded that the vibration characteristics, such as, the shape of the resonance curve, relating nonlinear components, and so on, in the FDOF system are qualitatively the same as those in the TDOF system.

5. Summary of Nonlinear Forced Oscillations in the FDOF system

The analytical and experimental results are summarized in Table 1. The component N(0) has influence on every kinds of oscillation and it determines

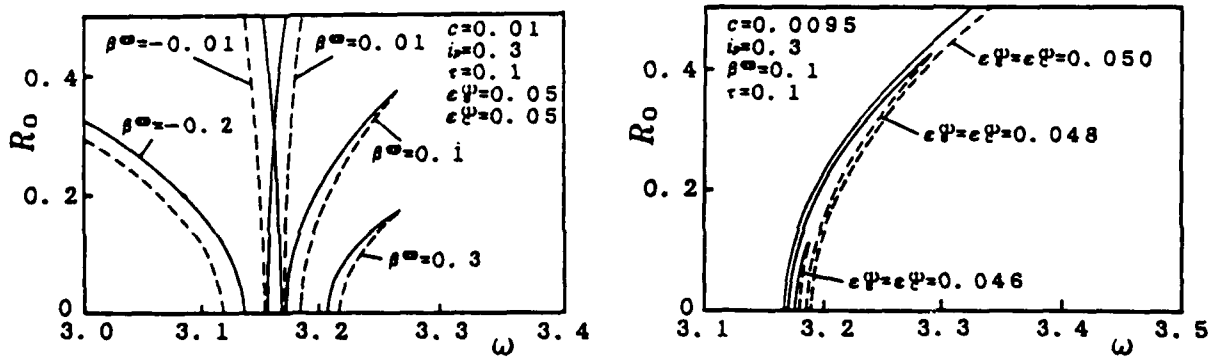

(a) Effects of $N(0)$. (b) Effects of $N(1)$.

Fig.3 The effects of the nonlinear components $N(0)$ and $N(1)$ on the subharmonic oscillation [$\omega = 2p_f$]

Table 1. Summary of theoretical and experimental results

			Precessional motion	Kinds of Oscillation	Nonlinear component	Experiments		
						A[1]-[3]	B-I[4]	B-II[4]
Forced Oscillation caused by Symmetrical Nonlinearity	Sub-H Oscil.		Forward(F)	$\omega \fallingdotseq 3p_1 (i_p<1/3)$ $\ddagger\ \omega \fallingdotseq 3p_2$	$N(0).N(2)$	×	×	○
			Backward(B)	$\ddagger\ \omega \fallingdotseq -3p_3$ $\ddagger\ \omega \fallingdotseq -3p_4$	$N(0).N(4)$	×	×	×
	S-and-D-H Oscil.	Two Components	F + F	$\omega \fallingdotseq 2p_1+p_2 (i_p<1/2)$ $\omega \fallingdotseq p_1+2\ p_2 (i_p<1)$	$N(0).N(2)$	no resonance points		
			F + B (2F+B)	$\omega \fallingdotseq 2p_1-p_3 (i_p<1/2).\ddagger\omega \fallingdotseq 2p_2-p_3$ $\omega \fallingdotseq 2p_1-p_4 (i_p<1/2).\ddagger\omega \fallingdotseq 2p_2-p_4$	$N(0)$	×	○	○
			F + B (F+2B)	$\omega \fallingdotseq p_1-2\ p_3 (i_p<1).\ddagger\omega \fallingdotseq p_2-2\ p_3$ $\omega \fallingdotseq p_1-2\ p_4 (i_p<1).\ddagger\omega \fallingdotseq p_2-2\ p_4$	$N(0).N(2)$	×	×	○
			B + B	$\ddagger\ \omega \fallingdotseq -2p_3-p_4$ $\ddagger\ \omega \fallingdotseq -p_3-2\ p_4$	$N(0).N(4)$	×	×	×
		Three	F + F + B	$\omega \fallingdotseq p_1+p_2-p_3 (i_p<1)$ $\omega \fallingdotseq p_1+p_2-p_4 (i_p<1)$	$N(0)$			
			F + B + B	$\omega \fallingdotseq p_1-p_3-p_4 (i_p<1)$ $\ddagger\ \omega \fallingdotseq p_2-p_3-p_4$	$N(0).N(2)$	×	×	○
by Unsymmetrical Nonlinearity	Sub-H Oscil.		F	$\omega \fallingdotseq 2p_1 (i_p<1/2)$ $\ddagger\ \omega \fallingdotseq 2p_2$	$N(0).N(1)$	○	○	○
			B	$\ddagger\ \omega \fallingdotseq -2p_3$ $\ddagger\ \omega \fallingdotseq -2p_4$	$N(0).N(3)$	△	×	×
	S-and -D-H Oscil.		F + F	$\omega \fallingdotseq p_1+p_2 (i_p<1)$	$N(0).N(1)$			
			F + B	$\omega \fallingdotseq p_1-p_3 (i_p<1).\ddagger\omega \fallingdotseq p_2-p_3$ $\omega \fallingdotseq p_1-p_4 (i_p<1).\ddagger\omega \fallingdotseq p_2-p_4$	$N(0),N(1)$	○	○	○
			B + B	$\ddagger\ \omega \fallingdotseq -p_3-p_4$	$N(0).N(3)$	△	×	×

the inclination of resonance curves. In addition, one of the components $N(0) \sim N(5)$ has influence on each oscillation and it determines the intensity of the occurrence. The experimental results reported previously[1)-(4)] are obtained in the apparatus consisting of an elastic shaft and a disc ($i_p \approx 2$). In these apparatus, the oscillations with * have their resonance points. Apparatus A are systems with strong unsymmetrical nonlinearity, and they are used on the literatures[(1)-(3)]. Apparatus B-I and B-II are systems treated in the literature[(4)]. The former apparata B-I is a system with strong symmetrical nonlinearity with no directional difference, and the latter apparata B-II is a system with strong symmetrical nonlinearity with directional difference. The symbol ○ means that the oscillation appeared often with large arplitude in experiments. The symbol △ means that the oscillation appeared sometimes with small amplitude. The × means that the oscillation did not appear through many experimemts. By comparing the theoretical and experimental results, it is known that (a) the oscillations to which simple-shaped nonlinear components, such as N(0) and N(1), have influence in their intensity often appear and (b) those to which complex-shaped nonlinear components, such as N(3) and N(4), have influence are difficult to appear. Therefore, it is concluded that, if we check the influencing nonlinear components, we can predict the occurrence of the oscillation.

6. A Simple Rule Predicting the Relating Nonlinear Components

From the above-mensioned results, the importance of nonlinear component is established. Concerning these nonlinear components which has influence on the intensity of occurrence, simple rule can be stated: namely, for the oscillation which appear when the relation $a\omega = bp_i + cp_j$ holds, the nonlinear component N(k) ($k=|a-b-c|$) have influence on the intensity.

[literatures] (1)Yamamoto, T., Trans. Japan Soc. Mech. Engrs, Vol.21, No.111(1955), p.853. (2)Yamamoto, T., Trans. Japan Soc. Mech. Engrs, Vol.22, No.115(1956), p.172. (3)Yamamoto, T., Bull. JSME, Vol.3, No.12(1960), p.397. (4) Yamamoto, T. et al., Bull. JSME, Vol.18, No.123(1975) p.965. (5)Yamamoto, T. et al., Bull. JSME, Vol.22, No.164, p.164

Nonlinear Effects in the Static and Dynamic Behavior of Beams and Rotor Blades

Dewey H. Hodges*
Georgia Institute of Technology
Atlanta, Georgia, U. S. A.

Marcelo R. M. Crespo da Silva†
Rensselaer Polytechnic Institute
Troy, New York, U. S. A.

and

David A. Peters*
Georgia Institute of Technology
Atlanta, Georgia, U. S. A.

Sponsored by the U. S. Army Research Office

Introduction

In work published recently in *Vertica*, Nagaraj and Sahu [1] analyze the static and dynamic behavior of an end-loaded cantilever beam. They develop solutions for the static behavior based on perturbation methods and present these results along with numerical results for the free-vibration frequencies. Contrary to known laws of physics, they allege that their various analyses exhibit non-negligible differences in tip deflection, tip rotation and free-vibration frequencies, in spite of the fact that these analyses are based on only one analytical model with differences arising only from the treatment of the finite rotation of the beam cross section frame. They conclude that, in modeling the finite deflections of an Euler-Bernoulli beam, the sequence of rotational transformations that is used to construct the matrix of direction cosines (of the deformed-beam cross-sectional frame) "affects the nonlinear corrections to the bending deflection." The authors also state that "the closed-form solutions derived in the present paper show that systematic differences exist in these quantities in solutions based on modified Euler angles ..." (See "Conclusions" on pages 661 - 662).

We show in this paper that these and other conclusions of [1] are patently false and result from *numerous errors in the analysis*. Most of the errors in [1] are not new; previous works with mistakes of a similar nature are discussed in [2]. The present paper is intended to be a critical analysis and discusion of the work presented in [1]. It seems

* Professor, School of Aerospace Engineering

† Professor, Department of Mechanical Engineering, Aeronautical Engineering, and Mechanics

apparent that only a brief look at the title is sufficient to know that [1] is seriously in error since the mathematical description of a system cannot affect its physical attributes. In the paper we discuss the nature of the errors of [1] in terms of the fundamentals of mechanics, nonlinear analysis, interpretation of experimental results, and rigid-blade modeling.

Uniqueness of Solution

For a given analytical model of any system, we expect to obtain the same answers for its behavior, regardless of the variables we use to describe the system. In the paper we discuss the concept of impenetrability and what it implies concerning the use of orientation angles in dynamics analysis.

One of the most fundamental of all the laws of physics is the law of impenetrability. This law states that, at any instant in time, a particle of matter can occupy only one position in space. On the basis of this law, it is not difficult to show that a rigid body can assume only one orientation at any particular instant in time. In continuum mechanics textbooks, this law is often stated in terms of the continuity of deformation resulting in a one-to-one mapping between deformed and undeformed structural configurations. As a consequence, when attempting to model a system which consists of particles and/or rigid bodies, the analyst develops appropriate mathematical expressions which convey the position of each particle and orientation of each rigid body at a particular time, generally grouped under the heading of kinematics. If these expressions are valid for all time within some range of interest, then the application of laws of motion will allow for analytical or numerical simulation of the motion of the system in question over the time interval of interest.

In the paper by Nagaraj and Sahu, this fundamental concept is severely violated. Nagaraj and Sahu, as have some other investigators such as some of those discussed in [2], developed more than one expression for the orthonormal transformation matrix between two reference frames. By unwisely using the same symbol for the third angle of two distinct sets of orientation angles, they were apparently then unable to see that these quantities are different angles. Since the expressions for the direction cosines are very different for different treatments of finite rotation, the development in [1] leads to a fundamental fallacy: that a frame (which is kinematically equivalent to a rigid body) can have more than one orientation at one time.

The consequences of this error appear in the numerical results of [1]. Recalling the one-to-one mapping between deformed and undeformed structures, a particular physical model of a beam can exhibit only one deformation for a given load. On the other hand, Nagaraj's and Sahu's results show a displacement of the elastic line and an orientation of the cross section at the tip of the beam that depend upon their choice of rotational variable – which is patently nonsensical!

It is well known to dynamicists that it is the values of the rotational variables (their being, in a sense, intermediate quantities) that depend on the choice of rotational

variables. That is, at some instant in time the direction cosines of some particular frame are unique, but the values of the variables used to evaluate the direction cosines will depend upon what those variables are, whether orientation angles of any of the 24 or more types [3], of Rodrigues parameters, or of any other measures [4]. However, the final answer for *a component of displacement, a component of angular velocity or velocity, a strain component, a direction cosine, or other measurable quantities*, cannot depend on the choice of rotational variables. We will see firm evidence of this when we correct the nonlinear analysis of [1] and properly compare their results with experiment.

When orientation angles (referred to by the authors of [1] as "modified Euler angles") are used, the third orientation angle is not the beam's total rotation at some particular value of the axial coordinate. It is simply *an orientation angle of the rotation sequence* and, thus, its value may, of course, depend on the particular sequence used. In the paper we show that if one were to assume that all the various torsional kinematical variables used in [1] were equal, then the distance from a particle to a plane is not unique at an arbitrary time. Thus, these quantities are not equal and, thus, cannot be all the same quantity!

Errors in the Nonlinear Analysis of [1]

To analyze nonlinear systems, special attention should be given to the formulation of the differential equations of motion for the system. Also, if an approximate solution to the governing differential equations is generated by a perturbation analysis, care should be taken so that the original nonlinear equations are expanded in terms of a small parameter, ϵ, to the same order that is desired of the solution. Here we let, the deflections and torsional kinematical variable each be $O(\epsilon)$, where ϵ is a bookkeeping parameter to identify the order to which each of these variables is retained in the equations of motion. If the nonlinearities in a set of equations are expanded to $O(\epsilon^n)$, then the solution to the expanded equations is, of course, only valid to $O(\epsilon^n)$. If a solution valid to $O(\epsilon^{m+n})$ is desired, with $m > 0$, then all terms of $O(\epsilon^{m+n})$ must be retained in the expanded equations. With this in mind, we address some other erroneous conclusions and results presented in [1].

There are two basic sources of error in the analysis of the end-loaded cantilever presented in [1]. The first and more important is in the approach in which the authors fail to fully develop Eqs. (16) to $O(\epsilon^3)$ in order to obtain a set of consistent $O(\epsilon^3)$ approximations for the deflections v and w. The main reason that Nagaraj and Sahu failed in their attempt to correct their Eqs. (16) to be valid to $O(\epsilon^3)$ is that they failed to include $O(\epsilon^3)$ terms in their expressions for bending curvature (their Eqs. 11b and 12b for k_y and k_z). It turns out that this, alone, is responsible for the authors' erroneous conclusion that the deflections v and w depend on the rotation sequence. The other basic source of error happens to be in Eqs. (8). We will prove that Eqs. (8) are in error by examining a special planar case of those equations. It should be noted that much of the erroneous analysis in [1] is developed properly in [5,6].

In the paper, it is shown that the entire analysis in [1], including static deformation, dynamics, and lateral buckling, is in error. By far the most serious of the errors are the failure to distinguish the rotational kinematical variables and the failure to properly develop Eqs. (16) to $O(\epsilon^3)$. Therefore, the conclusions of [1] regarding the influence of transformation sequence, many of which were derived from the faulty analysis therein, are blatantly in error and physically groundless.

Other Errors in [1]

There are two types of experiments described in [7,8] with which numerical results in [1] are compared. One deals exclusively with static behavior of an end-loaded cantilever beam for large deflections, and the other deals with the dynamic behavior. In the former, the tip displacements and one angle for determining the tip rotation are reported. In the latter, the fundamental flatwise and edgewise bending frequencies are reported. Nagaraj and Sahu compare with both and erroneously report a dependence of tip rotation, tip displacement, lateral buckling load, and fundamental frequency on transformation sequence. With the tip displacement, buckling load, and fundamental frequency, the errors noted above are responsible for this false conclusion. Indeed, it is easily shown that the correct form of the governing equations that were solved in [1] does not depend on the transformation sequence. For the tip rotation, Nagaraj and Sahu do not properly identify the quantity that was measured in the experiment. We properly identify it and show that it is, indeed, independent of transformation sequence.

We also show in the paper that partial differential equations of motion with nonlinear terms retained only through second degree are not sufficiently accurate to determine the large deflection behavior of end-loaded cantilever beams, a conclusion that can also be inferred from the work of [9 – 13]. The reason now is clear: recall that in the static problem, the torsional variable is $O(\epsilon^2)$ and always appears in the flexural equations multiplied by terms that are $O(\epsilon)$. Thus, the static equations which stem from dynamical equations with only second degree nonlinear terms, used in finding the nonlinear equilibrium solution about which to linearize, are *not* consistent since they contain some $O(\epsilon^3)$ terms, but not all. Thus, we should not be surprised that a formulation based on consistent partial differential equations of motion, with only second degree nonlinearities in v, w, and the torsional variable, would perform in a mediocre manner for this problem.

We also comment on the section of [1] which discusses the flap-lag stability of rigid, articulated blades. The paper presents stability boundaries for the so-called "sequence-free" transformation and shows that they are between the boundaries for blades with flap-lag and lag-flap hinge sequences. This observation is followed by the extraordinarily false conclusion, "Since the flap and lag hinges are assumed coincident, there is no preferred sequence which can be specified for this problem and the sequence-free formulation appears to be a natural choice."

References

1. Nagaraj, V. T., and Sahu, N., "Influence of Transformation Sequence on Nonlinear Bending and Torsion of Rotor Blades," *Vertica*, Vol. 11, No. 4, 1987, pp. 649 - 664.

2. Hodges, Dewey H., Ormiston, Robert A., and Peters, David A., "On the Nonlinear Deformation Geometry of Euler-Bernoulli Beams," NASA TP-1566, 1980.

3. Kane, Thomas R., Likins, Peter W., and Levinson, David A., *Spacecraft Dynamics*, McGraw-Hill, New York, 1983, chapter 1.

4. Hodges, Dewey H., "Finite Rotation and Nonlinear Beam Kinematics," *Vertica*, Vol. 11, No. 1/2, 1987, pp. 297 - 307.

5. Crespo da Silva, M. R. M., and Glynn, C. C., "Nonlinear Flexural-Flexural-Torsional Dynamics of Inextensional Beams: I. Equations of Motion," *Journal of Structural Mechanics*, Vol. 6, No. 4, 1978, pp. 437 - 448.

6. Crespo da Silva, M. R. M., and Glynn, C. C., "Nonlinear Flexural-Flexural-Torsional Dynamics of Inextensional Beams: II. Forced Motions," *Journal of Structural Mechanics*, Vol. 6, No. 4, 1978, pp. 449 - 461.

7. Dowell, E. H., and Traybar, J., "An Experimental Study of the Non-linear Stiffness of a Rotor Blade Undergoing Flap, Lag and Twist Deformations," AMS Report No. 1194, Princeton University, Jan. 1975.

8. Dowell, E. H., and Traybar, J., "An Experimental Study of the Non-linear Stiffness of a Rotor Blade Undergoing Flap, Lag and Twist Deformations," AMS Report No. 1257, Princeton University, Dec. 1975.

9. Hinnant, Howard E., and Hodges, Dewey H., "Application of GRASP to Nonlinear Analysis of a Cantilever Beam," AIAA Paper 87-0953, *Proceedings of the 28th Structures, Structural Dynamics and Materials Conference and Dynamics Specialists Conference (Part II)*, Monterey, California, Apr. 6 - 10, 1987, pp. 966 - 975.

10. Dowell, E. H., Hodges, D. H., and Traybar, J., "An Experimental-Theoretical Study of Nonlinear Bending and Torsion Deformation of a Cantilever Beam," *J. Sound and Vib.*, Vol. 50, No. 4, Feb. 22, 1977, pp. 533 - 544.

11. Rosen, A., and Friedmann, P., "The Nonlinear Behavior of Elastic Slender, Straight, Beams Undergoing Small Strains and Moderate Rotations," *Journal of Applied Mechanics*, Vol. 46, 1979, pp. 161 - 168.

12. Rosen, A., Loewy, R. G., and Mathew, M. B., "Nonlinear Analysis of Pretwisted Rods Using 'Principal Curvature Transformation' Part I: Theoretical Derivation," *AIAA Journal*, Vol. 25, No. 3, 1987, pp. 470 - 478.

13. Rosen, A., Loewy, R. G., and Mathew, M. B., "Nonlinear Analysis of Pretwisted Rods Using 'Principal Curvature Transformation' Part II: Numerical Results," *AIAA Journal*, Vol. 25, No. 4, 1987, pp. 598 - 604.

NONLINEAR FLEXURAL-FLEXURAL-TORSIONAL-EXTENSIONAL DYNAMICS OF BEAMS: FORMULATION AND RESPONSE

M.R.M. Crespo da Silva
Professor, Department of Mechanical Engineering,
Aeronautical Engineering and Mechanics
Rensselaer Polytechnic Institute
Troy, New York 12180-3590 U.S.A.

ABSTRACT

The nonlinear dynamics of beams capable of undergoing flexure along two principal directions (and, thus, flexure in any direction in space), torsion and extension, is discussed. The analysis presented here is based on a set of consistent nonlinear differential equations of motion that are valid for extensional and for inextensional beams. The beam's material is assumed to be Hookean, and the beam's properties may vary along its span. The nonlinearities in the differential equations of motion include contributions from the beam's curvature and torsion expressions, from inertia terms, and from midsurface extension if the beam is extensional. A number of studies are being conducted at R.P.I. dealing with the nonlinear flexural-flexural and flexural-flexural-torsional dynamics of inextensional beams and beam-like structures. In this paper the influence of several types of nonlinearities in the dynamics of inextensional and of extensional beams is discussed.

FORMULATION AND ANALYSIS

The nonlinear differential equations governing the flexural-flexural-torsional motions of Euler-Bernoulli inextensional beams were formulated by Crespo da Silva and Glynn [1]. The equations developed in [1] are valid for arbitrary property variations along the beam's span. They are also valid for the general case where the bending and torsional motions are of the same order. A number of cases were investigated by the same authors involving the nonlinear non-planar free and forced response of inextensional beams and for the case where the torsional natural frequencies were much higher than the bending natural frequencies [e.g. 2-8]. Non-planar motions of extensional beams were considered by Ho, Scott and Eisley [9,10] by making use of a set of differential equations where torsional effects and nonlinear contributions to the curvature were neglected a priori.

From a fundamentally rigorous point of view, the inextensional assumption and the differential equations of motion for beams with fixed-sliding or with fixed-fixed boundaries should be a by-product of a unified approach that treats both extensional and inextensional systems. One then could assess the validity of neglecting nonlinear terms, such as higher-

order contributions to bending curvature and the torsion terms, when analyzing the nonlinear response of such systems.

The details of the formulation of the nonlinear differential equations of motion, and their boundary conditions, for initially straight Euler-Bernoulli beams able to undergo flexure along two principal directions, torsion and extension, are presented in [11]. The nonlinearities present in the equations include contributions from the curvature and torsion expressions, and from inertia terms. The equations developed in [11] are also valid for the general case beam's stiffness and distributed mass may vary along its span, and when the flexural and torsional motions are of the same order. A particular form of these equations, valid for the simpler case when the beam's properties are constant along its span and when the distributed mass moments of inertia are neglected (and thus, when the torsional natural frequencies are much higher than the berding natural frequencies) are given below. Here, x denotes distance, normalized by the undeformed beam's length L, measured along the line joining the beam's supports at x = 0 and at x = 1, and t is normalized time as defined in [1].

$$\ddot{v} + c\dot{v} + \beta_y v'''' = Q_v(x,t) + \beta_A \frac{K_u v''}{1+K_u} \int_0^1 (v'^2 + w'^2)dx$$

$$+ \left\{ (1-\beta_y)\left[w'' \int_1^x v''w''dx - w''' \int_0^x v''w'dx - \frac{K_\gamma w''}{1+K_\gamma} \int_0^1 \int_1^x v''w''dx\,dx \right] - \beta_y v'(v'v'' + w'w'')' \right.$$

$$- \frac{(1-\beta_y)^2}{\beta_\gamma}\left[w'' \int_0^x \int_1^x v''w''dx - \frac{K_\gamma}{1+K_\gamma}(xw'') \int_0^1 \int_1^x v''w''dx\,dx \right]'$$

$$\left. + \beta_y \frac{K_u}{1+K_u} v''' \int_0^1 (v'^2 + w'^2)dx + \frac{v'}{2} \int_1^x \left[\frac{xK_u}{1+K_u} \int_0^1 (v'^2 + w'^2)dx - \int_0^x (v'^2 + w'^2)dx \right]^{\cdot} dx \right\}' \qquad (1a)$$

$$\ddot{w} + c\dot{w} + w'''' = Q_w(x,t) + \beta_A \frac{K_u w''}{1+K_u} \int_0^1 (v'^2 + w'^2)dx$$

$$- \left\{ (1-\beta_y)\left[v'' \int_1^x v''w''dx + v''' \int_0^x v''w'dx - v'''v'w' - \frac{K_\gamma v''}{1+K_\gamma} \int_0^1 \int_1^x v''w''dx\,dx \right] \right.$$

$$+ \frac{(1-\beta_y)^2}{\beta_\gamma}\left[v'' \int_0^x \int_1^x v''w''dx\,dx - \frac{K_\gamma}{1+K_\gamma}(xv'') \int_0^1 \int_1^x v''w''dx\,dx \right]' + w'(v'v'' + w'w'')'$$

$$\left. - \frac{K_u}{1+K_u} w''' \int_0^1 (v'^2 + w'^2)dx - \frac{w'}{2} \int_1^x \left[\frac{xK_u}{1+K_u} \int_0^1 (v'^2 + w'^2)dx - \int_0^x (v'^2 + w'^2)dx \right]^{\cdot} dx \right\}' \qquad (1b)$$

In equations (1a,b), $v(x,t)$ and $w(x,t)$ are the components, along orthogonal inertial directions, of the beam's elastic deformations due to bending; $\beta_A = EAL^2/(2EI_\eta)$, $\beta_y = EI_\zeta/(EI_\eta)$, $\beta_\gamma = GJ/(EI_\eta)$, where A and L are, respectively, the beam's "cross-sectional area" and length; EI_η and EI_ζ are the beam's bending stiffnesses and GJ is its torsional stiffness. The parameters K_u and K_γ are constants; $K_u = 0$ if the end at $x = 1$ is free to move, and $K_u = \infty$ if it is fixed; $K_\gamma =$ if the end at $x = 1$ is free to rotate, and $K_\gamma = \infty$ if it is restrained against rotation. The terms multiplied by β_A in equations (1a,b) are due to midplane stretching of the beam's mid-surface. For inextensional beams ($K_u = 0$) those terms are absent from the equations, of course.

The quantity $\mu \triangleq D_\eta/(EAL^2)$ is the square of the radius of gyration (normalized by the length L of the undeformed beam) of the beam's cross section and, thus, is very small. For extensional beams, where $K_u \neq 0$, the terms multiplied by β_A in equations (1a,b) are the "dominant" nonlinearities in those equations [12]. For such beams, the bending deflections are $O(\mu)$ and, thus, very small. When $K_u = 0$ the beams behaves as inextensional [12]. In this case, all nonlinearities for an initially straight beam are cubic. For $K_u = 0$, and for $K_\gamma = 0$, equations (1a,b) reduce to equations (5a,b) in [2].

NONLINEAR RESPONSE: A BRIEF OVERVIEW

The nonlinear coupling terms in equations (1a,b) can cause a resonant energy exchange between the v and w bending components of the response, and between different "modes" associated with the planar or with the nonplanar response of the beams. Figure 1 shows the single harmonic response of a homogeneous clamped-free beam ($K_u = K_\gamma = 0$) with $\beta_y = (1.01)^2$, driven by a periodic force $Q_v(s,t) = K(s) \cos \Omega t$ with $\Omega = 1.01 \times (1.875)^2$, $c = 0.05$ and $q = \int_0^1 K(s)F(s)ds$, where $F(s)$ is the beam's first modal eigenfunction associated with the linearized counterpart to equations (1a,b)(s is arc length along the deformed inextensional beam). For these parameter values, the planar response is unstable.

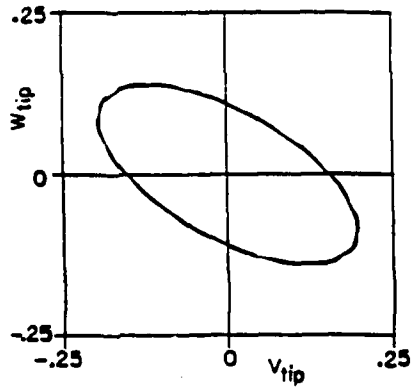

Figure 1. Nonlinear response of a beam subjected to a planar excitation.

The response shown in Figure 1 is non-planar and stable, and the beam's tip describes, to a first approximation, an ellipse in space. The spatial orientation of the ellipse depends on β_y, c, Ω and q.

Figure 2 shows the influence of EAL^2/D_η in a typical amplitude-frequency response characteristics of an extensional beam undergoing planar motion. The response shown is for a clamped-clamped beam subjected to a harmonic excitation with frequency Ω near the beam's first natural frequency ω, and with c = 0.002 and q = 0.0002.

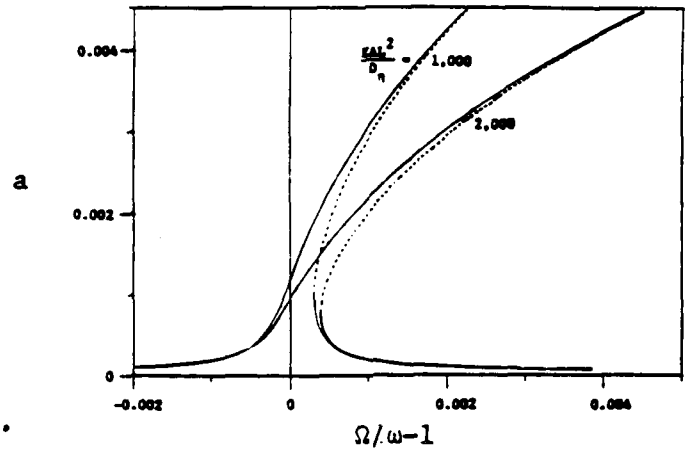

Figure 2. Typical amplitude-frequency response for an extensional beam

The same type of response shown in Figure 2 is exhibited by clamped-pinned and by pinned-pinned beams. An upper bound for the maximum amplitude, a_{max}, of the planar resonant response of extensional beams has been determined in [12]. With $\alpha = [\int_0^1 F'^2(x)dx]^2$, it was shown in [12] that

$$a_{max} << 4\omega\left[\frac{\sqrt{2}}{3\omega} D_\eta/(EAL^2)\right]^{1/2} \qquad (2)$$

A number of studies are being conducted at R.P.I. concerning the nonlinear non-planar response of inextensional beams and of beam-like structures. These include modal interactins both in the flexural-flexural and in the flexural-flexural-torsional dynamics of such beams. Beams with constant and with variable properties along the span are being conducted. A number of well-controlled experiments are also being performed at R.P.I. in order to generate data that can be used to verify the results of the analytical investigations being conducted.

REFERENCES

1. Crespo da Silva, M.R.M., and Glynn, C.C., Nonlinear flexural-flexural-torsional dynamics of inextensional beams. I. Equations of motion, J. Struct. Mech., Vol. 6, pp. 437-448 (1978).

2. Crespo da Silva, M.R.M., and Glynn, C.C., Nonlinear flexural-flexural-torsional dynamics of inextensional beams. II. Forced motions, J. Struct. Mech., Vol. 6, pp. 449-461 (1978).

3. Crespo da Silva, M.R.M., and Glynn, C.C., Nonlinear non-planar resonant oscillations in fixed-free beams with support asymmetry, Int. J. Solids and Struct., Vol. 15, pp. 209-219 (1979).

4. Crespo da Silva, M.R.M., and Glynn, C.C., Out-of-plane vibrations of a beam including non-linear inertia and non-linear curvature effects, Int. J. Non-Linear Mech., Vol. 13, pp. 261-271 (1979).

5. Crespo da Silva, M.R.M., Flexural-flexural oscillations of Beck's column subjected to a planar harmonic excitation, J. Sound and Vibr., Vol. 60, pp. 133-144 (1978).

6. Crespo da Silva,M.R.M., Harmonic non-linear response of Beck's column to a lateral excitation, Int. J. Solids and Struct., Vol. 14, pp. 987-997 (1978).

7. Crespo da Silva, M.R.M., Nonlinear resonances in a column subjected to a constant end force, J. Appl. Mech., ASME Trans., Vol. 47, pp. 409-414 (1980).

8. Crespo da Silva, M.R.M., On the whirling of a base-excited cantilever beam, J. Acoust. Soc. Am., Vol. 67, pp. 740-707 (1980).

9. Ho, C.H., Scott, R.A., and Eisley, J.G., "Non-planar, non-linear oscillations of a beam. I. Forced motions, Int. J. Non-linear Mech., Vol. 10, pp. 113-127 (1975).

10. Ho, C.H., Scott, R.A., and Eisley, J.G., "Non-planar, non-linear oscillations of a beam. II. Free motions, J. Sound and Vibr., Vol. 47, pp. 333-339 (1976).

11. Crespo da Silva, M.R.M., Nonlinear flexural-flexural-torsional-extensional dynamics of beams. I: Formulation. To appear in the Int. J. Solids and Struct.

12. Crespo da Silva, M.R.M., Nonlinear flexural-flexural-torsional-extensional dynamics of beams. II: Response analysis. To appear in the Int. J. Solids and Struct.

NONLINEAR MODAL COUPLING IN THE RESPONSE OF INEXTENSIONAL BEAMS

M.R.M. Crespo da Silva and C. L. Zaretzky
Department of Mechanical Engineering,
Aeronautical Engineering & Mechanics
Rensselaer Polytechnic Institute
Troy, New York 12180-3590 U.S.A.

ABSTRACT

Nonlinear inertia and curvature terms, as well as nonlinear terms that couple flexural and torsional motions, can have a dominant role in the response of inextensional beams or beam-like structural members. In this paper the effect of modal coupling in the nonlinear response of such members to a periodic excitation is discussed.

INTRODUCTION

Few authors have addressed problems associated with either nonlinear modal coupling in beams or nonlinear non-planar (with torsion) dynamic behavior of beams, or beam-like structures, or both. Such problems can be of primordial importance when, for example, one is dealing with large beam-like space-structure members. In this paper, nonlinear modal coupling phenomena in inextensional beams, due to geometric nonlinearities, are addressed. Due to space limitations, only a brief overview is presented. A detailed analysis of such motions is presented in [1].

An analysis of the flexural-flexural single-mode response of a cantilever subjected to a base excitation was first presented in [2]. The analysis presented in [2] was based on a set of differential equations of motion where nonlinear contributions from curvature and torsion were neglected a priori. A stability analysis of the motion was also performed in [2] based on a set of linearized differential equations with periodic coefficients. The problem considered in [2] was also addressed in [3] by making use of a consistent set of differential equations of motion that take into account all the geometric nonlinearities in the system [4,5]. In this paper, modal interactions in the response of inextensional structural beam-like elements are addressed. The differential equations of motion developed in [4] are applied to a beam with one end clamped and subjected to a periodic excitation that is either distributed or applied at one or at different points along its span. As in [5], we let $Lv(s,\tau)$ and $Lw(s,\tau)$ denote the bending deflections along two orthogonal inertial directions y and z, and $\gamma(s,\tau)$ denote the angle of twist of the beam. Before deformation, the principal axes along the beam's cross section at $s = s$ are aligned with the x and y directions. Here s denotes arc-length along the inextensional beam, normalized by the beam's length L, and τ denotes time. As shown in [1], the differential equations governing the flexural-flexural-torsional dynamics of an inextensional beam clamped at

$s = 0$ and with principal bending stiffnesses $EI_\eta(s)$ and $EI_\zeta(s)$, torsional stiffness $GJ(s)$, torsional distributed mass moment of inertia $j_\xi(s)$ and distributed mass $m^*(s)$, can be written as

$$\ddot{mv} + c\dot{v} + (\beta_y v'')'' = \left\{ w'' \int_1^s (\beta_\eta - \beta_y) v''w'' ds - [(\beta_\eta - \beta_y)w'']' \int_0^s v''w' ds - v'[\beta_y(v'v'' + w'w'')]' \right.$$
$$+ \left[(\beta_\eta - \beta_y)w'' \int_0^s \frac{1}{\beta_\gamma} \int_1^s [\mu\dot{g} - (\beta_\eta - \beta_y)v''w''] ds\, ds \right]'$$
$$\left. - \frac{v'}{2} \int_1^s m \left[\int_0^s (v'^2 + w'^2) ds \right]^{\cdot\cdot} ds - w'' \int_1^s \mu\dot{g}\, ds - \mu\dot{w}'g \right\}' + Q_v(s)\cos(\Omega_v t + \tau_v) \tag{1a}$$

$$\ddot{mw} + c\dot{w} + (\beta_\eta w'')'' = -\left\{ v'' \int_1^s (\beta_\eta - \beta_y) v''w'' ds - [(\beta_\eta - \beta_y)v'']' \int_0^s v'w'' ds + w'[\beta_\eta(v'v'' + w'w'')]' \right.$$
$$- \left[(\beta_\eta - \beta_y)v'' \int_0^s \frac{1}{\beta_\gamma} \int_1^s [\mu\dot{g} - (\beta_\eta - \beta_y)v''w''] ds\, ds \right]'$$
$$\left. + \frac{w'}{2} \int_1^s m \left[\int_0^s (v'^2 + w'^2) ds \right]^{\cdot\cdot} ds - v'' \int_1^s \mu\dot{g}\, ds + \mu\dot{v}'g \right\}' + Q_w(s)\cos(\Omega_w t + \tau_w) \tag{1b}$$

$$\mu\dot{g} - (\beta_\gamma\gamma')' - (\beta_\eta - \beta_y)v''w'' = Q_\gamma\cos(\Omega_\gamma t + \tau_\gamma) \tag{1c}$$

where $g = \dot{\gamma} + \dot{v}'w' - \left[\int_0^s v''w'' ds \right]^{\cdot}$.

In equations (1a-c), $(\,)' = \partial(\,)/\partial s$, $(\,)^{\cdot} = \partial(\,)/\partial t$, $\beta_\eta = EI_\eta/D_{\eta 0}$, $\beta_y = EI_\zeta/D_{\eta 0}$, $\beta_\gamma = GJ/D_{\eta 0}$, $\mu = j_\xi/(m_0 L^2)$ and $t = \tau\sqrt{D_{\eta 0}/m_0 L^4)}$, where $D_{\eta 0} = \int_0^1 EI_\eta(s) ds$, $m_0 = \int_0^1 m^*(s) ds$ and $m(s) = m^*(s)/m_0$; the parameter c is a normalized viscous damping coefficient. Also, $Q_\alpha(s)\cos(\Omega_\alpha t + \tau_\alpha)$, for $\alpha = v$ and w, are the components of the external excitation along the inertial y and z directions, respectively, and $Q_\gamma(s)\cos(\Omega_\gamma t + \tau_\gamma)$ is an externally applied moment. Here we will consider the case where $Q_w = Q_\gamma = 0$. The small effects of shear [6] and of the distributed mass moments of inertia on the bending deflections are neglected in these equations.

NONLINEAR MODAL INTERACTIONS

To analyze the response of the system, we first introduce an arbitrary perturbation parameter ε, which is used for "bookkeeping" purposes only,

three time scales $t_i = \varepsilon^i t (i = 0,1,2)$, and let $\alpha = \sum_{i=1}^{n} F_{\alpha_i}(s)\alpha_{t_i}(t)$ for $\alpha = v,w,\gamma$. Here the functions F_{α_i} are chosen to be the eigenfunctions associated with the linearized counterpart of equations (1a-c). The temporal part of the solution of the linearized, $O(\varepsilon)$, differential equations is obtained as

$$\alpha_{t_i} = A_{\alpha_i}(t_1,t_2)\cos\left[\omega_{\alpha_i} t_0 + B_{\alpha_i}(t_1,t_2)\right]; \quad \alpha = v,w,\gamma \tag{2}$$

When the solution to the linearized equations is substituted into the $O(\varepsilon^i)$, $i > 1$, differential equations, a number of resonances between the bending-bending and bending torsion motions are identified. The steady-state response (and the stability of the perturbed motion about that steady state) associated with each resonant motion is then obtained from the solvability conditions extracted from those differential equations. The amplitude-frequency response characteristics for the structure are readily obtained from the solvability conditions.

The bimodal amplitude-frequency response curve for a fixed-free homogeneous beam with torsional natural frequencies much higher than its bending natural frequencies is shown in Figure 1. The response shown is for a planar motion with $c = 0.002$ and $q = \int_0^1 F_{v_i}(s)Q_v(s)ds = 0.08$, for $i = 3$.

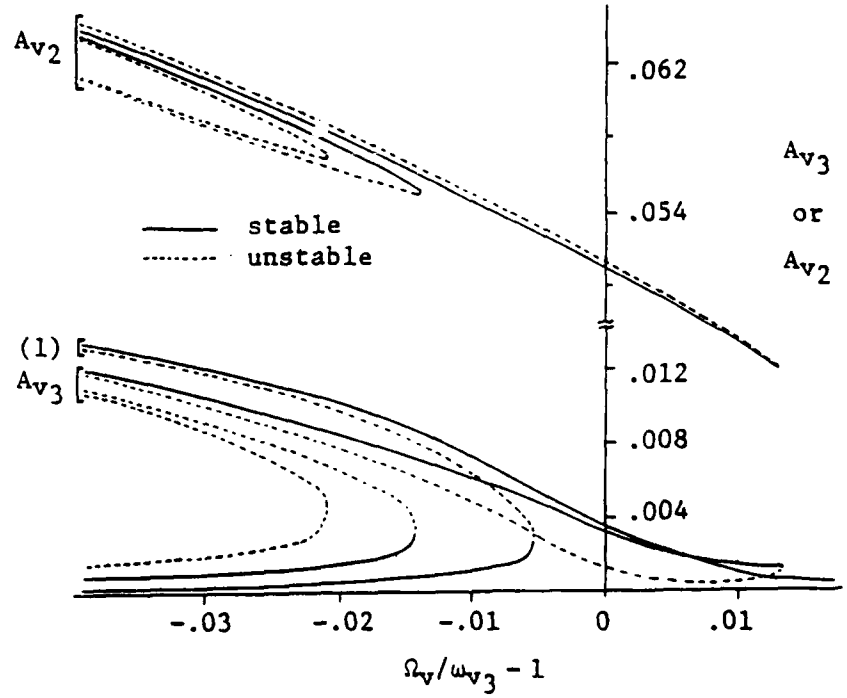

Figure 1. Amplitude (equilibrium) - frequency response curve for a clamped-free beam [(1): single mode response $(A_{v_2}) = 0$].

Figure 2 shows the amplitude response curves for a clamped-pinned/sliding beam with the same value of c and q (with i=2) given above. For the cantilever beam, the bimodal response exhibits modal interactions between the second and third linear modes; for the clamped-pinned/sliding beam the modal interaction is between the first and second modes. Nonlinear modal interactions in extensional beams were investigated by Nayfeh, Mook and their co-investigators [7-9]. For extensional beams, the main nonlinearity in the equations of motion is due to mid-surface stretching of the beam, and this nonlinearity is always of the hardening type [10].

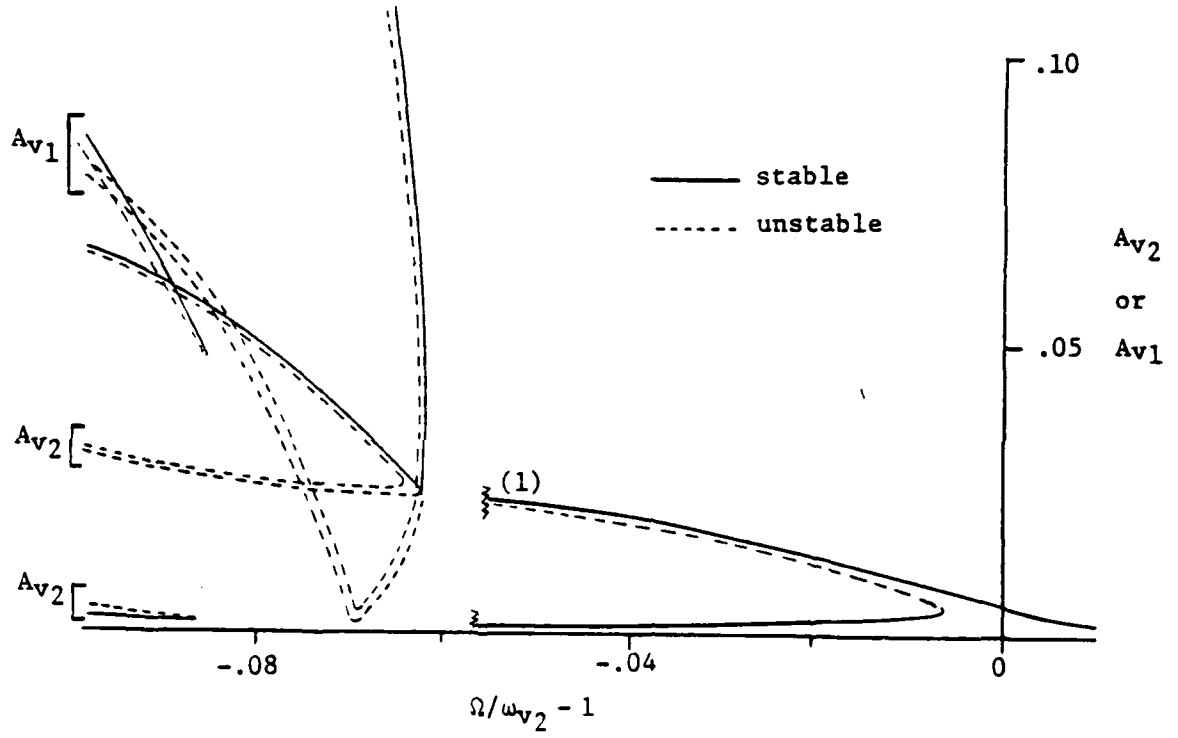

Figure 2. Amplitude (equilibrium) - frequency response for a clamped-pinned/sliding beam [(1): single mode response ($A_{v_1} = 0$)].

A number of experiments are being conducted by the authors to generate laboratory data that can be used to corroborate results of their various analytical investigations. These experiments involve beams with constant and variable cross sections, and long frames of the type to be employed in space structures. The results of these experiments will be reported in the near future.

ACKNOWLEDGMENTS

The work presented here was sponsored, in part, by the U.S. Air Force Contract No. F33615-87-C-3255 with the Flight Dynamics Laboratory, Air Force Wright Aeronautical Laboratories (AFSC).

REFERENCES

1. Crespo da Silva, M.R.M., and Zaretzky, C., Nonlinear Modal Coupling in the flexural-flexural and flexural-flexural-torsional motions of inextensional beams. In preparation.

2. Haight, E.C., King, W.W., Stability of nonlinear oscillations of an elastic rod. J. Acoust. Soc. Am., Vol. 52, pp. 899-911 (1971).

3. Crespo da Silva, M.R.M., On the whirling of a base-excited cantilever beam. J. Acoust. Soc. Am., Vol. 67, pp. 704-707 (1980).

4. Crespo da Silva, M.R.M., and Glynn, C.C., Nonlinear flexural-flexural-torsional dynamics of inextensional beams. I. Equations of motion, J. Struct. Mech., Vol. 6, pp. 437-448 (1978).

5. Crespo da Silva, M.R.M., and Glynn, C.C., Nonlinear flexural-flexural-torsional dynamics of inextensional beams. II. Forced Motions, J. Struct. Mech., Vol. 6, pp. 449-461 (1978).

6. Timoshenko, S., Young, D.H., and Weaver, W., Jr., Vibration Problems in Engineering, Wiley, New York (1974).

7. Nayfeh, A.H., Mook, D.T., and Sridhar, S., Nonlinear Analysis of the Forced Response of Structural Elements, J. Acoust. Soc. Am., Vol. 55, pp. 281-291 (1974).

8. Nayfeh, A.H., Mook, D.T., and Lobitz, D.W., Numerical perturbation method for the nonlinear analysis of structural vibrations, AIAA J., Vol. 12, pp. 1222-1228 (1974).

9. Nayfeh, A.H., Mook, D.T., and Nayfeh, J.F., Some aspects of the modal interactions in the response of beams, Paper No. 87-07777, AIAA Structures, Structural Dynamics and Materials Conference, Monterey, CA, April 6-8, 1987.

10. Crespo da Silva, M.R.M., Nonlinear flexural-flexural-torsional-extensional dynamics of beams. II. Response analysis. To appear in Int. J. Solids and Struct.

MODAL INTERACTIONS IN THE RESPONSE OF BEAMS TO A HARMONIC EXCITATION

J. F. Nayfeh, A. H. Nayfeh, and D. T. Mook
Department of Engineering Science and Mechanics
Virginia Polytechnic Institute and State University
Blacksburg, Virginia 24061

In this paper, we investigate some aspects of modal interactions in the response of beams. Specifically, we present a nonlinear analysis of the response of a hinged-clamped beam to a simple-harmonic excitation. For such a beam, the second natural frequency is approximately three times the first, leading to a state of internal (autoparametric) resonance which produces a strong coupling of these modes. This coupling is responsible for unusual responses that cannot be predicted by single-mode nonlinear analyses or by multi-mode linear analyses.

For a comprehensive review of the nonlinear response of beams to single- and multi-frequency excitations, we refer the reader to the textbook by Nayfeh and Mook[1].

A combination of geometric and material nonlinearitiers is considered[2]. The ends of the beam are immovable and a large lateral deformation or large amplitude vibration prduces stretching of the median line of the beam. The strain-displacement relation becomes nonlinear and is of the form

$$e = u^{o}_{,x} + \frac{1}{2} w^{2}_{,x} - zw_{,x} \tag{1}$$

In addition, the beam is assumed to be made of a nonlinear material. The Ramberg-Osgood material with cubic nonlinearity is used and the stress-strain relation is given by

$$\sigma_x = Ae - Be^3 \tag{2}$$

where A and B are the material constants. Neglecting the longitudinal and rotary inertia and the transverse shear, we find that the transverse deflection w(x,t) is governed by

$$w_{,tt} + \frac{AI}{\rho} w_{,xxxx} = -\frac{c}{\rho} w_{,t} + \alpha_1 w_{,xx} \int_0^L (w_{,x})^2 dx + 2\alpha_2 w_{,xx}(w_{,xxx})^2$$

$$+ \alpha_2 (w_{,xx})^2 w_{,xxxx} + \frac{Q(x,t)}{\rho} \tag{3}$$

where

$$\alpha_1 = \frac{Abh}{2\rho L}, \quad \alpha_2 = \frac{3Bbh^5}{40\rho} \tag{4}$$

Here ρ is the mass density of the beam, b, h and I are the width, height and moment of inertia of the cross section, c is the damping coefficient, and Q is the applied transverse load.

The linear free-vibration solution is

$$w(x,t) = \phi(x) \cos(\omega t + \beta) \tag{5}$$

where

$$\phi = b[\sin(s_1 x) - \frac{\sin(s_1 L)}{\sinh(s_2 L)} \sinh(s_2 x)] \tag{6}$$

$$s_n^2 = \mp \left(\frac{\rho \omega_n^2}{AI}\right)^{\frac{1}{2}} \tag{7}$$

$$s_2 \tan(s_1 L) - s_1 \tanh(s_2 L) = 0 \tag{8}$$

and b is chosen so that

$$\int_0^L \phi^2 dx = L \tag{9}$$

Next, we expand the solution of Eq. (3) in terms of the free undamped linear modes as

$$w(x,t) = \sum_{n=1}^{\infty} v_m(t)\phi_m(x) \tag{10}$$

Using the Galerkin procedure and assuming modal damping, we obtain the nondimensional temporal equations of motion

$$\frac{d^2\hat{v}_n}{d\hat{t}^2} + \Omega_n^2 \hat{v}_n = -2\varepsilon\mu_n \frac{d\hat{v}_n}{d\hat{t}} + \varepsilon \sum_{m,k,\ell} \Gamma_{nmk\ell} \hat{v}_m \hat{v}_k \hat{v}_\ell + \varepsilon F_n(\hat{t}) \tag{11}$$

where

$$c_{nn} = \frac{1}{\rho} \int_0^L c\phi_n(x)\phi_n(x)dx \tag{12}$$

$$Q_n(t) = \frac{1}{\rho} \int_0^L Q(x,t)\phi_n(x)dx \tag{13}$$

$$\omega_1^2 \Gamma_{nmk\ell} = -\alpha_1 \left[\int_0^L \phi_n' \phi_m' dx\right]\left[\int_0^L \phi_k' \phi_\ell' dx\right] - 2\alpha_2 \left[\int_0^L \phi_n' \phi_m' dx\right]\left[\int_0^L \phi_k'''' \phi_\ell'''' dx\right]$$
$$+ \alpha_2 \left[\int_0^L \phi_n'' \phi_m'' dx\right]\left[\int_0^L \phi_k'' \phi_\ell'' dx\right] \tag{14}$$

$$\Omega_n = \frac{\omega_n}{\omega_1}, \quad 2\varepsilon\mu_n = \frac{c_{nn}}{\omega_1}, \quad \varepsilon F_n = \frac{Q_n}{\omega_1^2} \tag{15}$$

and ε is a small parameter, which is introduced as a bookkeeping device and will be set equal to unity in the final analysis.

Method of Analysis

We use the method of multiple scales[3] to determine a uniform first-order expansion of the solutions of Eq. (11) when $F_n(t)$ is harmonic; that is,

$$F_n(\hat{t}) = f_n \cos\Omega\hat{t} \tag{16}$$

and Ω is near Ω_2. To express quantitatively the nearness of the primary and internal resonances, we introduce the detuning parameters σ_1 and σ_2 defined according to

$$\Omega_2 = 3\Omega_1 + \varepsilon\sigma_1 \quad \text{and} \quad \Omega = \Omega_2 + \varepsilon\sigma_2 \tag{17}$$

Applying the method of multiple scales, we obtain the modulation equations

$$2i(A_1' + \mu_1 A_1) - 8A_1 \sum_n \gamma_{1m} A_m \bar{A}_m - 8\delta_1 A_2 \bar{A}_1^2 e^{i\sigma_1 T_1} = 0 \tag{18}$$

$$2i\Omega_2(A_2' + \mu_2 A_2) - 8\Omega_2 A_2 \sum_n \gamma_{2m} A_m \bar{A}_m - 8\Omega_2 \delta_2 A_1^3 e^{-i\sigma_1 T_1} - \frac{1}{2} f_2 e^{i\sigma_2 T_1} = 0 \tag{19}$$

where

$$8\Omega_1\delta_1 = 3\Gamma_{1112}, \; 8\Omega_2\delta_2 = \Gamma_{1112} \tag{20a}$$

$$8\Omega_m\gamma_{mj} = 2(\Gamma_{mmjj} + 2\Gamma_{mjmj}), \; m \neq j, \; 8\Omega_m\gamma_{mm} = 3\Gamma_{mmmm} \tag{20b}$$

To analyze the solutions of Eqs. (18) and (19), we let

$$A_1 = \frac{1}{2}(p_1 - iq_1)e^{i\nu_1 T_1} \quad \text{and} \quad A_2 = \frac{1}{2}(p_2 - iq_2)e^{i\nu_2 T_1} \tag{21}$$

where

$$\nu_1 = \frac{1}{3}(\sigma_2 + \sigma_1) \quad \text{and} \quad \nu_2 = \sigma_2 \tag{22}$$

Substituting Eqs. (21) and (22) into Eqs. (16) and (17) and separating real and imaginary parts, we obtain the following autonomous equations describing the modulation in amplitude and phase:

$$p_1' + \mu_1 p_1 + \nu_1 q_1 + \gamma_{11} q_1 (p_1^2 + q_1^2) + \gamma_{12} q_1 (p_2^2 + q_2^2) + \delta_1 q_2 (p_1^2 - q_1^2) - 2\delta_1 p_1 p_2 q_1 = 0 \tag{23}$$

$$q_1' + \mu_1 q_1 - \nu_1 p_1 - \gamma_{11} p_1 (p_1^2 + q_1^2) - \gamma_{12} p_1 (p_2^2 + q_2^2) - \delta_1 p_2 (p_1^2 - q_1^2) - 2\delta_1 p_1 q_1 q_2 = 0 \tag{24}$$

$$p_2' + \mu_2 p_2 + \nu_2 q_2 + \gamma_{21} q_2 (p_1^2 + q_1^2) + \gamma_{22} q_2 (p_2^2 + q_2^2) + \delta_2 (3p_1^2 q_1 - q_1^3) = 0 \tag{25}$$

$$q_2' + \mu_2 q_2 - \nu_2 p_2 - \gamma_{21} p_2 (p_1^2 + q_1^2) - \gamma_{22} p_2 (p_2^2 + q_2^2) - \delta_2 (p_1^3 - 3p_1 q_1^2) - f_2/2\Omega_2 = 0 \tag{26}$$

Next, we present numerical results for the case $\omega_1 = 15.418$, $\omega_2 = 49.965$, $\Omega_2 = 3.241$, $\sigma_1 = 3.710$, $\mu_1 = \mu_2 = .01$, $3\Omega_2\gamma_{11}/\delta_1 = 3\Omega_2\gamma_{22}/\delta_1 = 1$, $3\gamma_{12}/\delta_1 = \Omega_2$ and $f_2 = 1$.

Periodic solutions of w correspond to the fixed points of Eqs. (23)-(26). There are two possibilities. First, $p_1 = q_1 = a_1 = 0$, and

$$\sigma_2 = -\gamma_{22}a_2^2 \pm \left[\frac{f_2^2}{4\Omega_2^2 a_2^2} - \mu_2^2\right]^{\frac{1}{2}} \tag{27}$$

where

$$a_1^2 = p_1^2 + q_1^2,\ a_2^2 = p_2^2 + q_2^2,\ \theta_2 = \sin^{-1}(q_2/a_2)$$

$$\text{and } \theta_1 = 3\sin^{-1}(q_1/a_1) - \theta_2 \tag{28}$$

The single-mode nonlinear solution is shown in Figures 1 and 2. Second, $p_1 \neq 0$ and $q_1 \neq 0$.

The stability of the fixed points is determined by the eigenvalues of the Jacobian matrix of the flow governed by (23)-(26). If all the eigenvalues have negative real parts, the fixed point is stable, otherwise it is not stable. Hopf bifurcation occurs when the real part of a complex conjugate pair of eigenvalues changes sign from negative to positive. In these ranges, steady state periodic solutions do not exist contrary to results predicted by linear multi-mode analyses or nonlinear single-mode analyses. Instead, the energy is continuously exchanged between the modes involved in the autoparametric resonance (Figure 3). Moreover, for small damping, the response experiences period-multiplying bifurcations and chaos. The stability of the periodic solutions is determined using Floquet theory. One of the Floquet multipliers is always unity because the system is autonomous. The unit circle is traversed at -1 giving a supercritical subharmonic bifurcation (Figures 4 and 5). An infinite sequence of period doubling takes place culminating in chaos (Figure 6). The mechanism is reported by Tonsi and Bajaj[4] in their studies of mechanical systems with cubic nonlinearities.

Acknowledgement

This work was supported by the Air Force Office of Scientific Research under Grant # AFOSR-86-0090.

References

1. Nayfeh, A. H. and Mook, D. T., Nonlinear Oscillations, Wiley-Interscience, New York, 1979.

2. Besseling, J. F., Ernst, L. J., et al., "Geometrical and Physical Nonlinearities: Some Developments in the Netherlands," Computer Methods Appl. Mech. Engrg., 17/18 (1), pp. 131-157, 1979.

3. Nayfeh, A. H., Perturbation Methods, Wiley-Interscience, New York, 1973.

4. Tonsi, S. and Bajaj, A. K., "Period-Doubling Bifurcations and Modulated Motions in Forced Mechanical Systems," ASME Journal of Applied Mechanics, Vol. 52, pp. 446-452, 1985.

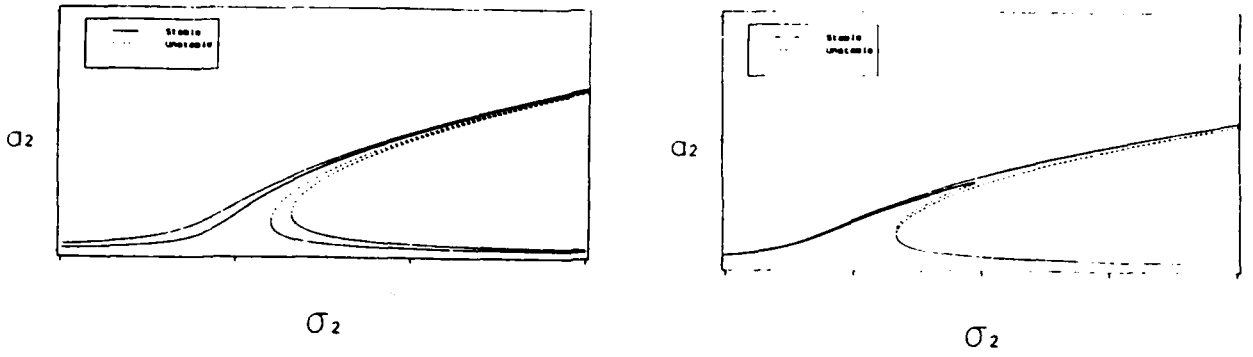

Figure 1. Single-mode nonlinear analysis. Left, effect of changing amplitude of excitation; right effect of changing damping.

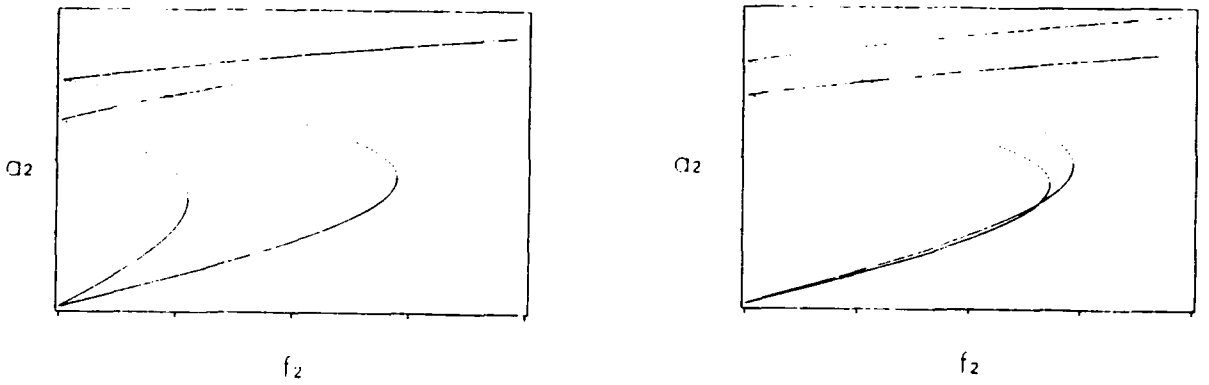

Figure 2. Single-mode nonlinear analysis. Left, effect of changing σ_2; right effect of changing damping.

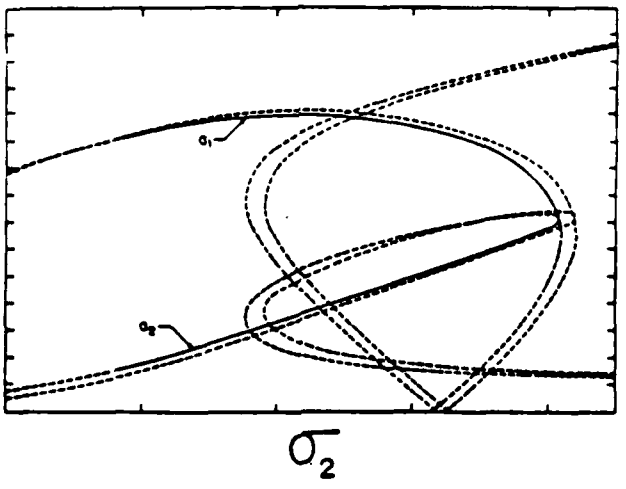

Figure 3. Multi-mode nonlinear analysis.

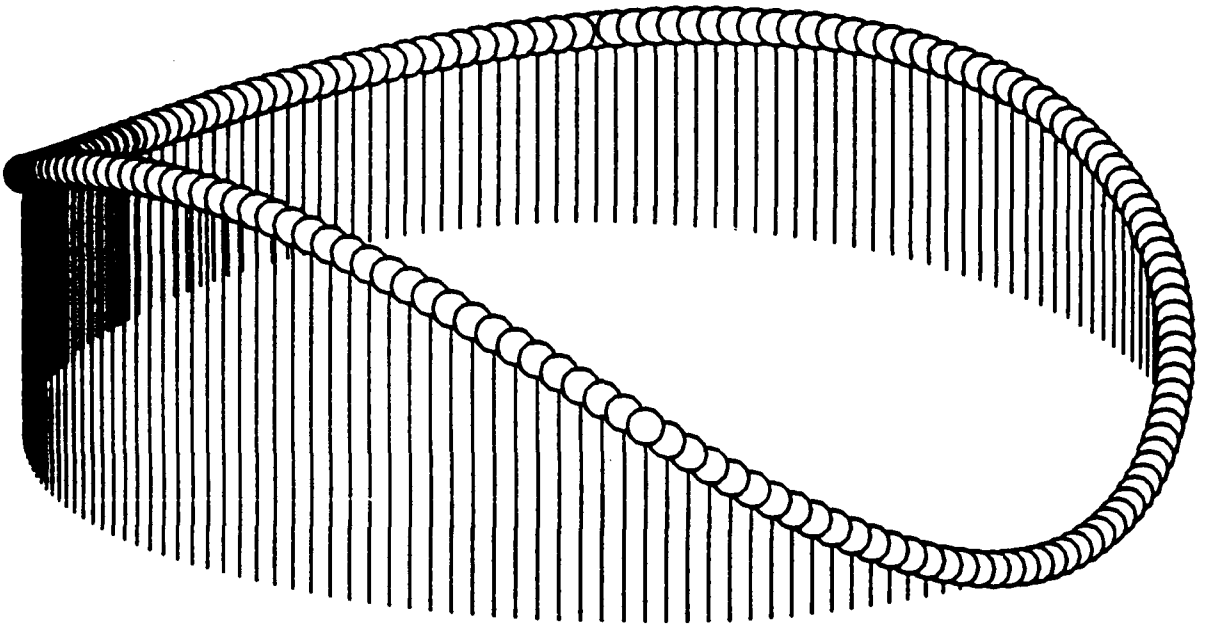

Figure 4. A 3-D projection of the limit cycle attractor for σ_2 = .3805. The needles show the 2-D projection of the attractor on the plane $a_2 - \theta_1$.

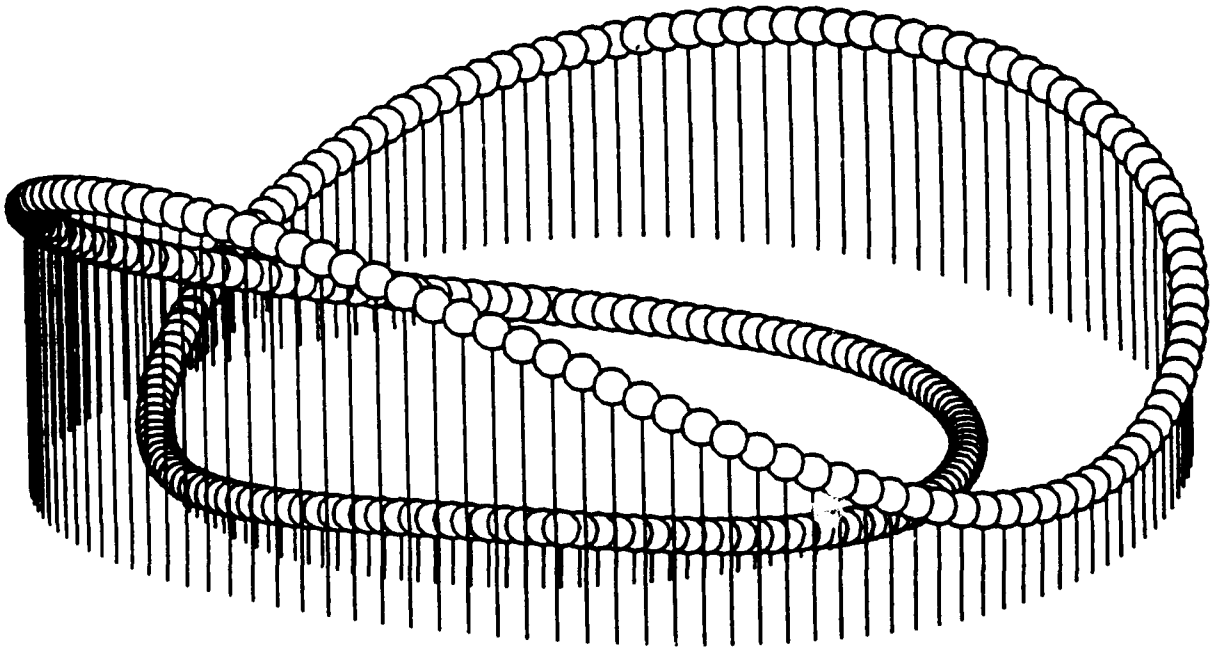

Figure 5. A 3-D projection of the period-doubled attractor at σ_2 = .3908. The needles show the 2-D projection of the attractor on the $a_2 - \theta_1$.

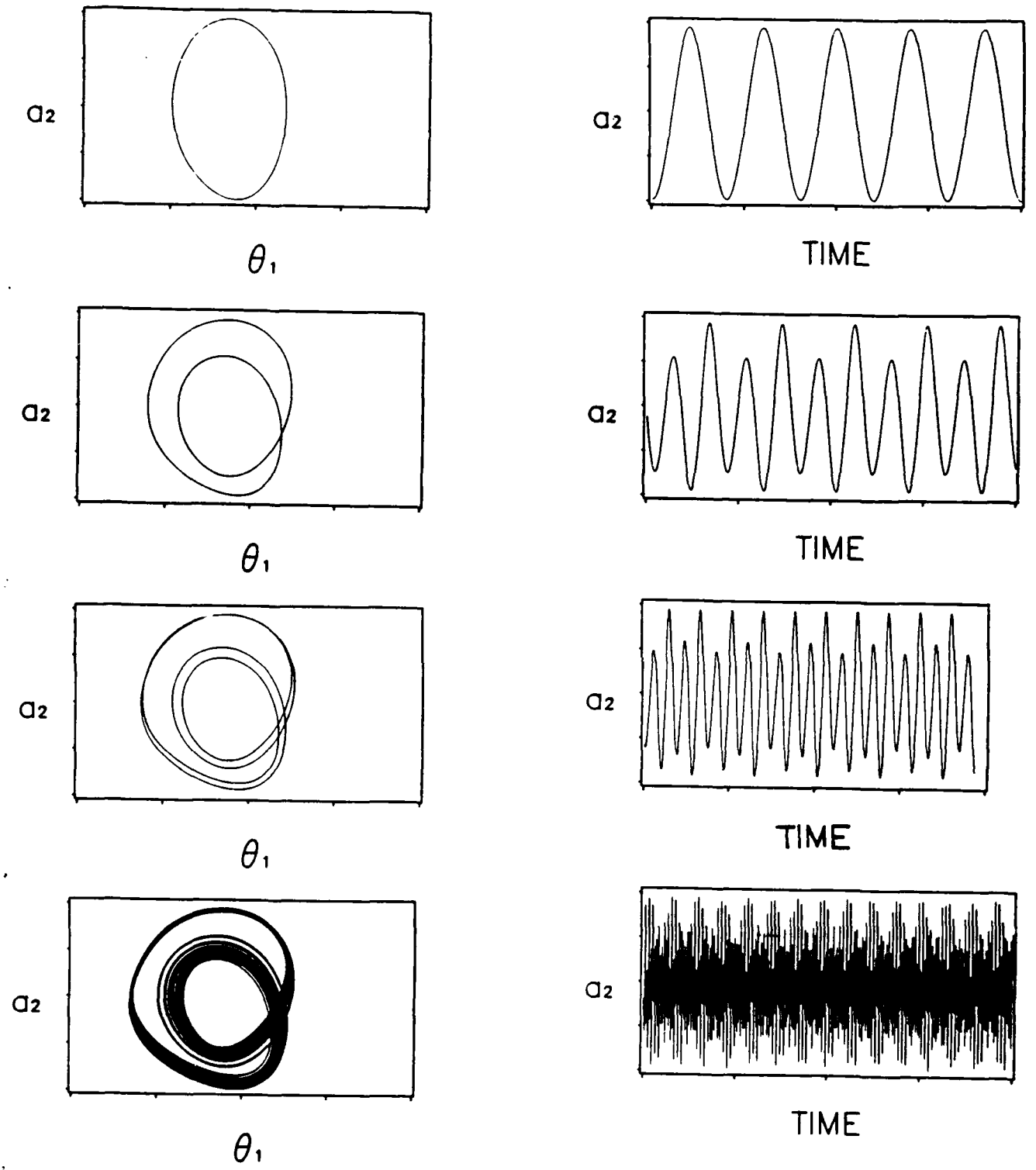

Figure 6. Phase diagrams of period-doubling bifurcations leading to chaos on the right and their corresponding wave forms on the left. From top to bottom σ_2 = (.3805, .3908, .3952, .4036).

ANALYSIS AND DESIGN SENSITIVITY CALCULATION OF NONLINEAR FORCED VIBRATIONS OF STEPPED BEAMS*

J. W. Hou, Y. X. Xue, C. Mei and C. Jackson
Department of Mechanical Engineering and Mechanics
Old Dominion University
Norfolk, VA 23529-0247

I. INTRODUCTION

In many engineering design textbooks, the failure criteria of fatigue are usually expressed in terms of stresses obtained by using linear vibration theory. However, nowadays many light-weight structures often experience large amplitude vibration. The effects of such large amplitude can not be ignored in designing structures against fatigue. Figure 1, in which the amplitude of the vibrating beam is more than half of its thickness, displays the relations between the number of cycles and the stresses calculated by linear and nonlinear vibration theories. It indicates that if the frequency of the harmonically excited force is lower than that of the natural frequency of the system, the stress obtained by using a linear vibration theory is higher than one obtained by using a nonlinear theory. Likewise, if the frequency of the excited force is greater than the natural frequency, the stress obtained by using a linear vibration theory is lower than one obtained by using a nonlinear theory. If the frequency of the excited force is greater than the natural frequency, the stress obtained by using a linear vibration theory is lower than one obtained by using a nonlinear theory. In other words, based upon the linear vibration theory, the structural or mechanical system can either be overdesigned or underdesigned depending upon the relation between the input force frequency and the natural frequency.

In order to consider this large amplitude in an automatic design environment, research efforts have been focused upon the enhancement of analysis capabilities and the development of design sensitivity analysis techniques. Some progress in this regard is reported in the following sections.

II. FINITE ELEMENT ANALYSIS OF NONLINEAR FORCED VIBRATION

There are many methods available to analyze responses of beams under nonlinear forced vibration. Because of its versatility and practical applications, the study will concentrate on the finite element approach proposed in reference [1]. It is initially used to find the response of a uniform beam, and is then modified to solve the responses of a stepped beam.

* This was partly supported by NSF Grant No. DMC-8657917 and NASA-Langley Grant No. NGT-70020.

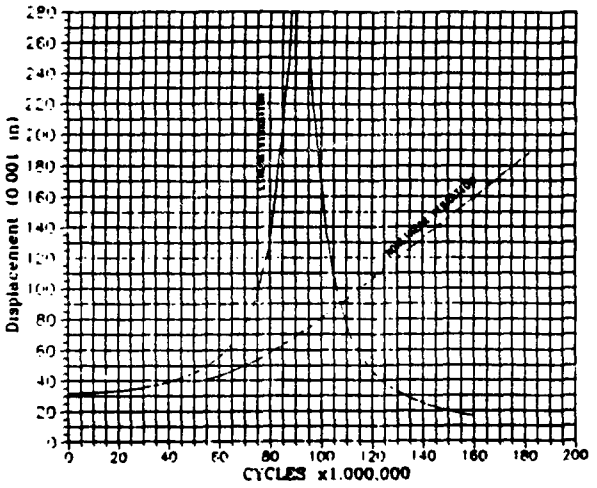

Fig. 1a Displacements of Beams Under Forced Vibrations

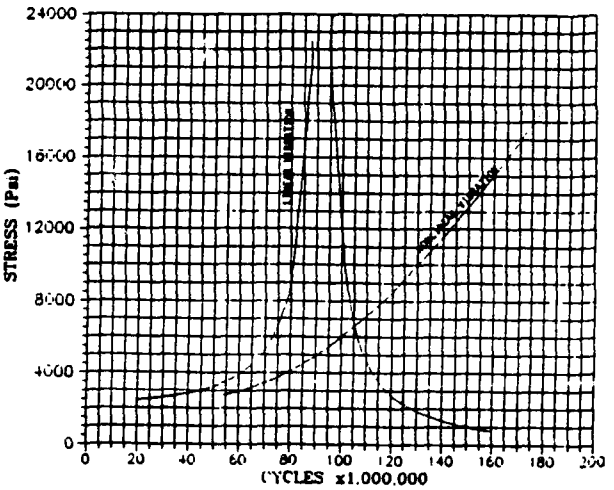

Fig. 1b Stresses of Beams Under Forced Vibrations

UNIFORM BEAM

The Lagrahgian of a uniform beam under harmonic excitation f(x,t) can be expressed as

$$L = \frac{1}{2}\int_0^L [EI\, w,_{xx}^2 + EA\,(u,_x + \frac{1}{2} w,_x^2)]\, dx - \frac{1}{2}\int_0^L (m\dot{w}^2 + m\dot{u}^2)\, dx$$
$$- \int_0^L f(x,t)\, w dx$$

After linearizing the strain energy, it can be discretized and approximated by finite element matrix equations:

$$[K]\{x\} + [G(\{x\})]\{x\} - [H(\{x\})]\{x\} - \lambda[M]\{x\} = 0 \qquad (1)$$

where $[G(\{x\})]$ corresponds to the nonlinear part of the strain energy and $[H(\{x\})]$ is the harmonic force matrix which is proportional to a constant B^0. The term $[H(\{x\})]\{x\}$ is a linear spring force which is an approximation of the harmonic excitation. The mathematical justification of the above statement can be found in Hsu's work [2]. The spring constant B^0 can be derived as

$$B^0 = \frac{CF_0}{\gamma\omega_L^2}\ ,\ c = \int_{\ell_1}^{\ell_2} \phi\, dx \Big/ \int_0^{\ell} \phi^2 dx \qquad (2)$$

where γ is the maximum amplitude, ϕ is the normalized mode shape, ω_L is the linear fundamental eigenvalue, and $F_0 \cos \sqrt{\lambda}t$ is the harmonic force.

Equation 1 represents n individual equations. The possible unknowns in that equation, however, can be the mode shape {x} with n components, the frequency, and the force density of the harmonic excitation. With different combinations of given and unknown variables, equation 1 can be used to simulate many practical applications in which either the mode shape, the force density, or the frequency of an excitation can be considered as the primary unknown.

As one practical example, it is assumed that the maximum amplitude of the mode shape and the force density of the harmonic excitation are given. In this case, with the specified maximum amplitude and the assumed mode shape, equation 1 is solved iteratively as a linear eigenvalue problem for the mode shape and the frequency of the harmonic excitation [1]. The same solution procedure can also be used to solve a nonlinear vibration problem in which the frequency of the excitation and the maximum amplitude are determined as a priori with the harmonic excitation force density and the mode shape considered as unknowns.

Another important application, from a designer's point of view, is one in which the harmonic excitation force is completely specified, that is both the frequency and the force density are known; and the mode shape is the only unknown. In this case, equation 1 becomes a set of n nonlinear equations which may be solved by using a root-finding algorithm. However, proving the existence and uniqueness of the solution is a very subtle issue and has not yet been solved.

STEPPED BEAM

Not much work has been done in dealing with nonlinear forced vibration of stepped beams. A method based upon Eq. 1 has been proposed in reference [3] in which the spring constant, B_i^0, is evaluated for each individual beam element, instead of being evaluated over the entire length of the beam. The purpose of this modification is to allow the spring constant, B_i^0, to be different for different elements according to the geometric properties of each element and the actual load applied onto each element. Figure 2 shows the difference between the new and the original definitions of B_i^0. The new formulation of B_i^0 defined over the ith beam element is given as

$$B_i^0 = \frac{\int_{\ell_{i-1}}^{\ell_i} \phi \, dx}{\int_{\ell_{i-1}}^{\ell_i} \phi \, dx} \cdot \frac{F_{oi}}{A_{mp}}$$

where F_{oi} is the force density applied to the ith beam element. The matrix equation 1 with the new definition of B_i^0 can be applied to beams with stepped cross sections and to beams subjected to nonuniformly distributed harmonic loads.

For nonlinear vibrations of a uniform beam, a maximum difference of 1.2% is observed between the eigensolutions calculated by the proposed finite element method with B_i^0 and those calculated by the original method with B_i^0. As

for a stepped beam, there is no finite element solution available currently. However, numerical comparison indicates that the nonlinear eigenvalue solution obtained by the proposed finite element method is at most 1.5% higher than that obtained by the classical solution.

In short, numerical experience seems to confirm that the proposed finite element formulation for a nonuniform beam is valid.

III. NONLINEAR EIGENVALUE-EIGENVECTOR DESIGN DERIVATIVES

The field of design optimization has gone through a period of extensive development over the last two decades. One fruitful area of such research efforts is design sensitivity analysis. It has been recognized that design sensitivity analysis is capable of approximation analysis, analytical model improvement, and assessment of design trends. Thus, design sensitivity analysis has become more than a utility as an optimization design tool in its own right.

There are many valid approaches for determining the design derivatives of eigensolutions. Nevertheless, the computational procedure presented hereafter is an extension of the one reported in reference [4].

For simplicity, the coefficient matrices of finite element solutions of the nonlinear forced vibration can be written as

$$[A]\{x\} = 0 \tag{3}$$

where $[A] = [K] + [G] - [H] - \lambda [M]$. Premultiplying eigenvector $\{x\}^T$ to the above equation, one immediately has the following equality

$$\{x\}^T [A] \{x\} = 0. \tag{4}$$

There are n+1 unknowns in the last two matrix equations that can be used to find n+1 design derivatives of $\{x\}$ and λ. Let the subscript b denote the design derivative and $[E]$ denote the derivative of the vector $[G-H]\{x\}$, in which $\{x\}$ is held fixed, with respect to the eigenvector. With some manipulations, it is straightforward to obtain the design derivatives of Eqs. 3 and 4 as

$$\lambda_b = \frac{1}{\{x\}^T[M]\{x\}} \left[\{x\}^T [A_b]\{x\} + \{x\}^T[E]\{x_b\}\right] \tag{5}$$

and

$$\left([A] + [E] - \frac{[M]\{x\}\{x\}^T[E]}{\{x\}^T[M]\{x\}}\right), \{x_b\} = [A_b]\{x\} + \frac{[M]\{x\}}{\{x\}^T[M]\{x\}} \{x\}^T[A_b]\{x\}$$

or symbolically,

$$[B]\{x_b\} = \{c\} \tag{6}$$

where [B] and {c} are defined according to the last equation. In contrast to the linear eigenvalue problem, as indicated in Eq. 5, the design derivative of eigenvalue, λ_b, can not be calculated without knowing the design derivative of eigenvector $\{x_b\}$ in advance. Because $\{x\}^T[B]\{x_b\}=0$ and $\{x\}^T\{c\}=0$, it can be also concluded that [B] in Eq. 6 is singular based on the alternative theorem.

In order to avoid the singularity of [B] one can express the eigenvector design derivative $\{x_b\}$ as $\{x_b\} = \{\bar{x}\} + \alpha\{x\}$, where the unknown variables are $\{\bar{x}\}$ and the coefficient α. The $\{\bar{x}\}$ can be attained by the following matrix equations

$$([A] + [E])\{\bar{x}\} = [A_b]\{x\} - \alpha\,[E]\{x\} \tag{7}$$

$$\{\bar{x}\}^T\,[M]\{x\} = 0 \tag{8}$$

where the constraint Eq. 8 restricts $\{\bar{x}\}$ to be orthogonal to {x}. Applying the theorem of Lagrange multipliers to the above equations yields n+1 simultaneous equations for $\{\bar{x}\}$ and u

$$\begin{bmatrix} [A] + [E] & [M]\{x\} \\ \{x\}^T\,[M] & 0 \end{bmatrix} \begin{Bmatrix} \{\bar{x}\} \\ u \end{Bmatrix} = \begin{Bmatrix} [A_b]\,\{x\} \\ 0 \end{Bmatrix} - \alpha \begin{Bmatrix} [E]\,\{x\} \\ 0 \end{Bmatrix} \tag{9}$$

The leading coefficient matrix on the left side of the above equation is nonsymmetric, and there is an undetermined coefficient, α, appearing on the right side. Since the above equation is linear, one may superpose the solutions as

$$\begin{Bmatrix} \{\bar{x}\} \\ u \end{Bmatrix} = \begin{Bmatrix} \{\bar{x}_1\} \\ u_1 \end{Bmatrix} + \alpha \begin{Bmatrix} \{\bar{x}_2\} \\ u_1 \end{Bmatrix}$$

where the first and the second terms are the solutions of Eq. 9 with $\{([A_b]\{x\})^T, 0\}^T$ and $\{([E]\{x\})^T, 0\}^T$, as the forcing terms, respectively. The coefficient, α, is usually determined by considering the normalization of the corresponding eigenvector. For example, the maximum amplitude is often fixed in the formation of nonlinear forced vibration. In this case,

$$\alpha = -\frac{\bar{x}_1\,(x_o)}{\bar{x}_2\,(x_o) + x(x_o)}$$

where x_o is the position of the maximum amplitude.

The proposed computational scheme for design sensitivity analysis has been validated by several numerical examples. Table 1 tabulates the comparisons between the predicted and actual changes of the lateral deflection measured at a location 40 inches away from the center of the beam. It shows that the change predicted by the first order design sensitivity $w_b \cdot \Delta b$ can be used to approximate the actual change Δw. It is also important to note that, as indicated in the last row of Table 1, the design sensitivity analysis takes only one-seventh of the CPU time required for the direct analysis.

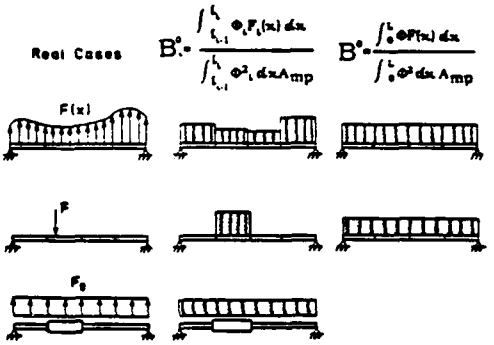

Fig. 2 Differences between two definitions of B°

IV. CONCLUSIONS AND REMARKS

This research has achieved the following goals:
1) Modification of the harmonic force matrix of an existing finite element method in order to treat stepped beams under nonlinear forced vibration.
2) Design sensitivity analysis of nonlinear vibration of stepped beams where the effects of both longitudinal displacement and inertia are included.

As mentioned before, many physical behaviors pertaining to nonlinear vibrations can not be realized by using the linear theory. The impact of these new physical behaviors on design considerations should be investigated carefully. Thus, it is important not only to enhance the nonlinear vibration formulations and analysis capability, but also to emphasize the research in the design sensitivity analysis of nonlinear eigensolutions. However, further efforts are needed in order to achieve the research goal.

REFERENCE

1. Mei, C. and Decha-Umphai, K., "A Finite Element Method for Nonlinear Forced Vibrations of Rectangular Plates," AIAA Journal, Vol. 23, 1985, pp. 1104-1110.
2. Hsu, C. S., "On the application of Elliptic Functions in Nonlinear Forced Oscillations," Quarterly of Applied Mathematics, Vol. 17, 1960, pp. 393-407.
3. Xue, Y. X., Analysis and Design Sensitivity Computations of Nonlinear Free and Forced Vibrations of Stepped Beams, M.S. thesis, Old Dominion University, Norfolk, VA, December 1987.
4. Hou, J. W., and Yuan, J. Z., "Calculation of Eigenvalue and Eigenvecter Derivatives for Nonlinear Beam Vibrations," AIAA paper No. 86-0963, presented at the 27th SDM conference, San Antonio, TX, May 19-21, 1986.

Table 1 Design sensitivity analysis of eigenvectors (displacements) associated with various perturbations of design variable for hinged, stepped beam under free vibration.

New H_1 (in.)	Change of H_1 (%)	New w_{40}** (in.)	Actual Change of w_{40}(in.)	Prediction $w_h \times H_1$(in.)	Error (%)
7.4825	-25.	9.36738	-0.45036	-0.47898	6.35
8.4801	-15.	9.53766	-0.28008	-0.28739	2.61
8.9790	-10.	9.62873	-0.18901	-0.19159	1.37
9.4778	- 5.	9.72243	-0.09531	-0.09580	0.51
10.475	+ 5.	9.91371	0.09597	0.09580	0.18
10.974	+10.	10.00945	0.19171	0.19159	0.06
11.473	+15.	10.10416	0.28642	0.28739	0.34
12.471	+25.	10.28788	0.47014	0.47898	1.88
CPU time ***		14.05 (s)^{o}	2.06 (s)^{oo}		

* $$\text{Error} = \left| \frac{w_h \times \Delta H_1 - \Delta w}{\Delta w} \right| \times 100\%$$

** w_{40} denotes the deflection at the location 40 in. away from the center of the beam.

*** On CDC 830, Single Precision

o Analysis at H_1=9.97661 in.

oo Design Sensitivity Analysis at H_1=9.97661 in.

Non Linear Oscillations and Limit Cycles: A Time Finite Element Approach

M. Borri
Center for the Advancement of Computational Mechanics
Georgia Institute of Technology, Atlanta, GA 30332
and
P. Mantegazza
Dipartimento di Ingegneria Aerospaziale
Politecnico di Milano
Via Golgi 40 - 20133 Milano - ITALY

1 Introduction

The importance of non linear oscillations in the study of vibration problems is well known to engineers and scientists. Several alternative analytical and numerical methods have been developed to solve these kind of problems [1-2].

These methods often require a lot of manual work even when they are applied to systems of a few degrees of freedom and are therefore too cumbersome for analyzing systems with many degrees of freedom.

The aim of the present paper is to show how the finite element approach in the time domain when applied to Hamilton's principle can provide a fully automated numerical scheme for solving problems of this type.

During the last decade much attention has been given to the numerical applications of Hamilton's principle, often called Hamilton's law of varying action, promoting also vigorous discussions about this subject [3-11]. The use of Hamilton's principle to solve periodic non-autonomous problmes has been proposed in Ref. [12], [13].

The present paper deals with more general periodic non linear problems in which the period is not known in advance. Finite elements in the time domain applied to Hamilton's principle provide a suitable numerical approach.

It is believed that the approach proposed here can be used for a wider class of problem than that shown. It is sufficient to remark that the method can be applied to initial and final value problems and that the linear stability can be analyzed by the eigenvalue analysis of the same matrices computed during the search for the solution [10, 12].

Moreover it is important to note that the proposed method is nothing but a suitable application of the virtual work principle and of finite element method to dynamics, so that the well known numerical algorithms and techniques of the finite element method can be profitably used.

In order to simplify the presentation, the method is formulated only for holonomic systems. Non-holonomic constraints could be accounted for in a natural way [16].

2 Hamilton's Principle and Finite Element Approximation

Let us consider a holonomic system with n degrees of freedom. At any given time t, the position of a representative point P in the configuration space is described by the set of n coordinates $\mathbf{q}$, i.e. $\mathbf{q} = (q_1, q_2, \cdots q_n)$ and let Γ be any trajectory of the system with equation $\Gamma = \Gamma(u)$ where u is an aribitrary independent parameter that assumes the role of independent variable.

Let $L(\mathbf{q}, \dot{\mathbf{q}}, t)$ be the ordinary Lagrangian function of the system, and S the Lagrangian action along any oriented curve Γ in the configuration space, drawn from the point P_1 (where $u = u_1$ and $t = t_1$) to the point P_2 (where $u = u_2 > u_1$ and $t = t_2 > t_1$) i.e.

$$S(\Gamma) = \int_{t_1}^{t_2} L(\mathbf{q}, \dot{\mathbf{q}}, t) dt$$

In addition to the conservative forces, whose potential is accounted for in the Lagrangian of the system, we will consider also a non-conservative force vector $\mathbf{Q}$ for which the virtual work is $\delta_c \mathbf{q} \cdot \mathbf{Q}$ and the virtual action is given by [1]:

$$\delta_c A = \int_{t_1}^{t_2} \delta_c \mathbf{q} \cdot \mathbf{Q} dt$$

Hamilton's principle can be written as:

$$\delta_c S + \delta_c A - \delta_c \mathbf{q} \cdot \mathbf{p}|_{t_1}^{t_2} = 0 \tag{1}$$

In view of the numerical applications, the boundary terms are of vital importance and cannot be dropped by constraining the virtual displacement to zero at the end points P_1, P_2. Moreover the generalized momenta $\mathbf{p}$ cannnot be overspecified by constraining them to be equal to $\frac{\partial L}{\partial \dot{\mathbf{q}}}$ since, their definition is naturally included in the principle.

This principle is very suitable for numerical approximation using the finite element approach. To this end we subdivide the interval $u_2 - u_1$ into consecutive non overlapping subintervals. We define with $\mathbf{u} = (u_1, u_2, \cdots, u_{N+1})$ the values of the parameter at the nodal points. Without loss of generality we assume $u_1 = 0$ and $u_{N+1} = 1$.

In the numerical formulation of the problem we assume the Lagrangian coordinate vector $\mathbf{q}$ ranging in some limited class of admissible functions $f(u)$ and we set:

$$\mathbf{q}(u) = \sum f_k(u) \mathbf{q}_k \tag{2}$$

where

$$\mathbf{q}_k = \mathbf{q}(u_k) \qquad k = 1, 2, \cdots N+1$$

Moreover in order to preserve the orientation of time t with the parameter u we assume:

$$t = t_1 + Tu \tag{3}$$

where $T > 0$ is the time interval $t_2 - t_1$.

For notational reasons and for sake of conciseness we define the following vectors $\mathbf{X}$ and $\mathbf{Y}$.

$$\mathbf{X} = (\mathbf{q}_1, \mathbf{q}_2, \cdots \mathbf{q}_{N+1}) \qquad \mathbf{Y} = (\mathbf{q}_1, \mathbf{q}_2, \cdots \mathbf{q}_{N+1}, t_1, t_2) \tag{4}$$

So Eq. 2 can be shortly rewritten as:

$$\mathbf{q} = f \cdot \mathbf{X} \tag{5}$$

[1] here and in the following δ_c denotes the corotational virtual change

and the collection of Eqs. 2 and 3 is briefly identified by:

$$\mathbf{r} = g \cdot \mathbf{Y} \tag{6}$$

With the present approximation the functional $S(\Gamma)$ turns out to be a function of the vector Y and the virtual action related to external forces $\mathbf{Q}$ can be expressed in the following form:

$$\delta_c A = \delta_c \mathbf{X} \cdot \int_{t_1}^{t_r} f \cdot \mathbf{Q} dt = \delta_c \mathbf{X} \cdot \mathbf{A} \tag{7}$$

where $\mathbf{A}$ represents the generalized impulses corresponding to the forces $\mathbf{Q}$. The trailing terms of the variational principle, can be also changed into the following:

$$\delta_c \mathbf{q} \cdot \mathbf{p}|_{t_1}^{t_r} = \delta_c \mathbf{X} \cdot \mathbf{B} \tag{8}$$

where

$$\mathbf{B} = (-\mathbf{p}_1, 0, 0, \cdots 0, \mathbf{p}_{N+1})$$

and the variational principle leads to the following:

$$\frac{\partial S}{\partial \mathbf{X}} + \mathbf{A} - \mathbf{B} = 0 \tag{9}$$

These equations constitute an approximate functional relation onto which the integral curve Γ joining the points $\mathbf{P}_1$ and $\mathbf{P}_2$ must fit. They further constitute the approximate parallel of Hamilton's partial differential equations. Obviously to solve a particular dynamic problem the initial or boundary conditions must also be specified. When applied to autonomous periodic problems, we enforce $\mathbf{q}_{N+1} = \mathbf{q}_1$ and $\mathbf{B}_{N+1} = \mathbf{B}_1$.

Morover, we can set to zero the value of the time instant t_1 so that $t_2 = T$, and we can also prescribe the value of one component of the vector $\mathbf{q}_1$, then Eq. (6) can be solved for the remaining components of $\mathbf{q}$ and t_2.

Since Eq. (6) are nonlinear, their practical implementation requires the use of a nonlinear algebric equations solver. We select the use of Newton-Raphson method that, in addition to its property of quadratic convergence within the attraction domain, implies the use of a consistent linearization of the equations that can be profitably used for Floquet's stability analysis of the solution [11-12].

The preceding developments have been verified with a few simple examples. These examples were related to systems with one or two degrees of freedom chosen with the aim of verifying the basic concepts and the feasibility of the numerical approximations but without taking care of numerical efficiency.

The first example refers to a self excited system governed by the equation:

$$\ddot{q} = .2(1 - 2\dot{q}^2)\dot{q} - q + q^3 = 0 \tag{10}$$

showing, a stable limit cycle enclosing all the critical points $q = -1$, $q = 0$, $q = +1$.

The harmonic balance method gives the approximation, q= 1.35sin(.605t). The present approach, with the period subdivided into eight four node elements, gives a limit cycle period $T = 2\pi/.636$ and a peak value $q_p = 1.46$; the contribution of higher harmonics is significant.

The second example refers to a single degree of freedom system possessing two limit cycles and governed by the equation:

$$\ddot{q} + (.3 - .02q^2 + .0001q^4)\dot{q} + q = 0 \tag{11}$$

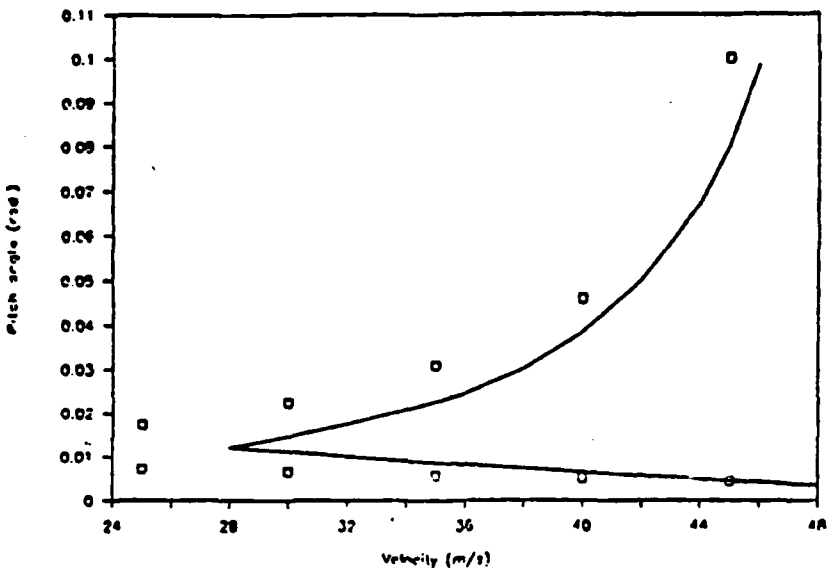

Figure 1: Bending-torsion flutter boundary □ - FEM ——— Ref. [17]

The first harmonic balance approximation gives two limit cycles both possessing the same circular frequency $\Omega = 1$. The first is unstable and has an approximate amplitude equal to 8.514 while the second is stable with a larger amplitude equal to 17.368. The resulting limit cycle periods obtained with the same finite element mesh as the previous example are respectively 6.322 and 6.392.

The third example refers to the bending torsion flutter of a two dimensional airfoil in incompressible flow and is taken from Ref. [17]. The system restoring force is linear in translation and has the non linear torsional stiffness, with backlash.

Figure 1 shows the results obtained with the present method compared with those of Ref. [17].

Despite the different aerodynamic approximation used the comparision shows an acceptable matching with a more pronounced separatation in the large and small amplitude limit cycles.

3 Concluding Remarks

The paper has shown the extension of Hamilton's Principle to problems showing periodic solutions with unknown period. The present and companion works [10], [12] clearly show the power of Hamilton's Principle coupled with finite elements in time domain as a unifying tool in the numerical solution of dynamic and response problems of mechanical systems.

In fact their coupling allows an easy set up of the approximating equations in linearized form which is the basis for an iterative solution of the nonlinear problem and for the analysis of the linear stability of periodic solutions of any type.

Nonetheless practical, efficient and robust numerical methods capable of dealing with multiple solutions of nonlinear systems of equations remain to be developed in order to allow the present method to be used for practical problems.

4 References

1. Schmidt, G. and Tondl, A., "Non-Linear Vibrations", Cambridge University Press, 1986.

2. Hagedorn, P., "Non-Linear Oscillations", Clarendon Press, Oxford, 1981.

3. Baily, C.D., "A New Look at Hamilton's Principle", Foundations of Physics, Vol. 5, No. 3, 1975, pp. 433-451.

4. Simkins, T.E. "Unconstrained Variational Statements for Initial and Boundary-Value Problems" AIAA Journal, Vol. 16, No. 6, June 1978, pp. 559-563.

5. Smith, C.V., Jr., "Comment on 'Unconstrained Variational Statements for Initial and Boundary-Value Problems'", AIAA Journal, Vol. 17, No. 1, Feb. 1979, pp. 126-127.

6. Simkins, T.E., "Finite Elements for Initial Value Problmes in Dynamics", AIAA Journal, Vol. 19, No. 10, October 1981, pp. 1357-1362.

7. Baruch, M. and Riff, R., "Hamilton's Principle, Hamilton's Law - 6n Correct Formulations", AIAA Journal, Vol. 20, No. 5, May 1982, pp. 687-692.

8. Smith, C.V., Jr., "Comment on 'Hamilton's Principle, Hamilton's Law - 6n Correct Formulations'", AIAA Journal, Vol. 22, No. 8, Aug. 1984, pp. 1181-1182.

9. Borri, M., Lanz, M., and Mantegazza, P., "Helicopter Rotor Dynamics by Finite Element Time Discretization", L'Aerotecnica Missili e Spazio 60, pp. 193-200, 1981.

10. Borri, M., et al, "Dynamic Response of Mechanical Systems by a Weak Hamiltonian Formulation", Computers and Structures, Vol. 20, No. 1-3, 1985, pp. 495-508.

11. Borri, M., Lanz, M., and Mantegazza, P., "Comment on 'Time Finite Element Discretization of Hamilton's Law of Varying Action'", AIAA Journal, Vol. 23, No. 9, September 1985, pp. 1457-1458.

12. Borri, M., "Helicopter Rotor Dynamics by Finite Element Time Approximation", Special Issue of Computers and Mathematics with Applications, Vol. 12A, No. 1, 1986.

13. Peters, David A. and Izadpanah, P., "hp-version Fiinite Elements for the Space-Time Domain", Computational Mechanics, Vol. 3, No. 2, 1988, pp. 73-88.

14. Agrawal, O. P., "An Application of Modified Hamilton's Law Varying Action", The Pennsylvania State University, October 7-9, 1985.

15. Synge, J. L., "Principles of Classical Mechanics and Field Theory", Encyclopedia of Physics, Vol. III/1, Springer-Verlag Berlin Gottingen Heidelberg, 1960.

16. Borri, M., and Mantegazza, P., "Finite Time Elements Approximation of Dynamics of Nonholonomic Systems", Presented at ASME Congress, Williamsburg, Virginia, August 1986.

17. Shen, S. F., "An Approximate Analysis of Non-Linear Flutter Problems", Journal of Aero/Space Science, January 1959.

Dynamics of Beams with Tip Masses and Attached to a Moving Base

S. Hanagud* and S. Sarkar†
Georgia Institute of Technology
Atlanta, Georgia-30332

Introduction

Studies involving the transient responses of beams attached to bases that are restricted to translational and angular acceleration have many practical applications. The results of such an analysis can be applied to spinning helicopter blades starting from rest, rapid maneuverings of space based arms as which carry payloads from one place to another, deployment of space structures and numerous other fields. Even when such systems are physically stable and controllable, an inaccurate analysis could lead to a wrong conclusion of unstable motion. In a rotating beam, contribution towards stability is provided by a nonlinear phenomenon known as the centrifugal stiffening. The purpose of this paper is to account for some of the significant nonlinearities in the analysis. The dynamic analysis has been performed by using Kane's method because it leads to the final equations more directly as compared to the Hamilton's principle or other virtual work methods.

An elementary analysis of the centrifugal stiffening has been given in Ref.(1). The beam has been assumed to be inextensible and the virtual work done by the centrifugal force field due to axial foreshortening has been considered in the potential energy expression which leads to the centrifugal stiffening terms. This analysis has been refined by Likins et.al[2] by considering a steady state axial stretch term due to centrifugal force. Vigneron[3] has a assumed foreshortening of the beam and has shown that the centrifugal stiffening terms arise from the kinetic energy terms. Simo[4-5] has taken all displacements to be measured from an inertial frame instead of a rotating frame and has used finite strain measures to obtain the centrifugal stiffening effect. In all analyses mentioned so far, Hamilton's principle has been used to derive the equations of motion. In Ref.(6), Kane.et.al have used Kane's method to obtain the equations by considering stretch and two bending deflections as the independent variables to describe the neutral axis but the stretch term has not been applied in a consistent manner. In this paper, the same Kane's approach has been used to derive the equations of motion but the stretch has been replaced by the axial variable as the independent variable. Large deflections have been included by taking into considerations all the significant nonlinear terms in the strain energy terms. Numerical studies have been performed to study the effect of a tip mass on the motion of the beam. The result has been compared with the case where no tip mass is present. The response of the beam has been also studied for the case where the base is subjected to a linear acceleration along the plane of the beam motion. Finally, all the second and third order stiffening terms have been dropped from the equations and the resulting loss of stability has been observed.

Formulation

The dynamical equations for the axial, bending, translational and rotational equations has been derived in this section. The deformation of the neutral axis has been

*Professor

†Graduate Research Assistant

sketched in Fig.(1). The neutral axis lies parallel to the $\mathbf{a_1}$ axis prior to deformation. The axial displacements u_1 and the bending displacements u_2 and u_3 can be written as functions of x. In Ref.(6), the basic kinematical variables to determine the neutral axis have been the stretch and the bending displacements. They are written in terms of chosen modal functions. The axial and transverse speeds and the corresponding partial velocities have been obtained in terms of the independent variables by using an expression for stretch as given below.

$$x_1 + s(x_1, t) = \int_0^{\sigma_1} [1 + \hat{u}_{2,\sigma}^2 + \hat{u}_{3,\sigma}^2]^{1/2} d\sigma \tag{1}$$

The stretch given by Eq.(1) will be correct if the bending displacements $\hat{u}_2$ and $\hat{u}_3$ are expressed in terms of a variable which is the projection of the deformed neutral line on the $\mathbf{a_1}$ axis, denoted by σ, or deformed coordinate. In Ref.(7), Kane has clarified that it is indeed so. However in all subsequent derivations the bending displacements have been written as function of the undeformed x coordinate, in which case, the stretch should be written as below

$$x_1 + s(x_1, t) = \int_0^{x_1} (1 + u_{1,x})^2 + u_{2,x}^2 + u_{3,x}^2]^{1/2} dx \tag{2}$$

Both the stretch expressions given in Eq.(1) and Eq.(2) are correct, they appear different because the effect of axial displacement has been taken into account in Eq.(1) in an implicit manner. However, care must be exercized in choosing the proper independent variable.

In this section dynamical equations have been derived for the independent transverse and axial displacements which are expressed as functions of undeformed coordinate x. The mass and moments of inertia of the base have been assumed to be zero. The cross-sections have been assumed to remain normal after deformation. The effects of warping and rotary inertia have not been included in this formulation. Since the displacements could be large, nonlinear strain-displacement relationships have been used to determine the strain energy function of the beam and terms upto fourth order are retained. The generalized active forces due to elastic deformation have been determined by differentiation of the strain energy function while the generalized inertial forces have been found by taking the dot products between accelerations and partial velocities.

In fig.(1.a), the quantities $\mathbf{a_1}, \mathbf{a_2}$ and $\mathbf{a_3}$ are orthogonal unit vectors which are attached to the base and they undergo the same inertial motion as that of the base. The quantities v_1, v_2, v_3 and $\omega_1, \omega_2, \omega_3$ are the translation and rotational velocity components respectively of the base along $\mathbf{a_1}, \mathbf{a_2}$ and $\mathbf{a_3}$. The beam displacements are given in the rotating frame and they are expressed as functions of x. Then, the assumed displacements take the following form

$$u_j(x, t) = \sum_{i=1}^{N_j} \phi_{ji}(x, t) q_{ji}(t) \qquad j = 1, 2, 3 \tag{3}$$

It is to be noted that different sets of genaralized coordinates are chosen for displacement u_1, u_2 and u_3. Velocities and accelerations are derived from Eq.(3) and subsequently generalized inertial forces are obtained. The generalized active forces due to elastic effects are determined by differentiating the strain energy function.

The strain energy function U is written as follows

$$U = 1/2\int_0^l [EI_2 u_{3,xx}^2 + EI_3 u_{2,xx}^2 + EAu_{1,x}^2 + EA\, u_{1,x}(u_{2,x}^2 + u_{3,x}^2) + 1/4\, EA(u_{2,x}^4 + u_{3,x}^4 + 2u_{2,x}^2 u_{3,x}^2)]dx \quad (4)$$

The dynamical equations have been obtained by using the Kane's method [8]. EA is the axial rigidity and EI_2 and EI_3 are the bending rigidities. The axial equations corresponding to the generalized speed $\dot{q}_{1i}$ are written as follows

$$\sum_{i=1}^{N_1} W_{11ki}\ddot{q}_{1i} + \sum_{i=1}^{N_1} K_{11ki}q_{1i} + 1/2\sum_{m=1}^{N_2}\sum_{n=1}^{N_2} G_{122kmn}q_{2m}q_{2n} + 1/2\sum_{m=1}^{N_3}\sum_{n=1}^{N_3} G_{133kmn}q_{3m}q_{3n} + (\dot{\omega}_2 + \omega_2\omega_3)\sum_{i=1}^{N_3} W_{13ki}q_{3i} + (-\dot{\omega}_3 + \omega_1\omega_2)\sum_{i=1}^{N_2} W_{12ki}q_{2i} - (\omega_2^2 + \omega_3^2)\sum_{i=1}^{N_1} W_{11ki}q_{1i} + 2\omega_2\sum_{i=1}^{N_3} W_{13ki}\dot{q}_{3i} - 2\omega_3\sum_{i=1}^{N_2} W_{12ki}\dot{q}_{2i} = -(\dot{v}_1 + \omega_2 v_3 - \omega_3 v_2)W_{1k} + (\omega_2^2 + \omega_3^2)X_{ik} \quad (5)$$

Similiarly the transverse dynamical equations corresponding to $\dot{q}_{2i}$ and $\dot{q}_{3i}$ can be obtained and are given in Ref.(9).

The translational and rotational dynamic equations correspond to v_i's and ω_i's . For v_1, The dynamical equations can be written as

$$(\dot{v}_1 + \omega_2 v_3 - \omega_3 v_2)M + \sum_{i=1}^{N_1} W_{1i}\ddot{q}_{1i} - 2\omega_3\sum_{i=1}^{N_2} W_{2i}\dot{q}_{2i} + 2\omega_2\sum_{i=1}^{N_3} W_{3i}\dot{q}_{3i} - (\omega_2^2 + \omega_3^2)(\sum_{i=1}^{N_1} W_{1i}q_{1i} + J) + (\omega_1\omega_2 - \dot{\omega}_3)\sum_{i=1}^{N_2} W_{2i}q_{2i} + (\omega_1\omega_2 + \dot{\omega}_2)\sum_{i=1}^{N_3} W_{3i}q_{3i} = P_1 \quad (6)$$

Similiarly the other two translational equations corresponding to v_2 and v_3 can be obtained. The rotational dynamical equations for ω_1 is

$$(\omega_2\omega_3 + \dot{\omega}_1)\sum_{k=1}^{N_2}\sum_{i=1}^{N_2} W_{22ki}q_{2k}q_{2i} - (\omega_2\omega_3 - \dot{\omega}_1)\sum_{k=1}^{N_3}\sum_{i=1}^{N_3} W_{33ki}q_{3k}q_{3i} + (\omega_1\omega_3 - \dot{\omega}_2)(\sum_{k=1}^{N_2}\sum_{i=1}^{N_1} W_{21ki}q_{2k}q_{1i} + \sum_{k=1}^{N_2} X_{2k}q_{2k}) - (\omega_1\omega_2 + \dot{\omega}_3)(\sum_{k=1}^{N_3}\sum_{i=1}^{N_1} W_{31ki}q_{3k}q_{1i} + \sum_{k=1}^{N_3} X_{3k}q_{3k}) + 2\omega_1(\sum_{k=1}^{N_3}\sum_{i=1}^{N_3} W_{33ki}q_{3k}\dot{q}_{3i} + \sum_{k=1}^{N_2}\sum_{i=1}^{N_2} W_{22ki}q_{2k}\dot{q}_{2i}) -$$

$$2\omega_3 \sum_{k=1}^{N_3}\sum_{i=1}^{N_1} W_{31ki} q_{3k}\dot{q}_{1i} - 2\omega_2 \sum_{k=1}^{N_2}\sum_{i=1}^{N_1} W_{21ki} q_{2k}\dot{q}_{1i} +$$
$$(\omega_3^2 - \omega_2^2) \sum_{k=1}^{N_3}\sum_{i=1}^{N_2} W_{32ki} q_{3k} q_{2i} + \sum_{k=1}^{N_2}\sum_{i=1}^{N_3} W_{23ki}(q_{2k}\dot{q}_{3i} - q_{3i}\dot{q}_{2k})$$
$$- \sum_{k=1}^{N_3} W_{3k} q_{3k}(\dot{v}_2 + \omega_3 v_1 - \omega_1 v_3) + \sum_{k=1}^{N_2} W_{2k} q_{2k}(\dot{v}_3 + \omega_1 v_2 - \omega_2 v_1) = M_1 \quad (7)$$

Similiarly, the two rotational equations corresponding to ω_2 and ω_3 can be obtained. In these equations the following quantities have been defined.

$$W_{mnij} = \int_0^l \rho\phi_{mi}(x)\phi_{nj}(x)dx + M_t\phi_{mi}(l)\phi_{nj}(l);\ m,n = 1,2,3;\ i = 1..N_m;\ j = 1..N_n \quad (8.a)$$

$$W_{pi} = \int_0^l \rho\phi_{pi}(x)dx + M_t\,\phi_{pi}(l);\ p = 1,2,3\ i = 1..N_p \quad (8.b)$$

$$X_{pi} = \int_0^l \rho x\phi_{pi}(x)dx + M_t\, l\,\phi_{pi}(l);\ p = 1,2,3\ i = 1..N_p \quad (8.c)$$

The definitions of other quantities can be found in Ref.(9).

Results and Discussion

The spin-up problem in Ref.(6) is also considered here to study the effect of nonlinear structural terms. The beam is initially at rest and an angular velocity is given along $\mathbf{a_3}$ axis at the base. Only the inplane motions are excited in line with the assumptions. The beam parameters are as follows, E=68950000000 N/mt^2, ρ= 1.2 Kg/mt,M_t(tip mass)=3 Kg, A=0.0004601 mt^2, I_3= 0.0000002031 mt^4, l=10 mt. The angular velocity history is taken to be identical with the one in Ref.(6).

$$\begin{aligned} \omega_3 &= 6/15\left[t - \frac{15}{2\pi}\sin\frac{2\pi t}{15}\right] \text{ rad/s} \quad 0 \le t \le 15 \text{ s} \\ \omega_3 &= 6 \text{ rad/s} \quad t \ge 15 \text{ s} \end{aligned} \quad (9)$$

The transverse mode shapes are taken as the fixed-free nonrotating eigenfunctions of an uniform beam under transverse vibration while the longitudinal modes are taken as the eigen-functions of a fixed-free uniform rod under longitudinal vibrations. The axial and transverse motions are represented by one and three modes respectively. The axial and bending responses of the tip of the cantilever beam resulting from the formulation presented in this paper have been shown in Fig.(2.a) and Fig.(2.b) respectively. The solid and dashed curved are for nonlinear analysis and they correspond to the cases without tip mass and with tip mass respectively. In the nonlinear analysis, the transverse deflection initially grows in a direction opposite that of the base motion. After reaching a maximum displacement, the tip goes back towards the equillibrium position and settles down to a steady oscillation. The nonlinear stiffening action in the beam prevents it from instability. As one might expect, the maximum displacement and the amplitude of the final steady state oscillations are more when the tip mass is present. The dotted curves

in Fig.(2.a) and Fig.(2.b) correspond to the cases where all the second and third order terms in the final equations are dropped . The beam rapidly goes unstable which clearly illustrates the necessity of retaining the higher order terms in order to obtain stable motion. In the analysis of in Ref.(3), foreshortening of the beam has been assumed a-priori to derive the centrifugal stiffness terms. In the present analysis, the solid and dashed curves in Fig.(2.a) indicate that the initial foreshortening of the beam is a pure consequence of the imposed base motion. The physical interpretation is that in the first few seconds, the neutral axis does not stretch and as a result an axial shortening results for all bending displacements. After the beam has reached the maximum bending displacement and starts coming back towards the equillibrium configuration, the axial displacement grows and finally achieves a more or less steady state displacement under the centrifugal force field. Finally, the effects of base translational motion on the axial and bending motion are studied by imposing a constant base acceleration along a fixed inertial axis and along the plane of the beam motion for the initial five seconds. The axial and bending responses are plotted in Fig.(3.a) and Fig.(3.b) respectively.

Conclusions

In this paper, we have formulated the problem of a cantilever beam with a tip mass and attached to a moving support by using Kane's method. The formulation is valid for large displacements and all significant geometric nonlinearities have been considered in the strain-displacement relations. The method has been validated by studying the stability characteristics of a beam under the spin-up maneuver. It has been demonstrated that structural nonlinearities play a major role in the transient response characteristics and they cannot be ignored.

References

1.Meirovitch, Leonard.,Analytical Methods in Vibrations.
2.Likins,P.W. et.al, AIAA Journal, 11, 1973, 1251-1258.
3. Vigneron, F.R., AIAA Journal,13, 1975, 126-128.
4.Simo,J,C. and Vu-Quoc,L., J. Appl. Mech, 1986, 53, 849-854
5.Simo,J,C. and Vu-Quoc,L., J. Appl. Mech, 1986, 53, 855-863
6.Kane, T.R. et.al, J. Guid. Cont. Dyn.,10, 2, 1987, 139-151
7.Kane, T,R., " Private communication with S.Hanagud," August,1987.
8.Kane, T.R. et.al," Spacecraft Dynamics," McGraw-Hill Book Company, 1983.
9.Hanagud, S. et.al, J. Guid. Cont. Dyn., To be published.

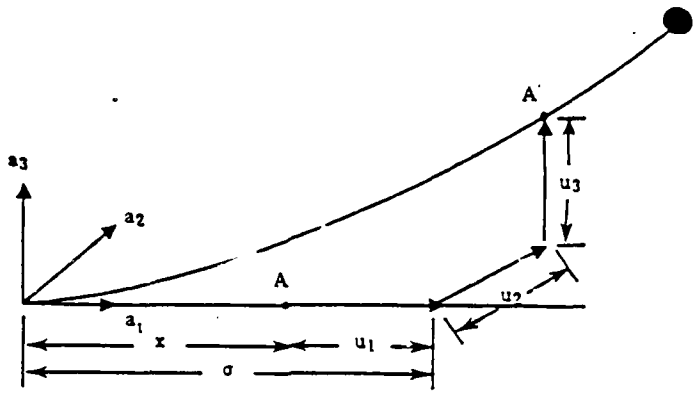

Figure 1 : Displacements at neutral axis

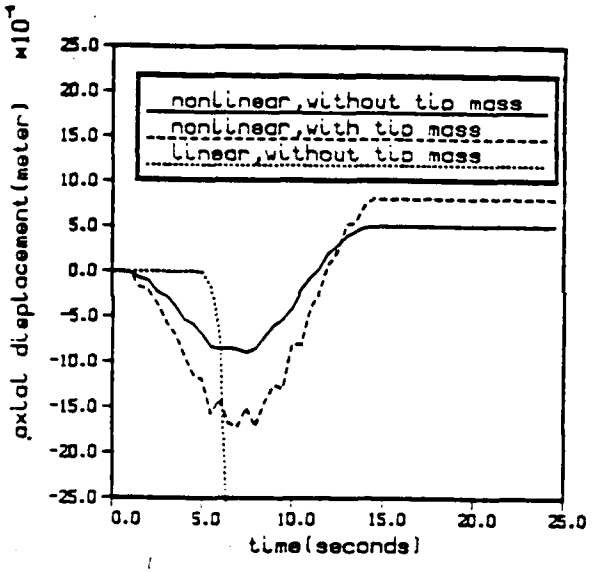

Figure.(2.a) Effect of tip mass on axial response

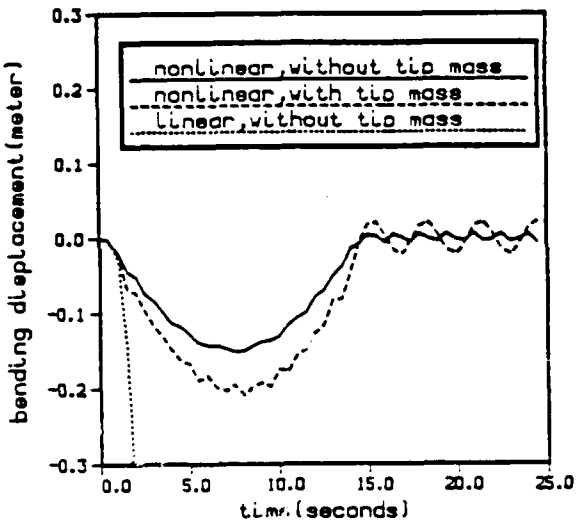

Figure.(2.b) Effect of tip mass on bending response

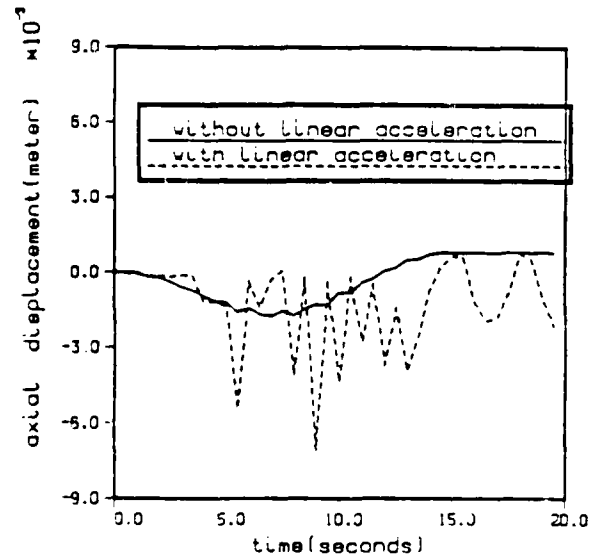

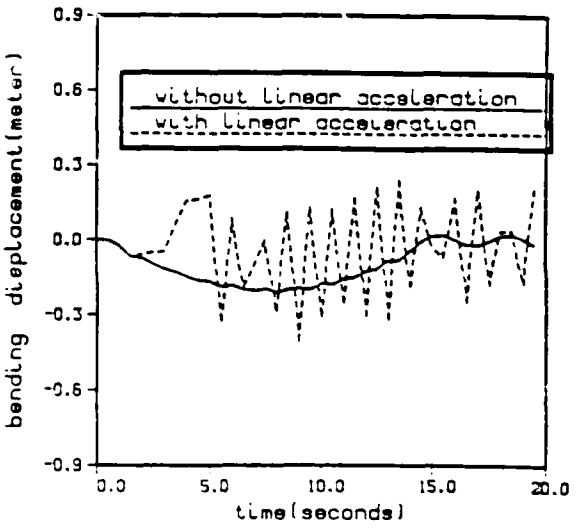

SESSION 7

NONLINEAR ANALYSIS OF PLATES AND SHELLS

THURSDAY - 1330 - 1515

June 2, 1988

NON-LINEAR OSCILLATIONS OF AN INEXTENSIBLE, AIR-INFLATED, CYLINDRICAL MEMBRANE

Raymond H. Plaut
Department of Civil Engineering
Virginia Polytechnic Institute and State University
Blacksburg, Virginia 24061

ABSTRACT

A long cylindrical membrane, attached to a horizontal base along two generators and inflated with air, is considered. The material is assumed to be inextensible and its weight is neglected, so that the equilibrium shape of the cross section is circular, as shown in the figure. Two-dimensional, undamped, nonlinear oscillations about this equilibrium configuration are investigated.

The radial displacement is a function of the coordinate θ and time t. Weakly nonlinear motions are considered, and terms of fourth order and higher are neglected in the equation of motion. Galerkin's method is applied, first with one term and then with two terms, to yield ordinary differential equations for the displacement amplitudes as functions of time. In the one-term case, the equation has the form

$$c_1\ddot{U} + c_2\ddot{U}U + c_3\ddot{U}U^2 + c_4U + c_5U^2 = 0.$$

For anti-symmetric modes, c_2 and c_5 vanish.

The method of multiple scales is used to obtain approximate solutions. It is found that the response frequencies tend to decrease as the response amplitude increases. For the case of two terms, the response may grow large if the internal resonance $\omega_2 \approx 2\omega_1$ exists. However, the internal resonance $\omega_2 = 3\omega_1$ has little influence on the response.

Numerical integration is also utilized to determine frequencies and amplitudes. The results show good agreement with the asymptotic solutions when the motion is sufficiently small.

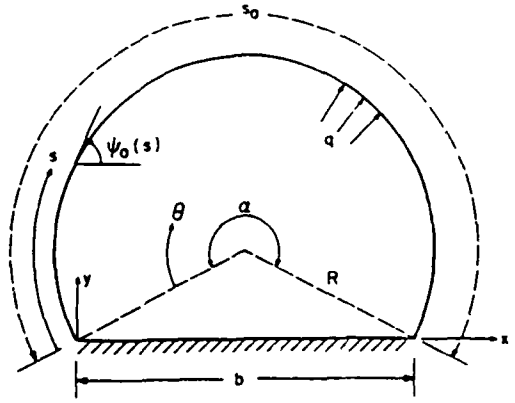

IMPACT OF SHELLS

by

Charles R. Steele
Division of Applied Mechanics
Stanford University
Stanford, CA 94305

Introduction

The analysis of large displacement of thin shells is generally a difficult problem. Guidance can be found from Love's "principle of applicable surfaces", which is based on the fact that higher levels of strain energy are required for deformations which involve extensional distortion of the reference surface, than are required for inextensional bending. The consequence is that even elaborate post-buckling patterns are usually characterized by regions of inextensional deformation joined by lines of localized bending. Ashwell (1960) utilizes this concept for the problem of a spherical shell with a static radial point load, for which the geometry is quite simple, and showed that a good approximation can be obtained for the large displacement behavior. The procedure consists of assuming that a portion of the sphere, a "cap", undergoes a reversal in curvature and becomes a "dimple". Continuity of stress and displacement is obtained by solutions of the linear equations for the inverted cap and the remaining portion of shell. Ashwell uses the Bessel function solutions of the shallow shell equations. Ranjan and Steele (1977) show that a much simpler solution can be obtained by using the exponential, "steep shell" approximate edge stiffness coefficients. Furthermore, the accuracy is increased by including the geometric nonlinearity, obtained from a perturbation expansion of the moderate rotation equations by Ranjan and Steele (1980). Parnell (1984) gives further considerations to this problem.

The purpose for the present paper is to show that the inverted cap solution permits insight into the response of a shell in various transient loadings. The results are interesting because the specific problems are of practical concern and are useful as nontrivial examples for verification of general purpose finite element programs.

Displacement under static point load

First the basic point load solution is reviewed. A spherical shell under a point load P has the displacement x according to the linear solution by Reissner (1946) given by

$$\frac{x}{c} = \frac{PR}{8D} = P^* \tag{1}$$

where R, h and D are the spherical radius, thickness and plate bending stiffness, respectively. The reduced thickness is c, which gives the ratio of bending to stretching stiffness of the shell wall. The simplest form is obtained with the assumption that the edge angle α of the inverted cap, or dimple, shown in Fig. 1 is both "shallow":

$$\alpha \leq 0.3 \tag{2}$$

and "steep":

$$\sqrt{\frac{R}{c}}\alpha >> 1 \tag{3}$$

The two conditions are easily satisfied for a range of edge angles when the shell is very thin. Adding the inverted dimple modifies the potential energy. The dominant terms are the change in potential of the external force because of the increase in displacement and the strain energy of bending of the edge of the dimpie and the edge of the remaining shell to obtain continuity of the slope of the meridian. The approximate potential change is

$$U(\alpha) = 2\pi D\sqrt{\frac{2R}{c}}\,\alpha^3 - PR\alpha^2 \tag{4}$$

For equilibrium, the potential must be stationary with respect to a change in the edge angle. This provides the relation between the edge angle and the load magnitude P. Adding the linear result to the additional displacement due to the dimpling gives the total displacement:

$$\frac{x}{h} = P^* + K\left(P^*\right)^2 \tag{5}$$

where the constant is

$$K = \left(\frac{8}{3\pi}\right)^2\sqrt{3\left(1-\nu^2\right)} = 1.19 \quad \text{for } \nu = 0.3 \tag{6}$$

The geometric nonlinearity in the edge bending, as obtained by Ranjan and Steele (1980), provides a 20 percent reduction in the strain energy and an increase in the constant:

$$K_{NL} = K\left(\frac{5}{4}\right)^2 = 1.86 \quad \text{for } \nu = 0.3 \tag{7}$$

The result (5) agrees well with the experiments of Penning and Thurston (1965) and the numerical results of Fitch (1968), all on rather thin spherical shells for displacement magnitude up to about fifteen shell thicknesses. More remarkable are the results of Taber (1982) showing that the equivalent of (5) provides good agreement with experiments on a thick shell. In addition, Taber considered the problem of a shell filled with an incompressible fluid, for which the strain energy of the wall extension due to the internal pressure must be added. The comparison with experiment is reasonable for displacements in magnitude up to about half the radius. For displacements much larger than the thickness, the linear contribution in (5) may be ignored and the result written as a nonlinear spring:

$$P = \gamma x^{1/2} \tag{8}$$

where the constant is

$$\gamma = \frac{4}{5}\frac{6\pi D}{R}\sqrt{\frac{2}{c}} \tag{9}$$

The conclusion is that the key feature is the dimple with the strain energy of edge bending approximated by the one-term, steep shell solution. In the experiments and numerical computation, bifurcations to nonsymmetric patterns occur. However, a substantial load loss with such bifurcations apparently does not take place, so the symmetric solution remains a good approximation.

Impact of a rigid mass

A rigid obstacle of mass M striking the spherical shell with an initial velocity of sufficient magnitude will cause a large displacement of the shell. This displacement can be approximated by the dimple just as in the static case, as indicated in Fig. 1. Adding the inertia terms to the previous static formulation leads to the following equation of motion:

$$\frac{d}{dt}\left[\left(M + \pi R \rho h x\right)\frac{dx}{dt}\right] + \gamma x^{1/2} = 0 \tag{10}$$

in which ρ is the density of the shell wall. Note that the moving mass of the wall is the dimple region which increases with the displacement x. When either the obstacle mass or the mass of the shell wall is dominant, the equation may be integrated exactly. The numerical solution for the general case is straightforward.

Impact of shell against a rigid wall

In the case of the shell impacting a rigid wall, as indicated in Fig. 2, the contact force acts against the edge of the dimple region, so the displacement x is half that of the concentrated load case for a given dimple size. The result for the static effective spring is

$$P = 2^{3/2}\gamma x^{1/2} \tag{11}$$

The inertia is easy in this situation, since the dimple region merely changes direction but must have the same magnitude of velocity as the remaining part of the shell. Therefore the approximate equation of motion is

$$M_s \frac{d^2x}{dt^2} + 2^{3/2}\gamma x^{1/2} = 0 \tag{12}$$

in which M_s is the total mass of the shell and whatever may be attached to the shell, away from the dimple region of contact. The integrals of this equation are readily obtained. For instance the maximum displacement is

$$x_{max} = \frac{1}{2}\left(\frac{3 M_s v_0^2}{2\gamma}\right)^{2/3} \tag{13}$$

in which v_o is the velocity of the shell at the instant of initial contact.

Extensions

Various additional effects can be readily included. These include the generalization to a composite shell. The asymptotic edge stiffness coefficients for a composite, as computed from classical shell theory, are already available from Fettahlioglu and Steele (1974). The inclusion of transverse shear deformation and composite wall construction in the analysis of Ranjan and Steele (1980) should be possible. Bennett (1979) shows that the dimple can be extended to a general elliptic surface. In that case the boundary of the dimple is an ellipse. The asymptotic solution for the general surface with edge bending is integrated around the boundary, with the interesting result that the behavior is exactly the same as that for the sphere but with the spherical radius of curvature replaced by the mean radius of curvature. Impulsive pressure loading can also be treated in a similar manner. The effective nonlinear spring is, however, unstable which substantially changes the response.

It seems that much can be done with the shell of positive gaussian curvature. The challenging problem is to find an equivalent simple method for the shells of zero and negative gaussian curvature.

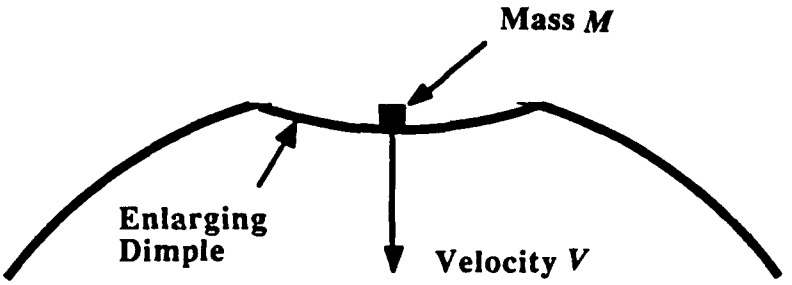

Figure 1 – Spherical shell impacted by mass *M*. For large amplitude displacement an effective approximation is that an inverted dimple forms. The significant strain energy is in the localized bending at the edge of the dimple which provides the effect of a nonlinear spring.

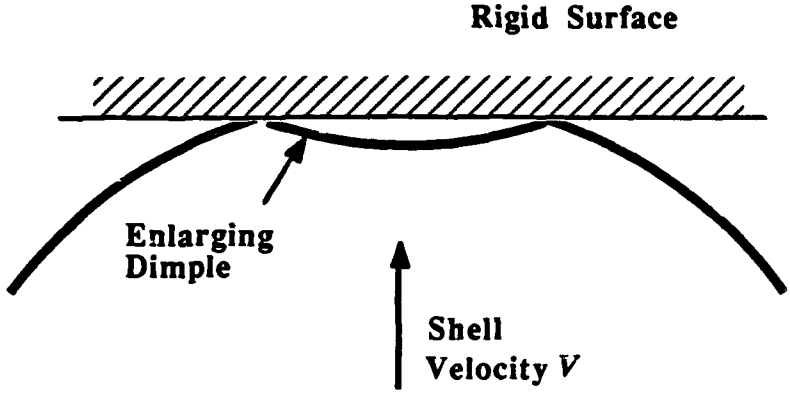

Figure 2 – Impact of shell against a rigid surface. For this problem as well, the inverted dimple can be utilized. Since the dimple has the same velocity magnitude as the center of the shell, the kinetic energy is the same with or without the rigid surface.

References

Ashwell, D.G., (1960). "On the large deflection of a spherical shell with an inward point load", *Theory of Thin Elastic Shells*, W. Koiter, ed. (North-Holland, Amsterdam), 44-63.

Bennett, B.E. (1979). "Studies in dynamics and the application of asymptotic methods in solid mechanics", Ph.D. Thesis, Stanford University.

Fettahlioglu, O.A., and Steele, C.R. (1974). "Asymptotic solutions for inhomogeneous, orthotropic shells of revolution", *J. Appl. Mech.*, **41**, 753-758.

Fitch, J.R., (1968). "The buckling and post-buckling behavior of spherical caps under concentrated load", *Int. J. Solids Struct.*, **4**, 421-446.

Parnell, T.K. (1984). "Numerical improvement of asymptotic solutions and nonlinear shell analysis", Ph.D. Thesis, Stanford University.

Penning, F.A., and Thurston, G.A., (1965). "The stability of shallow spherical shells under concentrated load", NASA CR-265.

Reissner, E. (1946). "Stresses and displacements in shallow spherical shells", Part I, *J. Math. and Phys.*, **25**, 80-85, Part II, *J. Math. and Phys.*, **25**, 279-300.

Ranjan, G.V., and Steele, C.R. (1977). "Large deflection of deep spherical shells under concentrated load", *Proc. 18th Structures, Structural Dynamics, and Materials Conference*, San Diego, (March 1977).

Ranjan, G.V., and Steele, C.R. (1980). "Nonlinear corrections for edge bending of shells", *J. Appl. Mech.*, **47**, 861-864.

Taber, L.A., (1982). "Large deflection of a fluid-filled spherical shell under a point load", *J. Appl. Mech.*, **49**, 121-128.

Nonlinear Dynamic Stability of Laminated Composite Shear Deformable Flat Panels Subjected to In-Plane Periodic Edge Loads"

L. Librescu and S. Thangjitham
Department of Engineering Science & Mechanics
Virginia Polytechnic Institute & State University
Blacksburg, Virginia 24061

Abstract

Laminated composite structures are being increasingly used in the construction of aeronautical and space vehicles. Employment in their construction of the new material systems that exhibit exotic properties such as high degrees of anisotropy and high flexibility in transverse shear requires a better knowledge of their instability behavior.

The present paper is devoted to an analysis of the dynamic stability of laminated composite shear-deformable flat panels subjected to in-plane bi/uniaxial periodic edge forces. The analysis is based on a refined geometrically nonlinear theory of anisotropic symmetrically-laminated composite panels. The improved theory is developed i) by incorporating transverse shear deformation and transverse normal stress effects, ii) by fulfilling the static conditions on the bounding planes of the panel and iii) by incorporating the higher-order effects. The theory is formulated within the Lagrangian description considered in conjunction with the von Kármán concept allowing one a reduction of the complexity of nonlinear expressions. The linear counterpart of the obtained governing equation (which is of a Mathieu-type) is used to determine the boundaries of the instability regions while the full nonlinear equation is used to obtain the behavior of the plate within the instability region.

Comparisons of the obtained results with their counterparts obtained within the first order transverse shear deformation theory and the classical one (based upon the Kirchhoff constraints) are made. These allow one to infer about the influence of transverse shear deformation as well as of higher order effects on the parametric instability boundaries.

In addition, a thorough numerical analysis intended to put into evidence the various effects played by the physical and geometrical parameters of shear deformable composite panels on the instability characteristics is performed and pertinent conclusions are formulated.

The Method of Multiple Scales for Nonlinear Resonances in the Forced Response of Orthotropic Rectangular Plates

Habib Eslami*
Embry-Riddle University
Daytona Beach, FL 32014

Osama A Kandil**
Old Dominion University
Norfolk, VA 23529-0247

Introduction

Amplitudes of harmonic transverse deflections of thin laminated composite plates could be as large as the order of the plate thickness. For these large deflections, the nonlinear governing equations of motion of laminated composite plates and nonlinear methods of analysis must be used to study the nonlinear responses. The literature survey shows that there are significant contributions in the area of nonlinear vibrations of isotropic plates and laminated composite plates. For isotropic plates, the reader is referred to the book by Nayfeh and Mook[1], and for composite plates, the reader is referred to the book by Chia[2] and the survey article by Bert[3].

For the nonlinear forced vibrations of rectangular and circular isotropic plates subjected to harmonic excitations, several investigations have been reported by Yamaki, et. al.[4], Mei and Decha-Umphai[5] and Sridhar, et. al.[6], among others. For the nonlinear forced vibration of laminated composite plates subjected to harmonic excitations, a few investigations has been reported, e.g.; Bennett[7], and Mei and Chiang[8]. Unfortunately, the literature lacks research work on the nonlinear forced vibrations of laminated composite plates including the effect of damping for all possible resonances.

In the present paper, we use the method of multiple scales (MMS) to study the nonlinear forced oscillations of orthotropic rectangular plates subjected to harmonic excitations. The Galerkin method is used to reduce the nonlinear partial differential equations to a set of nonlinear ordinary differential equations with cubic nonlinearity. The resulting nonlinear equations are solved by using the method of multiple scales which makes it possible to study all possible nonlinear resonances; primary as well as secondary resonances (subharmonics and superharmonics).

Formulation and Method of Solution

The nondimensional governing equations, which are based on the von Karman large-deflection analysis, for a rectangular orthotropic panel subjected to harmonic loading including the effect of damping and in-plane loadings are given by

---

*Assistant Professor, Department of Aeronautical Engineering.

**Professor, Department of Mechanical Engineering and Mechanics.

$$L(\bar{w},F) = \bar{w}_{,\tau\tau} + C\,\bar{w}_{,\tau} + \bar{w}_{,\xi\xi\xi\xi} + 2D^{*}\, r_o^2\, \bar{w}_{,\xi\xi\eta\eta} + r_o^4\, \bar{w}_{,\eta\eta\eta\eta}$$

$$- r_o^2\,[(F_{,\eta\eta} + N_{\xi}^{a})\bar{w}_{,\xi\xi} + (F_{,\xi\xi} + N_{\eta}^{a})\,\bar{w}_{,\eta\eta} - 2\,F_{,\xi\eta}\,\bar{w}_{,\xi\eta}]$$

$$- P_o \cos\Omega\tau = 0 \qquad (1)$$

$$\alpha\, F_{,\xi\xi\xi\xi} + \beta\, r^2\, F_{,\xi\xi\eta\eta} + \gamma\, r^4\, F_{,\eta\eta\eta\eta} = r^2\,(\bar{w}^2_{,\xi\eta} - \bar{w}_{,\xi\xi}\,\bar{w}_{,\eta\eta}) \qquad (2)$$

where the dimensionless quantities $\bar{w}$ is the deflection, F the Airy stress function, $r = a/b$ the plate aspect ratio, C the damping parameter, N_{ξ}^{a} and N_{η}^{a} the in-plane loadings, $D^{*} = (D_{12} + 2\,D_{66})/\sqrt{D_{11}\,D_{22}}$, $r_o = a_o/b_o = (D_{22}/D_{11})^{1/4}/b$, $\alpha = A_{22}^{*}\,\sqrt{D_{11}\,D_{22}}/h^2$, $\beta = (2\,A_{12}^{*} + A_{66}^{*})\,\sqrt{D_{11}\,D_{22}}/h^2$, $\gamma = A_{11}^{*}\,\sqrt{D_{11}\,D_{22}}/h^2$, A_{ij}^{*} and D_{ij} the laminate extensional and bending stiffness and h the plate thickness. For additional definitions of the dimensionless quantities, the reader is referred to the paper by Eslami and Kandil[9]. Assuming a solution of the Galerkin form

$$\bar{w}(\xi, \eta, \tau) = \sum_{m}\sum_{n} q_{mn}(\tau)\, X_m(\xi)\, Y_n(\eta) \qquad (3)$$

where X_m and Y_n are admissible functions satisfying the boundary conditions, substituting the solution into the linear equation, Eq. (2), solving the resulting equation for F as a combination of a homogeneous part and a particular part, substituting Eq. (3) and the solution of F into Eq. (1) and setting the weighted residual equal to zero, we obtain

$$\int_0^1 \int_0^1 L(\bar{w}, F)\, X_{\ell}(\xi)\, Y_j(\eta)\, d\xi\, d\eta = 0 \qquad (4)$$

Equation (4) yields a set of ordinary differential equations with cubic nonlinearities which can be reduced to the form

$$\ddot{\tilde{q}}_k + c_k\,\dot{\tilde{q}}_k + \omega_k^2\,\tilde{q}_k + \sum_{\ell}\sum_{m}\sum_{n} L_{k\ell mn}\,\tilde{q}_{\ell}\,\tilde{q}_m\,\tilde{q}_n = P_{ok}\cos\Omega\tau \qquad (5)$$

where the time functions q_{mn} have been redefined as

$$\{\tilde{q}_k\}^T = \{q_{11}, q_{21}, \ldots, q_{N1}, \ldots, q_{MN}\}^T \qquad (6)$$

Using the transformation $\tilde{q} = \varepsilon^{1/2} U_k$, Eq. (5) reduces to

$$\ddot{U}_k + 2\,\varepsilon\xi_k \dot{U}_k + \omega_k^2 U_k + \varepsilon \sum_m \sum_n L_{k\ell mn} U_\ell U_m U_n = F_{ok} \cos\Omega\tau \qquad (7)$$

where

$$\xi_k = \frac{c_k}{2\varepsilon} \quad \text{and} \quad F_{ok} = P_{ok}/\varepsilon^{1/2} \qquad (8)$$

Equation (7) is solved by using the method of multiple scales by introducing the time scales $T_n = \varepsilon^n \tau$ and assuming the expansion

$$U_k(\tau; \varepsilon) = U_{ko}(T_o, T_1) + \varepsilon U_{k1}(T_o, T_1) + \ldots\ldots \qquad (9)$$

The time derivative $\frac{d}{d\tau}$ is transformed by using

$$\frac{d}{d\tau} = D_o + \varepsilon D_1 + \ldots\ldots; \quad D_i = \frac{\partial}{\partial T_i} \qquad (10)$$

Using the MMS, primary and secondary resonances can be studied. Primary resonances occur when $\Omega \approx \omega_k$ (kth mode frequency), and one has to order the forcing amplitude F_{ok} as $F_{ok} = \varepsilon f_k$ and introduce the detuning parameter σ_k such that $\Omega = \omega_k + \varepsilon\sigma_k$. Secular terms develop in the U_{k1}-equation and one has to eliminate them, a process which yields governing equations for the amplitudes and phases of U_{ko}. For simply supported panel, the deflection function, Eq. (3), is given by

$$\tilde{w} = \sum_m \sum_n q_{mn}(\tau) \sin(m\pi\xi) \sin(n\pi\eta) \qquad (11)$$

and it can be shown that only symmetric-symmetric modes are excited. Considering the case of m = 1, 3 and n = 1, two cases of primary resonance might occur; $\Omega \approx \omega_1$ or $\Omega = \omega_3$.

For secondary resonances, F_{ok} need not be ordered, and for simply supported panels superharmonic resonances might occur when $3\,\Omega \approx \omega_1$ or $3\,\Omega \approx \omega_3$, while subharmonic resonances might occur when $\Omega \approx 3\,\omega_1$ or $\Omega \approx 3\,\omega_3$.

Numerical Applications

Here, we show a few samples of numerical applications for primary and secondary resonances. The material considered is a single-layered boron-epoxy[9] and ε is kept as $\varepsilon = 0.0001$. For the primary resonances, we show the frequency response curves at different forcing amplitudes with a damping ratio $\xi = 0.05$ for $\Omega \approx \omega_1$ (Fig. 1) and for $\Omega \approx \omega_3$ (Fig. 2). Comparisons of the MMS solution and the method of harmonic balance show excellent agreement. The frequency response equations (not given here) show that there is no coupling

between the modes. For the first mode, the jump phenomen becomes visible as the forcing function is increased while for the second mode, the jump phenomenon is not visible for the considered range of F_o. Figure 3, shows the results for the second mode for the same range of F_o but with a damping ratio $\xi = 0.005$, which is one order of magnitude less than that of Fig. 2. Figure 4 shows the contribution of the second mode solution for superharmonic response when $\Omega \approx \frac{1}{3}\omega_1$. The solution is compared with the superharmonic response obtained by the first mode only. Additional results will be shown in the presentation for superharmonic and subharmonic resonances.

References

1. Nayfeh, A. H., Mook, D. T., Nonlinear Oscillations, Wiley & Sons, Inc.

2. Chia, C. Y., Nonlinear Analysis of Plates, McGraw-Hill, 1980.

3. Bert, C. W., "Research on Dynamics of Composite and Sandwich Plates," Shock and Vibration Digest, Vol. 14, 1982, pp. 17-34.

4. Yamaki, N., Otomo, K. and Chiba, M., "Nonlinear Vibrations of a Clamped Circular Plate with Initial Deflection and Initial Edge Displacemnt, Pa I: Theory, "J. Sound and Vibration, Vol. 79, 1981, pp. 23-42.

5. Mei, C. and Decha-Umphai, K., "A Finite Element Method for Nonlinear Forced Vibrations of Rectangular Plates," Proceedings of 25th Structures, Structural Dynamics and Materals Conference, Part 2, Palm Springs, CA, 1984, pp. 81-89. Also in AIAA Journal, May 1985.

6. Sridhar, S. D., Mook, D. T. and Nayfeh, A. H., "Nonlinear Resonances in the Forced Response of Plates," Part II: Asymmetric Responses of Circular Plates, Journal of Sound an Vibrations, 1978, Vol. 59, pp. 15-170.

7. Bennett, J. A., "Nonlinear Vibration of Simply Supported Angle-Ply Laminated Plates," AIAA Journal, Vol. 9, Oct. 1971, pp. 1977-2003.

8. Mei, C. and Chiang, C. K., "Finite Element Nonlinear Forced Vibration Analysis of Symmetrically Laminated Composite Rectangular Plates," Proceedings of 26th Structures, Structural Dynamics and Materials Conference, Paper No. 85-0654, Orlando, FL, 1985.

9. Eslami, H. and Kandil, O. A., "A Peturbation Method for Nonlinear Forced Vibration of Orthotropic Rectangular Plates with In-Plane Loads," Proceedings of the 28th Structures, Structural Dynamics and Material Conference, Monterey, CA, 1987, pp. 522-532, accepted for publication in the AIAA Journal.

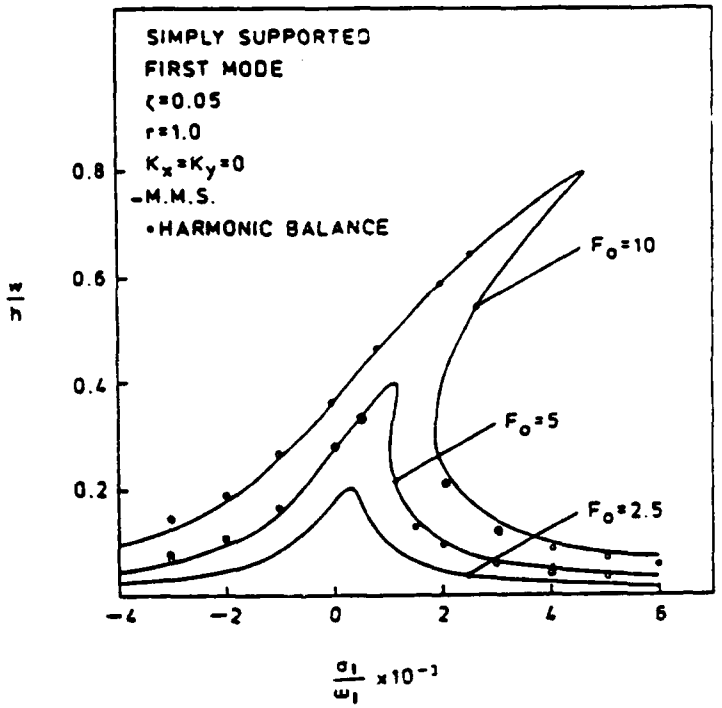

Fig. 1. Frequency response of primary resonance for different forcing amplitude for the orthotropic simply-supported panel and the comparison with the harmonic balance method.

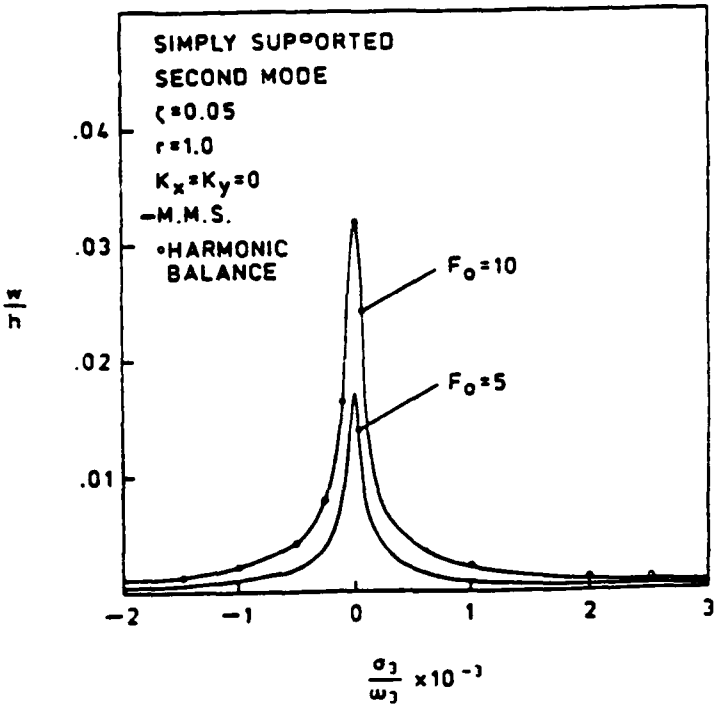

Fig. 2. Frequency response of primary resonance of a simply-supported panel for the second mode and comparison with the harmonic balance method.

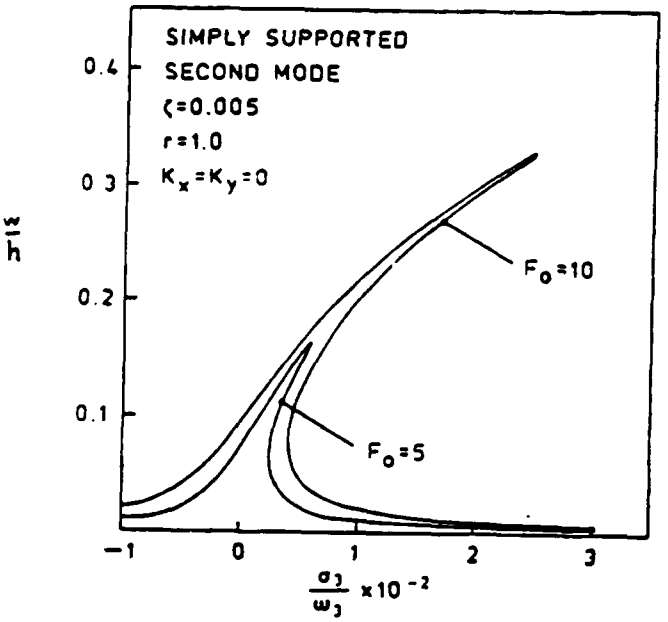

Fig. 3. The effect of lower damping ratio on frequency response of primary resonance for the second mode.

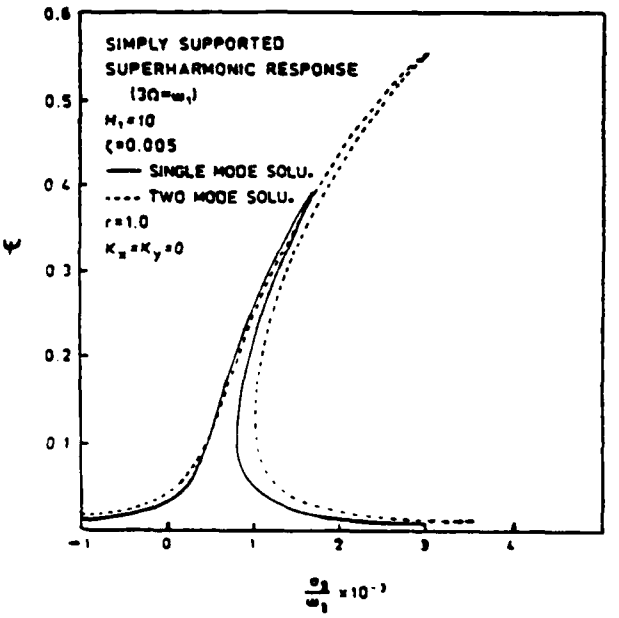

Fig. 4. Contribution of the second mode solution over the single mode solution for the superharmonic response when $3\Omega = \omega_1$.

A FINITE ELEMENT METHOD FOR NONLINEAR PANEL FLUTTER OF COMPOSITE LAMINATES

Chuh Mei
Department of Mechanical Engineering and Mechanics
Old Dominion University, Norfolk, VA 23529-0247

Carl E. Gray, Jr.
Systems Engineering Division
NASA Langley Research Center, Hampton, VA 23665-5225

ABSTRACT

Panel flutter is the self-excited oscillations of a plate in supersonic flow. Panel flutter differs from wing flutter in that the aerodynamic force acts only on one side of the panel. In the framework of small deflection linear structural theory, there is a critical value of the dynamic pressure, λ, (or air velocity); above which the panel motion becomes unstable and grows exponentially with time, and below which any disturbance to the panel decays. Linear theory can determine the critical dynamic pressure, mode shape and frequency at the instability but gives no information about the panel's deflections and stresses. Thus, the service life of the panel can not be predicted. A great quantity of literature exists on linear panel flutter using different aerodynamic theories, for example [1-3] and many others. The aerodynamic theory employed for panel flutter at high supersonic Mach numbers ($M>1.7$) is a quasi-steady first-order aerodynamic piston theory. This theory calculates the aerodynamic loads on the panel from local pressures generated by the body's motion as related to the local normal component of the fluid velocity; thus, a point-function relationship between the normal component of the fluid velocity (no penetration fluid-panel boundary) and the local panel pressure is known. Assuming exponential dependence on time, the aerodynamic pressure can be separated into two forces. The primary aerodynamic force is proportional to the local panel slope, while the other force, which is the aerodynamic damping force (g_a), is proportional to the transverse panel displacement. Hence, the damping force is combined with the usual inertial force to yield an effective inertial force.

In reality, the panel not only bends but also stretches due to vibrations with large amplitude. Such membrane tensile forces in the panel due to stretching, provides a limited stabilizing effect that restrains the panel motion to bounded amplitude limit-cycle oscillations with increasing amplitude as the dynamic pressure increases. The external skin of a flight vehicle can, thus, withstand velocities beyond the linear critical value. Nonlinear structural theory determines the limit-cycle oscillating frequency, and also panel deflections and stresses. Panel fatigue life, therefore, can be predicted. For a more thorough understanding of panel flutter behavior, the geometrical nonlirearity effects due to large deflections should be considered in the formulation. An outstanding survey on the subject for both linear and nonlinear panel flutter was given by Dowell [4], and most recently by Reed, Hanson and Alford [5].

A number of classic analytical methods exists for the investigation of limit-cycle oscillations of panels in supersonic flow. In general, the Galerkin's method is used in the spatial domain, and the panel deflection is expressed in terms of two to six linear normal modes; and various techniques in the temporal domain such as the time numerical integration [6-8], harmonic balance [9,10] and perturbation method [10,11] are also employed. Nonlinear flutter of orthotropic panels was recently studied [12] using the harmonic balance method. All of the analytical investigations have been limited to two-dimensional or three-dimensional rectangular plates with all four edges simply supported or clamped. The classic approaches also indicated that at least six linear normal modes are required to achieve a converged solution.

Extension of the finite-element method to study the linear panel flutter problems was due to Olson [13,14]. Because of its versatile applicability, effects of aerodynamic damping, complex panel configuration (delta and rhombic planforms, etc.), flow angularity, inplane pre-stresses, and laminated anisotropic panel properties can be conveniently included in the formulation. A review of the linear panel flutter using finite-element methods was given by Yang and Sung [15].

Application of the finite element method to study the limit-cycle oscillations of two-dimensional panels was given by Mei and Rogers [16,17]. Rao and Rao [18] investigated the large amplitude supersonic flutter of two-dimensional panels with ends elastically restrained against rotation. Mei and Weidman [19], Han and Yang [20], and Mei and Wang [21] further extended the finite element methods to treat limit-cycle oscillations of three-dimensional rectangular and triangular isotropic plates, respectively. In deriving the nonlinear stiffness matrices due to large deflections in refs. 18, 19 and 21, the strain components $(\partial u/\partial x)$ and $(\partial v/\partial y)$ have been neglected from the von Karman strain-displacement relations. A high-order triangular plate element with 54 degrees-of-freedom was used in ref. 20 and excellent agreement on limit-cycle oscillations has been obtained between the finite element single-mode and the classic analytical six-mode solutions.

The eigenvalues, κ, versus dynamic-pressure parameter, $\lambda(= 2qa^3/\beta D)$, for a simply-supported square panel at two different amplitude ratios, c/h=0.0 and 0.6, for aerodynamic damping $g_a = 0$ are shown in Fig. 1. A 3x8 gridwork in a half plate was used. The curves for c/h=0.0 correspond to the linear small-deflection theory. When λ=0 (in-vacuo), the nonlinear flutter problem degenerates to large amplitude vibrations of plates and the eigenvalues are real and positive. As λ is increased monotonically from zero, the symmetric stiffness matrix is then perturbed by the nonsymmetric aerodynamic influence matrix, two of the eigenvalues approach each other, and after coalescence they become complex conjugate pairs. The critical dynamic pressure λ_{cr} corresponds to the lowest value of λ for which first coalescence occurs among all limit-cycle amplitudes c/h, and it usually corresponds to the linear case c/h=0.0.

In the case of negligible aerodynamic damping $g_a \to 0$, the flutter boundary simply corresponds to λ_{cr}. When $\lambda<\lambda_{cr}$, any disturbance to the panel decays and $c/h \to 0$. For $\lambda>\lambda_{cr}$, a limit-cycle oscillation exists with increasing amplitude as λ increases. This situation can be seen more clearly by plotting the panel damping-rate α and frequency ω against dynamic pressure λ as shown

in Fig. 2. For the case of very small damping, $g_a \to 0$, instability that corresponds to a positive α does not set in until after the two undamped natural frequencies ω_1 and ω_2 have merged. If some damping is present, $g_a > 0$, the instability sets in a somewhat higher value of λ than for the case of zero-damping as indicated by the arrows in Fig. 2. This instability is, however, not catastrophic. The panel response does not grow indefinitely, but rather a limit-cycle oscillation is developed with increasing amplitude as dynamic pressure λ increases.

The limit-cycle panel deflections for a simply supported square panel at several dynamic pressures λ are shown in Fig. 3. It should be emphasized that only an updated single-mode is needed in the finite element solution.

In Fig. 4, the panel amplitude of the limit-cycle oscillations is given as a function of dynamic pressure ratio for simply supported square and isosceles triangular plates. The critical dynamic pressures λ_{cr} obtained from the analysis are 511.8 and 2022 for square and triangular, respectively. It clearly indicates that the triangular panel is much stiffer than the square one.

The increasing use of advanced composite materials on high-performance aircraft and missile structures necessitates the determination of limit-cycle motions of laminated composite panels. A finite element formulation for analyzing nonlinear flutter of arbitrarily laminated composite rectangular panels will be presented. The linear stiffness matrix is coupled between the bending and the inplane nodal degrees-of-freedom due to unsymmetric lamination, in addition the nonlinear stiffness matrix is also coupled due to large deflections. The quasi-steady aerodynamic theory is used. Finite element limit-cycle oscillation results of composite laminates will be presented.

REFERENCES

1. Laurenson, R. M. and McPherson, J. I., "Design Procedures for Flutter-Free Surface Panels," NASA CR-2801, 1977.

2. Cunningham, H. J., "Flutter Analysis of Flat Rectangular Panels Based on Three-Dimensional Supersonic Unsteady Potential Flow," NASA TR R-256, 1967.

3. Dugundji, J., "Theoretical Considerations of Panel Flutter at High Supersonic Mach Numbers," AIAA J., Vol. 4, July 1966, pp. 1257-1266.

4. Dowell, E. H., "Panel Flutter: A Review of the Aeroelasic Stability of Plates and Shells," AIAA J., Vol. 8, March 1970, pp. 385-399.

5. Reed, W. H., Hanson, P. W. and Alford, W. J., "Assessment of Flutter Model Testing Relating to the National Aero-Space Plane," NASP Contractor Report 1002, 1987.

6. Ventres, C. S. and Dowell, E. H., "Comparison of Theory and Experiment for Nonlinear Flutter of Loaded Plates," AIAA J., Vol. 8, Nov. 1970, pp.2022-2030.

7. Dowell, E. H., "Nonlinear Oscillations of a Fluttering Plate II," AIAA J., Vol. 5, Oct. 1967, pp. 1856-1862.

8. Dowell, E. H., "Nonlinear Oscillations of a Fluttering Plate," AIAA J., Vol. 4, July 1966, 1267-1275.

9. Eastep, F. E. and McIntosh, S. C., "Analysis of Nonlinear Panel Flutter and Response Under Random Excitation or Nonlinear Aerodynamic Loading," AIAA J., Vol. 9, March 1971, pp. 411-418.

10. Kuo, C. C., Morino, L. and Dugundji, J., "Perturbation and Harmonic Balance Methods for Nonlinear Panel Flutter," AIAA J., Vol. 10, Nov. 1972, pp. 1479-1484.

11. Morino, L., "A Perturbation Method for Treating Nonlinear Panel Flutter Problems," AIAA J., Vol. 7, March 1969, pp. 405-410.

12. Eslami, H., "Nonlinear Flutter and Forced Oscillations of Rectangular Symmetric Cross-Ply and Orthotropic Panels Using Harmonic Balance and Perturbation Method," Ph.D. Dissertation, Old Dominion University, Norfolk, VA 1987.

13. Olson, M. S., "Finite Elements Applied to Panel Flutter," AIAA J., Vol. 5, Dec. 1967, pp. 2267-2270.

14. Olson, M. D., "Some Flutter Solutions Using Finite Elements," AIAA J., Vol. 8, April 1970, pp. 747-752.

15. Yang, T. Y. and Sung, S. H., "Finite Element Panel Flutter in Three-Dimensional Supersonic Unsteady Potential Flow," AIAA J., Vol. 15, Dec. 1977, pp. 1677-1683.

16. Mei, C. and Rogers, J. L., Jr., "Application of NASTRAN to Large Deflection Supersonic Flutter of Panels," NASA TM X-3428, Oct. 1976, pp. 67-97.

17. Mei, C., "A Finite Element Approach for Nonlinear Panel Flutter," AIAA J., Vol. 15, Aug. 1977, pp. 1107-1110.

18. Rao, K. S. and Rao, G. V., "Large Amplitude Supersonic Flutter of Panels with Ends Elastically Restrained Against Rotation," Computers and Structures, Vol. 11, 1980, pp. 197-201.

19. Mei, C. and Weidman, D. J., "Nonlinear Panel Flutter-A Finite-Element Approach," in Computational Methods for Fluid-Structure Interaction Problems, Ed. by Belytscnke, T. and Geers, T. L., AMD-Vol. 26, ASME, 1977, pp. 139-165.

20. Han, A. D. and Yang, T. Y., "Nonlinear Panel Flutter Using High-Order Triangular Finite Elements," AIAA J., Vol. 21, Oct. 1983, pp. 1453-1461.

21. Mei, C. and Wang, H. C., "Finite Element Analysis of Large Amplitude Supersonic Flutter of Panels," Proceedings International Conference on Finite Element Methods, Shanghai, China, Gordon and Breach Science Publishers, Inc. 1982, pp. 944-951.

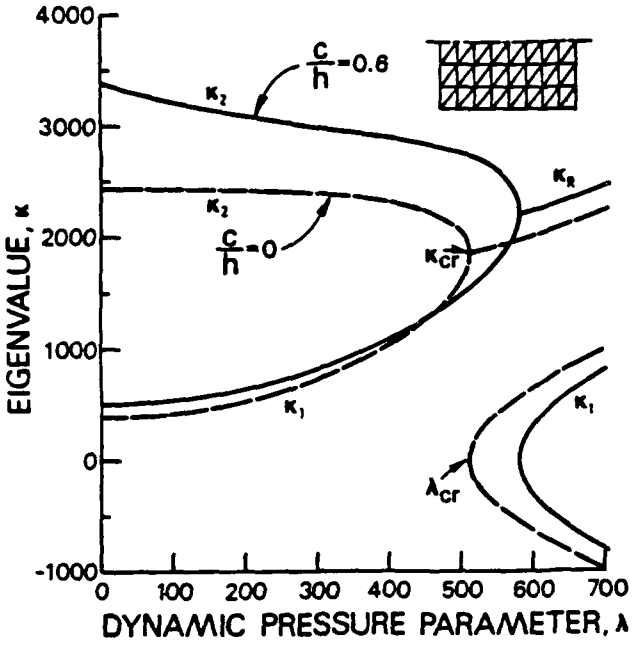

Fig. 1 Variation of eigenvalues with dynamic pressure for a simply supported square panel at small (c/h=0) and large (c/h=0.6) deflections, g_a=0.

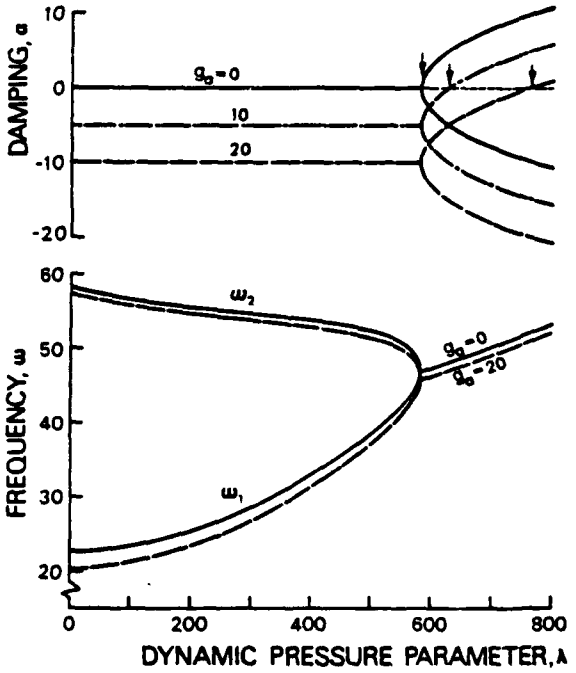

Fig. 2 Damping rate and frequency versus dynamic pressure for a simply supported square panel with several values of g_a at c/h=0.6.

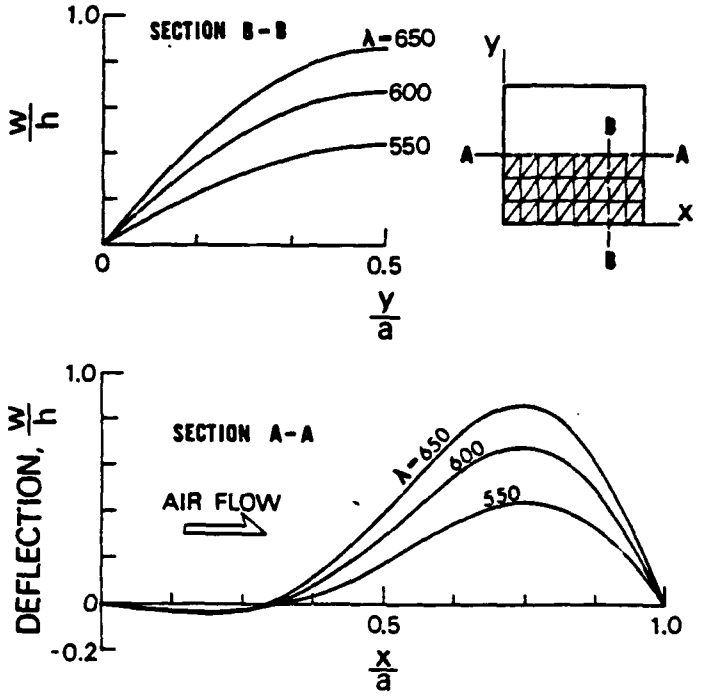

Fig. 3 Large-amplitude deflections at various dynamic pressure for a simply supported square panel, g_a=0.

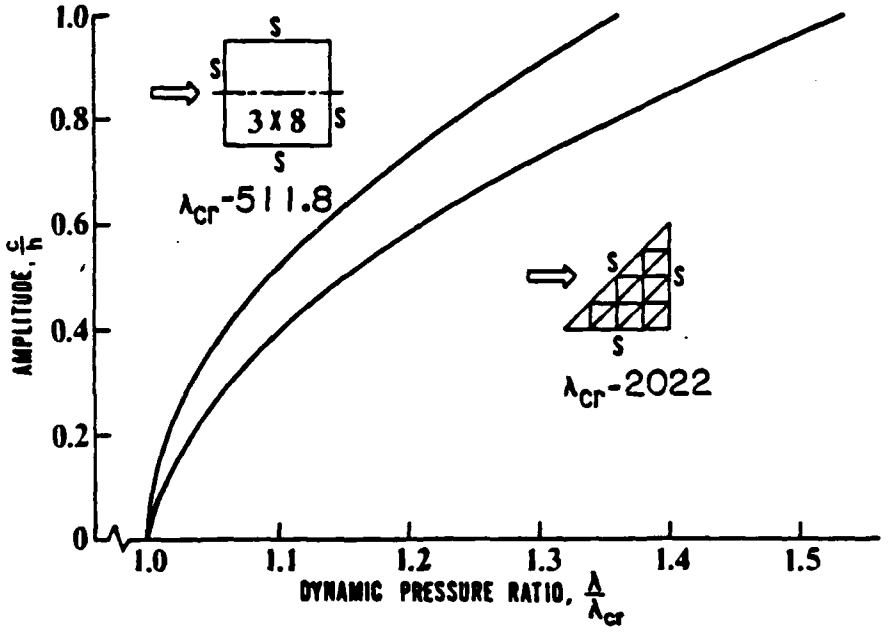

Fig. 4 Limit-cycle amplitude versus dynamic pressure ratio for simply supported square and triangular panels, g_a=0.

DYNAMIC STABILITY OF LAMINATED COMPOSITE SHELLS USING A SHEAR DEFORMATION THEORY

by

E. Yogeswaren and J. N. Reddy
Department of Engineering Science and Mechanics
Virginia Polytechnic Institute and State University
Blacksburg, Virginia USA

EXTENDED ABSTRACT

1. Introduction

Dynamic instability of plates and shells includes such phenomena as buckling under impulsive mechanical loads, vibrations induced by sudden thermal loads, and instability due to pulsating mechanical loads. This type of instability has been observed in the first walls of inertial confinement fusion reactors and in the skin shells of aerospace vehicles in transonic or low supersonic flights. In these cases failures may occur at loads far below the static critical load and dynamic stability analysis is an essential part of the design. For example, a flat plate subjected to an in-plane load varying at a multiple of plate natural frequency will exhibit parametric instability and may buckle at load amplitudes far below the static critical buckling load. The load is considered parametric since it perturbs the coefficients of the governing equations of motion and thus appears as a parameter in the equation.

Studies of dynamic instability of laminated composite structures [1-3] are often based purely on analytical methods thus restricting the scope of problems to simple geometries, loadings and boundary conditions. The present study deals with the use of a shear deformation shell theory and the finite element method to investigate dynamic stability of laminated composite cylindrical shells.

2. Governing Equations and Finite Element Model

The Sanders shell theory [4] used in the present study has the following equations of motion:

$$\frac{\partial N_1}{\partial x_1} + \frac{\partial N_6}{\partial x_2} = \bar{I}_1 \ddot{u} + \bar{I}_2 \ddot{\phi}_1$$

$$\frac{\partial N_6}{\partial x_1} + \frac{\partial N_2}{\partial x_2} = \bar{I}_1 \ddot{v} + \bar{I}_2 \ddot{\phi}_2$$

$$\frac{\partial Q_1}{\partial x_1} + \frac{\partial Q_2}{\partial x_2} - \frac{N_1}{R_1} - \frac{N_2}{R_2} + q = I_1 \ddot{w}$$

$$\frac{\partial M_1}{\partial x_1} + \frac{\partial M_6}{\partial x_2} - Q_1 = \bar{I}_2 \ddot{u} + \bar{I}_1 \ddot{\phi}_1 \qquad (1)$$

$$\frac{\partial M_6}{\partial x_1} + \frac{\partial M_2}{\partial x_2} - Q_2 = \bar{I}_2'\ddot{v} + \bar{I}_1'\ddot{\phi}_2$$

where superposed dot denotes differentiation with respect to time, q is the distributed transverse load, and N_i, M_i and Q_i are the stress resultants

$$(N_i, M_i) = \sum_{k=1}^{N} \int_{\zeta k-1}^{\zeta k} \sigma_i^{(k)}(1,\zeta)d\zeta \quad (i = 1,2,6)$$

$$(Q_2, Q_1) = \sum_{k=1}^{N} \int_{\zeta_{k-1}}^{\zeta_k} (\sigma_4^{(k)}, \sigma_5^{(k)})d\zeta. \tag{2}$$

The inertias, $\bar{I}_i$ $(i = 1,2)$ are defined by the equations,

$$\bar{I}_1 = I_1 + \frac{2}{R_1} I_2 \ , \ \bar{I}_2 = I_2 + \frac{1}{R_1} I_3 \ ,$$

$$(I_1, I_2, I_3) = \sum_{k=1}^{N} \int_{\zeta_{k-1}}^{\zeta_k} \rho^{(k)}(1,\zeta,\zeta^2)d\zeta, \tag{3}$$

and $\bar{I}_i'$ are the same as $\bar{I}_i$ except that R_1 is replaced by R_2.

The resulting finite element model is of the form

$$[M]\{\ddot{u}\} + [C]\{\dot{u}\} + [K]\{u\} = \{0\} \tag{4}$$

where

$$[C] = \lambda[M]$$

$$[K] = [K_L] + [K_{NL}] + [S_s] + [S_D]\cos\omega t \tag{5}$$

and

$[K_L]$ - linear stiffness matrix

$[K_{NL}]$ - nonlinear stiffness matrix

$[S_s]$ - stability matrix due to static loads

$[S_D]$ - stability matrix due to dynamic loads.

The equation (4) with a time-dependent parameter is a Mathieu-Hill equation. The analysis presented here establishes the principal and second order unstable regions of the system with and without damping.

3. Numerical Results

Numerical results for sample problems are discussed here. The following material properties of a lamina are used:

$$E_1 = 25E_2;\ G_{23} = 0.2E_2;\ G_{13} = G_{12} = 0.5E_2;\ \nu_{12} = 0.25$$

A cylindrical shell made of four layer (0°/90°/90°/0°) cross-ply lamination is studied. An axial sinusoidally oscillating load N_1 is used. Advantage of the symmetry is taken to model a quadrant of the cylinder (see Fig. 1a). The instability regions are shown in Fig. 1b.

A cylindrical panel made of four-ply (0°/90°/90°/0°) lamination is investigated (see Fig. 2a) next. An axial sinusoidally oscillating load N_1 is used, and a quadrant of the cylindrical panel is modeled. The boundaries of instability are plotted in the Ince-Strutt diagram of Fig. 2b.

In order to study the effect of thickness and aspect ratio on the instability regions, three cases of plates were considered. The boundary conditions used are the same as those for the cylindrical panel. The Ince-Strutt instability charts are shown in Fig. 3 for comparison of thickness effects and by Fig. 4 for comparison of aspect ratio effect. Increasing thickness shifts the principal region towards the origin while narrowing the instability region itself. Larger aspect ratios shift the principal region away from the origin and narrows the instability region.

References

1. Ambartsumyan, S. A., Theory of Anisotropic Plates, Technomic, Lancaster, PA, 1970.

2. Ray, H. and Bert, C. W., "Dynamic Instability of Suddenly Heated Thick Composite Shells," International Journal of Engineering Science, Vol. 22, No. 11/12, pp. 1259-1268, 1984.

3. Bert, C. W. and Birman, V., "Dynamic Instability of Shear Deformable Antisymmetric Angle-Ply Plates," International Journal of Solids and Structures, Vol. 23, No. 7, pp. 1053-1061, 1987.

4. Reddy, J. N., Energy and Variational Methods in Applied Mechanics, John Wiley, New York, 1984.

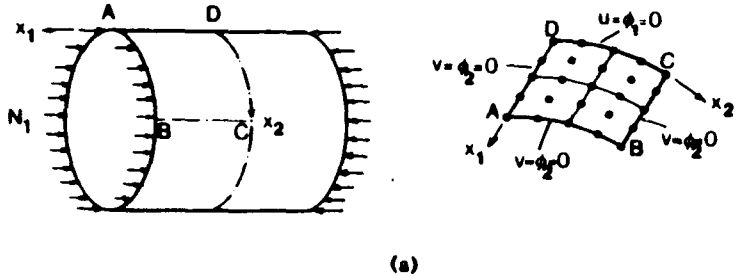

(a)

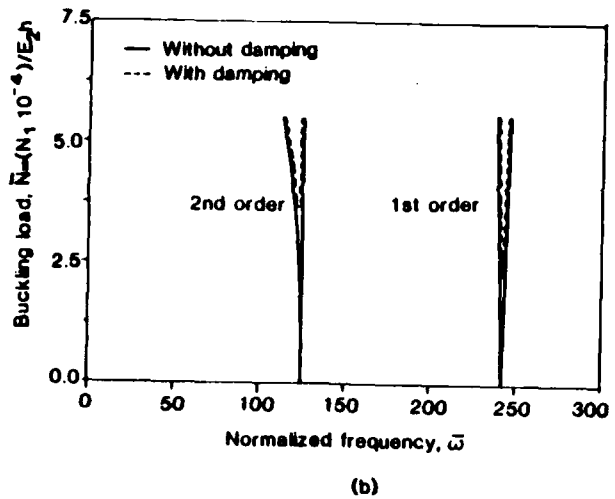

(b)

Figure 1. Geometry and instability regions for four-ply (0/90/90/0) cylindrical shell.

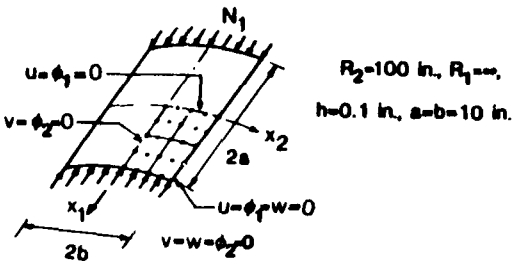

(a)

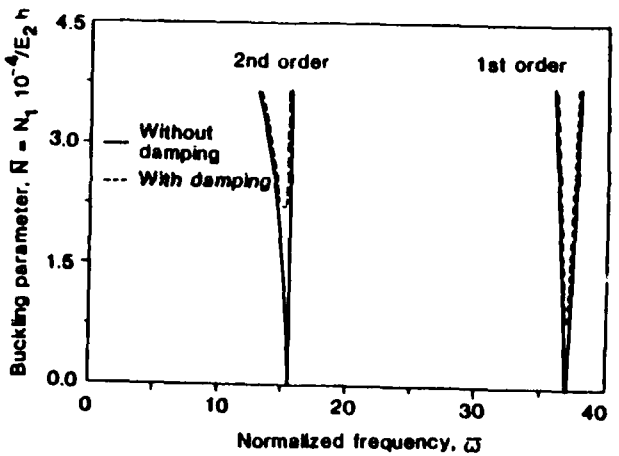

(b)

Figure 2. Geometry and instability regions for four-layer (0/90/90/0) cylindrical panel.

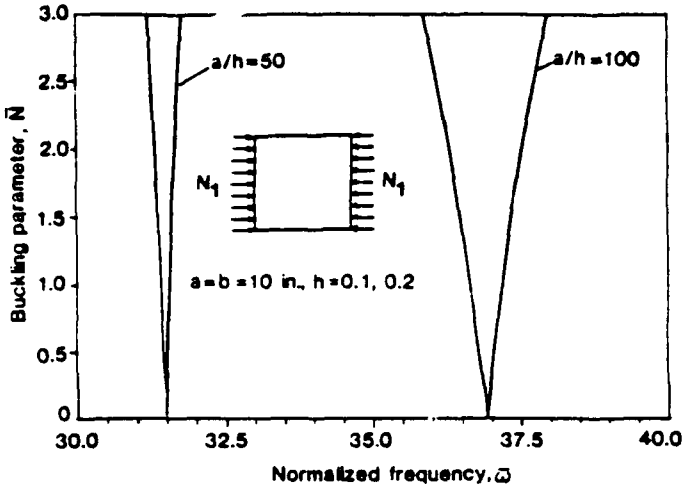

Figure 3. Instability regions for simply-supported four-layer (0/90/90/0) square laminates under axial compressive load.

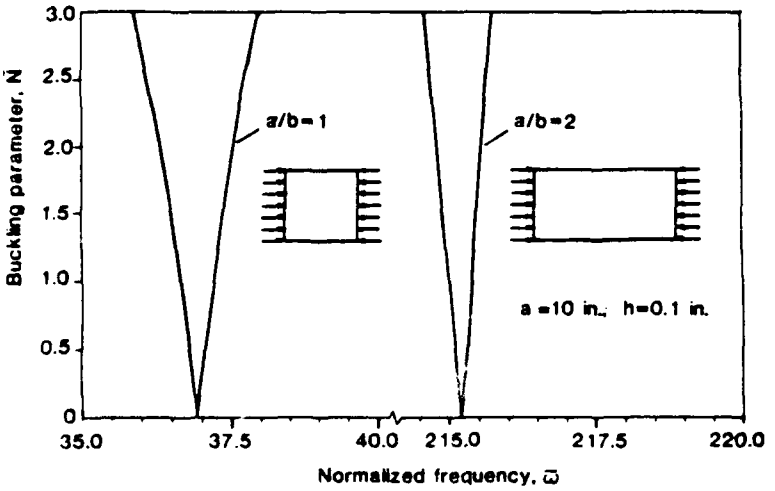

Figure 4. Instability regions for simply-supported cross-ply (0/90/90/0) laminates under axial compressive load.

SESSION 8

MISCELLANEOUS TOPICS IN NONLINEAR DYNAMICS

THURSDAY - 1545 - 1900

June 2, 1988

PLANAR RESPONSE OF ELASTIC CABLES TO A SUBHARMONIC OR SUPERHARMONIC EXCITATION

Francesco Benedettini and Giuseppe Rega

Dipartimento di Ingegneria delle Strutture, delle Acque e del Terreno
Università dell'Aquila
Monteluco di Roio, 67040 L'Aquila, ITALY

ABSTRACT

Planar non-linear oscillations of a onedegree-of-freedom model of elastic cables under subharmonic or superharmonic resonance conditions are studied. Second-order perturbation analyses and numerical integrations of the equation of motion are developed. Parametric investigations are performed for technical cables with various sag-to-span ratios to enlight the main features of the dynamic phenomena.

INTRODUCTION

The planar motion of a parabolic elastic cable subjected to a vertical distributed load p(x, t) is described by the equation

$$[Hv' + EA/l \cdot (y' + v') \int_0^l (y'v' + v'^2/2)\, dx] + p - \mu\dot{v} = m\ddot{v} \qquad (1)$$

in the vertical displacement unknown v(x, t). This equation, which is valid in the case of moderately large rotations and negligible longitudinal inertia forces, is accurate for studying nonlinear dynamics of cables used in overhead transmission lines. Referring to assumed spatial distribution of the excitation and deflected shape of the cable, and applying the Galerkin method, equation (1) reduces to one dimensionless ordinary differential equation

$$\ddot{\tilde{q}} + \tilde{q} + \mu^*\dot{\tilde{q}} + c_2\tilde{q}^2 + c_3\tilde{q}^3 = p^* \cos \Omega t \qquad (2)$$

where quadratic and cubic nonlinearities occur, associated with initial curvature and stretching of cable axis respectively.

Though primary and secondary resonances of systems described by equation (2) have been analysed in several recent papers [1-4], few works have been concerned with elastic cables [5-7]. In this paper, subharmonic resonances are studied through second order perturbation analyses and numerical integration of equation (2), and the main features of these dynamic phenomena are discussed for technical cables with various sag-to span ratios.

ANALYSIS

Secondary resonances due to quadratic nonlinearity

Weakly nonlinear oscillations in the neighbourhood of these resonances are investigated

by letting $\tilde{q} = \varepsilon q$, $\mu^* = \varepsilon\mu$, $p^* = \varepsilon p$, where q, μ, p are 0(1) variables and ε is a small but finite parameter. Equation (2) reads

$$\ddot{q} + q + \varepsilon\mu\dot{q} + \varepsilon c_2 q^2 + \varepsilon^2 c_3 q^3 = p \cos \Omega t \tag{3}$$

and a second-order approximation to its solution is sought through the multiple time scales method. Secondary resonances occur if $\Omega \cong 1/2$ or $\Omega \cong 2$.

To study the former case [2], *superharmonic resonance of order two*, the frequency of the excitation in written as $2\Omega = 1 + \varepsilon\hat{\sigma}$, where a detuning parameter $\varepsilon\hat{\sigma}/2$, describing quantitatively the nearness of Ω to one half the cable natural frequency, appears. In terms of dimensionless actual quantities, the frequency response equation for steady-state oscillation is obtained

$$\frac{\mu^2 a^2}{4} + (\sigma + c_4 a^2 + c_5 \Lambda^2 + \frac{\mu^2}{8})^2 a^2 = c_2^2 \Lambda^4 [(1 - \frac{\sigma}{2})^2 + \mu^2 c_6^2] \tag{4}$$

where $2\Lambda = p/(1 - \Omega^2)$ is the amplitude of the forced term occurring in the time law for q(t) and a is the amplitude of the superharmonic component of order two. This latter exists for all initial conditions.

To study the case $\Omega \cong 2$, *subharmonic resonance of order one half*, we let $\Omega = 2 + \varepsilon\hat{\sigma}$. With the ordering assumed for damping and excitation, so called second-order theory [1], the frequency-response equation for steady-state oscillation reads

$$\frac{\mu^2 a^2}{4} + (\frac{\sigma}{2} + c_4 a^2 + c_7 \Lambda^2 + \frac{\mu^2}{8})^2 a^2 = c_2^2 \Lambda^2 a^2 [(1 - \frac{\sigma}{2})^2 + \mu^2 c_8^2] \tag{5}$$

and shows the possible occurrence of both the trivial and a non trivial subharmonic of order one half in the response. Stable finite amplitude subharmonic occurs only in some regions in the parameter space of the excitation. Where both the trivial and the non-trivial solution can occur, which one actually settles down depends on the initial conditions.

Secondary resonances due to cubic nonlinearity

The new ordering $\tilde{q} = \varepsilon q$, $\mu^* = \varepsilon^2\mu$, $p^* = \varepsilon p$ is let, leading to the equation

$$\ddot{q} + q + \varepsilon^2\mu\dot{q} + \varepsilon c_2 q^2 + \varepsilon^2 c_3 q^3 = p \cos \Omega t \tag{6}$$

Secondary resonances are seen to occur to the ε^2-order if $\Omega \cong 1/3$ or $\Omega \cong 3$.

To study the former case, *superharmonic resonance of order three*, we let $3\Omega = 1 + \varepsilon^2\hat{\sigma}$ and obtain the frequency-response equation

$$\sigma = -(c_4 a^2 + c_5 \Lambda^2) \pm (c_9^2 \Lambda^6/a^2 - \mu^2/4)^{1/2} \tag{7}$$

where a is the amplitude of the superharmonic component of order three occurring again in the response for all initial conditions.

To study the case $\Omega \cong 3$, *subharmonic resonance of order one third*, we let $\Omega = 3 + \varepsilon^2\hat{\sigma}$ and obtain the frequency-response equation for the non-trivial subharmonic component of order one third

$$\sigma = -3(c_4 a^2 + c_5 \Lambda^2) \pm 3(c_{10}^2 \Lambda^2 a^2 - \mu^2/4)^{1/2} \tag{8}$$

Since the trivial solution is a possible stable steady-state solution, regions of existence and stability of the finite amplitude subharmonic are determined.

RESULTS

Some results are presented for prestressed cables vibrating with the first (symmetric) mode, with sag-to-span ratio ranging from zero up to about 1/40 and technical values of the axial rigidity-to-initial tension parameter ($EA/H \cong 500$). Equation (4) is plotted in figure 1. The order-two superharmonic resonance phenomenon is as stronger as the cable is slacker. Apart from the nearly taut cables showing hardening behaviour, the response is more and more softening as d/l increases due to the increased importance of the quadratic nonlinearity. Two curves obtained to the first order approximation are also reported in figure 1 (thick line) for comparison. Besides the absence of bending, the main difference is concerned with the peak amplitude value, which is lower for a sagged cable and slightly higher for a nearly taut cable.

The curves obtained by plotting equation (7) for the order-three superharmonic resonance are very similar to the former ones: the more strongly nonlinear response still occurs for the slacker cables, notably influenced by the quadratic nonlinearity, but the peak amplitude values are quite lower than in the order-two resonance.

In the two time laws of steady-state response obtained perturbatively in the neighbourhood of $\Omega = 1/2$ and $\Omega = 1/3$, both the superharmonic component of order two and that of order three are present, to a different order which is exchanged in the two cases. This interaction is confirmed by the results of numerical integrations of equation (2) which are in good agreement with the perturbation results (fig. 2) and show how the 2Ω-harmonic becomes the more important one even in the neighbourhood of $\Omega = 1/3$ as the excitation amplitude increases (fig. 3). Moreover, in this case, the numerical results become more and more hardening and show the occurrence of an upper branch of superharmonic response at amplitude and frequency values of technical interest, contrary to the perturbation results which predict such branch to occur at unreliable response parameter values.

Equation (5) for the order one half subharmonic resonance is plotted in the lower part of figure 4 for a nearly taut cable (thick line) and an actually sagged cable (thin line). Intermediate cables exhibit higher response amplitudes close to perfect tuning. In the upper part, the regions of existence (II), of possible existence (III) and of non-existence (I) of the stable non-trivial subharmonic are shown in the parameter space of the excitation. Region I and III are exchanged for the two cables since they exhibit different spring behaviour. Results of numerical integrations validate the predictions of this second-order perturbation solution, except for the occurrence of the subharmonic component at large negative σ-values with the sagged cable, a physically unrealistic finding which is likely to be due to the order considered in the asymptotic expansion.

For the same two cables, figure 5 shows in the lower part the frequency response equation (8) for the order one third subharmonic resonance and in the upper part the regions of possible existence (III) and of non-existence (I) of the stable non-trivial subharmonic. These regions differ notably from each other for the two cables. In particular, as p increases, this subharmonic phenomenon becomes meaningful mostly for the sagged cable, whose region of existence extends over perfect tuning. However the response is found to be more weakly nonlinear in the one third than in the one half subharmonic oscillations, confirming the behaviour obtained in the corresponding superharmonic.

CONCLUSIONS

The main conclusions are summarized as follows.

1) The quadratic nonlinearity associated with the initial curvature plays an important role in the cable forced dynamics. This gives rise to some interesting features of the response. i) The oscillation amplitude is notably higher for the sagged cables than for the nearly taut cables, even in the neighbourhood of the secondary resonances due to the cubic nonlinearity. ii) In this neighbourhood, the response of the system is more weakly non-linear than close to the resonances due to the quadratic nonlinearity, where the amplitude of the secondary component can reach important values, some times higher than those of the forced component. iii) In the superharmonic cases, in which significant interaction between the two main (2Ω and 3Ω) superharmonic components of the motion occurs in the neighbourhood of the two resonant frequencies, the order-two superharmonic becomes the more important one also near $\Omega = 1/3$ as the excitation amplitude increases. iv) As larger is the sag, as lower is the excitation amplitude to which the one half subharmonic can occur, and as more important is the one third subharmonic with increasing excitation amplitude.
2) Use at least of a second-order approximation in the perturbation solutions is essential to accurately describe the cable nonlinear dynamics. In particular, the so called second-order theory must be referred to when treating the order one-half subharmonic resonance.
3) The findings of the approximate solutions obtained are validated by the results of numerical integrations in a rather large range of values of amplitude and frequency around perfect tunings. As the excitation amplitude increases, the perturbation solutions fail to the approximation considered.

ACKNOWLEDGMENT

This research was partially supported by the Italian Ministry of Education (M.P.I. 60%)

REFERENCES

[1] A.H. NAYFEH 1983 *Journal of Sound and Vibration* **89**, 457-470. The response of single degree of freedom systems with quadratic and cubic nonlinearities to a subharmonic excitation.
[2] A.H. NAYFEH 1984 *Journal of Sound and Vibration* **92**, 363-377. Quenching of primary resonance by a subharmonic resonance.
[3] D.T. MOOK, R.H. PLAUT and N. HAQUANG 1985 *Journal of Sound and Vibration* **102**, 473-492. The influence of an internal resonance on non-linear structural vibrations under subharmonic resonance conditions.
[4] R.H. PLAUT, N. HAQUANG and D.T. MOOK 1986 *Journal of Sound and Vibration* **106**, 361-376. Simultaneous resonances in non-linear structural vibrations under two-frequency excitation.
[5] S.I. AL-NOURY and S.A. ALI 1985 *Journal of Sound and Vibration* **101**, 451-462. Large-amplitude vibrations of parabolic cables.
[6] F. BENEDETTINI and G. REGA 1987 *International Journal of Non-linear Mechanics* **22**, 497-509. Nonlinear dynamics of an elastic cable under planar excitation.
[7] K. TAKAHASHI and Y. KONISHI 1987 *Journal of Sound and Vibration* **118**, 85-97. Non-linear vibrations of cables in three dimensions, Part II: Out-of-plane vibrations under in-plane sinusoidally time-varying load.

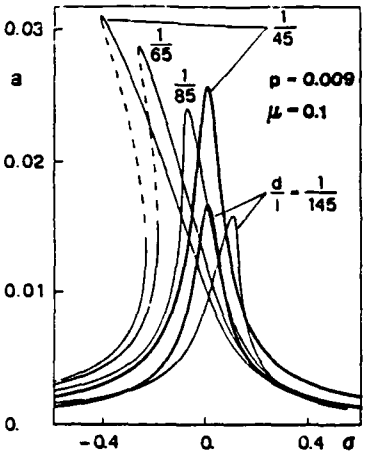

Fig. 1 - Order-two superharmonic

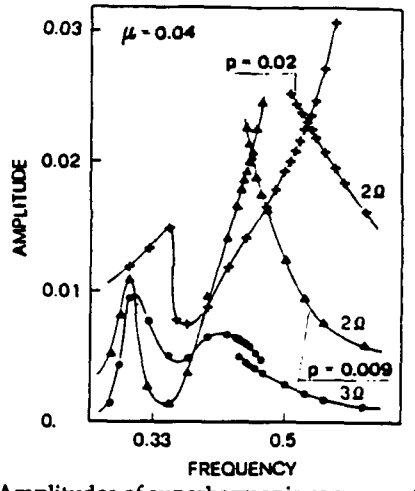

Fig. 3 - Amplitudes of superharmonic components with two excitation amplitudes, numerical results

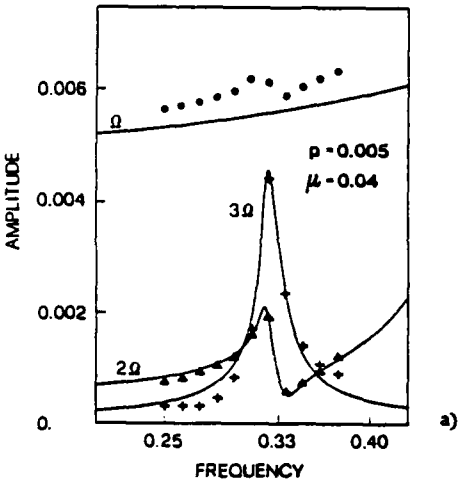

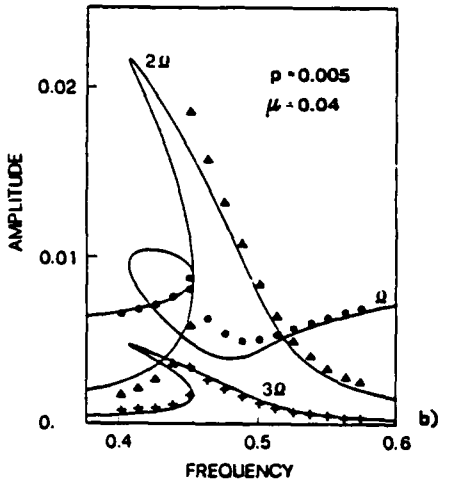

Fig. 2 - Order-three (a) and order-two (b) superharmonic, perturbation (curves) and numerical (dots) results

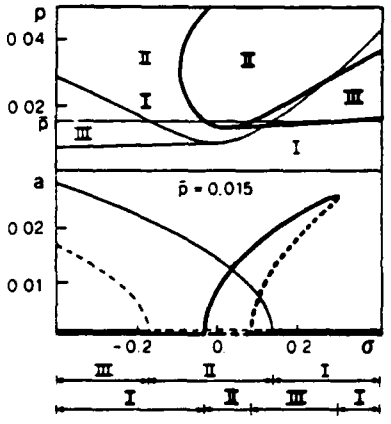

Fig. 4 - One-half subharmonic

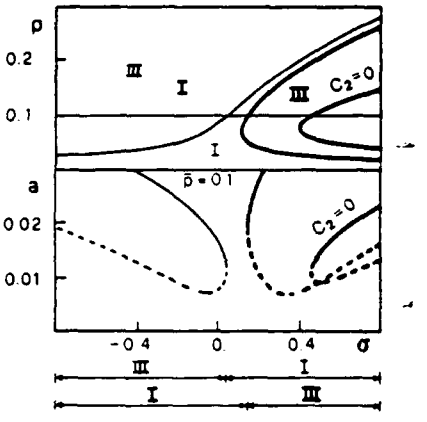

Fig. 5 - One-third subharmonic

THE RESPONSE OF SEISMICALLY MOUNTED ROTOR SYSTEM WITH CUBIC NON–LINEARITIES

A. ERTAS AND E. K. CHEW

Department of Mechanical Engineering
Texas Tech University
Lubbock, Texas

The dynamic response of a two-degree-of-freedom seismically mounted rotor system with cubic non-linearities is investigated. The rotating machine is subjected to internal forces caused by the eccentricity of the center of mass of the rotor. The equations of motion of the system are determined using Lagrange's equation. The method of multiple scales is then used to determine the response of the system. The response of the system is determined when the excitation frequency is near the first and second modal frequency under noninternal and internal resonance conditions.

INTRODUCTION

Rotor machinery such as turbines and compressors are designed to operate in a vibration free manner. However, bearing misalignment, material heterogeneity, geometric variations, and rotor shaft deflections, collectively or selectively, cause the rotor axial mass center distribution to be non-coincident with the bearing axis. In general, the locus of the mass centers of the discretized rotor cross sections defines a space curve with respect to the bearing axis. Such a deviation is termed rotor mass center eccentricity and causes time dependent bearing forces to occur in the rotor housing. If the housing is mounted on a foundation isolation support system, the time dependent bearing forces will cause a motion of the housing and also gives rise to internal stresses.

The housing support system is supposed to decrease the foundation forces from the values appearing at the bearing support. However, in order to determine the extent of the decrease, the motion of the housing, which dictates the transmitted foundation forces, must be known. In turn, the housing motion is affected not only by the bearing forces but also by the foundation support system forces. The net result is a complex interdependent set of relationships between the housing motion and the foundation forces [1].

Vibration, due to motion of the housing–rotor system, may be enough to cause malfunctions in sensitive equipment located nearby. The quality of the work from fine machining may deteriorate as a result of this vibration. Hence, the source of the vibration should be isolated from sensitive equipment. If the vibration cannot be reduced by dynamic balancing, or by relocating the rotating machine, it is often possible to isolate the rotating machine on a seismic mounting [2]. A seismic mounting is formed by interposing resilient materials between the machine and its supports. The resilient material is typically in the form of steel springs, rubber isolators, or air springs. One of the most common materials that is used to isolate machines is rubber [3]. Under compression, a rubber spring will have the characteristics of hardening spring. Often, designers ignore the non-linearity of actual springs. However, non-linear systems exhibit phenomena that are not predicted using a linearized analysis. Many excellent analytical

and numerical studies have been done on the oscillations of non-linear systems with quadratic and cubic non-linearities by Abu–Aris and Nayfeh [4], Burton and Rahman [5], Mook et al. [6, 7], Nayfeh [8-12], Nayfeh and Zavodney [13], Nayfeh and Jerbil [14], Plaut et al. [15, 16], Tezak et al. [17], and Ibrahim and Barr [18]. To investigate the effects of the seismic mounting on the dynamic response of a rotating machine the two mass–hardening spring–damper model is used in this paper. The principal resonances in the rotor system tuned to an internal resonance due to cubic non-linearities ($\omega_2 = 3\omega_1$) are investigated.

EQUATIONS OF MOTION

The equations of motion of the rotating machine are derived by using Lagrange's equation. The generalized coordinates used for the two–degree–of–freedom rotating machine, as shown in Figure 1, are x_1 and x_2 which are the vertical displacements of the center of mass of the housing and base from the static equilibrium positions, respectively. The springs and dashpots are assumed to be identical for all the supports. All the springs have a non–linear cubic type hardening characteristics. The load–displacement curve is described by

$$F(x) = kx + \frac{k\pi^2}{12d^2}x^3 \tag{1}$$

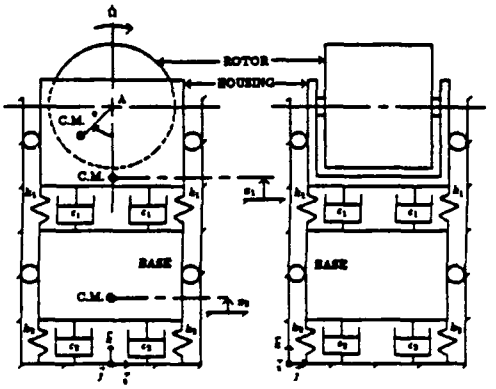

Fig. 1 Schematic of rotating machine

The equations of motion of the rotating machine can be written as

$$M_H(1+r_{MD})\ddot{x}_1 + 4k_1(x_1 - x_2) = 4c_1(\dot{x}_2 - \dot{x}_1) + \frac{k_1\pi^2}{3d_1^2}(x_2^3 - x_1^3) + \frac{k_1\pi^2}{d_1^2}(x_1^2x_2 - x_1x_2^2)\delta - M_H(r_{MD}e\Omega^2\cos(\Omega t)) \tag{2}$$

$$M_H r_{MB}\ddot{x}_2 + 4k_1\left[(1+r_k)x_2 - x_1\right] = 4c_1\left[\dot{x}_1 - (1+r_c)\dot{x}_2\right] + \frac{k_1\pi^2}{3d_1^2}\left[x_1^3 - (1+r_k/r_d)x_2^3\right] + \frac{k_1\pi^2}{d_1^2}(x_1x_2^2 - x_1^2x_2) \tag{3}$$

where M_B, M_D, M_H, c, d, k, r_{MB}, r_{MD}, r_k, t, Ω, are the mass of the base, mass of the rotor, mass of the housing, damping coefficient, asymptote of the load–deflection curve

of spring, stiffness, mass ratio of the rotor to housing, mass ratio of the base to housing, ratio of the initial stiffness of springs, excitation frequency, and time, respectively. Dots indicate differentiation with respect to the time t. The equation of motion of the system in a non-dimensional normalized form can be written as

$$Y_n'' + \lambda_n^2 Y_n = \varepsilon^2 \left\{ \sum_{m=1}^{2} [C_{nm} Y_m' + NL_{1nm} Y_m^3 + NL_{2nm} Y_1 Y_2 Y_m] + E_n \Omega^2 \cos(\nu\tau) \right\}, \quad n = 1, 2 \qquad (4)$$

where the λ_n^2, C_{nm}, NL_{1nm}, NL_{2nm}, E_n, and ν, are constants, ε is a small non–dimensional parameter, and the prime denotes derivatives with respect to the non–dimensional time τ. In equation (4) the damping matrix C_{nm} can be decoupled by using the modal orthogonality condition.

METHOD OF SOLUTION AND RESULTS

Following the multiple scale method [19], an approximation to the solution of the non–dimensional normalized equations (3) and (4) can be expressed as

$$Y_1 = Y_{10}(T_0, T_2) + \varepsilon^2 Y_{12}(T_0, T_2) + 0(\varepsilon^3) \qquad (5)$$

$$Y_2 = Y_{20}(T_0, T_2) + \varepsilon^2 Y_{22}(T_0, T_2) + 0(\varepsilon^3) \qquad (6)$$

Through the solution of equations (5) and (6) the influence of stiffness and damping of the supports and the overall eccentricity of the rotor housing system on the response amplitude has been investigated. Some of the numerical results are presented in Figures 2-4 for the following cases:

1. Noninternal resonance conditions with $\Omega \approx \omega_1$ and $\Omega \approx \omega_2$
2. Internal resonance conditions when
   a. $\Omega \approx \omega_1$ and $\omega_2 \approx 3\omega_1$
   b. $\Omega \approx \omega_2$ and $\omega_2 \approx 3\omega_1$

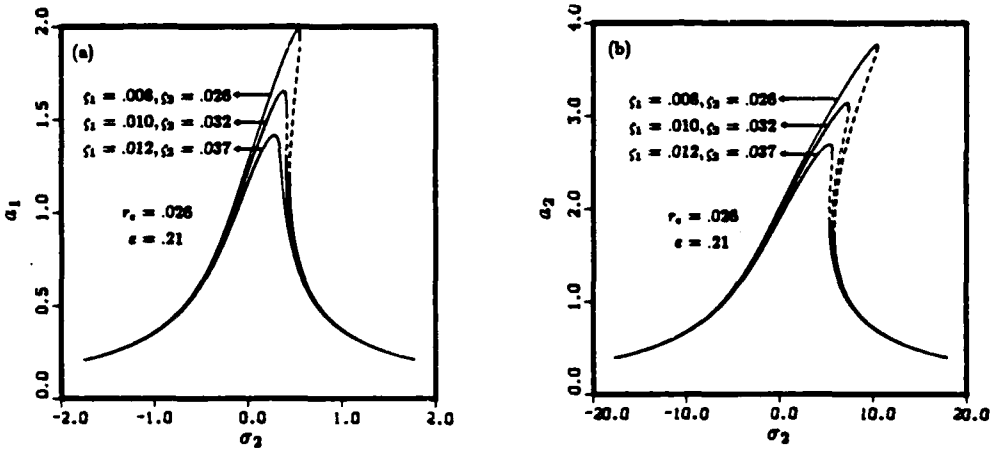

Fig. 2 The variation of response amplitude a, as a function of detuning parameter σ_2, with damping ratio ζ. ($M_H = 37.27$ *Slugs*, $k = 4{,}658$ lb_f/Ft, $r_{MB} = 10$, $r_{MD} = 0.3$, eccentricity=$e = 0.008$ Ft, $d = 0.05$ Ft, $r_e = e^2/d^2$). (a) Noninternal resonance condition with $\Omega \approx \omega_1$; (b) noninternal resonance condition with $\Omega \approx \omega_2$.

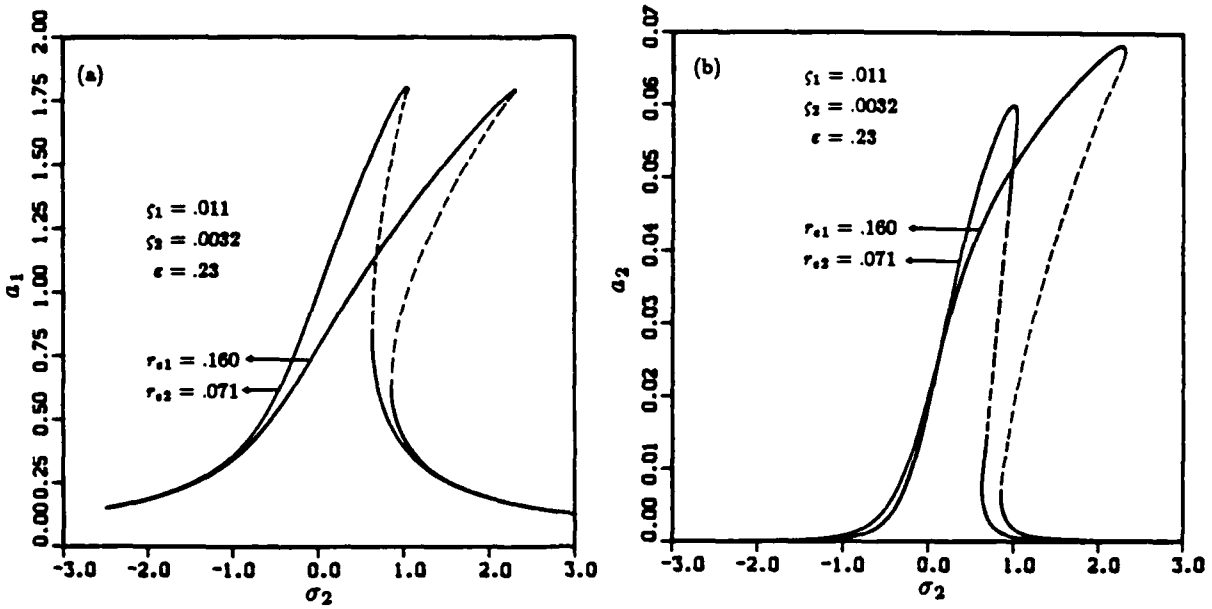

Fig. 3 The variation of response amplitude a, as a function of detuning paprameter σ_2, with asymtote d (M_H = 37.27, *Slugs*, k = 4,658 lb_f/Ft, r_{MB} = 8.44, r_{MD} = 0.3, eccentricity=e = 0.008 Ft, d_1 = 0.02 Ft, d_2 = 0.03 Ft). (a), (b) Internal resonance condition with $\Omega = \omega_1$ when $\omega_2 = 3\omega_1$.

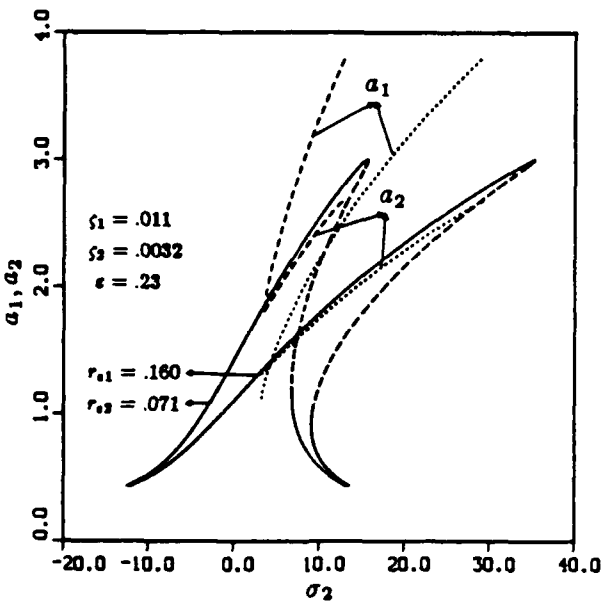

Fig. 4 The variation of response amplitude a, as a function of detuning parameter σ_2, with asymptote d (M_H = 37.27 *Slugs*, k = 4,658 lb_f/Ft, r_{MB} = 8.44, r_{MD} = 0.3, eccentricity=e = 0.008 Ft, d_1 = 0.02 Ft, d_2 = 0.03 Ft). Internal resonance condition with $\Omega = \omega_2$ when $\omega_2 = 3\omega_1$. —$a_1 = 0, a_2 \neq 0$ with $r_{e1} = 0.16$ and $r_{e2} = 0.071$, - - - $a_1 \neq 0, a_2 \neq 0$ with $r_{e2} = 0.071$, $\cdots a_1 \neq 0, a_2 \neq 0$ with $r_{e1} = 0.16$.

REFERENCES

1. A. Ertas and T. J. Kozik 1987 *ASME Journal of Energy Resources Technology* 109, 174-179. Fatigue loads on the foundation due to turbine rotor eccentricity.
2. J. A. Macinanth 1984 *Seismic Mounting for Vibration Isolation.* New York: Wiley-Interscience.
3. C. M. Harris and C. E. Crede 1976 *Shock and Vibration Handbook.* MaGraw–Hill Book Co.
4. A. M. Abu-Arish and A. H. Nayfeh 1985 *Journal of Sound and Vibration* 103, 253-272. The response of one–degree of–freedom systems with cubic and quadratic non–linearities to a harmonic excitation.
5. T. D. Burton and Z. Rahman 1986 *Intern'l J. Non-linear Mechanics* 21, 135-146. On the multiple–scales analysis of strongly non–linear forced oscillators.
6. D. T. Mook, R. H. Plaut and N. HaQuang 1985 *Journal of Sound and Vibration* 102, 473–492. The influence of an internal resonance on non–linear structural vibrations under subharmonic resonance conditions.
7. D. T. Mook, N. HaQuang and R. H. Plaut 1986 *Journal of Sound and Vibration* 104, 229–241. The influence of an internal resonance on non–linear structural vibrations under combination resonance conditions.
8. A. H. Nayfeh 1983 *Journal of Sound and Vibration* 89, 457–470. The response of single degree of freedom systems with quadratic and cubic non–linearities to a subharmonic excitation.
9. A. H. Nayfeh 1983 *Journal of Sound and Vibration* 90, 237–244. The response of multidegree–of–freedom systems with quadratic non–linearities to a harmonic parametric resonance.
10. A. H. Nayfeh 1983 *Journal of Sound and Vibration* 88, 1–10. Response of two–degree–of–freedom systems to multifrequency parametric excitation.
11. A. H. Nayfeh 1983 *Journal of Sound and Vibration* 88, 547–557. The response of two–defree–of–freedom systems with quadratic non–linearities to a parametric excitation.
12. A. H. Nayfeh 1985 *Journal of Sound and Vibration* 102, 403–414. The response of non-linear single–degree–of freedom systems to multifrequency excitations.
13. A. H. Nayfeh and L. D. Zavodney 1986 *Journal of Sound and Vibration* 107, 329–350. The response of two–degree–of freedom systems with quadratic non–linearities to a combination parametric resonance.
14. A. H. Nayfeh and A. E. S. Jerbil 1987 *Journal of Sound and Vibration* 115, 83–101. The response of two–degree–of–freedom systems with quadratic and cubic non–linearities to multifrequency parametric excitations.
15. R. H. Plaut, N. Haquang and D. T. Mook 1986 *Journal of Sound and Vibration* 106, 361–376. Simultaneous resonances in non–linear structural vibrations under two–frequency excitation.
16. R. H. Plaut, N. Haquang and D. T. Mook 1986 *Journal of Sound and Vibration* 107, 309–319. The influence of an internal resonance on non–linear structural vibrations under two–frequency excitation.
17. E. G. Tezak, A. H. Nayfeh and Mook 1982 *Journal of Sound and Vibration* 85, 459–472. Parametrically excited non–linear multidegree–of–freedom systems with repeated natural frequencies.
18. R. A. Ibrahim and A. D. S. Barr 1978 *Shock and Vibration Digest* 10, 9-24. Parametric vibration Part II: Mechanics of non–linear problem.
19. A. H. Nayfeh and D. T. Mook 1979 *Non-linear Oscillations.* Newyork: Wiley–Interscience.

NONLINEAR OSCILLATIONS UNDER TWO-FREQUENCY PARAMETRIC EXCITATION

Raymond H. Plaut
Department of Civil Engineering
Virginia Polytechnic Institute and State University
Blacksburg, Virginia 24061, USA

and

Jeanette J. Gentry and Dean T. Mook
Department of Engineering Science and Mechanics
Virginia Polytechnic Institute and State University
Blacksburg, Virginia 24061, USA

ABSTRACT

Forces acting on structural and mechanical systems often appear in the coefficients of the equations of motion and are called parametric excitations. A parametric excitation containing two harmonic components is considered here. In the resonance case which is treated, the sum of the two parametric frequencies is approximately equal to twice a natural frequency of the system. Multidegree-of-freedom systems with weak quadratic and cubic nonlinearities are investigated, and results are obtained by means of the method of multiple scales.

ANALYSIS

The following system of equations in $u_n(t)$ is considered:

$$\ddot{u}_n + 2\varepsilon^2\mu_n\dot{u}_n + \omega_n^2 u_n + 2\varepsilon \sum_{m=1}^{2} \cos(\lambda_m t + \tau_m) \sum_{j=1}^{\infty} Q_{jn}^m u_j + \varepsilon \sum_{j=1}^{\infty}\sum_{k=1}^{\infty} \Lambda_{jkn} u_j u_k + \varepsilon^2 \sum_{j=1}^{\infty}\sum_{k=1}^{\infty}\sum_{\ell=1}^{\infty} \Gamma_{jk\ell n} u_j u_k u_\ell = 0; \quad n = 1,2,... \tag{1}$$

The ω_n are the natural frequencies of the linearized system; ε is a small, constant parameter; the Λ_{jkn} and $\Gamma_{jk\ell n}$ are constant coefficients of the

nonlinear terms; the μ_n are constant damping coefficients; and the Q_{in}^m, λ_m, and τ_m are constant excitation amplitudes, frequencies, and phases, respectively.

Assume that

$$\lambda_1 + \lambda_2 = 2\omega_q + \varepsilon^2\sigma \tag{2}$$

where σ is a detuning parameter. The method of multiple scales leads to the asymptotic solution

$$u_n(t) = a_n(T_2)\cos[\omega_n t + \beta_n(T_2)] + O(\varepsilon) \tag{3}$$

where $T_2 = \varepsilon^2 t$. In the steady state, $a_n = 0$ for $n \neq q$ (assuming $\mu_n > 0$), and solutions a_q depend on the parameters of the system.

RESULTS

Various plots of the steady-state amplitude a_q are presented in Figures 1-4. Solid lines denote stable solutions and dashed lines denote unstable solutions. There is always a trivial solution, $a_q = 0$. When no nontrivial solutions exist, the trivial solution is stable. When there is one nontrivial solution, it is stable and the trivial solution is unstable. When there are two nontrivial solutions, the larger one is stable, the smaller one is unstable, and the trivial solution is stable.

In Figure 1, a_q is plotted as a function of σ for two sets of system parameters. The behavior may be hardening, as in (A), or softening, as in (B). For Figure 2, $Q_{qq}^1 = Q_{qq}^2 = Q$ and the other excitation amplitudes are assumed to be zero. In (A), μ_q and σ are both zero, and the nontrivial solution a_q is proportional to Q. In (B) and (C), $\mu_q = 0$ while σ has opposite signs. In (D) and (E), $\mu_q > 0$ and different sets of parameters are chosen.

The response amplitude depends on the relative values of λ_1 and λ_2. Let $\gamma = \lambda_1/2\omega_q$. The variation of a_q with γ is shown in Figure 3 for three typical cases, with $\mu_q = 0$ in (A) and $\mu_q > 0$ in (B) and (C). The relative values of the excitation amplitudes also affect the response amplitude. For Figure 4, $Q_{qq}^1 = Q$, Q_{qq}^2 is fixed, and the other excitation amplitudes are assured to be zero. In (A) and (D), $\mu_q = 0$, while $\mu_q > 0$ in (B) and (C). It is seen that various types of behavior can occur, depending on Q_{qq}^2 and the system parameters.

ACKNOWLEDGEMENT

This research was supported by the U.S. Army Research Office.

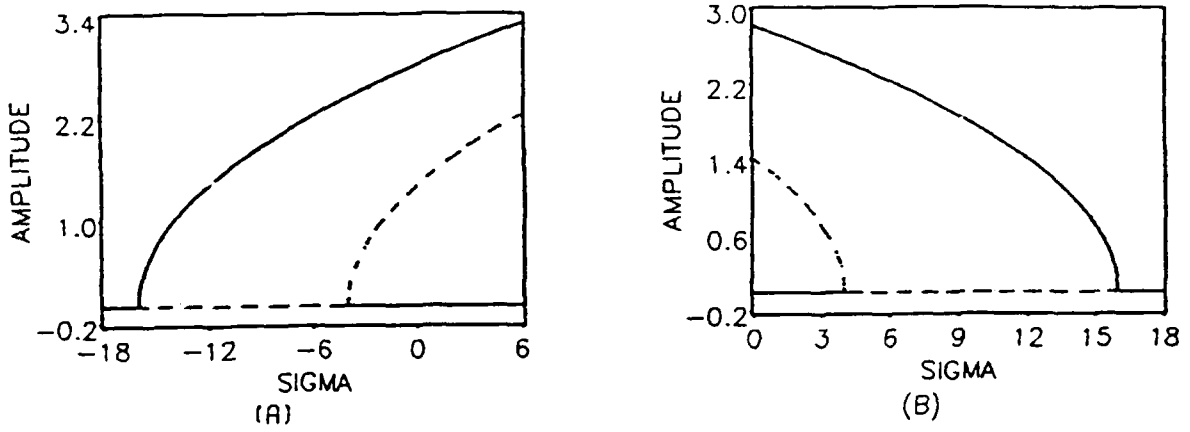

Figure 1. Response amplitude a_q as a function of detuning parameter σ.

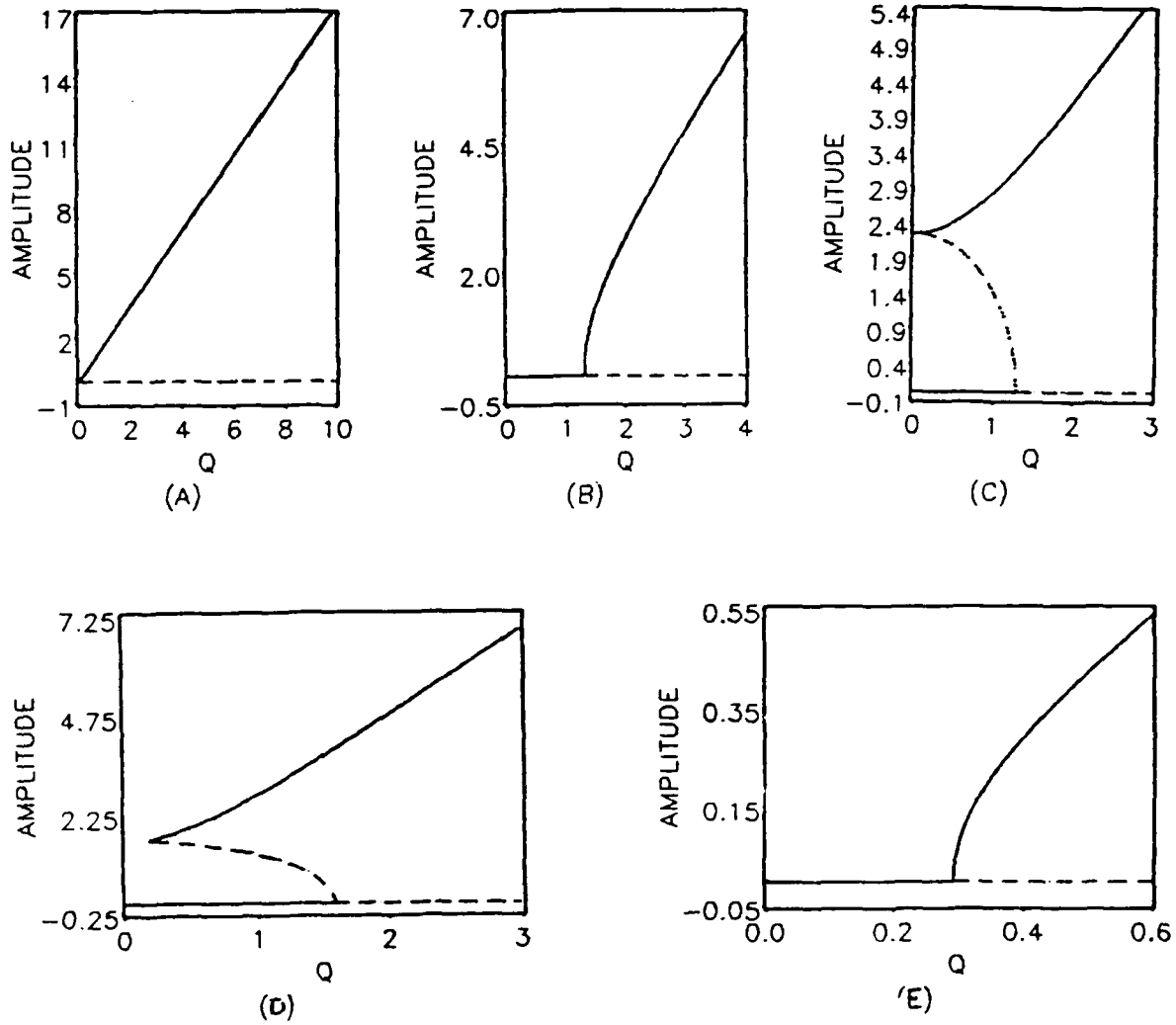

Figure 2. Response amplitude a_q as a function of Q, where $Q=Q^1_{qq}=Q^2_{qq}$.

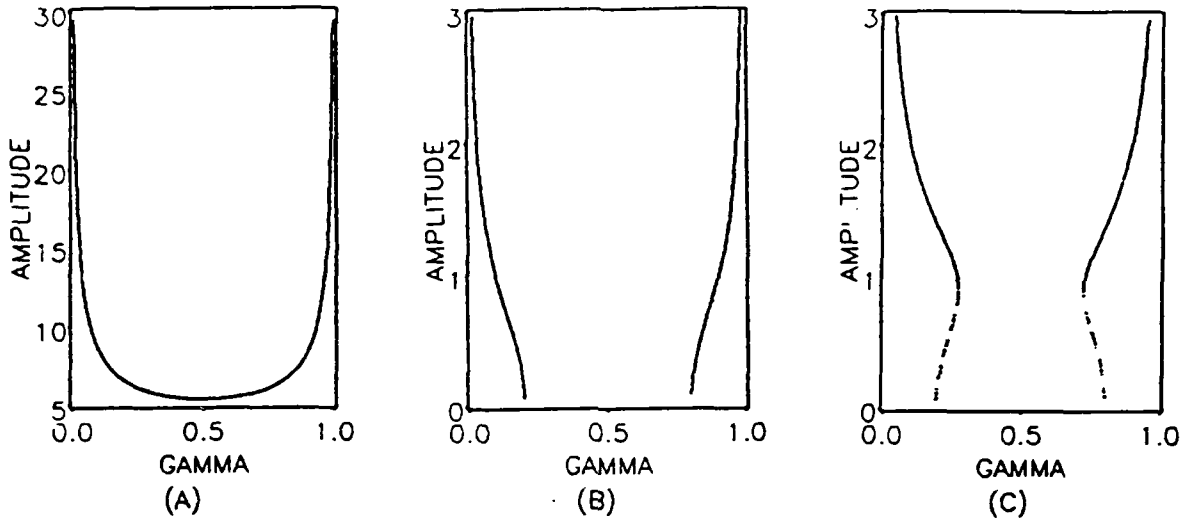

Figure 3. Response amplitude a_q as a function of γ; $\gamma=\lambda_1/2\omega_q$.

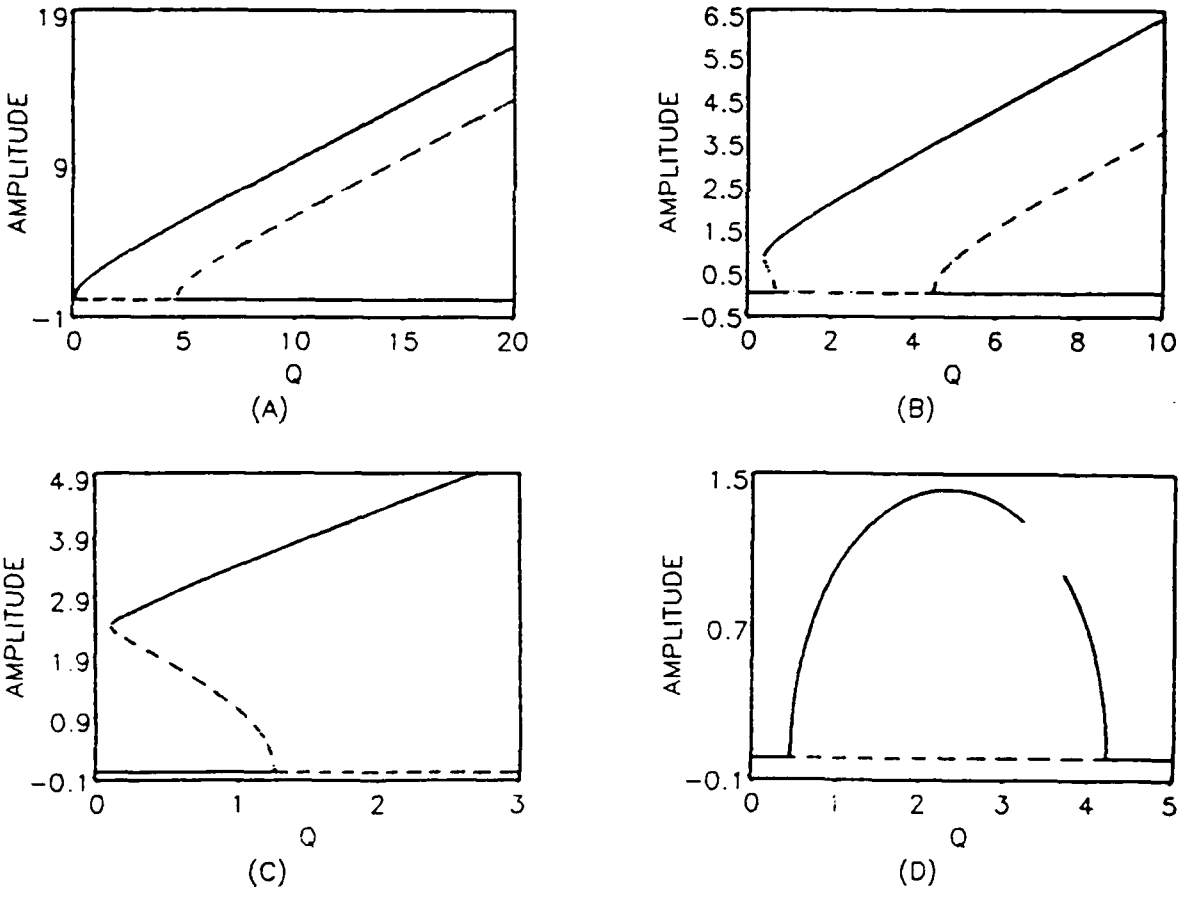

Figure 4. Response amplitude a_q as a function of Q; $Q=Q^1_{qq}$, Q^2_{qq} fixed.

QUENCHING OF SELF-EXCITED VIBRATIONS

Khaled R. Asfar
Department of Mechanical Engineering
Jordan University of Science and Technology
Irbid, Jordan

ABSTRACT

A passive method for suppressing self-excited vibrations is proposed. The system consists of a mass and damper attached to the main self-excited system. Free and forced vibrations are considered. A first-order approximate solution of the governing nonlinear equations is obtained using the method of multiple scales. The analysis shows that complete quenching of self-excited free vibrations is possible for some values of the system parameters. The results are verified by numerical integration of the governing equations. For the forced self-excited system, the case of primary resonance is investigated. The analysis shows that the proposed system is quite effective in suppressing the amplitude of vibrations. Furthermore, it causes a frequency shift and eliminates the unstable region in the response.

1. INTRODUCTION

Quenching of self-excited vibrations has been attempted using active and passive methods. Asfar et al [1] analyzed the response of self-excited oscillators to multifrequency excitations. They concluded that under certain conditions, the free oscillations may be suppressed by the presence of non-resonant excitations. The dynamic vibration absorber for self-excited systems was first investigated by Mansour [2]. He concluded that an absorber may not be quite effective in suppressing self-excitation effects due to negative damping. Tondl [3] extended further the analysis of Mansour. In conclusion, the absorber can be effective in suppressing self-excited vibrations only when the ratio between its mass and that of the main system is adequately high. In the present paper, a vibration suppression system known as the Lanchester damper is proposed for the quenching of free and forced self-excited vibrations.

2. PROBLEM FORMULATION

The differential equations of motion are

$$\frac{d^2u_1}{dt^2} + u_1 = \varepsilon\left[\frac{du_1}{dt} - \frac{1}{3}\left(\frac{du_1}{dt}\right)^3\right] + \varepsilon R\left(\frac{du_2}{dt} - \frac{du_1}{dt}\right) \qquad (1)$$

$$\frac{d^2u_2}{dt^2} + \gamma\left(\frac{du_2}{dt} - \frac{du_1}{dt}\right) = 0 \qquad (2)$$

In what follows, we determine a first-order approximation to the solutions of equations (1) and (2) for $\varepsilon \ll 1$.

3. ANALYSIS

Using the method of multiple scales [4], we seek an approximate solution in the form

$$u_j(t;\varepsilon) \approx u_{j0}(T_0,T_1) + \varepsilon u_{j1}(T_0,T_1) + \ldots, \quad j = 1,2 \tag{3}$$

The solutions of the equations governing u_{10} and u_{20} are written as

$$u_{10} = A(T_1)e^{iT_0} + \bar{A}\, e^{-iT_0} \tag{4}$$

$$u_{20} = a_{20}(T_1) + \frac{\gamma}{\gamma+i} A\, e^{iT_0} + \frac{\gamma}{\gamma-i} \bar{A}\, e^{-iT_0} \tag{5}$$

The solution of the equation governing u_{11} contains secular-producing terms. Therefore, to render the expansion (3) uniform, these terms must be eliminated. This condition leads to the following equations governing the amplitude and phase

$$a' = \frac{a}{2}\left(1 - \frac{1}{4}a^2 - \frac{R}{1+\gamma^2}\right) \tag{6}$$

$$\beta' = -\frac{R\gamma}{2(1+\gamma^2)} \tag{7}$$

The condition for which $a \to 0$ (written in terms of the system parameters c,μ,k,M) is

$$C_{cr} = \frac{km^2}{2\mu M} - \left(\frac{km^2}{M}\right)^{\frac{1}{2}} \left[\frac{km^2}{4M\mu^2} - 1\right]^{\frac{1}{2}} \tag{8}$$

Figure 1 shows the relation between the critical damping coefficient and the mass m. Any point on the curve (c,m) would produce complete quenching of the self-excited motion amplitude. There is a threshold of the damper mass m below which no quenching is possible unless a very high value of damping coefficient is used. Beyond this threshold, a sharp drop in the value of C_{cr} occurs.

Equations (1) and (2) are numerically integrated to verify the result obtained by the perturbation solution. A point with the values c = 10 and m = 20 is picked on the curve in Figure 1, for K = 100 and M = 100, for the numerical integration. Starting with arbitrary initial conditions, we find that the amplitude of the self-excited motion decays with a small rate and continues to decay and goes to zero after a long time, Figure 2a. If the damping coefficient is decreased below the critical value (keeping m constant), the amplitude of the limit cycle remains unchanged and no quenching is produced, Figure 2b. When the damping coefficient is taken higher than the critical value, the decay rate increases and a trivial response is obtained after few time cycles, Figure 2c.

4. FORCED RESPONSE

Here, the response of the self-excited system to a monofrequency excitation subjected to the action of the mass-dashpot system is investigated. The governing equations are

$$\ddot{u}_1 + u_1 = \varepsilon(\dot{u}_1 - \frac{1}{3}\dot{u}_1^3) + \varepsilon R(\dot{u}_2 - \dot{u}_1) + \hat{f}\cos\Omega t \qquad (9)$$

$$\ddot{u}_2 + \gamma(\dot{u}_2 - \dot{u}_1) = 0 \qquad (10)$$

The case of primary resonance is considered here. Therefore, the excitation amplitude $\hat{f}$ is ordered as $\hat{f} = \varepsilon f$. An approximate solution using the method of multiple scales is sought in the forms (3) and (4). The equations governing the amplitude a and phase ψ are given by

$$a\psi' = a\sigma - \frac{1}{2}\frac{R\gamma}{1+\gamma^2}a + \frac{1}{2}f\cos\psi \qquad (11)$$

$$a' = \frac{1}{2}(1 - \frac{R}{1+\gamma^2})a - \frac{1}{8}a^3 + \frac{1}{2}f\sin\psi \qquad (12)$$

where $\psi = \sigma T_1 - \beta$. The steady-state frequency-response equation is

$$\sigma = \frac{1}{2}\frac{R\gamma}{1+\gamma^2} \pm \{\frac{f^2}{a^2} - (1 - \frac{R}{1+\gamma^2} - \frac{a^2}{4})^2\}^{\frac{1}{2}} \qquad (13)$$

where σ is defined by $\Omega = 1 + \varepsilon\sigma$.

Figure 3 shows the effect of varying the amplitude of the excitation f on the response. For small values of f, there exists two branches; a lower single-valued branch close to the σ-axis, and a higher closed curve branch in the form of an oval. As f increases, the oval expands and the lower branch moves closer to the oval. At some value of f (which depends on R and γ), the two branches coalesce and form one continuous multivalued curve. As f increases further, the multivalued region decreases and eventually becomes a single-valued response curve. The curve also moves away from the σ-axis as f increases. In all figures, the solid curve represents the stable solution, while the dashed line represents the unstable solution.

Figure 4 shows the effect of the parameter R on the response. When R is equal to zero, the response curves are those discussed in [5]. As R increases, the two branches approach each other and eventually form a single continuous curve. The maximum amplitude decreases, and the axis of symmetry shifts to the right. As R increases further, the curve becomes single valued and moves to the right and closer to the σ-axis. The effective damping in the system becomes positive for $R > 5$ (for $\gamma = 2$). All of the response curve becomes stable.

The effect of changing γ on the response is shown in Figure 5. For small values of γ, the response curve is single valued and its axis of symmetry is away from the $\sigma = 0$ axis. As γ increases, the axis of symmetry shifts to the left, the curve becomes multivalued, and the peak amplitude increases. As γ increases further, the curve separates into two branches; an oval and a lower branch. The axis of symmetry shifts further to the left, the oval moves away from the σ-axis, while the lower branch moves closer to the σ-axis. For higher values of γ, the axis of symmetry becomes very close to the $\sigma = 0$ axis, and there is little change in the response curves. The response of the system approaches the case with no damper.

5. CONCLUSIONS

The results presented in this paper show that the mass-damper system is quite effective in quenching both free and forced self-excited vibrations. When compared to the dynamic vibration absorber, it is found that the present system is superior since it has less components and does not require any tuning to the excitation frequency. Furthermore, it can be used in those systems where resilient foundations are impractical to use.

REFERENCES

1. Asfar, K. R., Nayfeh, A. H., and Mook, D. T., "Response of Self-Excited Oscillators to Multifrequency Excitations". Journal of Sound and Vibration 79(4), 589-604, 1981.

2. Mansour, W. M., "Quenching of Limit Cycles of a van der Pol Oscillator". Journal of Sound and Vibration 25, 395-405, 1972.

3. Tondl, A., "Quenching of Self-Excited Vibrations; Equilibrium Aspects". Journal of Sound and Vibration 42, 251-260, 1975.

4. Nayfeh, A. H., Introduction to Perturbation Techniques. Wiley Interscience, New York, 1981.

5. Nayfeh, A. H. and Mook, D. T., Nonlinear Oscillations. Wiley Interscience, New York, 1979.

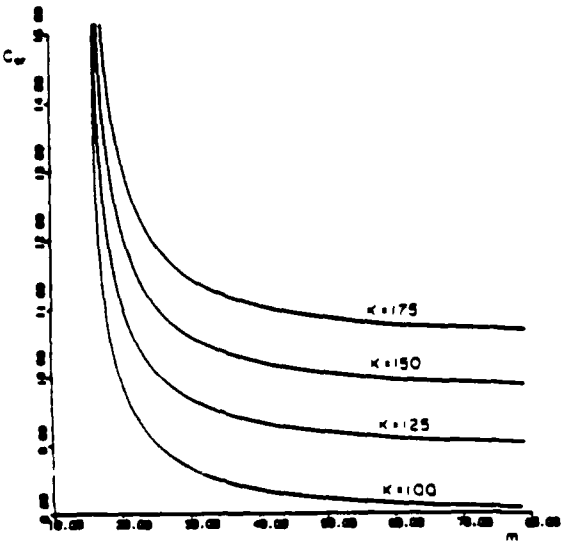

Figure 1. The relation between the critical damping coefficient and the damper mass.

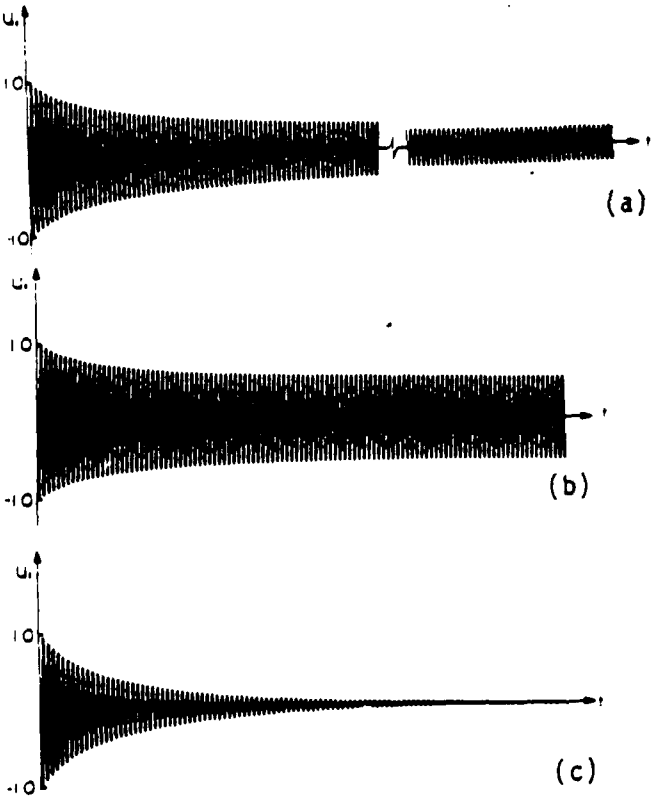

Figure 2. Numerical integration of the governing equations: (a) $c = c_{cr}$, (b) $c < c_{cr}$, (c) $c > c_{cr}$.

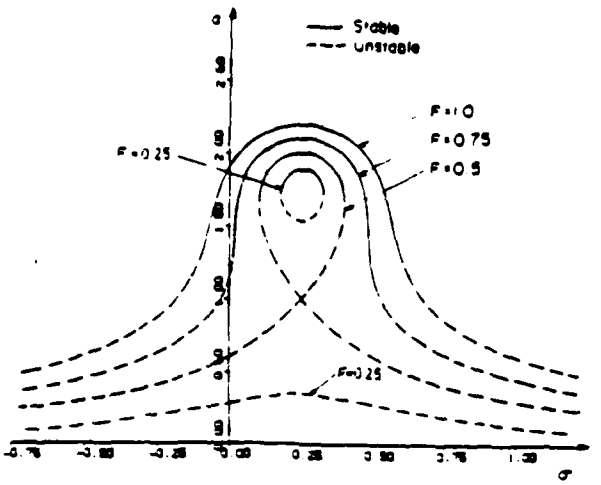

Figure 3. The effect of f on the response.

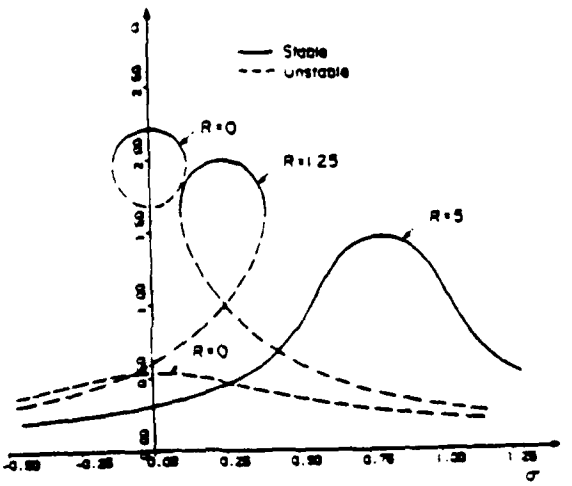

Figure 4. The effect of R on the response.

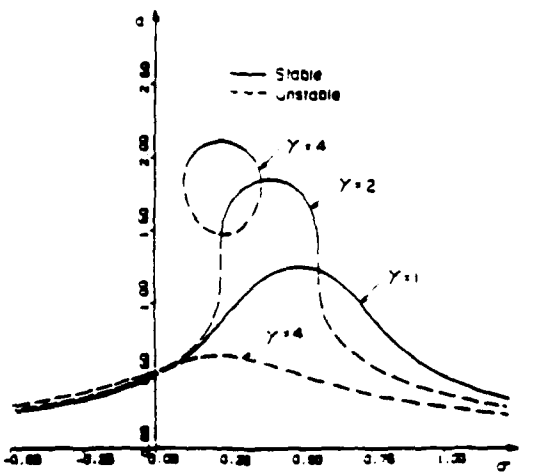

Figure 5. The effect of γ on the response.

Efficient Solution of Constrained Equations of Motion by Recursive Projection

by

Roger A. Wehage

Mechanical Engineer
US Army Tank-Automotive Command
Warren, MI 48397-5000

This paper illustrates a method for representing joints, equations of motion and topology of articulated mechanical systems in factored matrix form, which results in large systems of loosely coupled equations amenable to sparse matrix manipulation. Optimal matrix permutation, partitioning and recursive projection techniques are then applied to symbolically lay out an O(n) solution strategy which follows the system's natural topological profile and generates the necessary uncoupled equations. When combined with symbolic equation generation and optimization techniques, it offers the potential for highly efficient and general purpose computer programs.

An n degree-of-freedom (dof) mechanical system is composed of joints and generalized coordinates defining joint and absolute displacements and motion relative to a global reference frame. Each joint is assigned a reference and referenced side, a center and a positive orientation or direction as indicated by an arrow. The referenced side of a joint holds other entities such as inertias, profiles, force elements, joints, etc. and it is the only entry point into an element. The reference side of a joint can be held by only a single joint (element) or the global frame (ground).

Define an inertial global Cartesian reference frame with $1 \le d \le 6$ orthogonal spatial directions (for example, $d = 3$ implies planer and $d = 6$ implies three dimensional or spatial) and joints a, b, c, ..., p (p = number of joints) with resp. d_a, d_b, d_c, ..., d_p internal dof. Each joint has d reference and referenced absolute coordinates relative to global. Mechanical systems are composed of trees formed from roots, branches and leaves of interconnected joints and elements. The tree represents a path for traversal of the system of joints. Moving from root toward leaves represents upward traversal of the tree and its joints. All joints are oriented upward in the tree.

Joint connectivity and reachability is defined by sparse, lower triangular, inversely related ($dp \times dp$) **C** and **R** matrices with unit determinant. To construct **C** and **R**, refer to Figs. 1 and 2 and think of them as a $p \times p$ arrays of $d \times d$ cells filled with zeros into which $\pm I$'s are inserted. Label the rows and columns as a, b, c, ..., p. Trace upward through the tree of joints labeling them in sequentially increasing order. For each joint *, place **I** in cell (row *, column *) of **C**, resp. **-I** in cell (*, *-1), where *-1 means holder of *, not necessarily the next lower letter in the sequence. To construct **R**, start at each joint * in the tree, trace outward traversing each reachable joint @ in the path and enter **I** in the corresponding cell (@, *), or simply invert **C**.

To simplify the following development, all joint and element displacement, velocity, acceleration and force components are referenced directly to a global frame. Let joints a and b be adjacent where joint b allows $d_b \le d$ dof (specific joint characteristics are not important here), then a $d \times d_b$ velocity influence coefficient matrix $\mathbf{H}_b$, d_b generalized coordiantes q_b and product $\mathbf{H}_b\dot{q}_b$ define the displacement and velocity of b with respect to a. If v_a and v_b define element a and b absolute velocities (linear and angular components), then

$$v_b = v_a + \mathbf{H}_b\dot{q}_b \qquad (1)$$

Differentiating Eq. 1 yields absolute accelerations

$$a_b = a_a + \mathbf{H}_b\ddot{q}_b + \gamma_b \qquad (2)$$

where γ_b absorbs components of acceleration which are quadratic in first derivatives. The inertia matrix is given by $d \times d$ matrix M_b. Combined absolute force and moment components are denoted by $d \times 1$ vectors f_b, g_b, etc. The unconstrained equation of motion for element b is

$$M_b a_b = g_b + f_b \tag{3}$$

where g_b absorbs inertial forces due to those acceleration components quadratic in first derivatives and any external effects such as weight, springs, dampers, etc, and f_b represents the reaction and internal forces at joint b.

The matrix H_b defines tangents to the joint constraint surface along which relative motion takes place and upon which the internal constraint reaction force $f_b^{\perp}$ acts normal to, so that $H_b^T f_b^{\perp} = 0$. The remaining forces in the joint, $f_b^{\parallel}$, acting tangent or parallel to the surface (i.e. in the direction of q_b) are called generalized forces Q_b and thus $H_b^T f_b^{\parallel} = Q_b$. Let $f_b = f_b^{\perp} + f_b^{\parallel}$ and

$$H_b^T f_b = Q_b \tag{4}$$

Keeping in mind the sign conventions on a joint, the force f_b acts positively on element b as indicated in Eq. 3 and negatively on element a.

Using connectivity matrix C, the equations of motion for an arbitrary mechanical system are

$$C v = H \dot{q} \tag{5}$$

$$C a = H \ddot{q} + \gamma \tag{6}$$

$$M a = g + C^T f \tag{7}$$

$$H^T f = Q \tag{8}$$

where $\dot{q} = \left[\dot{q}_a^T, \dot{q}_b^T, ..., \dot{q}_p^T\right]^T$, $\ddot{q} = \left[\ddot{q}_a^T, \ddot{q}_b^T, ..., \ddot{q}_p^T\right]^T$, $Q = \left[Q_a^T, Q_b^T, ..., Q_p^T\right]^T$, $H = \text{diag}\left[H_a, H_b, ..., H_p\right]$, $v = \left[v_a^T, v_b^T, ..., v_p^T\right]^T$, $\gamma = \left[\gamma_a^T, \gamma_b^T, ..., \gamma_p^T\right]^T$, $a = \left[a_a^T, a_b^T, ..., a_p^T\right]^T$, $g = \left[g_a^T, g_b^T, ..., g_p^T\right]^T$, $f = \left[f_a^T, f_b^T, ..., f_p^T\right]^T$ and $M = \text{diag}\left[M_a, M_b, ..., M_p\right]$. Equations 6-8 are combined in matrix form as

$$\begin{bmatrix} M & -C^T & 0 \\ C & 0 & -H \\ 0 & H^T & 0 \end{bmatrix} \begin{bmatrix} a \\ f \\ \ddot{q} \end{bmatrix} = \begin{bmatrix} g \\ \gamma \\ Q \end{bmatrix} \tag{9}$$

Finding an efficient solution of Eq. 9 is relatively straight forward when the matrix structure is carefully analyzed. To illustrate the procedure, the 4-element serial mechanism shown in Fig. 1 is analyzed. For any system represented by a tree, the optimum pivotal strategy for minimum matrix fill and computational overhead requires forward elimination starting from the leaves, progressing toward the root and the reverse process for back substitution. Matrix C defines the optimum permutation order for forward elimination (up and to the left in C^T) and back substitution (down and to the right in C). Observe that this is exactly the reverse (only to keep the variables in natural order in the permuted matrices) of what one generally encounters in the literature, so think of UL factorization instead. For convenience in the previous examples, the elements were labeled a, b, ..., p in a natural ascending order so Eq. 9 can be permuted into

$$\begin{bmatrix} \bar{M}_a & \bar{I} & 0 & 0 \\ -\bar{I}^T & \bar{M}_b & \bar{I} & 0 \\ 0 & -\bar{I}^T & \bar{M}_c & \bar{I} \\ 0 & 0 & -\bar{I}^T & \bar{M}_d \end{bmatrix} \begin{bmatrix} \bar{x}_a \\ \bar{x}_b \\ \bar{x}_c \\ \bar{x}_d \end{bmatrix} = \begin{bmatrix} \bar{b}_a \\ \bar{b}_b \\ \bar{b}_c \\ \bar{b}_d \end{bmatrix} \tag{10}$$

where $\bar{M}_a = \begin{bmatrix} M_a & -I & 0 \\ I & 0 & -H_a \\ 0 & H_a^T & 0 \end{bmatrix}$, $\bar{I} = \begin{bmatrix} 0 & I & 0 \\ 0 & 0 & 0 \\ 0 & 0 & 0 \end{bmatrix}$, $\bar{x}_a = \begin{bmatrix} s_a \\ f_a \\ \ddot{q}_a \end{bmatrix}$, $\bar{b}_a = \begin{bmatrix} g_a \\ \gamma_a \\ Q_a \end{bmatrix}$, etc. One could solve this problem by UL factorization but the structure of the diagonal matrices makes that impractical. It is more easily handled by matrix partitioning. Consider the linear system of equations $Ax = b$ partitioned as $\begin{bmatrix} A_{11} & A_{12} \\ A_{21} & A_{22} \end{bmatrix} \begin{bmatrix} x_1 \\ x_2 \end{bmatrix} = \begin{bmatrix} b_1 \\ b_2 \end{bmatrix}$ where A_{22} is nonsingular. Then $A_{11}x_1 + A_{12}x_2 = b_1$, $A_{21}x_1 + A_{22}x_2 = b_2$ yields

$$x_2 = A_{22}^{-1}\left[b_2 - A_{21}x_1\right] \tag{11}$$

and

$$\left[A_{11} - A_{12}A_{22}^{-1}A_{21}\right]x_1 = b_1 - A_{12}A_{22}^{-1}b_2 \tag{12}$$

Rename this reduced system of equations in Eq. 12 as $By = c$ and partition again as above to obtain $B_{11}y_1 + B_{12}y_2 = c_1$, $B_{21}y_1 + B_{22}y_2 = c_2$ where B_{22} is nonsingular. These new equations yield

$$y_2 = B_{22}^{-1}\left[c_2 - B_{21}y_1\right] \tag{13}$$

and $\left[B_{11} - B_{12}B_{22}^{-1}B_{21}\right]y_1 = c_1 - B_{12}B_{22}^{-1}c_2$. The process continues until the last matrix is small enough so that it is easily invertible which completes the forward elimination step. Say $B_{11} - B_{12}B_{22}^{-1}B_{21}$ is obtained in the last step, then back substitution starts with $y_1 = \left[B_{11} - B_{12}B_{22}^{-1}B_{21}\right]^{-1}\left[c_1 - B_{12}B_{22}^{-1}c_2\right]$ and follows with Eqs. 13 and 11 where $x_1 = \left[y_1^T, y_2^T\right]^T$. Eventually the entire vector x is evaluated.

Following the above pattern, the first partitioning of Eq. 10 starts as

$$\begin{bmatrix} \bar{M}_a & \bar{I} & 0 & 0 \\ -\bar{I}^T & \bar{M}_b & \bar{I} & 0 \\ 0 & -\bar{I}^T & \bar{M}_c & \bar{I} \\ 0 & 0 & -\bar{I}^T & \bar{M}_d \end{bmatrix} \begin{bmatrix} \bar{x}_a \\ \bar{x}_b \\ \bar{x}_c \\ \bar{x}_d \end{bmatrix} = \begin{bmatrix} \bar{b}_a \\ \bar{b}_b \\ \bar{b}_c \\ \bar{b}_d \end{bmatrix} \tag{14}$$

where the submatrix $\bar{M}_d$ must be inverted. This inversion can be simplified by first partitioning $\bar{M}_d$ and noting that $\begin{bmatrix} M_d & -I \\ I & 0 \end{bmatrix}^{-1} = \begin{bmatrix} 0 & I \\ -I & M_d \end{bmatrix}$. After some effort and using the basic identity

$$\begin{bmatrix} A & -B \\ B^T & 0 \end{bmatrix}^{-1} = \begin{bmatrix} PA^{-1} & E \\ -F^T & D \end{bmatrix}$$ where $D = \left[B^T A^{-1} B\right]^{-1}$, $E = A^{-1}BD$, $F^T = DB^T A^{-1}$, $P = I - EB^T$ and P is a projection matrix such that $P^2 = P$, it can be verified that the desired inverse is

$$\bar{M}_d^{-1} = \begin{bmatrix} G_d & P_d^T & E_d \\ -P_d & M_d^p & F_d \\ E_d^T & -F_d^T & D_d \end{bmatrix} \tag{15}$$

where $M_d^e = M_d$, $D_d = \left[H_d^T M_d^e H_d\right]^{-1}$, $E_d = H_d D_d$, $F_d = M_d^e E_d$, $G_d = E_d H_d^T$, $\bar{P}_d = F_d H_d^T$, $P_d = I - \bar{P}_d$, $M_d^p = P_d M_d^e$. Matrices M_d^e / M_d^p are the effective/projected (across joint d) inertias of element d.

Now using Eq. 11 as a guide, the partitioned Eq. 14 and Eq. 15, it follows that

$$\ddot{\bar{x}}_d = \begin{bmatrix} G_d & P_d^T & E_d \\ -P_d & M_d^p & F_d \\ E_d^T & -F_d^T & D_d \end{bmatrix} \left(\bar{b}_d - \begin{bmatrix} 0 & 0 & -\bar{I}^T \end{bmatrix} \begin{bmatrix} \ddot{\bar{x}}_a \\ \ddot{\bar{x}}_b \\ \ddot{\bar{x}}_c \end{bmatrix} \right) \tag{16}$$

Only the last equation of Eq. 16 is necessary for solving the equations (see Eqs. 6 and 7), thus

$$\ddot{q}_d = D_d Q_d + E_d^T g_d^e - F_d^T \left[a_c + \gamma_d\right] \tag{17}$$

where $g_d^e = g_d$ and g_d^e is the effective force on element d. Note the introduction of redundant effective inertias $M_d^e = M_d$ and forces $g_d^e = g_d$ at leaf elements for consistency.

Using Eq. 12 as a guide, the matrix corresponding to $A_{11} - A_{12} A_{22}^{-1} A_{21}$ is now evaluated. Setting up the matrix products from the partitioned submatrices of Eq. 14 and Eq. 15 reveals that to update the entire expression requires only the single operation $M_c^e = M_c + M_d^p$ where, as above, M_c^e is the effective inertia of element c. Updating the right hand side, corresponding to Eq. 12 yields

$$\begin{bmatrix} \bar{b}_a \\ \bar{b}_b \\ \bar{b}_c \end{bmatrix}^e = \begin{bmatrix} \bar{b}_a \\ \bar{b}_b \\ \bar{b}_c \end{bmatrix} - \begin{bmatrix} 0 \\ 0 \\ \bar{I} \end{bmatrix}^T \begin{bmatrix} G_d & P_d^T & E_d \\ -P_d & M_d^p & F_d \\ E_d^T & -F_d^T & D_d \end{bmatrix} \bar{b}_d \tag{18}$$

which also requires only a single computation

$$g_c^e = g_c + g_d^p - M_d^p \gamma_d - F_d Q_d \tag{19}$$

where $g_d^p = P_d g_d^e$. The quantity g_c^e is the effective force acting on element c and g_d^p is the projected force across joint d. If element c should happen to hold more than one joint, then M_c^e and g_c^e would receive projected components across each such joint. At this point the first step of forward elimination is complete and the reduced system along with its next partitioning becomes

$$\begin{bmatrix} \bar{M}_a & \bar{I} & 0 \\ -\bar{I}^T & \bar{M}_b & \bar{I} \\ 0 & -\bar{I}^T & \bar{M}_c^e \end{bmatrix} \begin{bmatrix} \bar{x}_a \\ \bar{x}_b \\ \bar{x}_c \end{bmatrix} = \begin{bmatrix} \bar{b}_a \\ \bar{b}_b \\ \bar{b}_c^e \end{bmatrix} \tag{20}$$

where $\bar{M}_c^e = \begin{bmatrix} M_c^e & -I & 0 \\ I & 0 & -H_c \\ 0 & H_c^T & 0 \end{bmatrix}$, $\bar{b}_c^e = \begin{bmatrix} g_c^e \\ \gamma_c \\ Q_c \end{bmatrix}$. The remaining elimination steps follow by decrementing subscripts, i.e. (c → b and d → c), etc, and using the effective mass $\mathbf{M}^e$ and force $\mathbf{g}^e$. With the additional equations, Eqs. 6 and 7 and matrix $\mathbf{C}$, the sparse matrix algorithm is now complete. A more detailed development of O(n) solution algorithms for both open and closed kinematic-loop systems is given in Ref. 1.

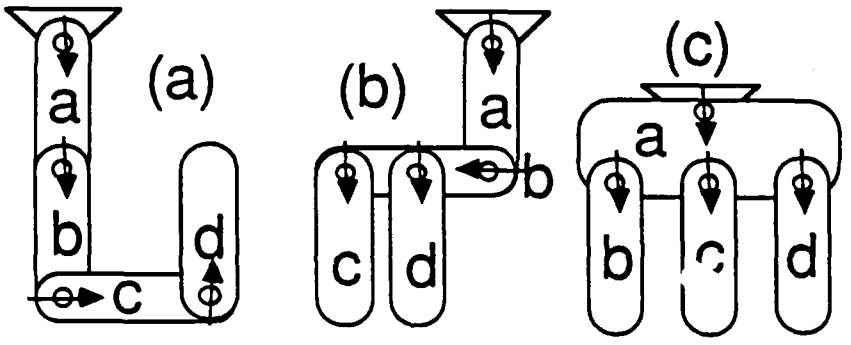

Figure 1 Example 4-Bar Mechanisms

$$C^a = \begin{array}{c} \\ a \\ b \\ c \\ d \end{array}\!\!\begin{array}{c} \begin{array}{cccc} a & b & c & d \end{array} \\ \begin{bmatrix} 1 & 0 & 0 & 0 \\ -1 & 1 & 0 & 0 \\ 0 & -1 & 1 & 0 \\ 0 & 0 & -1 & 1 \end{bmatrix} \end{array}; \quad C^b = \begin{array}{c} \\ a \\ b \\ c \\ d \end{array}\!\!\begin{array}{c} \begin{array}{cccc} a & b & c & d \end{array} \\ \begin{bmatrix} 1 & 0 & 0 & 0 \\ -1 & 1 & 0 & 0 \\ 0 & -1 & 1 & 0 \\ 0 & -1 & 0 & 1 \end{bmatrix} \end{array}; \quad C^c = \begin{array}{c} \\ a \\ b \\ c \\ d \end{array}\!\!\begin{array}{c} \begin{array}{cccc} a & b & c & d \end{array} \\ \begin{bmatrix} 1 & 0 & 0 & 0 \\ -1 & 1 & 0 & 0 \\ -1 & 0 & 1 & 0 \\ -1 & 0 & 0 & 1 \end{bmatrix} \end{array}$$

$$R^a = \begin{array}{c} \\ a \\ b \\ c \\ d \end{array}\!\!\begin{array}{c} \begin{array}{cccc} a & b & c & d \end{array} \\ \begin{bmatrix} 1 & 0 & 0 & 0 \\ 1 & 1 & 0 & 0 \\ 1 & 1 & 1 & 0 \\ 1 & 1 & 1 & 1 \end{bmatrix} \end{array}; \quad R^b = \begin{array}{c} \\ a \\ b \\ c \\ d \end{array}\!\!\begin{array}{c} \begin{array}{cccc} a & b & c & d \end{array} \\ \begin{bmatrix} 1 & 0 & 0 & 0 \\ 1 & 1 & 0 & 0 \\ 1 & 1 & 1 & 0 \\ 1 & 1 & 0 & 1 \end{bmatrix} \end{array}; \quad R^c = \begin{array}{c} \\ a \\ b \\ c \\ d \end{array}\!\!\begin{array}{c} \begin{array}{cccc} a & b & c & d \end{array} \\ \begin{bmatrix} 1 & 0 & 0 & 0 \\ 1 & 1 & 0 & 0 \\ 1 & 0 & 1 & 0 \\ 1 & 0 & 0 & 1 \end{bmatrix} \end{array}$$

Figure 2 Connectivity and Reachability matrices for the mechanisms in Fig. 1

References

1. Wehage, R.A., "Application of Matrix Partitioning and Recursive Projection to O(n) Solution of Constrained Equations of Motion," to appear in the ASME Journal of Mechanisms, Transmissions and Automation in Design.

GLOBALLY CONVERGENT NUMERICAL ALGORITHMS FOR NONLINEAR SYSTEMS OF EQUATIONS

Layne T. Watson
Department of Computer Science
Virginia Polytechnic Institute & State University
Blacksburg, VA 24061

Abstract. There are algorithms for finding zeros or fixed points of nonlinear systems of equations that are globally convergent for almost all starting points, i.e., with probability one. The essence of all such algorithms is the construction of an appropriate homotopy map and then tracking some smooth curve in the zero set of this homotopy map. There are three distinct, but interrelated, aspects of homotopy methods: 1) construction of the right homotopy map, 2) theoretical proof of global convergence for this homotopy map, and 3) tracking the zero curve of this homotopy map. The first aspect is currently still an art, although this is much better understood now due to the accumulation of computational experience. Although much remains to be done, significant progress has been made on the second aspect. Global convergence has been proved for Brouwer fixed point problems, certain classes of zero finding and nonlinear programming (both unconstrained and constrained) problems, and two-point boundary value approximations based on shooting, finite differences, spline collocation, and finite elements. Recently A. P. Morgan obtained some elegant results for polynomial systems, for which homotopy methods are guaranteed to find *all* the solutions.

Homotopies are a traditional part of topology, and only recently have begun to be used for practical numerical computation. The algorithms described here are known as probability one globally convergent homotopy algorithms, which are related to, but distinct from, continuation, parameter continuation, incremental loading, displacement incrementation, invariant imbedding, and continuous Newton methods. These algorithms are also referred to as "continuous" methods, to distinguish them from the simplicial homotopy methods, whose theoretical foundations date back to the very origins of topology.

The frameworks for fixed point and zero finding problems are slightly different, so they will be discussed separately. The fixed point problem will be considered first. Let B be the closed unit ball in n-dimensional real Euclidean space E^n, and let $f : B \to B$ be a C^2 map. Define $\rho_a : [0,1) \times B \to E^n$ by

$$\rho_a(\lambda, x) = \lambda(x - f(x)) + (1 - \lambda)(x - a). \tag{1}$$

The fundamental result is that for almost all a (in the sense of Lebesgue measure) in the interior of B, there is a zero curve $\gamma \subset [0,1] \times B$ of ρ_a, along which the Jacobian matrix $D\rho_a(\lambda, x)$ has rank n, emanating from $(0, a)$ and reaching a point $(1, \bar{x})$, where $\bar{x}$ is a fixed point of f. Thus with probability one, picking a starting point $a \in \text{int } B$ and following γ leads to a fixed point $\bar{x}$ of f. This justifies the phrase "globally convergent with probability one".

The zero finding problem

$$F(x) = 0, \tag{2}$$

where $F : E^n \to E^n$ is a C^2 map, is more complicated. Suppose there exists a C^2 map

$$\rho : E^m \times [0,1) \times E^n \to E^n$$

such that

1) the $n \times (m+1+n)$ Jacobian matrix $D\rho(a,\lambda,x)$ has rank n on the set

$$\rho^{-1}(0) = \{(a,\lambda,x) \mid a \in E^m, 0 \leq \lambda < 1, x \in E^n, \rho(a,\lambda,x) = 0\},$$

and for any fixed $a \in E^m$,

2) $\rho_a(0,x) = \rho(a,0,x) = 0$ has a unique solution x_0,

3) $\rho_a(1,x) = F(x)$,

4) $\rho_a^{-1}(0)$ is bounded.

Then the supporting theory says that for almost all $a \in E^m$ there exists a zero curve γ of ρ_a, along which the Jacobian matrix $D\rho_a$ has rank n, emanating from $(0,x_0)$ and reaching a zero $\bar{x}$ of F at $\lambda = 1$. γ does not intersect itself and is disjoint from any other zeros of ρ_a. The globally convergent algorithm is to pick $a \in E^m$ (which uniquely determines x_0), and then track the homotopy zero curve γ. A simple choice for ρ_a is

$$\rho_a(\lambda,x) = \lambda F(x) + (1-\lambda)(x-a). \tag{3}$$

This satisfies properties 1)–3), but not necessarily 4). There are fairly general sufficient conditions on $F(x)$ so that (3) will satisfy property 4), but for some practical problems of interest the homotopy map (3) will not suffice.

The Transversality Theorem from differential topology provides general conditions under which most homotopies (in a precise sense) will have smooth non-bifurcating curves. In practice an admissible homotopy is constructed by defining artificial parameters (a) so that a partial derivative condition is satisfied and then choosing these parameters independently of the structure and coefficients of the original system (F). For example, random choices of a will generally work.

Thus the artificial homotopy $\rho(a,\lambda,x)$ might be chosen so that the jth component includes a_j and not any a_k for $k \neq j$, and so that the partial derivatives

$$\frac{\partial \rho(a,\lambda,x)}{\partial a_j}$$

for $j = 1$ to n are nonzero for $0 \leq \lambda < 1$, for all x. Here $a = (a_1,\ldots,a_n)$ and λ are *artificial*; that is, they have nothing to do with x or any other parameter of the given problem. Then a is chosen at random. The Transversality Theorem guarantees that the resulting homotopy curves will be smooth, without bifurcations or singularities. In fact, in practice they tend to be very well conditioned. This mysterious usefulness of randomly chosen a is a feature of the "probability-one" approach to constructing homotopies.

Probability-one globally convergent homotopy curves have no bifurcations (with probability one) for $0 \leq \lambda < 1$. However, at the end of a curve (when $\lambda = 1$), singularities may be encountered. This happens precisely when the original problem is singular at the solution, because as $\lambda \to 1$ the homotopy becomes the original system. For some mild singularities in F, the homotopy can remain nonsingular at $\lambda = 1$, but in general this is not so.

The zero curve γ of the homotopy map ρ_a can be tracked by many different techniques. HOMPACK, currently under development at Sandia National Laboratories, General Motors Research Laboratories, Virginia Polytechnic Institute and State University, and the University of Michigan, is a suite of codes for tracking zero curves of probability one homotopy maps, and provides both high-level and low-level subroutines for three different approaches to tracking γ.

The three algorithmic approaches provided by HOMPACK are: 1) an ODE-based algorithm; 2) a predictor-corrector algorithm whose corrector follows the flow normal to the Davidenko flow (a "normal flow" algorithm); 3) a version of Rheinboldt's linear predictor, quasi-Newton corrector algorithm (an "augmented Jacobian" method). There are qualitatively different algorithms for dense and sparse Jacobian matrices; HOMPACK provides for both capabilities.

This talk surveys globally convergent homotopy methods, the HOMPACK software, and some applications to nonlinear dynamics.

References.

[1] L. T. WATSON, *A globally convergent algorithm for computing fixed points of C^2 maps*, Appl. Math. Comput., 5 (1979), pp. 297–311.

[2] L. T. WATSON AND D. FENNER, *Chow-Yorke algorithm for fixed points or zeros of C^2 maps*, ACM Trans. Math. Software, 6 (1980), pp. 252–260.

[3] L. T. WATSON, *Numerical linear algebra aspects of globally convergent homotopy methods*, SIAM Rev., 28 (1986), pp. 529–545.

[4] L. T. WATSON, S. C. BILLUPS, AND A. P. MORGAN, *HOMPACK: A suite of codes for globally convergent homotopy algorithms*, ACM Trans. Math. Software, 13 (1987), pp. 281–310.

SESSION 9

MULTIBODY DYNAMICS

FRIDAY - 0830 - 1000

June 3, 1988

Survey on the Generation and Solution of Multibody System Equations

by

R. Schwertassek

Institut für Dynamik der Flugsysteme, DFVLR, Oberpfaffenhofen, W. Germany

and

C. Führer

Mathematisches Institut, Technische Universität München, W. Germany

To be presented at the Nonlinear Mechanics Conference, Session Multibody Dynamics, June 1-3, 1988, VPI&SU, Blackbury, Virginia.

A b s t r a c t

Multibody system equations can be generated in various forms. All of these can be interpreted as results of two basic approaches, the augmentation- and the elimination-method. The former method yields the descriptor form of the system motion, a set of differential/algebraic equations, and the latter the state space representation, a set of pure differential equations. Both of these methods are surveyed.

For simulation purposes one would like to select that set of system equations which can be generated most efficiently and for which the most efficient and reliable solution techniques are available. Numerical solution techniques for pure differential equations have been studied in great detail and they are well-developed. By contrast, differential/algebraic equations have not been investigated for such a long time. The status of development in the latter field is surveyed and recent results on improving relability and efficiency of the corresponding solution techniques are discussed. A new method, avoiding the shortcomings of previous techniques for solving differential/algebraic equations, is presented.

ON THE USE OF THE FINITE ELEMENT METHOD AND CLASSICAL APPROXIMATION TECHNIQUES IN THE NONLINEAR DYNAMICS OF MULTIBODY SYSTEMS

A.A. Shabana
Dept. of Mechanical Engineering
University of Illinois at Chicago
P.O. Box 4348
Chicago, IL 60680

ABSTRACT

In this paper the finite element method and classical approximation techniques such as Rayleigh Ritz methods are used to develop a set of generalized Newton-Euler equations for deformable bodies that undergo large translational and rotational displacements. In the finite element formulation, a stationary (total) Lagrangian approach is used to formulate the generalized Newton-Euler equations for each finite element in terms of a set of invariants that depend on the assumed displacement field. The deformable body invariants are obtained by assembling the invariants of the finite elements using a standard finite element Boolean matrix approach. This leads to the nonlinear generalized Newton-Euler equations for the deformable bodies. These equations are presented in a simple closed form which is useful in developing recursive formulations for multibody systems consisting of interconnected deformable bodies. Both lumped and consistent mass formulations are discussed.

COMPARATIVE STUDY OF METHODOLOGIES EMPLOYED IN CONSTRAINED MULTIBODY DYNAMICS

F.M.L Amirouche
Assistant Professor
Mechanical engineering Dpt
University of Illinois at Chicago
Chicago il 60680

ABSTRACT

Popular methods used in the coordinate reduction of dynamical systems subjected to simple nomholonomic constraint include the zero eigenvalue theorem,the singular value decomposition,coordinates partioning based on LU factorization,and the QR decomposition method.Most recently Amirouche et al have introduced a new method called the Pseudo-uptriangular-decomposition which is beleived to be computational more efficient and provides a more stable algorithm to compute the orthogonal complement array to the Jacobian matrix.

Unlike the previous method which rely on the solution of eigenvalues and invertion of matrices,the PUTD is based strictly on multiplication type of operation suited for computer simulation.In this paper we intend to pre sent a comparative study between methods and draw a conclusion on their advantages and draw backs as it pertain to the solution of complex constrained dynamical systems.

Primal and Mixed Forms of Hamilton's Principle for Constrained Rigid and Flexible Dynamical Systems: Numerical Studies

M. Borri, F. Mello, M. Iura, and S. N. Atluri

Center for the Advancement of Computational Mechanics
Georgia Institute of Technology
Atlanta, GA 30332

Abstract

Constraint equations arise in the dynamics of mechanical systems whenever there is the need to restrict kinematically possible motions of the system. In practical applications constraint equations can be used to simulate complex, connected systems. If the simulation must be carried out numerically it is useful to look for a formulation that leads straightforwardly to a numerical approximation.

This can be done if the dynamics of the holonomic or nonholonomic system is cast in a variational form to which a finite element discretization can be easily applied.

This paper suggests the adoption of a new variational principle and shows how two different formulations can be used to achieve good numerical results.

Introduction

Very often the vectorial and variational theories of mechanics are considered completely equivalent and the differences between them are considered only a matter of style. Many times, the variational principles are used only as an alternative approach to obtain the differential equations of motion.

Here we assert that the variational formulations are superior, not only because they afford a generalized and unified treatment of complex mechanical systems, but also because they are more easily implementable in a numerical form. They are extremely well suited for obtaining, in a general way, an automatic appproximation for the treatment of the stability and response equations of very complicated nonlinear systems. The numerical approximation can be built on a few basic and easily controllable hand developed formulae.

It is worth remarking that, in the treatment of practical problems, many existing variational principles must be revised in order to make them suitable for numerical implementation.

During the last decade the variational formulations for complex dynamic systems and their numerical approximations have known a renewed interest [1-4]. An example of this is the direct use of Hamilton's Weak Principle for the time finite element approximation of the dynamics of holonomic systems [5]. In the case of nonholonomic systems, however, a general and sound variational formulation suitable for a direct numerical approximation is not yet available.

To contribute to a possible solution of this problem this paper suggests the adoption of a new variational principle for holonomically and nonholonomically constrained dynamic systems and shows how two different finite time element approximations can be derived.

Different Forms of Hamilton's Principle

Hamilton's Principle for unconstrained dynamics can be written as:

$$\int_{t_1}^{t_2}(\delta\mathcal{L}+\delta\mathbf{q}\cdot\mathbf{Q})dt=\delta\mathbf{q}\cdot\mathbf{p}|_{t_1}^{t_2} \tag{1}$$

where t_1, t_2 are the ends of the time interval of interest; $\mathbf{q}$ and $\mathbf{p}$ are respectively the generalized coordinates and the momenta of the system. $\mathcal{L}(\dot{\mathbf{q}},\mathbf{q},t)$ denotes the Lagrangian function and $\mathbf{Q}$ the external forces not included in $\mathcal{L}$.

By the use of the Hamiltonian transformation, Eq. (1) can be rewritten in the following mixed form:

$$\int_{t_1}^{t_2}(\delta\dot{\mathbf{q}}\cdot\mathbf{p}-\delta\dot{\mathbf{p}}\cdot\mathbf{q}-\delta H+\delta\mathbf{q}\cdot\mathbf{Q})dt=(\delta\mathbf{q}\cdot\mathbf{p}-\delta\mathbf{p}\cdot\mathbf{q})|_{t_1}^{t_2} \tag{2}$$

where $H(\mathbf{p},\mathbf{q},t)=\mathbf{p}\cdot\dot{\mathbf{q}}-\mathcal{L}$ denotes the Hamiltonian of the system.

The Eq. (1) and Eq. (2) can be denoted respectively as primal and mixed forms of Hamilton's Principle and they are very suitable for numerical approximations in the context of finite elements in time domain. [5]

Let us consider now a constrained system in which the velocity $\dot{\mathbf{q}}$ must satisfy the following equations:

$$\psi(\dot{\mathbf{q}},\mathbf{q},t)=\mathbf{A}(\mathbf{q},t)\cdot\dot{\mathbf{q}}+\mathbf{a}(\mathbf{q},t)=0 \tag{3}$$

These equations entail the following constraint on the virtual displacements:

$$\mathbf{A}\cdot\delta\mathbf{q}=0 \tag{4}$$

In order to enforce Eq. (3) and Eq. (4) in a weak form we use the Lagrangian multiplier technique. Let μ be these multipiers. We then weight Eq. (3) and Eq. (4) with the variation $\delta\mu$ and the time derivative $\dot{\mu}$ respectively. Obtaining:

$$\delta\mu\cdot\psi-\dot{\mu}\cdot\frac{\partial\psi}{\partial\dot{\mathbf{q}}}\cdot\delta\mathbf{q}=0 \tag{5}$$

The benefit of this form is that it allows another integration by parts that reduces the continuity requirements for the Lagrangian multipliers. So, substituting Eq. (5) into Eq. (1), after this integration by parts [9], we obtain:

$$\int_{t_1}^{t_2}(\delta\overline{\mathcal{L}}+\delta\mathbf{q}\cdot\overline{\mathbf{Q}})dt=\delta\mathbf{q}\cdot\overline{\mathbf{p}}|_{t_1}^{t_2} \tag{6}$$

where:

$$\overline{\mathcal{L}}=\mathcal{L}+\mu\cdot\psi\qquad\overline{\mathbf{p}}=\mathbf{p}+\mu\cdot\frac{\partial\psi}{\partial\dot{\mathbf{q}}}\qquad\overline{\mathbf{Q}}=\mathbf{Q}+\mu\cdot\left(\frac{d}{dt}\frac{\partial\psi}{\partial\dot{\mathbf{q}}}-\frac{\partial\psi}{\partial\mathbf{q}}\right) \tag{7}$$

The Eq. (6) constitutes the modified Hamilton's Principle for constrained systems and $\overline{\mathcal{L}}$, $\overline{\mathbf{p}}$, $\overline{\mathbf{Q}}$ are respectively the modified Lagrangian function, the modified generalized momenta and the external forces modified by the reactions due to the nonholonomic constraints [9]. It is interesting to note

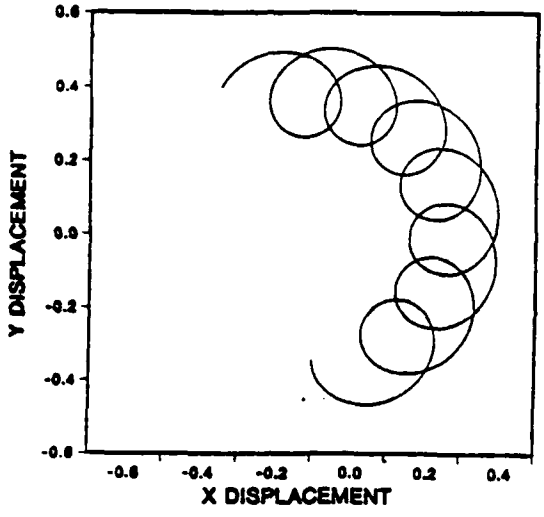

Figure 1: X-Y Displacement

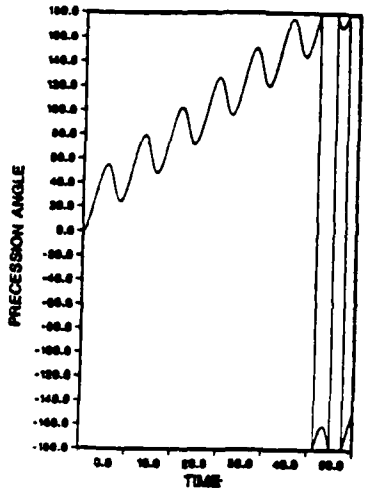

Figure 2: Precession angle

that $\overline{\mathbf{p}}$ are actually a generalized momenta of the augmented Lagrangian, in fact it can easily be seen that $\overline{\mathbf{p}} = \frac{\partial \overline{\mathcal{L}}}{\partial \dot{\mathbf{q}}}$.

Taking this property into account we can define the modified Hamiltonian function as $\overline{H} = \overline{\mathbf{p}} \cdot \dot{\mathbf{q}} - \overline{\mathcal{L}}$ and rewrite the Eq. (6) in the following mixed form:

$$\int_{t_1}^{t_2} (\delta \dot{\mathbf{q}} \cdot \overline{\mathbf{p}} - \delta \dot{\overline{\mathbf{p}}} \cdot \mathbf{q} - \delta \overline{H} + \delta \mathbf{q} \cdot \overline{\mathbf{Q}}) dt = (\delta \mathbf{q} \cdot \overline{\mathbf{p}} - \delta \overline{\mathbf{p}} \cdot \mathbf{q})|_{t_1}^{t_2} \tag{8}$$

It is worth emphasizing that the modified momenta $\overline{\mathbf{p}}$, from which the compatible momenta $\mathbf{p}$ and the Lagrangian multipliers μ can be recovered by a simple projection, are no longer constrained and can be viewed as independent variables.

For the sake of simplicity the formulations presented here are for finite degree of freedom systems, but they can be easily extended to continuous systems as in the ref. [11]. There, wave propagation in a rod is analyzed with the use of a mixed formulation, similar in concept to the two feild approach of Eq. (2). It is interesting to note that for linear problems the step by step marching scheme of that formulation produces very accurate results.

Numerical Results

The preceding developments have been verified with a few simple but significant numerical examples. The formulation corresponding to Eq. (6) has been used in order to solve the well known Caplygin's nonholonomic problem [8], [9].

The formulation corresponding to Eq. (8) has been used to solve the spinning top problem [10]. Since we intend to check the holonomic and nonholonomic constraints, the reference point is taken to coincide with the center of gravity and the velocity of the suspension point is enforced to be zero by appropriate constraint equations. Moreover, as a nonholonomic constraint, the constancy of the spinning angular velocity is considered. The results obtained are very encouraging and the method is very promising.

Figure 1 shows the plot of X and Y displacement of the mass center. This represents approximately 7500 calculation steps corresponding to 500 proper rotations. The numerical approach shows very stable behavior, even for this dynamically stiff problem. Figure 2 is the plot of precession angle, in which the discontinuity in the representation of finite rotation is clearly shown.

This does not present a problem in the numerical approach because the incremental finite rotation is adopted as a generalized coordinate. The physical data used in this problem are the same as in Ref.[12].

Aknowledgements

This work was supported by AFOSR and the SDIO/IST. The assistance of Ms. Deanna Winkler in the preparation of this manuscript is thankfully acknowledged.

References

1. C.D. Bailey, "Application of Hamilton's Law to Forced, Damped, Stationary Systems", *Journal of Sound and Vibration*, Vol. 75, pp. 117-126, 1981.

2. M.E. Simkins, "Finite Element for Initial Value Problems in Dynamics", *AIAA Journal*, Vol. 13, pp. 1154-1157, 1981.

3. M. Baruch and R. Riff, "Hamilton's Principle, Hamilton's Law, 6^n correct formulations", *AIAA Journal*, Vol. 21, pp. 687-692, 1982.

4. M. Borri, M. Lanz and P. Mantegazza, "Helicopter Rotor Dynamics by Finite Element Time Discretization", *L'Aerctecnica Missili e Spazio*, Vol. 60, pp. 193-200, 1981.

5. M. Borri, G.L. Ghiringhelli, M. Lanz, P. Mantegazza and T. Merlini, "Dynamic Response of Mechanical Systems by a Weak Hamilton's Formulation", *Computers & Structures*, Vol. 20, pp. 495-508, 1985.

6. T. Levi Civita and V. Amaldi, Lezioni di Meccanica Razionale, Zanichelli, Bologna 1979.

7. C. Lanczos, "The Variational Principles of Mechanics", University of Toronto, Toronto 1964.

8. Iu. I. Neimark and N.A. Fufaev, "Dynamics of Nonholonomic System", American Mathematical Society, Providence, Rhode Island 1972.

9. M. Borri and P. Mantegazza, "Finite Time Elements Approximation of Dynamics of Nonholonomic Systems", paper presented at ASME Congress, Williamsburg, Virginia, August 1986.

10. M. Borri and S.N. Atluri, "Time Finite Element Method for the Constrained Dynamics of a Rigid Body", Proceedings of ICES-88, Atlanta, Georgia, April 1988.

11. M. Iura, M. Borri, and S.N. Atluri, "Analysis of Traveling Wave Responses of Structures", Proceedings of ICES-88, Atlanta, Georgia, April 1988.

12. P.E. Nikravesh and E.J. Haug, "Generalized Coordinate Partitioning for Analysis of Mechanical Systems with Nonholonomic Constraints", Journal of Mechanisms, Transmissions, and Automation in Design, September 1983,Vol.105, pp. 379-384

ABSTRACT

ANALYSIS OF NONLINEARLY CONSTRAINED NONHOLONOMIC MULTIBODY SYSTEMS

Mingtao Xu
Chengqun Liu*
Department of Engineering Mechanics
Chongqing University
Chongqing, Sichuan
PEOPLE'S REPUBLIC OF CHINA

and

Ronald L. Huston
Department of Mechanical and
Industrial Engineering
University of Cincinnati
Cincinnati, Ohio 45221-0072
U.S.A.

*Currently, Ph.D. Candidate, University of Cincinnati

This paper presents a new method for studying multibody systems subjected to nonlinear nonholonomic constraints. The method is based upon Kane's equations as exposited by Kane, Levinson, Huston, et. al. Specifically, the method employs partial velocity and partial angular velocity vectors in developing generalized active, generalized constraint, and generalized inertia force arrays. Setting the sum of these force arrays to zero leads to the general dynamical equations of the system. Then by appending the constraint equations the governing equations of the constrained system are obtained. These equations are coupled nonlinear algebraic/differential equations for the constraint force components and the dependent variables. The solution to the equations is obtained by multiplying the matrix of dynamical equations by the orthogonal complement of the matrix of the constraint equations. This eliminates the constraint force components leaving a consistent system of differential equations for the dependent variables (generalized coordinates) of the system.

The principal analytical features of the method depend upon several intermediate results and observations. The first of these is the fact that even though the constraint equations are nonlinear, they may be differentiated into a linear form in terms of higher derivatives of the generalized coordinates. Next, it is observed that the velocity and angular velocity vectors are linear functions of the first derivatives of the generalized coordinates. The coefficients of these derivatives are the "partial velocity" and "partial angular velocity" vectors used by Kane, et. al. When the velocity and angular velocity vectors are differentiated these coefficients become the coefficients of the higher order derivatives of the generalized coordinates as occur in the differentiated constraint equations. Finally, it is observed that the generalized constraint force array may be represented as the transpose of the matrix of constraint equations multiplied by a constraint force array.

The method is illustrated with the classical problem of Appel and Hamel.

SESSION 10

MULTIBODY DYNAMICS

FRIDAY, 1030 - 1200

June 3, 1988

Nonlinear Analysis of Loss of Stability of Periodic Solutions with an Application to Robotic Motions

E. Lindtner, A. Steindl, H. Troger; Technische Universität Wien

1 Introduction

For many physical or technical systems the fundamental state is a periodic motion. Naturally this periodic motion is supposed to be stable for the standard operating conditions and the corresponding parameter values. However, it can lose its stability under variation of parameters at a critical parameter value. Sometimes only this critical parameter value is of interest. Then a linear stability analysis by means of Floquet's theory ([1]) is sufficient. However, there are many problems, for example in the dynamics of robots ([2]), where one also wants to know how the system behaves after a loss of stability of the fundamental periodic state. This, of course, requires a nonlinear analysis.

We want to show how, in a systematic way, such an analysis can be given by making use of the methods of bifurcation theory ([3,4,5]). The crucial step in doing a nonlinear analysis consists in replacing the equations of motion given by differential equations by a system of difference equations. This latter system is a point mapping called the Poincarè map ([3,4]). It can be given by a power series expansion in the neighborhood of the periodic solution, which is a fixpoint for the map. The coefficients of the power series expansion can be calculated numerically. If the Poincarè map is known then, in general, by means of Center Manifold theory ([6,7]) a further strong reduction of the dimension of the problem is possible.

In this paper these two steps, not well known to engineers, will be explained with emphasis to the practical calculations. Finally as an example the periodic motion of a robot will be studied.

2 Calculation of the Poincarè Map

We assume the stability problem of the periodic solution $y_0(t) = y_0(t+T)$ to be given in the form

$$\dot{x} = A(t,\lambda)x + f_2(x,t,\lambda) + f_3(x,t,\lambda) \tag{1}$$

where $A(t,\lambda), f_2(x,t,\lambda), f_3(x,t,\lambda)$ are periodic in t with period T and the N-vecors f_2 and f_3 contain the nonlinear functions in the variable x of second and third order respectively. (1) is obtained by introducing $y(t) = y_0(t) + x(t)$ into the original system of equations of motion. Hence the motion to be analyzed for stability is $x_0 = 0$. For a linear stability analysis of x_0 Floquet theory ([2]) could be used. But as it will be made clear below the calculation of the Poincarè map also includes the linear stability analysis supplied by Floquet's theory. The Poincarè map is defined in the neighborhood of the periodic solution by the map obtained from the transversal intersection of

the trajectories with a section surface. For example consider the trajectory in Fig. 1 leaving x_1 and intersecting after one revolution in x_2. Hence

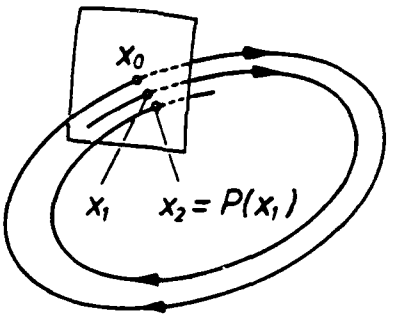

Fig. 1: Definition of the Poincarè map in the neighborhood of the periodic solution x_0

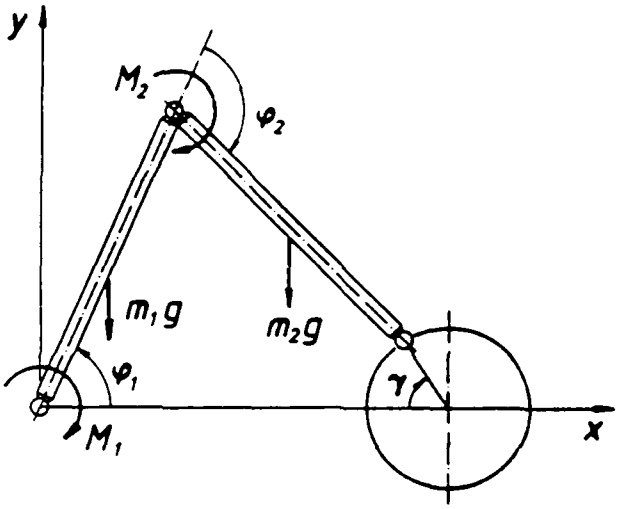

Fig. 2: DD-robot with 2 degrees of freedom φ_1, φ_2, and prescribed circular motion of the endpoint G

$$x_2 = x(T, x_1) = P(x_1) \tag{2}$$

where $x(t, x_1)$ is the solution of (1) starting at x_1. In order to calculate the mapping P in the neighborhood of the periodic solution which is given by the fixpoint x_0 in the section surface the following power series expansion is introduced.

$$P(x_0 + \xi) = P(x_0) + P'(x_0)\xi + \frac{1}{2}P''(x_0)(\xi, \xi) + \frac{1}{6}P'''(x_0)(\xi, \xi, \xi) + \dots \tag{3}$$

where $P(x_0) = x_0$ and $P'(x_0), P''(x_0), P'''(x_0), \dots$ are obtained from the solutions of a series of initial value problems ([8,9]). This follows immediately from (2) because

$$x(T, x_0 + \xi) = x(T, x_0) + \frac{\partial x}{\partial x_0}(T, x_0)\xi + \frac{1}{2}\frac{\partial^2 x}{\partial x_0^2}(T, x_0)(\xi, \xi) + \frac{1}{6}\frac{\partial^3 x}{\partial x_0^3}(T, x_0)(\xi, \xi, \xi) + \dots \tag{4}$$

Hence comparing (3) and (4)

$$P'(x_0) = \frac{\partial x}{\partial x_0}(T, x_0), \qquad P''(x_0) = \frac{\partial^2 x}{\partial x_0^2}(T, x_0), \qquad \dots \tag{5}$$

is obtained. For the calculation of $\frac{\partial x}{\partial x_0}$ the differential equation (1) is written in the form $\dot{x} = F(x, t)$. Taking the derivative of both sides with respect to x_0 a differential equation for $\frac{\partial x}{\partial x_0}$ of the form

$$\left(\frac{\partial x}{\partial x_0}\right)^{\cdot} = \frac{\partial F}{\partial x} \cdot \frac{\partial x}{\partial x_0} \tag{6}$$

is obtained. To obtain the first term in (5) (6) must be integrated from $t = 0$ until $t = T$ with the initial conditions $\frac{\partial x}{\partial x_0}(0) = I$, where I is the unit matrix. To calculate the next term in (5) the derivative of (6) with respect to x_0 is taken, yielding

$$\left(\frac{\partial^2 x}{\partial x_0^2}\right)^{\cdot} = \frac{\partial^2 F}{\partial x^2}\left(\frac{\partial x}{\partial x_0}\right)^2 + \frac{\partial F}{\partial x}\frac{\partial^2 x}{\partial x_0^2}. \tag{7}$$

Again (7) must be integrated from 0 to T with the initial conditions $\frac{\partial^2 x}{\partial x_0^2}(0) = 0$. Proceeding in this way also the coefficients of the third and higher order terms can be calculated.

The result of these calculations is a discrete dynamical system

$$\xi_{n+1} = L(\lambda)\xi_n + Q_2(\xi_n, \xi_n, \lambda) + Q_3(\xi_n, \xi_n, \xi_n, \lambda) + \dots \tag{8}$$

where $\xi_n \in R^N$ and λ is a parameter vector. $Q_2, Q_3, \dots$ are quadratic, cubic and higher order terms in the variables. For example Q_2 is a vector in R^N the components of which have the form $(N = 2) : \alpha_1 \xi_{n,1}^2 + \beta_1 \xi_{n,1}\xi_{n,2} + \gamma_1 \xi_{n,2}^2$.

Returning now to the stability problem of x_0. It is determined by the eigenvalues of the linear part of (8). The periodic solution $y_0(t)$ or the corresponding fixpoint of the map is stable if all eigenvalues of $L(\lambda)$ have absolute value smaller than 1. If only one eigenvalue has absolute value larger than 1 then the fixpoint is unstable. If all eigenvalues have absolute value smaller than 1 except some with absolute value equal to 1 the system is just at the stability boundary.

We assume now $\lambda \in R^1$. Then it is shown ([3]) that generically at loss of stability only one of the following three critical eigenvalues can occur: (i) $\mu_1 = 1$, (ii) $\mu_2 = -1$, (iii) $\mu_3 = \nu \pm i\eta$ with $|\mu_3| = 1$. If the calculation gives a more complicated case it can be made to disappear by a small change of other parameters in the system.

3 Calculation of the point map on the Center Manifold

Following [6,7] it is possible to reduce (8) to a system of dimension k, which locally in the neighborhood of the bifurcation point ($\lambda = \lambda_c$), describes the stability problem completely. k is equal to the number of eigenvalues with absolute value 1. Hence for the one parameter bifurcation problem either $k = 1$ for cases (i) and (ii) or $k = 2$ for case (iii) of the preceding section. As first step in the reduction process L in (8) is transformed into Jordan form by setting $y_n = T^{-1}x_n$ ([3,4,5,8,9]).

$$y_{n+1} = Jy_n + R_2(y_n, y_n) + R_3(y_n, y_n, y_n) + \dots \tag{9}$$

where $J = TLT^{-1}$ is in Jordan form. The equations in (9) are ordered in such a way that the first k equations correspond to eigenvalues of absolute value equal to 1 and the remaining $N - k$ to eigenvalues of absolute value smaller than 1. Hence (9) can be written

$$\begin{aligned} y_{n+1,c} &= J_c y_{n,c} + F_c(y_{n,c}, y_{n,s}) \\ y_{n+1,s} &= J_s y_{n,s} + F_s(y_{n,c}, y_{n,s}) \end{aligned} \tag{10}$$

where all the eigenvalues of J_c are located at the unit circle and those of J_s are inside the unit circle. J_c and J_s are $k \times k$ and $(N-k) \times (N-k)$ matrices respectively. $y_{n,c}$ are the active variables or the amplitudes of the eigenvectors corresponding to the eigenvalues with absolute value equal to 1. $y_{n,s}$ are the passive variables which still show up in the equation for the active variables $(10)_1$ and have to be eliminated from them. This can be done by making an ansatz of the form ([6,7]): $y_{n,s} = h(y_{n,c})$, where h has the following two properties: $h(0) = 0, h'(0) = 0$. Hence if a series expansion for h is made it starts at least with second order terms.

As an example for the practical calculation we pick the case (i) of the preceding section. Then (10) takes the form

$$\begin{aligned} y_{n+1,1} &= y_{n,1} + F_1(y_{n,1}, y_{n,i}) \\ y_{n+1,i} &= \mu_i y_{n,i} + F_i(y_{n,1}, y_{n,i}) \qquad i = 2, \ldots, N \end{aligned} \tag{11}$$

where for simplicity it has been assumed that the remaining eigenvalues μ_i form a diagonal matrix. From above follows

$$y_{n,i} = h_i(y_{n,1}) = a_{i,2} y_{n,1}^2 + a_{i,3} y_{n,1}^3 + \ldots \tag{12}$$

The coefficients $a_{i,j}$ follow from introducing (12) into $(11)_2$ and making use of $(11)_1$ yielding

$$\begin{aligned} &a_{i,2}\ [y_{n,1} + F_1(y_{n,1}, h_i(y_{n,1})]^2 + a_{i,3}[y_{n,1} + F_1(y_{n,1}, h_i(y_{n,1}))]^3 + \ldots \\ &\quad = \mu_i(a_{i,2} y_{n,1}^2 + a_{i,2} y_{n,1}^3 + \ldots) + F_i(y_{n,1}, h_i(y_{n,1})). \end{aligned} \tag{13}$$

If, for example, $(11)_1$ is only calculated up to third order terms then it is sufficient to calculate only quadratic terms in h, which will be done now. Equating the quadratic terms in (13) results in $a_{i,2} = \frac{f_{i,2}}{1-\mu_i}, (i = 2, \ldots, N)$ where $f_{i,2}$ are the coefficients of the quadratic terms in the Taylor expansion of F_i. One easily convinces himself that no other terms make a contribution.

4 Application to the motion of a simple robot

In [2] a DD-robot consisting of a planar double pendulum (Fig. 2) with moments acting at the hinges is studied. The motion of the endpoint G is supposed to be a circle with constant speed $\omega = \dot{\gamma}$. Further introducing a control-loop which serves to compensate deviations from the prescribed path, the equations of motion can be given in the form of (1) with $N = 4$. Calculating the Poincarè map according to section 2 results in a point map of the form of (8). In this problem depending on the control mechanism by increasing the speed of the endpoint of the double pendulum all three types of loss of stability can be found. Hence the following equations on the Center Manifold are obtained $(y_{n,1} = u_n)$

$$\begin{aligned} (i) \quad u_{n+1} &= (1+\varepsilon)u_n + a u_n^2 + O(|u_n|^3) \\ (ii) \quad u_{n+1} &= -(1+\varepsilon)u_n + a u_n^3 + O(|u_n|^5) \\ (iii) \quad z_{n+1} &= (\nu + i\eta)(1 + \varepsilon + \alpha z_n \bar{z}_n) z_n \end{aligned} \tag{14}$$

ϵ is the unfolding parameter proportional to ω and a and α must be calculated from the system data. (i) is called transcritical bifurcation, (ii) Flip-bifurcation and (iii) Hopf bifurcation ([3] p. 285). In Fig. 3 the motion of the endpoint G of the double pendulum is shown for the different three cases (14). For the transcritical bifurcation after loss of stability a shifted motion is obtained. In case of the Flip-bifurcation a double periodic motion sets in. For the Hopf bifurcation a motion on a torus is obtained.

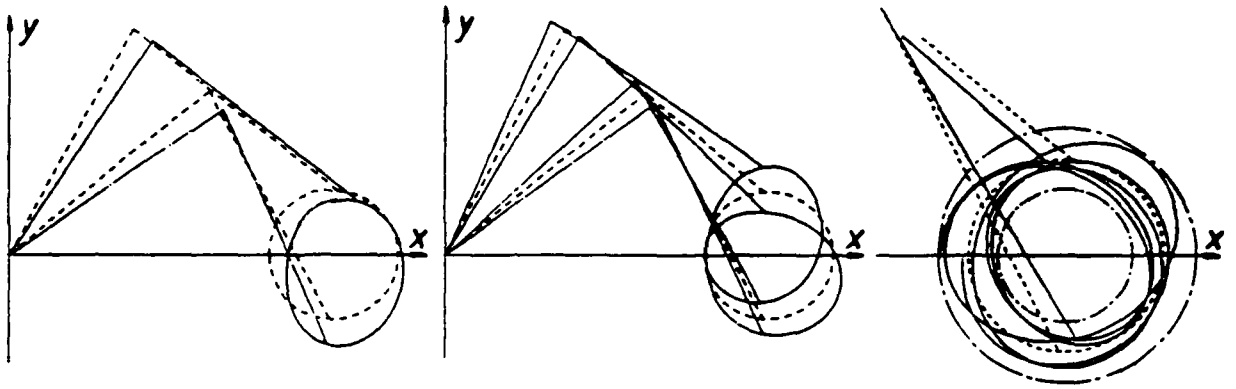

Figure 3: Motion of the endpoint G after a generic one parameter loss of stability due to: (a) Transcritical bifurcation ($\mu = 1$), (b) Flip bifurcation ($\mu = -1$), (c) Hopf-bifurcation ($\mu = \nu \pm i\eta$).

Acknowledgement

This research has been supported by the "Fonds zur Förderung der wissenschaftlichen Forschung" in Austria under project P 5519.

References

1. A. H. Nayfeh, D. T. Mook, *Nonlinear Oscillations*, J. Wiley and Sons, New York 1979.
2. E. Lindtner, A. Steindl, H. Troger, *Generic One-parameter Bifurcations in the Motion of a DD-Robot*, submitted for publication to J. of Computational and Applied Mathematics.
3. V. I. Arnold, *Geometrical Methods in the Theory of Ordinary Differential Equations*, Grundlehren der Math. Wissenschaften 250, Springer Verlag, Heidelberg, New York 1983.
4. J. Guckenheimer, Ph. Holmes, *Nonlinear Oscillations, Dynamical Systems and Bifurcations of Vector Fields*, Appl.Math. Sciences 42, Springer Verlag, Heidelberg, New York 1983.
5. M. Golubitsky, D. Schaeffer, *Singularities and Groups in Bifurcation Theory*, Appl. Math. Sciences 51 Springer Verlag, Heidelberg, New York 1985.
6. J. Carr, *Center manifold theory and its applications*, Appl. Math. Sciences 35, Springer Verlag, Heidelberg, New York 1981.
7. G. Iooss, *Bifurcation of Maps and Applications*, Math. Studies 36, North Holland, Amsterdam 1979.
8. H. Amann, *Gewöhnliche Differentialgleichungen*, deGruyter Verlag, Berlin, New York 1983.
9. E. A. Coddington, N. Levinson, *Theory of Ordinary Differential Equations*, McGraw-Hill, New York 1955.

SYSTEMATIC REDUCTION OF MULTIBODY EQUATIONS OF MOTION TO A MINIMAL SET

Parviz E. Nikravesh

Department of Aerospace and Mechanical Engineering
University of Arizona, Tucson, AZ 85721

This paper presents a two-step process to convert the equations of motion for closed-loop systems from Cartesian coordinates to a minimal set of relative joint coordinates. Initially, Cartesian coordinates are used to define the position of each body, the kinematic joints, and the forces acting on the bodies. Prior to numerical integration of the equations of motion, the equations are converted to a minimal set in order to gain computational efficiency. It is also shown that the equations of motion can be expressed in terms of the time derivative of the system momenta, instead of the accelerations, in order to reduce numerical integration error and, in turn, to gain computational stability.

Use of Linear and Nonlinear Structural Theories in Flexible Multibody Dynamics *

R. R. Ryan† and H. H. Yoo*

Department of Mechanical Engineering and Applied Mechanics
University of Michigan, Ann Arbor, Michigan, 48109-2125

Abstract

The present research involves an investigation of the roles of nonlinear and linear elastic structural theories in accurately predicting transient dynamic behavior of flexible multibody systems comprised by structural elements undergoing arbitrarily large and arbitrarily fast overall rotations and translations as well as small deformations. Coupling effects between deformation and overall motion are carefully scrutinized in the context of assumed-mode discretization techniques. Consistently linearized beam, plate, and shell formulations involving in-plane stretch variables are proposed and shown to yield very accurate simulation results and extremely fast modal convergence for most motions involving small strains. In some particular cases, however, in which membrane stiffness dominates bending stiffness, a nonlinear strain formulation is required in order to capture proper coupling between deformation and overall motion. Unfortunately, with standard component modes, algorithmic formalisms involving nonlinear strain-displacement expressions show very slow modal convergence. A procedure involving use of constraint modes is proposed to alleviate this problem.

1. Introduction

Fig. 1 shows a proposed Earth-orbiting satellite consisting of a number of hinge-connected rigid and deformable bodies which serve as rotors, antennae, solar panels, and other structural components designed to accomplish various mission objectives. This satellite is representative of a large class of systems known as flexible multibody systems, which are characterized by interconnected structural elements undergoing large overall motion and concomitant small deformation. Since these systems are extremely costly to deploy and are often difficult to test realistically on Earth, more and more emphasis is being placed on the prediction of dynamical behavior and the evaluation of active control systems via numerical simulations.

Development of multibody dynamic analysis formalisms aimed at facilitating such simulations was begun in the mid-1960's[1,2] and has proceeded continuously to the present time. Originally, these formalisms were restricted to joint-connected rigid bodies arranged in specific topologies, but were later extended to treat flexible bodies, arbitrary topologies, and arbitrary forcing functions. In fact, there now exists numerous nonlinear computational algorithms (*e.g.*, [3-7]) which were designed to treat quite general systems of rigid bodies, deformable solids, and flexible structures in open- or closed-loop topologies.

Many of the present multibody formalisms and associated computational algorithms are based on a flexible body model involving a three-dimensional continuum with mass and stiffness distribution described in terms of modal data derived from a linear finite element eigensolution. If the flexible body characterized in this way is not undergoing large

* This research work was partially supported by Mechanical Dynamics Inc.

† Assistant Professor

* Graduate Student

overall motion relative to other bodies in the multibody system, and if the overall system rotational motion remains small, then the formalisms can quite accurately predict system dynamical behavior. Solving for component displacements in this case is equivalent to a straightforward expansion in terms of the component modes. However, as shown in detail in Refs.[8-10], the algorithms are very limited in their ability to accurately treat coupled small deformation and large overall rotational motions of structural elements, regardless of speed of overall motion. For example, consider a simple uniform, cantilever channel-section beam undergoing a smooth slewing (repositional) maneuver from one orientation to another orientation 180° away. Suppose the axis of rotation is parallel to the cross-section symmetry axis of the beam, and assume that the properties of the beam are as specified in Fig. 2. Due to the offset between the centroidal axis and the elastic axis of the beam, one would expect noticeable torsion of the beam as well as bending of the beam in both principal planes of the cross-section during the maneuver. The correct solution is shown by the solid curves of in-plane displacement $u_2(t)$, out-of-plane displacement $u_3(t)$, and torsional rotation $\theta_1(t)$ in Fig. 2. Unfortunately, the flexible body model used in the conventional multibody formalisms does not provide the capability to automatically model the interaction of the mass offsets and the overall inertial forces necessary to provide an accurate description of the dynamic behavior. The result of applying the formalisms is as shown by the dotted curves in Fig. 2, where it is clear that both the out-of-plane response and the torsional response are poorly predicted.

This example, as well as many others involving both slow and fast translational and rotational overall motions of structural components of multibody systems, has pointed out the necessity of treating each structural element type distinctly in both the multibody model and the linear finite element model used to obtain descriptive modal data. It is not sufficient to model a structure as a plate or a beam or an assemblage of such structural elements in a linear finite element model and then use the resulting modal data in a flexible multibody model wherein the details of the structural component are ignored in favor of a simple continuum model.

These observations have led to vigorous new efforts to develop element-specific structural models within the framework of jointed multibody systems. These models must be capable of treating the intracacies of the structure, representing the proper membrane and bending stiffness, and providing for accurate coupling between overall motion and small deformation. Recent research efforts in this area have generally followed one of three paths, namely, (a)some form of physical discretization or substructuring combined with finite element stiffness descriptions[11], (b)straightforward fully nonlinear finite element procedures[12,13], and (c)modified assumed-mode representations. Our approach has been to attempt to retain all of the attractive features of the modal methods, such as ease of control design, model reduction, and solution; while building element specific models which can be assembled in a multibody formalism.

To do this, we have investigated two possibile avenues. First, we have taken advantage of the extensive literature and methods formulated for rotational analyses of rotorcraft and turbomachinery and have developed a set of *consistently-linearized models* for specific beam, plate, and shell elements which allow for abritrarily general overall translation as well as rotation, and permit general boundary conditions. These methods have been shown to yield very accurate predictions of flexible multibody system behavior for most motions involving small strain (see Fig. 3). These methods also provide rates of modal convergence which are far superior to fully nonlinear strain-displacement based theories when a standard set of assumed mode trial functions are employed. This is illustrated in Fig. 3, wherein a consistently linearized beam formulation is used with four standard assumed modal functions to model a spin-up maneuver of a uniform cantilever beam. This produces a solution which is indistiguishable from the known correct solution. However, using the same set of assumed modal functions with a fully nonlinear strain-based model yields the results labelled *non-*

linear in the same figure. Obviously, covergence has not yet been acheived. Studies with many more modal functions in the nonlinear model have shown eventual convergence to the known solution.

In attempting to treat large rotational motions of plate structures which are simply-supported by rotating rigid frames, we found that the consistently-linearized theories yield results which exhibit much too little membrane stiffness (see Fig. 4). To deal with problems where membrane effects are expected to be of predominant importance, we have developed an appropriate second-order nonlinear theory for various element types in the context of multibody systems.

In order to overcome the convergence problems with the nonlinear methods, we have developed a method involving nonlinear constraint modes which more closely match the structural boundary conditions of the nonlinear models. For more details on these issues, refer to [14].

REFERENCES

1. Hooker, W. W., and Margulies, G., "The Dynamical Attitude Equations for an n-Body Satellite," *The Journal of Astronautical Sciences*, Vol. XII, No. 4, 1965, pp. 123-128.
2. Roberson, R. E., and Wittenburg, J., "A Dynamical Formalism for an Arbitrary Number of Interconnected Rigid Bodies, with Reference to the Problem of Satellite Attitude Control," *Proceedings 3rd International Congress on Automatic Control* (London, 1966) London, 1967, pp. 46D.1-46D.8.
3. Bodley, C. S., Devers, A. D., Park, A. C., and Frisch, H. P., "A Digital Computer Program for the Dynamic Interaction Simulation of Controls and Structure (DISCOS)," Vols. 1 & 2, NASA Technical Paper 1219, May 1978.
4. Frisch, H. P., "A Vector-Dyadic Development of the Equations of Motion for N-Coupled Flexible Bodies and Point Masses." NASA Technical Note TN D-8047, Aug. 1975.
5. Ho, J. Y. L., and Herber, D. R., "Development of Dynamics and Control Simulation of Large Flexible Space Systems," AIAA *Journal of Guidance, Control, and Dynamics*, Vol. 8, No. 3, 1985, pp. 374-383.
6. Singh, R. P., VanderVoort, R. J., and Likins, P. W., "Dynamics of Flexible Bodies in Tree Topology - A Computer Oriented Approach," Paper No. AIAA-84-1024, AIAA/ASME/ASCE 25th Structures, Structural Dynamics and Materials Conf., Palm Springs, Ca., May 14-18, 1984.
7. Song, J. O., and Haug, E. J., "Dynamic Analysis of Flexible Mechanisms," Technical Report No. 55, Division of Materials Engineering, University of Iowa, May 1979.
8. Ryan, R. R.,"Flexibility Modeling Methods in Multibody Dynamics," Stanford University Ph.D Dissertation, University Microfilms, Ann Arbor, Mi. 1986.
9. Kane, T. R., Ryan, R. R., and Banerjee, A. K., " Dynamics of a Cantilever Beam Attached to a Moving Base," *Journal of Guidance, Control, and Dynamics*, Vol. 10, No. 2, March-April, 1987, pp. 139-151.
10. Ryan, R. R.,"Deployment, Pointing, and Spin of Active-Controlled Spacecraft Containing Elastic Beam-like Appendages," Presented at the AAS/AIAA Astrodynamics Specialist Conference, Paper No. AAS 87-478, Kalispell, Montana, Aug. 10-14, 1987.
11. Haug, E. J., Discussion of Modal Substructuring, NASA/SDIO Workshop on Multibody Dynamics, Pasadena, California, Sept. 1-3, 1987.
12. Simo, J. C., and Vu-Quoc, L.,"On the Dynamics of Flexible Beams under Large Overall Motions - the Plane Case: Part I and Part II," *Journal of Applied Mechanics*, Vol. 53, Dec., 1986, pp. 849-863.
13. Christensen, E. R., and Lee, S. W., " Nonlinear Finite Element Modeling of the Dynamics of Unrestrained Flexible Structures," *Computers and Structures*, Vol. 23, No. 6, 1986, pp. 819-829.
14. Yoo, H. H., Ryan, R. R., and Scott, R. A., "The Use of Assumed Modes in Large-Displacement Elastodynamic Plate Behavior," ACC Paper, Atlanta, Ga., June 1988.

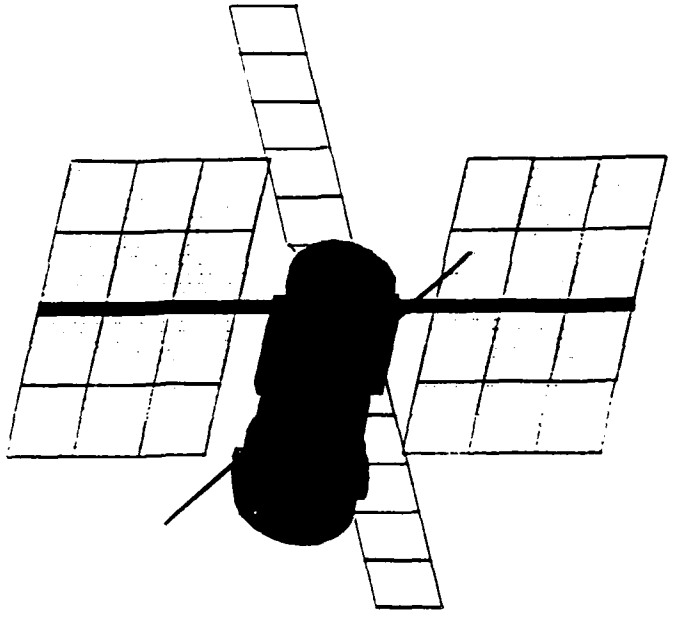

Fig. 1 - Representative Flexible Multibody System

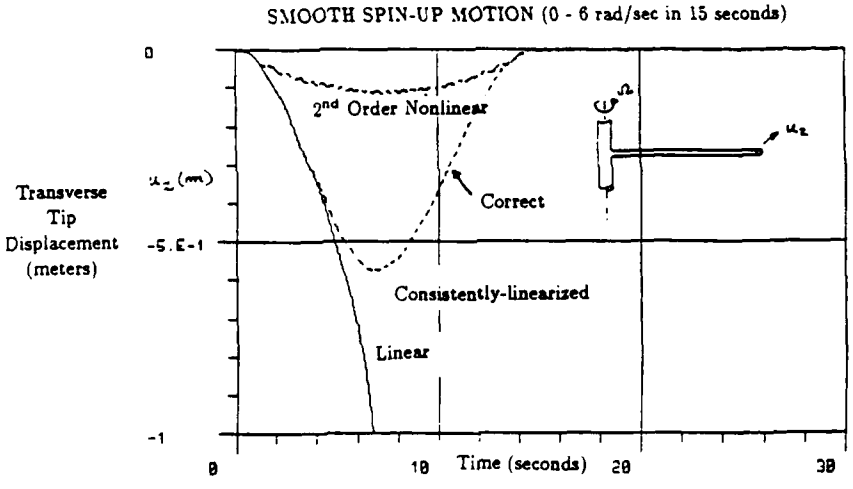

Fig. 3 - Uniform Beam Spin-up Maneuver

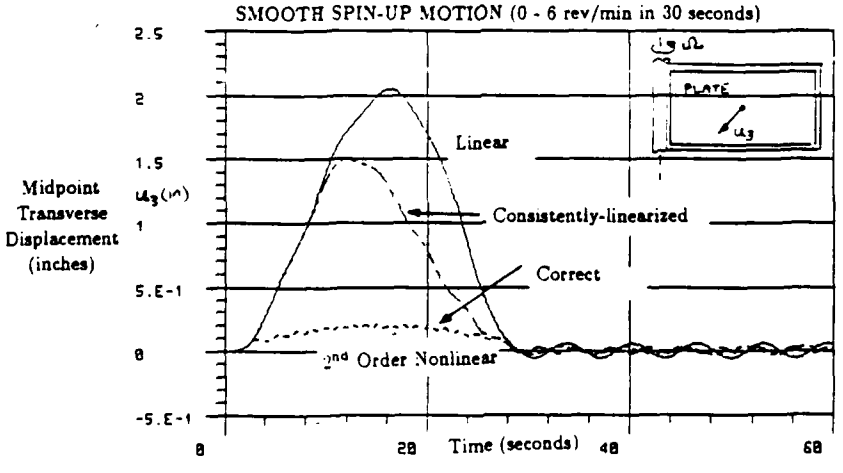

Fig. 4 - Simply-Supported Plate Spin-up Maneuver

SLOW REPOSITIONAL MANEUVER OF CHANNEL BEAM

Length:
L=8 m
Young's Modulus:
E=6.895E10 N/m^2
Shear Modulus:
G=2.6519E10 N/m^2
Mass per unit volume:
ρ=27766.67 kg/m^3
Cross-sectional area:
A=7.3E-5 m^2
Area moments:
I_2 = 4.8746E-9 m^4
I_3 = 8.2181E-9 m^4

Shear area ratios:
α_2 =3.174
α_3 =1.520
Torsional constant:
κ = 2.4330E-11 m^4
Warping constant:
Γ = 5.0156E-13 m^6
Eccentricities:
e_2 = 0
e_3 = 0.01875 m
Modes Employed: 5 .

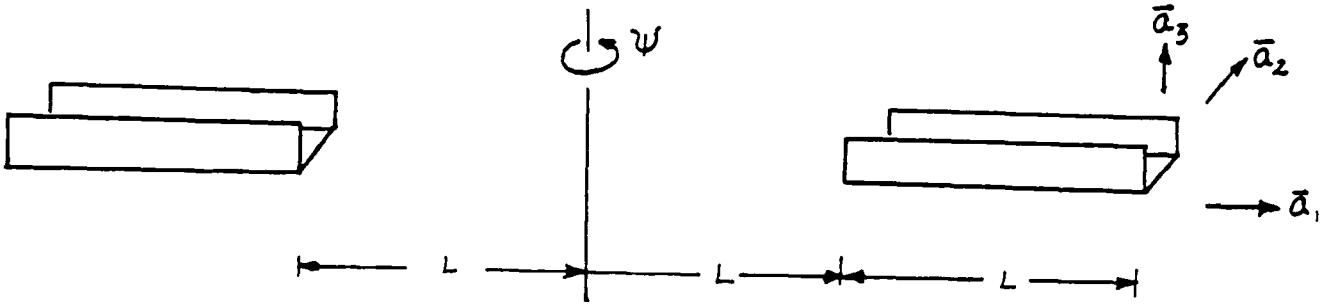

$$\Psi(t) = \begin{cases} \pi - \frac{\pi}{15}(t - \frac{15}{2\pi}\sin\frac{2\pi}{15}t) \text{ rad} & 0 < t < 15 \text{ seconds} \\ 0 \text{ rad} & t > 15 \text{ seconds} \end{cases}$$

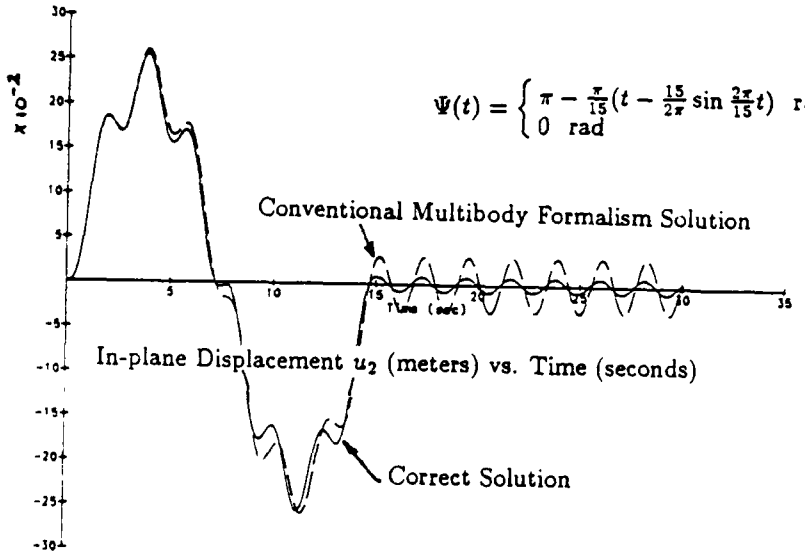

In-plane Displacement u_2 (meters) vs. Time (seconds)

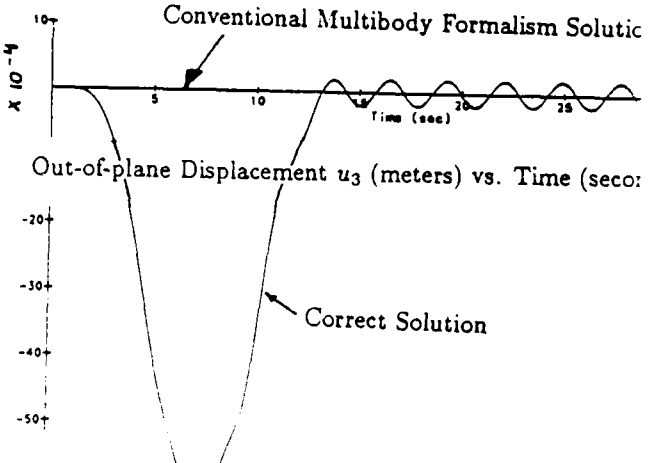

Out-of-plane Displacement u_3 (meters) vs. Time (seco:

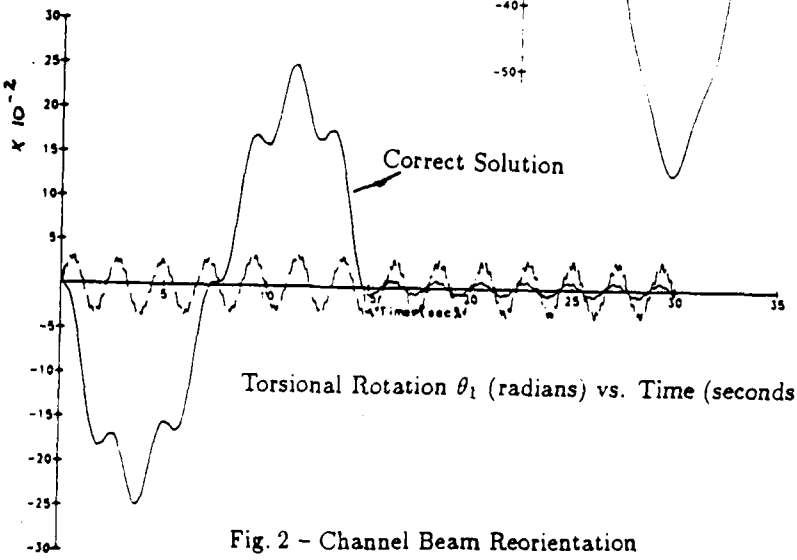

Torsional Rotation θ_1 (radians) vs. Time (seconds)

Fig. 2 – Channel Beam Reorientation

Nonlinear Large Rotational Structural Dynamics

M. Iura and S. N. Atluri

Center for the Advancement of Computational Mechanics
Georgia Institute of Technology

Summary

The objective of this paper is to present a novel theory, and its computational implementation, for the analysis of strongly nonlinear dynamic response of highly-flexible beam structures, and also to extend this theory to the case of highly-flexible shell structures.

The beam model used is based on Timoshenko's hypothesis; the effects of stretching, bending, torsion and transverse shear are taken into account. This kinematic hypothesis has been employed by many investigators (Antman and Jordan 1975, Reissner 1973, 1981, and Simo and Vu-Quoc 1986). In these papers, the existence of configuration-independent external moments has been postulated a priori. Argyris, Dunne and Scharpf (1978) and Iura and Atluri (1987), however, have made the point that the external moments generated by the conservative forces are generally configuration dependent. Therefore, the external virtual work associated with the moments does not, on first sight, appear to correspond to the first variation of an external energy functional. Argyris, Dunne, and Scharpf (1978) have derived a nonsymmetric tangent stiffness matrix at the element level using the rotational degrees of freedom referred to fixed axes of a global Cartesian system. Simo and Vu-Quoc (1986) have concluded that using the variation of a rotational variable introduced by Atluri (1984), the tangent stiffness matrix become symmetric only at an equilibrium configuration, provided that no distributed external moments are assumed to exist. This lack of symmetry (Argyris, Dunne, and Scharpf 1978) and the recovery of symmetry at only an equilibrium configuration (Simo and Vu-Quoc 1986) have been attributed to the fact that the finite rotation field is noncommutative. Iura and Atluri (1987), on the other hand, have shown that the use of any three independent components of the finite rotation tensor, as rotational variables, leads to a symmetric tangent stiffness matrix, not only at the equilibrium but also the nonequilibrium configuration, even if the distributed external moments exist in the problem. It should be emphasized that the rotation field remains noncommutative.

The shell model used is based on Reissner's hypothesis; the membrane, bending and transverse shear effects are taken into account. It is well known that the independent parameters in this shell model are three translational and two rotational ones, while the number of independent rotational parameters in the beam model is three. Based on this fact, Basar (1987) has introduced the finite rotation vector with two independent parameters. The momentum equations of Basar are based on the unacceptable assumption that

the Green strain tensor is a linear function of the shell thickness. Furthermore there are physically uninterpretable terms which appear in the angular momentum balance conditions. It is shown in this paper that, for certain choices of the rotation parameters, the momentum equations derived from the energy method take on the same form as those derived from the static method. For other choices of parameters the form of the momentum balance equations is different but completely equivalent to that derived from the static method. The resulting momentum equations are physically interpretable. As with the case of the present beam theory, the external moment vectors caused by the conservative forces are deformation dependent. In spite of this fact, we can derive the symmetric tangent stiffness matrix for the shell element in a manner similar to that employed in the beam theory.

The large deformation dynamics of a continuum body have been formulated with the use of the total Lagrangian, updated Lagrangian, Eulerian, Euler-Lagrangian and the moving coordinate formulations. The inertia effects are readily taken into account in the total Lagrangian formulation. Therefore, we employ the total Lagrangian formulation for both beam and shell theory. It should be noted that no simplification is made in the present formulation; not only the rotatory inertia but also the Coriolis and the centrifugal effects are accounted for.

Several numerical examples for transient dynamic responses are considered to demonstrate the validity and applicability of the theoretical methodology developed in this paper. A flexible in-plane beam in free flight is simulated in Fig. 1.

Aknowledgements

This work was supported by AFOSR and the SDIO/IST. The assistance of Ms. Deanna Winkler in the preparation of this manuscript is thankfully acknowledged.

References

1. S.S. Antman and K.B. Jordan, *Proc. R. Soc. Edinb.* 73A (5), 85-105 (1975).

2. J.H. Argyris, P.C. Dunne and D.W. Scharpf, *Comp. Meth. Appl. Mech. Engng.*, 14, 401-451 (1978).

3. S.N. Atluri, *Comput. and Struct.* 18, 93-116 (1984).

4. Y. Basar, *Int. J. Solids Structures*, 23 (10), 1401-1415 (1987).

5. M. Iura and S.N. Atluri, *Computational Mechanics* (In Press).

6. E. Reissner, *Studies Appl. Math.*, Vol. 52, 87-95 (1973).

7. E. Reissner, *J. Appl. Math. Phy* (ZAMP) 32, 734-744 (1981).

8. J.C. Simo and L. Vu-Quoc, *Comp. Meth. Appl. Mech. Engng.*, 58, 79-116 (1986).

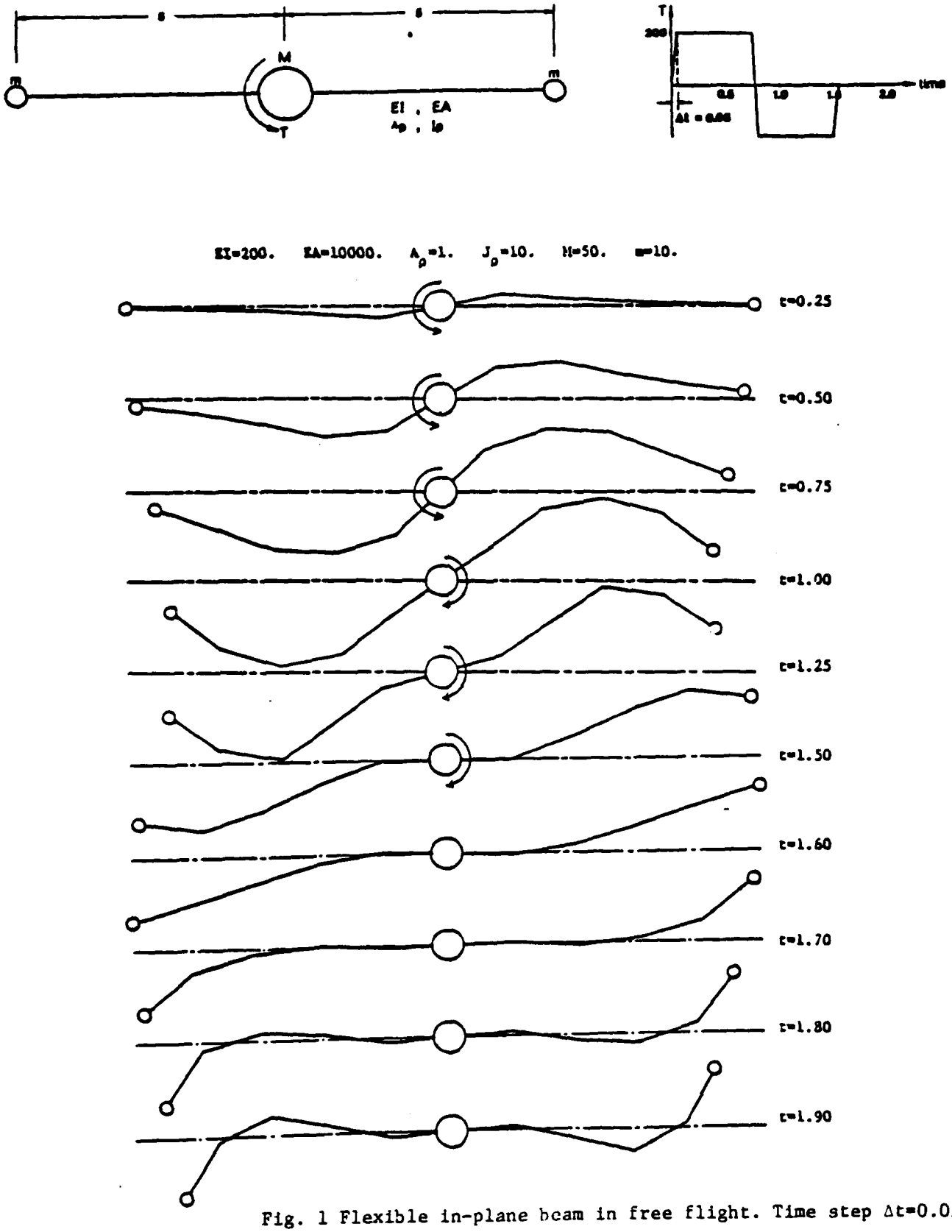

Fig. 1 Flexible in-plane beam in free flight. Time step Δt=0.05

DYNAMICS AND BIFURCATIONS OF ELASTIC SPACE STRUCTURES

by Mark Levi,
Mathematics department
Boston University, Boston, MA 02215.

Abstract

Coupling of two well-understood classical systems – an oscillator and a free rigid body in space produces a system which, on the one hand, is amenable to mathematical analysis using the ideas and methods of geometric theory of dynamical systems, and on the other hand, exhibits interesting and perhaps unexpected dynamical phenomena which give a good indication of what is likely to occur in more complex systems such as beams, platforms, etc. One such phenomenon is the bifurcation in which stable rotations become destabilized and vice versa, and more than three pure rotations are possible with the same parameters.

SESSION 11

FRICTION AND DAMPING

FRIDAY - 1300 - 1415

June 3, 1988

THE EFFECT OF SOFTENING OF THE SUPPORTS ON THE STABILITY AND DYNAMICS OF STRUCTURES

Marco Antonio Souza
Associate Professor
Departamento de Engenharia Civil
PUC-Rio Rio de Janeiro BRAZIL

ABSTRACT

A simplified model is used in order to illustrate how the softening of the supports change the stability and the vibration characteristics of structural elements liable to buckling. Damping is not included in the analysis.

INTRODUCTION

The accurate design of the support conditions represents an essential part in any experimental set up. It is not unusual to find out that experimental and theoretical results do not coincide. There are a few reasons for this to happen, the inacuracy of the theoretical assumptions being maybe the most common. But any inadequacy in the design of the supports to be used in the experimental set-up will also lead to the very same conclusion that the theoretically predicted results are different from the ones measured during the tests.

In order to highlight this fact, a very simple model is used to show how the softening of the supports can affect both the stability and the vibration characteristics of structural elements liable to buckling. The stability and the vibration characteristics will be illustrated by the equilibrium paths and the characteristic curves, respectively.

THE RIGID-BARS MODEL

The simplified rigid-bars model of figure 1 has been previously used by the author [1,2] to illustrate different effects. This model reproduces the behavior of beam-columns, plates and shells.

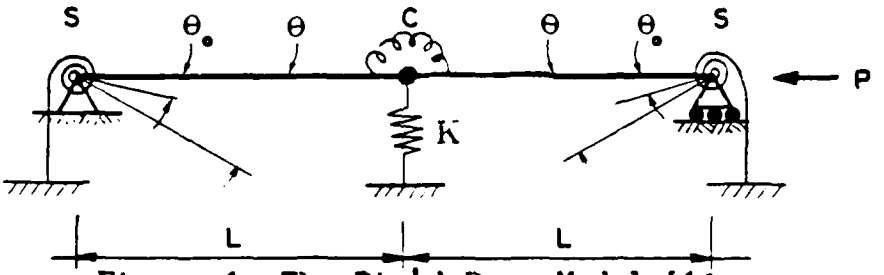

Figure 1- The Rigid-Bars Model [1]

The softening of the supports is modelled by the non-linear springs S, figure 1, which have the characteristics shown in figure 2, represented by $s=S/\bar{S}$ versus the rotation at the supports, θ.

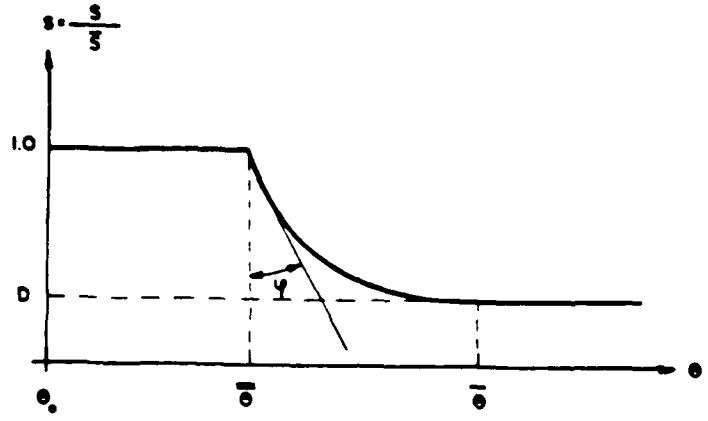

Figure 2 - The Non-linear Springs

The incremental stiffness function $s=S/\bar{S}$ to be used in the present analysis is defined as follows:

i) $\theta_o \le \theta \le \bar{\theta}$

$$s = 1.0 \qquad (1)$$

ii) $\bar{\theta} \le \theta \le \bar{\bar{\theta}}$

$$s = 1.0 + \psi\Delta + \Delta^3[\psi(-6 + 8\Delta - 3\Delta^2) + (1-D)(-10 + 15\Delta - 6\Delta^2)] \qquad (2)$$

where:

$$\psi = (\bar{\bar{\theta}} - \bar{\theta})\tan\varphi \; ; \; \Delta = (\theta - \bar{\theta})/(\bar{\bar{\theta}} - \bar{\theta}) \qquad (3)$$

iii) $\theta \ge \bar{\bar{\theta}}$

$$s = D \qquad (4)$$

Two cases of the incremental stiffness function s will be used in the analysis and are shown in figure 3, corresponding to φ = -1.2Rad., D=0.5 and D=0.0.

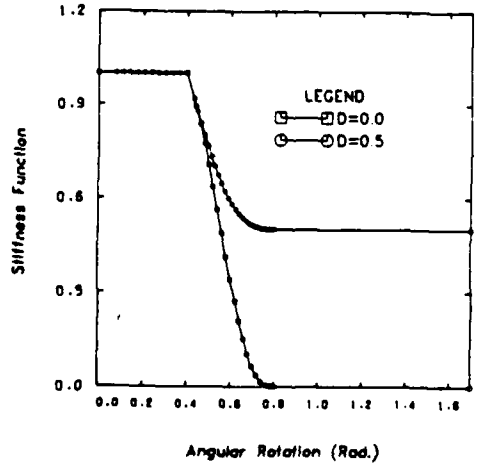

Figure 3 - The Incremental Stiffness Function s (φ=-1.2Rad.)

THEORETICAL ANALYSIS

The change of the total potential energy, V, can be written as:

$$V = 2C(\theta - \theta_o)^2 + (1/2)KL^2(\sin\theta - \sin\theta)^2 + \int_{\theta^*}^{\theta} \bar{S}\,[s(\theta)](\theta-\theta^*)d\theta \qquad (5)$$

where θ^* can be θ, $\bar{\theta}$, or $\bar{\theta}$ depending on the range of the angular deflection θ at the supports, i.e. $\theta_o \le \theta \le \bar{\theta}$; $\bar{\theta} \le \theta \le \bar{\theta}$ or $\theta \ge \bar{\theta}$.

The equilibrium paths are obtained from the equilibrium equation

$$V_{,\theta} = 0 \qquad (6)$$

and can be summarized as:

i) $\theta_o \le \theta \le \bar{\theta}$

$$p = \frac{(\theta - \theta_o)}{\sin\theta}(1 - \alpha + R) + \alpha\left(1 - \frac{\sin\theta_o}{\sin\theta}\right)\cos\theta \qquad (7)$$

where:

$$\alpha=(KL^2)/(KL^2+4C);\quad p=2PL/(KL^2+4C);\quad R=2/(KL^2+4C) \qquad (8)$$

ii) $\bar{\theta} \le \theta \le \bar{\theta}$

$$p = \alpha\left(1 - \frac{\sin\bar{\theta}}{\sin\theta}\right)\cos\theta + \frac{(\theta - \bar{\theta})}{\sin\theta}\left\{(1 - \alpha) + \psi + (1 - D)\Delta^3\left[R(-10 + 15\Delta - 6\Delta^2) + \psi(-6 + 8\Delta - 3\Delta^2)\right]\right\} \qquad (9)$$

where ψ, Δ, α, R are defined by equations (3) and (8) respectively;

iii) $\theta \ge \bar{\theta}$

$$p = \alpha\left(1 - \frac{\sin\bar{\theta}}{\sin\theta}\right)\cos\theta + (1 - \alpha + DR)\frac{(\theta - \theta_o)}{\sin\theta} \qquad (10)$$

Equilibrium paths for different values of the parameters R and ψ for $\alpha = 0.0$ are shown in figure 4 corresponding to the stiffness function s of figure 3.

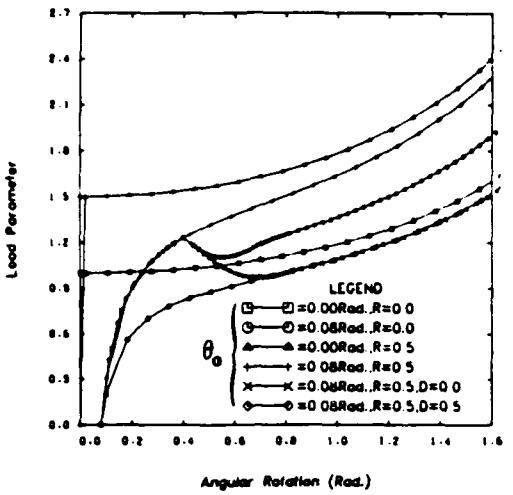

Figure 4 - Equilibrium Paths (α = 0.0)

The natural frequency of vibration corresponding to a load level p is obtained by means of a small perturbation δ from the equilibrium configuration represented by θ. The equation of motion is obtained from the Euler-Lagrange equation [3]:

$$\frac{d}{dt}\left(\frac{\partial T}{\partial \dot{\delta}}\right) + \frac{\partial V}{\partial \delta} = 0 \qquad (11)$$

where T is the kinetic energy $T=(1/2)I^{*}\dot{\delta}^{2}$ I^{*} being the generalized rotatory inertia, δ is the velocity associated to δ and $\dot{(\ )}=d(\ )/dt$ and neglecting terms of $O(\delta)^{2}$ can be written as:

$$\ddot{\delta} + \frac{(KL^{2} + 4C)}{I^{*}} f^{2}\delta = 0 \qquad (12)$$

where f^{2} is the square of the natural frequency given by:

i) $\theta_{o} \le \theta \le \bar{\theta}$

$$f_{o}^{2} = (1 - \alpha) + R + \alpha(\cos 2\theta - \sin\bar{\theta}\sin\theta) - p\cos\theta \qquad (13)$$

ii) $\bar{\theta} \le \theta \le \bar{\theta}$

$$f^{2} = f_{o}^{2} + R\left[1 - \Delta^{3}(1-D)(40 - 75\Delta + 36\Delta^{2})\right] \qquad (14)$$

iii) $\theta \ge \bar{\theta}$

$$f^{2} = f_{o}^{2} - R(1 - D) \qquad (15)$$

Characteristic curves relating the applied load and the square of the natural frequency are shown in figure 5, and correspond

to the equilibrium paths shown in figure 4.

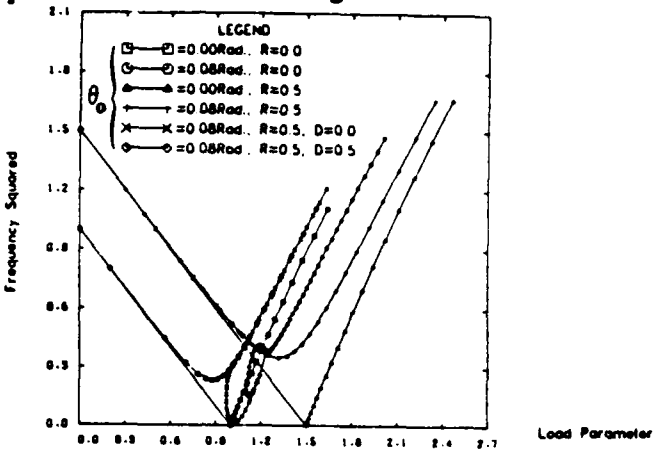

Figure 5 - Characteristic Curves (α = 0.0)

CONCLUSIONS

The results presented illustrate how the softening of the supports affects the stability and the vibration characteristics of structural elements liable to buckling. This is clear from the comparison between the curves, figures 4 and 5, corresponding to R≠0.0 and R=0.0 in the range of $\bar{\theta} \leq \theta \leq \bar{\theta}$.

The implications of the results on experiments are clear: unless the actual support conditions are properly designed the results obtained can exhibit a different pattern from that expected theoretically. It will not necessarily mean that the theory is not accurate only that the theoretical and the experimental supports do not have the same characteristics.

ACKNOWLEDGEMENT

This work was done during the two months visit to the Department of Civil Engineering of the University of Alberta, Canada, to which the author is deeply thankful.

REFERENCES

1. Souza, M. A., Post-buckling Vibration Characteristics of Structural Elements, Engineering Structures, Vol. 9, pp. 134-137, 1987.

2. Souza, M. A., The Effects of Initial Imperfection and Changing Support Conditions on the Vibration of Structuralof Structural Elements Liable to Buckling, International Journal of THIN-WALLED STRUCTURES, to appear, 1988.

3. Clough, R. W. & Penzien, J., Dynamics of Structures, McGraw-Hill Book Co., 1975.

JOINT DAMPING AND JOINT NONLINEARITY EFFECTS IN DYNAMICS OF SPACE STRUCTURES

Mary Bowden
John Dugundji

Space Systems Laboratory
Department of Aeronautics and Astronautics
Massachusetts Institute of Technology
Cambridge, MA 02139

The presence of joints can strongly affect the dynamics of space structures in weightlessness, especially if the joints are numerous, of low stiffness, have damping, or are nonlinear. In order to obtain an idea of these joint effects, a simple free-free system of four beams connected by three joints is investigated, as shown in Figs. 1 and 2.

Linear analyses of these beams were performed by using a standard finite element formulation and including various linear joint stiffness values k_L and linear joint damping values c_L. These analyses were formulated in the standard form,

$$\underset{\sim}{M}\,\ddot{\underset{\sim}{q}} + \underset{\sim}{c}\,\dot{\underset{\sim}{q}} + \underset{\sim}{K}\,\underset{\sim}{q} = \underset{\sim}{F} \qquad (1)$$

and then reduced to state space form,

$$\dot{\underset{\sim}{x}} = \underset{\sim}{A}\,\underset{\sim}{x} + \underset{\sim}{P} \qquad (2)$$

for ease in obtaining solutions. The corresponding lowest six symmetric modes and frequencies for no damping, $c_L = 0$, are shown in Fig.3 for a finite and an infinite joint stiffness. The effect of including joint damping c_L on these modes is shown in Fig.4. Increasing the joint damping increases resonant frequencies and modal damping, but only to the point where the joint gets "locked up" by the damping and approaches a continuous beam. This behavior is different from that predicted by proportional damping, as shown in Fig.5. The maximum amount of passive modal damping obtainable from the joints is greater for low stiffness joints and for modal vibrations in which many joints are participating. A joint participation function JPF, based on geometrical arguments of joint location, was used to quantify this phenomenon.

Nonlinear effects of the joints were introduced by using describing functions to represent the first harmonic of the

nonlinear joint forces. Assuming sinusoidal motion $q = A \sin \phi$ where $\phi = \omega t$, the nonlinear symmetrical joint force $F_{NL}(q, \dot{q})$ was expressed as,

$$F_{NL} = a \sin \phi + b \cos \phi = \frac{a}{A} q + \frac{b}{A\omega} \dot{q}$$

$$= c_p q + c_q \dot{q} \qquad (3)$$

where c_p and c_q are frequency and amplitude dependent stiffness (phase) and damping (quadrature) coefficients defined as

$$c_p = \frac{1}{\pi A} \int_0^{2\pi} F_{NL}(A \sin \phi, A \omega \cos \phi) \sin \phi \, d\phi$$

$$c_q = \frac{1}{\pi A \omega} \int_0^{2\pi} F_{NL}(A \sin \phi, A \omega \cos \phi) \cos \phi \, d\phi \qquad (4)$$

A joint with a simple cubic spring nonlinearity $F_{NL} = k_L q + k_{cs} q^3$ was used to illustrate nonlinear behavior, although other nonlinearities (free play, coulomb friction, etc.) were also considered. Figure 6 shows the typical forced response of a single degree of freedom system with a cubic spring. The response plots nondimensional amplitude $\tilde{A} = A\sqrt{\kappa}$ rather than A in order to collapse all results onto one universal curve. The forced response of the four beam model with cubic spring joints, to a vertical harmonic excitation at its center was then studied. Figure 7 shows typical log-log responses for the beam with linear spring joints, while Fig.8 shows the corresponding responses for the nonlinear cubic spring joints. These were computed using Newton-Raphson method with appropriate initial displacements. The nonlinear analyses show the classical single degree of freedom nonlinear behavior at each resonance: multiple solutions, jump behavior, resonant frequency shifts, and non-doubling of response for doubling of forcing amplitudes. These properties are illuminated by characteristic backbone curves, which show the locus of resonant peaks for increasing forcing amplitudes. These peaks shift from the small amplitude (linear) frequencies to the large amplitude)locked, continuous beam) frequencies and depend on the amount of joint participation. A modal coupling due to joint nonlinearity is also exhibited, as was the case for linear joint damping.

The present studies help to illustrate how multiple discrete nonlinearities interact with the global dynamics of continuous systems. The jointed beam model studied here can be

interpreted as truss bays with linear characteristics, and the joints as bay interfaces with nonlinear characteristics.

Acknowledgement

This work was supported in part by NASA and in part by McDonnell Douglas Astronautics Company.

References

1. Bowden, M.L., and Dugundji, J., "Effects of Joint Damping and Joint Nonlinearity on the Dynamics of Space Structures," AIAA SDM Issues of the International Space Station Conference, Williamsburg, VA, April 21-28, 1988, AIAA paper 88-2480.

2. Bowden, M.L., "Dynamics of Space Structures with Nonlinear Joints," M.I.T. Department of Aeronautics and Astronautics, ScD. Thesis, May 1988.

3. Crawley, E.F., and O'Donnell, K.J., "A Procedure for Calculating the Damping in Multi-Element Space Structures," 27th Congress of the International Astronautical Federation, Innsbruck, Austria, October 1986.

4. Den Hartog, J.P., Mechanical Vibrations, McGraw-Hill, 4th Edition, New York, 1956.

5. Woolston, D.S., Runyan, H.L., and Andrews, R.E., "An Investigation of Effects of Certain Types of Structural Nonlinearities on Wing and Control Surface Flutter," J. of Aero. Sciences, Vol. 24, No. 1, January 1957. See also Vol. 26, No. 1, pp. 51-53, January 1959.

6. Breitbach, E., "Effects of Structural Nonlinearities on Aircraft Vibration and Flutter," NATO AGARD Report R-665, January 1978.

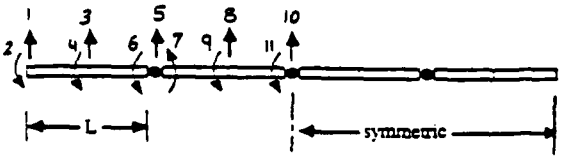

Figure 1 Three Joint Model

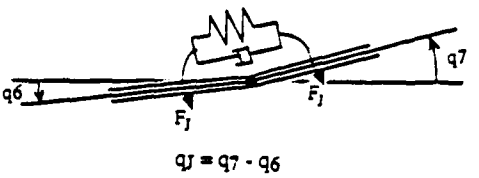

Figure 2 Joint Forces

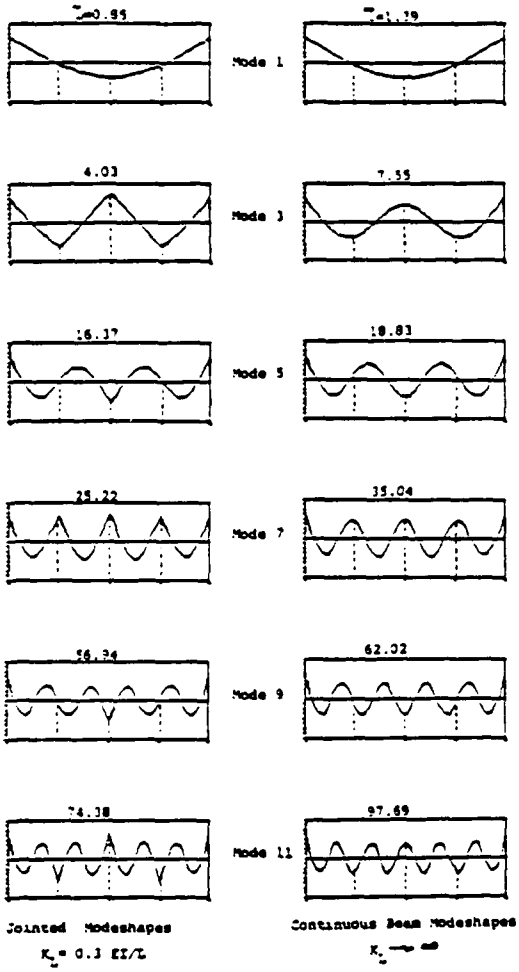

Figure 3 Jointed and Continuous Beam Modeshapes

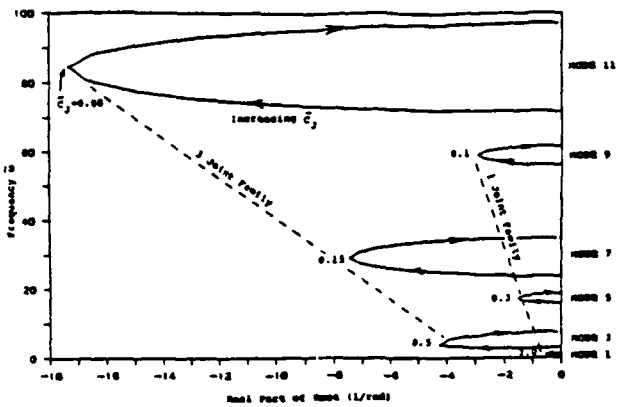

Figure 4 Root Locus for First 6 Symmetric Modes

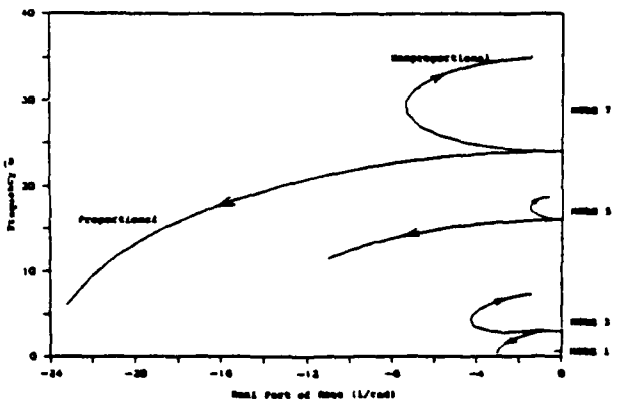

Figure 5 Nonproportional Damping

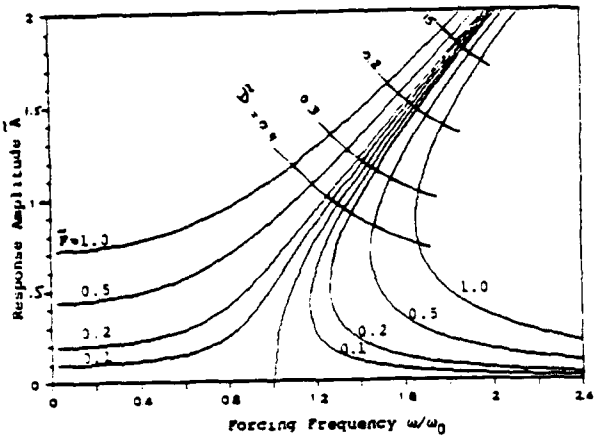

Cubic Spring Equation of Motion:

$$M\ddot{q} + C_L\dot{q} + K_L q + K_{CS} q^3 = F_0 \sin \omega t$$

Define the following quantities using $\kappa = K_{CS}/K_L$

$$\bar{q} = q\sqrt{\kappa} \qquad \bar{A} = A\sqrt{\kappa}$$

$$\bar{F} = \frac{F_0}{K_L}\sqrt{\kappa} \qquad \bar{D} = \frac{\zeta}{\bar{F}}$$

to obtain the following non-dimensional, universal form:

$$\frac{1}{\omega_0^2}\ddot{\bar{q}} + 2\zeta\frac{1}{\omega_0}\dot{\bar{q}} + \bar{q} + \bar{q}^3 = \bar{F}\sin\omega t$$

Figure 6 Cubic Spring Nonlinearity (1 dof)

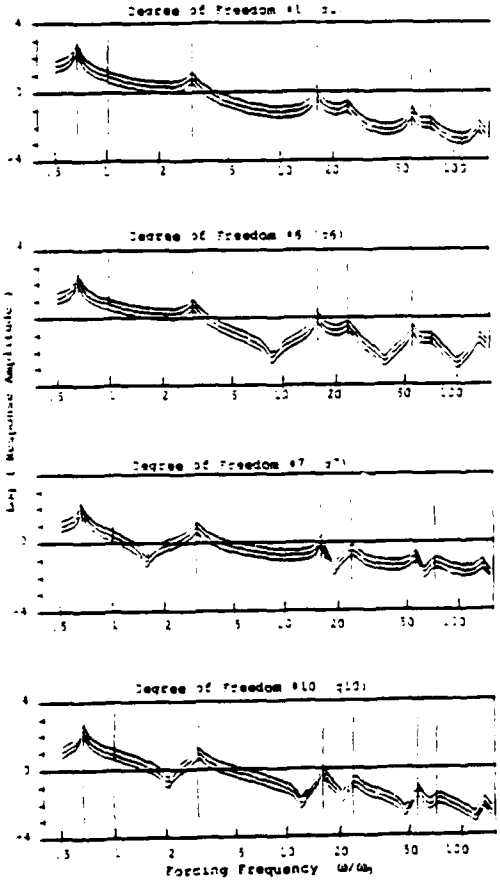

Figure 7 Response of Linear 3 Joint System

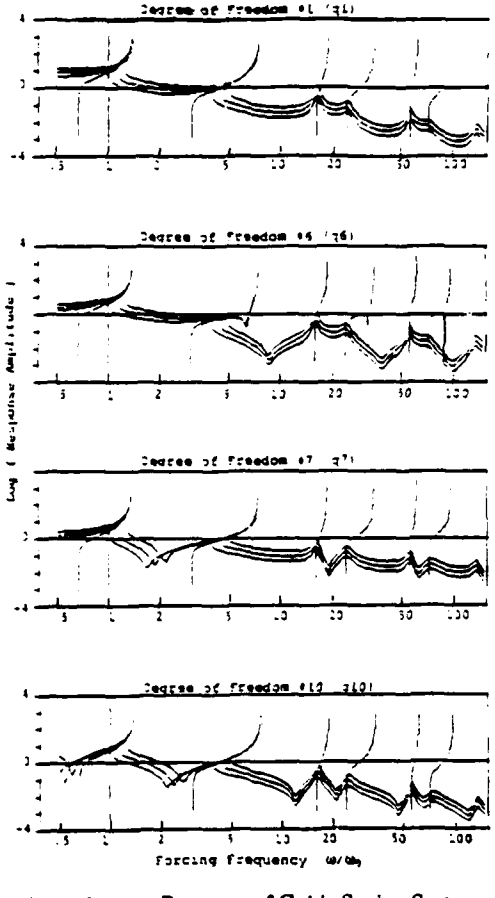

Figure 8 Response of Cubic Spring System

EFFECTS OF VELOCITY-DEPENDENT FRICTION ON PERFORMANCE OF A RESILIENT-FRICTION BASE ISOLATOR

Lin Su, Goodarz Ahmadi
Department of Mechanical and Industrial Engineering
Clarkson University, Potsdam, NY 13676

and

Iradj G. Tadjbakhsh
Department of Civil Engineering
Rensselaer Polytechnic Institute, Troy, NY 12181

ABSTRACT

Performances of a resilient-friction base isolator (R-FBI) as an aseismic bearing under a variety of conditions are analyzed. In particular, the effects of velocity-dependence of friction coefficient on the overall performance of the R-FBI system are studied. Based on experimental data, two expressions for velocity-dependence of friction coefficient are assumed. A nonuniform shear beam structural model is considered and the accelerogram of the N00W component of El Centro 1940 earthquake are used as the earthquake excitation. The presented results show that for a finite static friction coefficient the velocity-dependence of dynamic friction coefficient has no noticeable effects on the response spectra of the base-isolated structure. On the other hand, a zero static friction coefficient leads to significant differences and improves the effectiveness of the R-FBI system to a considerable extend.

INTRODUCTION

Using base isolation systems for aseismic design of relatively stiff structures has attracted considerable interest in the recent years. The main concept is to isolate the structure from ground during earthquake strong motions. Excellent reviews on the subject were provided by Kelly [1,2]. Recently, an interesting frictional base isolation system (R-FBI) was introduced by Mostagel and Khodaverdian [3]. This isolator consists of concentric layers of teflon coated plates that are in friction contact with each other and contains a central core of rubber. The system provides isolation through the parallel action of friction, damping and restoring springs. This design essentially uses a rubber bearing and a pure-friction isolator in parallel. Figure 1 shows a schematic diagram of mechanical behavior of the R-FBI system.

For the friction-type base isolators, the friction coefficient is an important parameter. In most earlier studies, a constant coefficient of friction in according to Coulumb's law

was used for response analyses. However, recent experimental data [4,5] suggest that the friction coefficient is not a constant and varies with velocity, normal pressure, and other parameters.

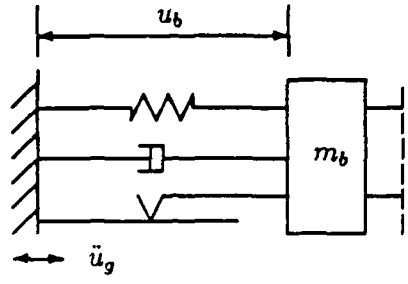

Figure 1. Schematic diagram of the R-FBI systems

In this work, a shear beam model for structure is considered and the acceleration record of El Centro 1940 earthquake is used. The performances of the R-FBI system for different structural systems are analyzed. Particular attention is given to the effect of velocity-dependence of friction coefficient. It is shown that for a finite static friction coefficient the velocity-dependence of dynamic friction coefficient has no noticeable effects on the response spectra of the base-isolated structure. On the other hand, should a negligible static friction coefficient for teflon-teflon or teflon-steel interfaces be substantiated, it could significantly alter the behavior of the frictional base isolators.

TECHNIQUE OF ANALYSIS

The equations of motion of a nonuniform shear beam structure with a base isolation system subject to an earthquake excitation are described at length in [6] and hence is not repeated here. It suffices to point out that the first ten modes of vibration are used in the response analysis. The computer program developed in [6] for numerical integration of equations of motion is modefied and is used in this study.

A modal damping coefficient of 0.02 for the structure, a nonuniformity coefficient of 0.1 and a mass ratio of 0.75 are used. The recommended values of parameters for the R-FBI system ($\mu_1 = 0.04$, $\zeta_o = 0.1$ and natural period of 4.0 sec) are employed. The accelerogram of the N00W component of El Centro 1940 earthquake is used as seismic excitation. The peak relative displacements and the maximum absolute accelerations of the base-isolated shear beam structure at its base raft and its roof under a variety of conditions are evaluated.

VELOCITY-DEPENDENT FRICTION

Recently Constantinou et al. [5] presented a series of experimental data for frictional characteristics of teflon-steel interfaces. The following two expressions for the velocity-dependence of friction coefficient given as

$$\mu = 0.02 + c_1(v/n), \tag{1}$$

$$\mu = c_2(v/n) + c_3(v/n)^2 + c_4(v/n)^3 \tag{2}$$

are fitted to the data of Constantinou et al. in [5]. Here, v is the slip velocity, n is the number of friction plates used in the R-FBI system ($n = 8$ is used in the analysis), and the values of c's are given as

$$c_1 = 1.0762 \times 10^{-3} \text{ sec/cm}, \qquad c_2 = 2.5086 \times 10^{-3} \text{ sec/cm},$$

$$c_3 = -3.1316 \times 10^{-3} \text{ sec}^2/\text{cm}^2, \qquad c_4 = 2.2545 \times 10^{-7} \text{ sec}^3/\text{cm}^3. \tag{3}$$

Figure 2 compares the predictions of equations (1) and (2) with the experimantal data. Equation (1) assumes a linear relationship between μ and the slip velocity with a static friction coefficient of 0.02. Constantinou et al. [5] have also reported that continuous non-stick sliding occured in their experiments, which implies that $\mu = 0$ for $v = 0$. Equation (2) satisfies this latter condition and leads to a zero static friction coefficient.

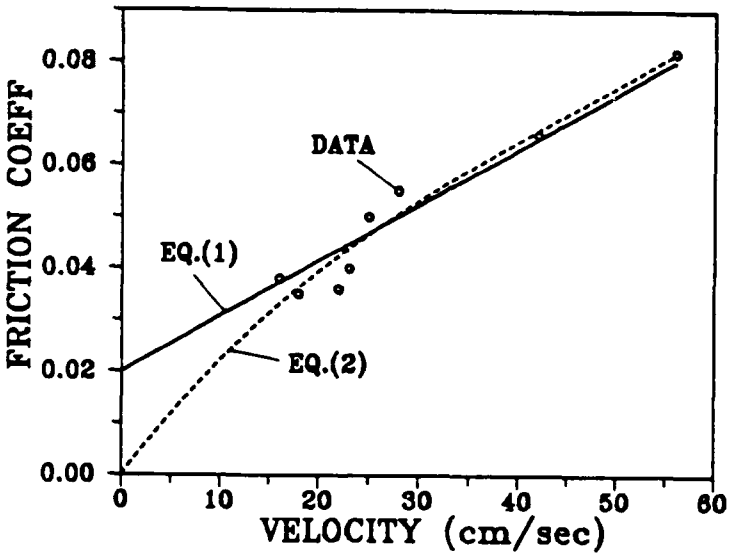

Figure 2. Velocity-dependence of friction coefficient

RESULTS

For friction coefficient as given by equations (1) and (2), as well as a constant value of 0.02, the response spectra of the base-isolated shear beam structure versus its natural period T_1 are evaluated. The results are shown in figure 3. It is observed that the response

spectra for μ given by equation (1) are almost the same as those for a constant friction coefficient. That is, the velocity-dependence of friction coefficient as given by equation (1) does not affect the peak responses. This figure also shows that the response spectra obtained by using equation (2) defer significantly from those obtained for a constant friction coefficient. The peak deflection and the peak acceleration are lower by a factor of 2 to 4 and the peak base displacement is higher by about 10 to 30 percent.

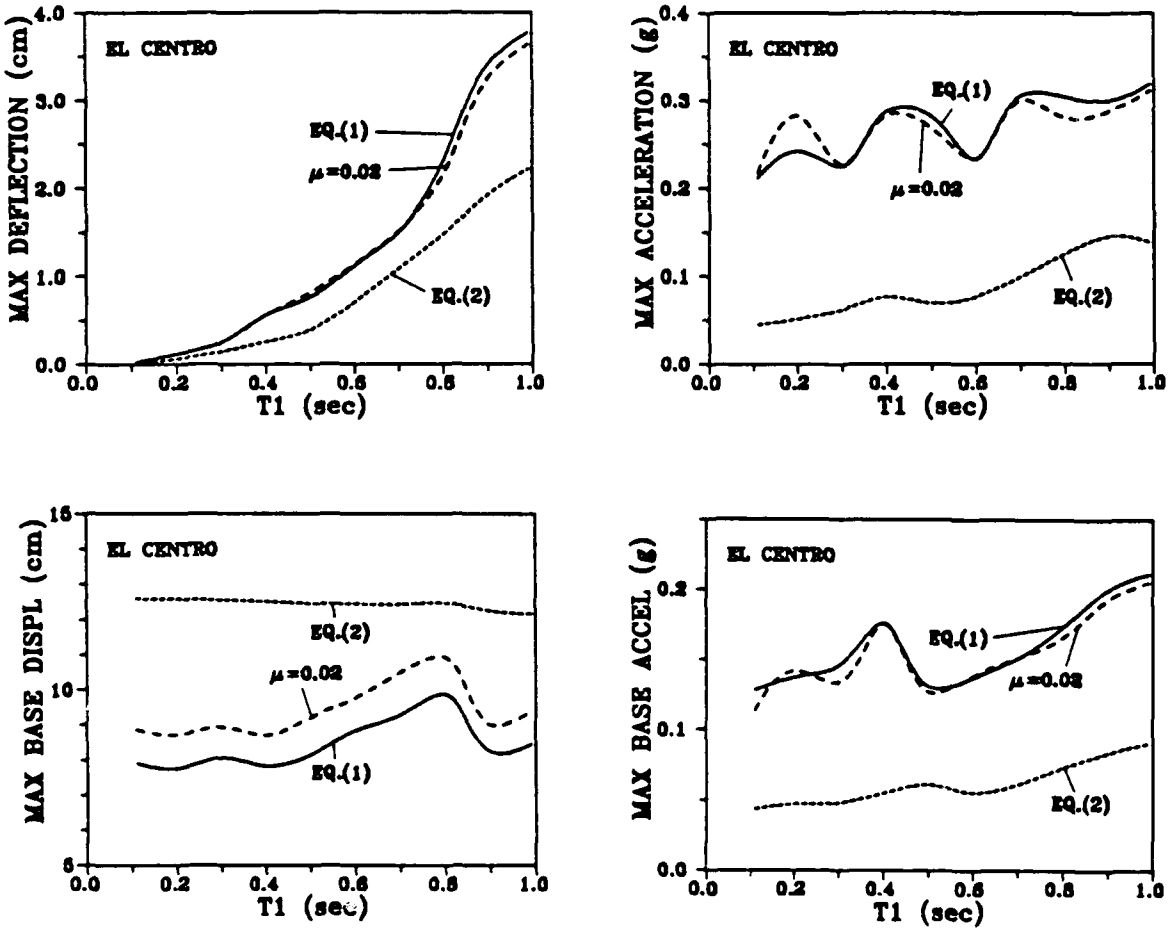

Figure 3. Variations of the peak responses of the structure with its natural period for the R-FBI systems with velocity-dependent friction coefficient

CONCLUSIONS

From the presented results, it may be concluded that the response spectra of the structure with the R-FBI system are not sensitive to the velocity-dependence of friction coefficient for a nonzero static friction coefficient. However, should it be proved that continuous nonstick sliding with zero static friction coefficient occurs for certain inter-

faces, then the velocity-dependence of μ can significantly affect the peak responses of the friction-type base isolators. The effects, in this case, are generally favorable and results in significant reductions in the peak deflection and the maximum acceleration of the structure. At the present time, however, the available meager data are inconclusive and additional experiments are needed.

ACKNOWLEDGMENT

This work is supported by the National Center for Earthquake Engineering Research, State University of New York at Buffalo under the Grants No. NCEER 872007.

REFERENCES

1. Kelly, J.M., *Aseismic Base Isolation, Shock Vib. Dig.*, 14, *pp. 17-25 (1982).*
2. Kelly, J.M., *Aseismic Base Isolation: Review and Bibliography, Soil Dyn. Earthquake Engng.*, 5, *pp. 202-216 (1986).*
3. Mostaghel, N. and Khodaverdian, M., *Dynamics of Resilient-Friction Base Isolator (R-FBI), Earthquake Engng. Struct. Dyn.* 15, *pp. 379-390 (1987).*
4. Kragelskii, I.V., *Friction and Wear, Butterworths, (1965).*
5. Constantinou, M.C., Caccese, J. and Harris, H.G., *Frictional Characteristics of Teflon-Steel Interfaces under Dynamic Conditions, Earthquake Engng. Struct. Dyn.*, 15, *pp. 751-759 (1987).*
6. Su, L., Ahmadi, G. and Tadjbakhsh, I.G., *A Comparative Study of Performances of Various Base Isolation Systems — Part I: Shear Beam Structures, Report No. MIE-153, Clarkson University, October 1987.*

NONLINEAR DYNAMIC RESPONSE OF FRACTIONALLY DAMPED STRUCTURAL SYSTEMS *

Joseph Padovan
Dept. Mechanical and Polymer Engineering
The University of Akron
Akron, Ohio 44325

Introduction

The modelling of structural damping has been a long standing problem. Most typically, differential type simulations have been employed to represent such behavior, i.e. Kelvin-Voigt, Maxwell, as well as combined models. Interestingly, this is in spite of the fact that such simulations do not generally define the proper frequency sensitivities over wide ranges of spectral input. As a result of this, alternative formulations have been sought. Generally, this has meant the development of nonlinear type representations. To extend the range of validity of differential type formulations, the integer derivatives have been recently replaced by fractional integro differential operators, i.e. of the Liouville-Riemann form. Such a formulation enables the powers of the various derivatives to be cast in terms of experimentally derived fractional numbers. Such expressions yield better results over wider spectral ranges than the usual integer version. Note while fractional operators yield significant modelling advantages, they are awkward to handle both analytically and numerically [2].

In the context of the foregoing, the presentation will develop efficient and stable numerical schemes enabling the solution of the nonlinear dynamic response of structure with viscoelastic components, as well as discretely attached dampers. The damping will be modelled by fractional integrodifferential operators of the Grunwald type [3]. To generalize the results, the numerical analysis will be generalized to FE type simulations.

Overall the dampers treated fall into three categories, namely

i) Those attached to external support structures;

ii) Internal dampers which may be linked between various components of the given structure; and,

iii) Viscoelastic type material behavior.

For the fractional formulation of such problems, the solution development consists of two levels, i.e. the establishment of the numerical approximation of the fractional operator and the global level transient algorithm.

---

* Work partially supported by NASA Langley under grant NAG-1-144.

To generalize the results, the algorithm will be developed for nonlinear structural simulations involving large deformation kinematics.

For the presentation, detailed discussions will be given on:

i) The numerical approximation of fractional operators;

ii) The FE simulation of nonlinear structure with fractionally defined dampers; and,

iii) Outlining the benchmarking experiments defining the stability and efficiency of the overall development.

Generalized Fractional Integrodifferential Dampers

As noted earlier, traditional dissipative characteristics are defined by the following differential type expression, namely

$$\underset{\sim}{F}_D \sim C_1 \frac{d}{dt}(\underset{\sim}{Y}) + C_2 \frac{d^2}{dt^2}(\underset{\sim}{Y}) + .. \qquad (1)$$

where $\underset{\sim}{F}_D$, C_i and $\underset{\sim}{Y}$ respectively represent the damper force, damping coefficient, and deflection. It is well known that due to the proportional nature of (1), C_i apply only for a small range of exciting frequencies. To extend the range of application, d^n/dt^n ( ); $n\epsilon[1,..]$ can be replaced by fractional operators, i.e. [2]

$$\underset{\sim}{F}_D = \sum_i C_i \, Dq_i (\underset{\sim}{Y}) \qquad (2)$$

where $Dq_i( )$ is defined by the Riemann-Liouville relation, namely

$$Dq_i(\underset{\sim}{Y}) = \frac{1}{\Gamma(-q_i)} \int_o^t \left(\frac{1}{t-\tau}\right)^{q_i+1} \underset{\sim}{Y}(\tau)d\tau \qquad (3)$$

such that Γ is the gamma function. The main draw back to employing fractional simulations lies in the fact that from a purely analytical point of view, such operators are somewhat cumbersome to handle. To bypass such a shortcoming, we shall employ an alternative but equivalent definition developed by Grunwald. In particular

$$Dq_i(Y) \sim \lim_{N\to\infty} \left(\frac{t}{N}\right)^{-1} \sum_{j=0}^{N-1} (-1)^j \binom{q}{j} T(t-jt/N) \qquad (4)$$

The foregoing definition can be extended to represent either an integral or differential type operator. This is achieved by letting q range over both positive and negative numbers. As will be seen from the presentation, (4) can be approximated by employing a finite series where Δt is discrete.

To generalize the results, the algorithm will be developed for nonlinear structural simulations involving large deformation kinematics.

For the presentation, detailed discussions will be given on:

i) The numerical approximation of fractional operators;

ii) The FE simulation of nonlinear structure with fractionally defined dampers; and,

iii) Outlining the benchmarking experiments defining the stability and efficiency of the overall development.

Generalized Fractional Integrodifferential Dampers

As noted earlier, traditional dissipative characteristics are defined by the following differential type expression, namely

$$\underset{\sim}{F}_D \sim C_1 \frac{d}{dt}(\underset{\sim}{Y}) + C_2 \frac{d^2}{dt^2}(\underset{\sim}{Y}) + .. \qquad (1)$$

where $\underset{\sim}{F}_D$, C_i and $\underset{\sim}{Y}$ respectively represent the damper force, damping coefficient, and deflection. It is well known that due to the proportional nature of (1), C_i apply only for a small range of exciting frequencies. To extend the range of application, d^n/dt^n ( ); $n\varepsilon[1,..]$ can be replaced by fractional operators, i.e. [2]

$$\underset{\sim}{F}_D = \sum_i C_i \, Dq_i (\underset{\sim}{Y}) \qquad (2)$$

where $Dq_i( )$ is defined by the Riemann-Liouville relation, namely

$$Dq_i(\underset{\sim}{Y}) = \frac{1}{\Gamma(-q_i)} \int_o^t \left(\frac{1}{t-\tau}\right)^{q_i+1} \underset{\sim}{Y}(\tau)d\tau \qquad (3)$$

such that Γ is the gamma function. The main draw back to employing fractional simulations lies in the fact that from a purely analytical point of view, such operators are somewhat cumbersome to handle. To bypass such a shortcoming, we shall employ an alternative but equivalent definition developed by Grunwald. In particular

$$Dq_i(Y) \sim \lim_{N\to\infty} \left(\frac{t}{N}\right)^{-1} \sum_{j=0}^{N-1} (-1)^j \binom{q}{j} T(t-jt/N) \qquad (4)$$

The foregoing definition can be extended to represent either an integral or differential type operator. This is achieved by letting q range over both positive and negative numbers. As will be seen from the presentation, (4) can be approximated by employing a finite series where Δt is discrete.

Finite Element Formulation

The main emphasis of the presentation will be to consider the analysis of nonlinear structure containing varying types of dampers. These shall be modelled by fractional integrodifferential type operators. The system nonlinearity treated is a direct result of kinematic, material and boundary condition induced nonlinearity. In this context, the FE model will employ the 2nd Piola Kirchhoff stress and Lagrangian strain tensor combination of measures. The overall "fractional" viscoelastic FE formulation will be established via the virtual work principle.

The solution of the resulting FE model will be developed via an implicit type formulation. As noted earlier, this consists of two operational levels, i.e. the fractional operator representation of the damping characteristics and secondly, the remaining formulation involving the structural stiffness, boundary conditions as well as inertial effects. The fractional operator is approximated by an appropriately truncated Grunwaldean representation. Note truncation is controlled via self-adaptively updated remainder expressions. These streamline the use of the Grunwald representation. The results of this level are employed in conjunction with the implicit transient formulation of the inertial terms. Overall this yields an incremental time stepping solution. For demonstration purposes a least square type [3] Newmark Beta type expression is used to represent the appropriate inertial fields. Due to the generality of the fractional formulation, both stress and strain rate dependencies can be handled, i.e. Maxwell-Kelvin-Voigt type representations.

Benchmarking

Based on the Grunwaldean Newmark Beta type implicit formulation, an incremental algorithm will be developed to enable the nonlinear dynamic solution of structure containing dampers modelled by more comprehensive fractional type operators. To benchmark the stability, efficiency and capabilities of such algorithms, the results of several numerical experiments will be presented, namely:

i) The simulation of a full scale rolling vehicle traversing rough terrain; and,

ii) The response of various structure with damped viscoelastic coatings.

The simulations will be used to establish the unique modelling features of fractional type operators.

References

1. Ross, B., Lecture notes in Mathematics, Vol. 455, Springer, Berlin, 1975.

2. Padovan, J., Computational Mechanics, Vol. 2, pp 271-28., 1987.

3. Padovan, J., Jr. of FE in Analysis and Design (in press).

PERIODIC RESPONSE OF A CLASS OF HYSTERETIC OSCILLATORS

Danilo Capecchi and Fabrizio Vestroni

Dipartimento di Ingegneria delle Strutture, Acque e Terreno
Universita' dell'Aquila, 67040 Monteluco di Roio (AQ), Italy

Introduction

A great number of papers, some very sophisticated, have been devoted to the response of nonlinear systems under sinusoidal excitation. Most of them concern the large-amplitude oscillations of structural systems; they can be described by simplified models which exhibit nonlinear force-deflection relationship of holonomic type [1].

Only a few studies, however, dealth with the dynamic analysis of hysteretic oscillators (e.g. Refs.2-6); the earlier ones concerned bilinear constitutive relationships, and subsequent ones more general yielding cases. Several models, whose stationary dynamic behaviour does not seem altogether enlightened, have been recently introduced to represent the hysteretic characteristics of different physical systems under severe excitation.

The aim of this paper is to explore this matter more throughly by studying the steady-state oscillations of a class of simple but general hysteretic systems.

Solution of steady-state response

Let us consider a hysteretic oscillator with a restoring force f, viscous damping ζ and a frequency ω_o of small amplitude under a sinusoidal excitation $F \cos \omega t$. If f_y is the maximum value of f and x_y the displacement at nominal yielding such that $\omega_o^2 = f_y/mx_y$, by introducing the non-dimensionalized quantities:

$$\tilde{x} = x/x_y, \quad \tilde{f} = f/f_y, \quad \tilde{F} = F/f_y, \quad \tilde{t} = \omega_o t, \quad \alpha = \omega/\omega_o \qquad (1)$$

the equation of motion reads:

$$\ddot{x} + 2\zeta\dot{x} + f(x) = F \cos \alpha t \qquad (2)$$

where the tilde has been omitted.

Along a stable cycle the force-deflection relation f(x) has to be described by two single-valued funtions, $f_1(x)$ and $f_2(x)$

for the upper ($\dot{x}>0$) and lower ($\dot{x}<0$) side of the cycle respectively. Typical examples are the bilinear model and the Ramberg-Osgood model, studied in [2,3].

Due to the non-holonomic character of the restoring force, the steady-state response is obtained by means of an integral procedure. The solution is sought for in the form:

$$x(t) = \Sigma_n A_n \cos n\alpha t + \Sigma_n B_n \sin n\alpha t \qquad (3)$$

Substitute eq.(3) into eq.(2) and expand the periodic function $f[x(t)]$ in a Fourier series; A_n, B_n are determined by equating the coefficients of the same harmonics.

It is assumed here that n=1 and damping is neglected; the amplitude X and the phase ϕ of the solution can be obtained from:

$$[\, C(X) - \alpha^2 X \,]^2 + S(X)^2 = F^2 \qquad (4)$$

$$\operatorname{tg} \phi = \frac{S(X)}{C(X)-\alpha^2 X} \qquad (5)$$

where:

$$C(X) = \frac{2}{\pi} \int_0^{\pi} f(X \cos\theta) \cos\theta \, d\theta \qquad (6)$$

$$S(X) = \frac{2}{\pi} \int_{\pi}^{0} f(X \cos\theta) \sin\theta \, d\theta \qquad (7)$$

Eq.(4) completely describes the relation $h(X,\alpha,F)$ among the oscillation amplitude, the intensity of the force and its frequency.

For the bilinear (EPL) and Ramberg-Osgood (ROM) models the solution has been obtained in [2,3] and the frequency-response curves (f.r.c.) are plotted in Fig.1. The main features of the response are:

a) the 'soft' resonance exibited by the systems
b) the single valued and stable nature of the response curves
c) the occurrence of unbounded resonance above a certain value of force intensity.

In comparison with nonlinear elastic oscillators the existence of a maximum value in the restoring force is responsible for the unbounded amplitude resonance, while the hysteresis seems to make branches of unstable solutions disappear, although multi-valued f.r.c. have been obtained in [4] for a particular hysteretic model.

The stability analysis, performed in many works on periodic oscillations of nonlinear systems, have shown that when the response amplitude is multi-valued the part of curve between two loci of vertical tangency is a region of unstable solution.

Frequency-response curves

To gain insigth into the behaviour of hysteretic models and to better ascertain the role of the hysteresis, it is convenient to develop a qualitative study of the eq.(4). Since it is clear that the solution is governed by the pattern of C(X) and S(X), to make reference in the analysis tc a range that is wide but at the same time meaningful, a class of hysteretic models, illustrated in Fig.2, has been considered. Due to linearity of the single branch and a very low number of parameters, the model is simple and sufficiently general so as to represent some characteristics of stiffness-strength degrading force-deflection laws of real engineering systems.

The parameter ϱ is the post-elastic stiffness which can be positive or negative; β governs the magnitude of hysteresis, that is minimum for $\beta=0$, while the model becomes bilinear for $\beta=1$. When ϱ and β change, C(X) and S(X) change as well; they are plotted in fig. 3 for three different cases. It is worthing to notice that the functions are regular and S(X) may or may not decrease.

In Fig. 4 the frequency-response curves for the model are illustrated with various values of β and ϱ (the latter is always positive). If β is even a little smaller than unity the curve becomes multi-valued, showing that the curve of bilinear model is marginally stable. The frequency range of unstable solution, for a given force level, becomes wider as β decreases and tends to disappear for high β values. Notwithstanding the simplicity of hysteretic model, a rich variety of the periodic response, depending on the pattern of C(X), S(X) and on the value of F is evidenced. Study of eq.(4) leads to the conclusion that the number of the roots of the equations:

$$C(X)^2 + S(X)^2 = F^2 \quad , \quad S(X)^2 = F^2 \qquad (8)$$

governs the intersections of the curve with the $\alpha=0$ axis, (eq.8_1) and with the backbone curve the second (eq.8_2).

For the model considered four different circumstances, illustrated in fig. 5, are possible acccrding to the number of the roots of eqs.8 reported in Tab.1. In case (a) S(X) is

monotonic, while in the others it is not monotonic; the curves (b),(c) and(d) refer to the same oscillator for increasing F values. In cases (b) and (c), there is always a frequency range where the curve is multi-valued and unstable solutions occur. In case (a) this can occur depending on the parameters of the model, in any case it happens for $\beta < 1$; curve (d) seems to be always stable.

Fig.6 describes the relation X-F for different frequency values in the range $\alpha < 1$ for an assigned model. On this plane for each frequency the value of F above which the response is unbounded is evident as well as the range where the curve is multivalued.

A detailed study of the stability of the steady-state solutions of the hysteretic systems presented is a natural development of the present work.

References

1. Nayfeh, A.H., and Mook, D.T., Nonlinear Oscillations, John Wiley & Sons, Inc.,New York,NY,1979.

2. Caughey, T.K., "Sinusoidal excitation of a system with bilinear hysteresis", Journal of Applied Mechanics, 27, Dec., 1960,pp.640-643.

3. Jennings, P.C., "Response of a general yielding structure", Journal of Engineering Mechanics Division, ASCE, 90, No.EM2, Apr., 1964, pp. 131-166.

4. Iwan, W.D., "The steady-state response of the double bilinear hysteretic model", Journal of Applied Mechanics, 32, 1965, pp.921-925.

5. Masri, S.F., "Forced vibration of the damped bilinear hysteretic oscillator", Journal of the Acoustical Society of America, 57, Jan.,1975, pp.105-112.

6. Capecchi, D., and Vestroni, F., "Steady-state dynamic analysis of hysteretic systems", Journal of Engineering Mechanics, ASCE, 111, Dec.,1985, pp.1515-1531.

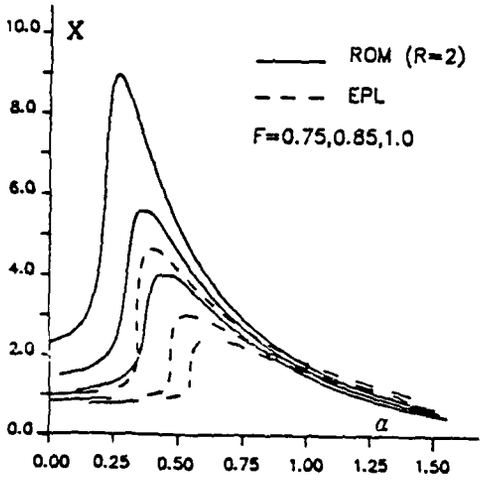

Fig. 1

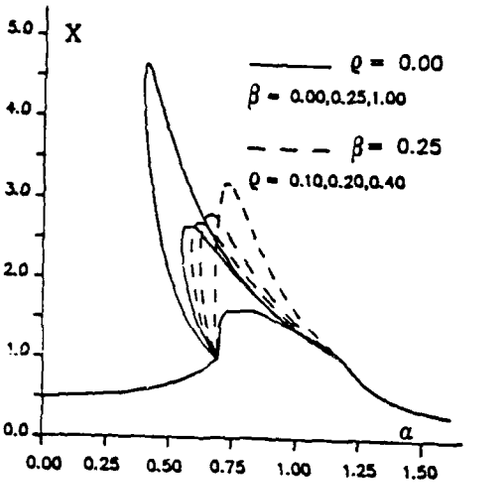

Fig. 2

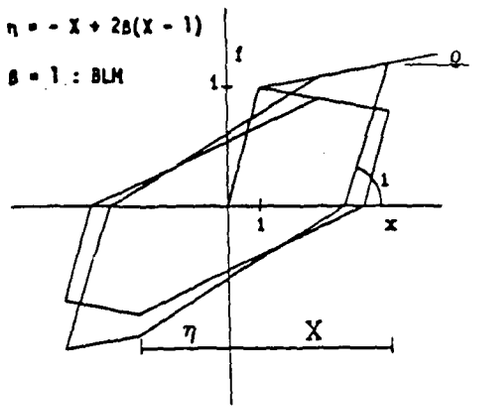

Fig. 3

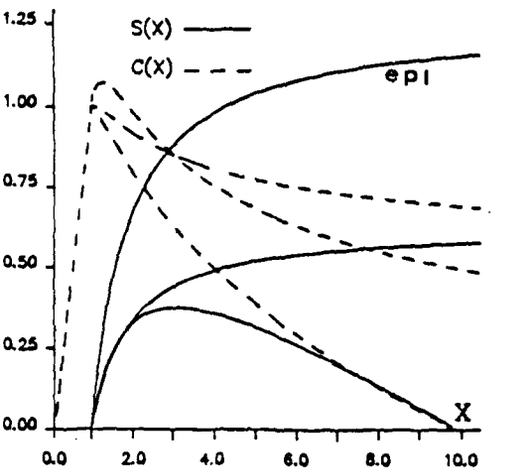

Fig. 4

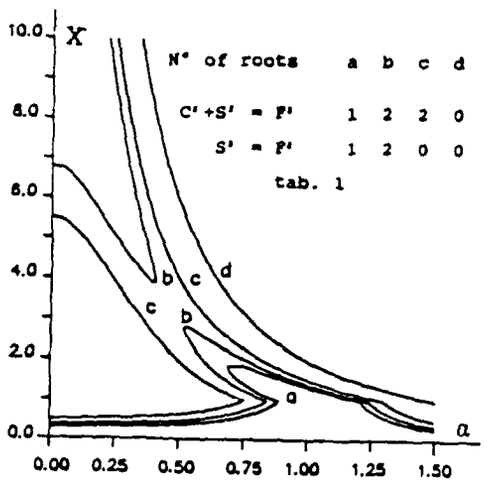

Fig. 5

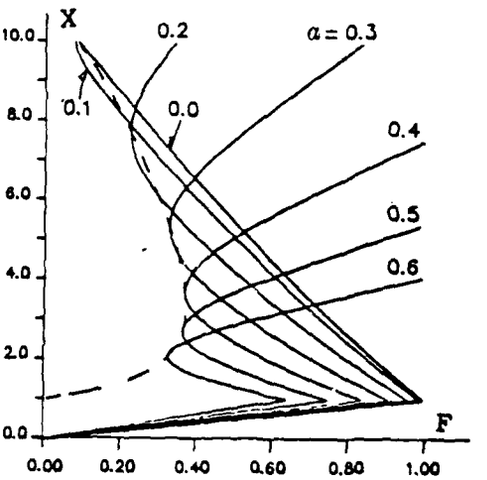

Fig. 6

DYNAMICS OF NONLINEAR AUTOMOBILE SHOCK-ABSORBERS

Jörg Wallaschek

Institut für Mechanik II
Technische Hochschule Darmstadt
Hochschulstr. 1
D-6100 Darmstadt
West-Germany

1. Introduction

Active and semi-active control of vehicle dynamics has become a subject of major interest during the past years, and today simple "damping control systems" are already incorporated in serial constructions of passenger cars. The fast progress in the analysis, design and technology of the control systems leads to the need of an accurate description of the dynamics of all components involved, like e.g. the tire or the shock-absorber.

The models used to analyze vehicle dynamics are mainly linear, with some isolated nonlinear elements. Usually, for ride-comfort investigations only the nonlinear dynamics of the shock-absorbers and the tires have to be taken into account. If only the system's overall dynamic response is of interest, these isolated elements can be taken care of by equivalent linearization techniques. The parameters of the linearized model can then be determined analytically, if the governing nonlinear equations are known. Most often, however, this is not the case and one must resort to experimental data. The parameters of the linearized model do of course depend on the type of test-signal. By using various test signals it is thus possible to determine the coefficients of an ad-hoc postulated nonlinear differential equation for the shock-absorber.

In what follows we first describe a simple mathematical model for shock-absorbers, discuss the linearization technique and estimate the parameters of the mathematical model from experimental data.

2. A mathematical model of the shock-absorber

Here only a very basic description of a shock-absorber is given. Its dynamic behavior does of course strongly depend on constructive details. Although there are many different types of shock-absorbers, they share one common feature: in principle they all consist of a piston moving in a closed cylinder as shown in Fig. 1.

Assuming that the two chambers are interconnected by a channel with constant circular cross-section a and length l and that the liquid is

incompressible one can derive the piston's equation of motion

$$m\ddot{x}(t) + d_1\dot{x}(t) + d_2\dot{x}^2(t)\ sgn[\dot{x}(t)] + d_3 sgn[\dot{x}(t)] = F(t), \qquad (1)$$

with

$$d_1 = \frac{8\mu\ A\pi l}{a^2}\ , \quad d_2 = \alpha\ \frac{\rho}{2}\ A^2\ , \quad d_3 = \mu N\ . \qquad (2)$$

where A is the effective piston area, υ and ρ are the dynamic viscosity and the mass density of the fluid and α is a constant. Coulomb friction between piston and cylinder has been taken into account, μN being the friction force. The three damping terms in (1) describe energy dissipation due to laminar flow, throttle losses and friction, respectively. In some types of dampers the liquid is suspended by pneumatic springs. Then one has to take into account this elasticity by introducing a spring in series with the piston. This model can also be used, if the foaming of oil and air becomes significant. We will however concentrate on the simplest case of Fig.1.

3. Equivalent linearization

From the various linearization methods only harmonic linearization is considered here. This technique corresponds to the first order approximation in the method of Krylov-Bogoljubow-Mitropolski for quasiperiodic differential equations /1/. It is therefore limited to a description of the damper dynamics for harmonic motion or nearly harmonic motion only.

The basic idea of harmonic linearization is to replace the nonlinear equation

$$m\ddot{x} + g(x(t),\dot{x}(t)) = F(t), \qquad (3)$$

where $g(x,\dot{x})$ usually is an odd function and $F(t)$ is harmonic by a linear one

$$m\ddot{y} + d\dot{x} + cx = F(t) \qquad (4)$$

and to chose the coefficients c and d so as to minimize the difference between $x(t)$ and $y(t)$ in a certain sense.

For shock-absorbers $g(x,\dot{x})$ is not an odd function and the method can not be applied directly. Taking into account that the operation point of the system will not be fixed in the case of a purely harmonic $F(t)$, we allow $F(t)$ to have a constant component

$$F(t) = \overline{F} + \hat{F}\ sin(\Omega t + \varphi) \tag{5}$$

so that

$$\overline{F} = \frac{1}{T}\int_0^T g(x(t),\dot{x}(t))\ dt\ , \quad T = \frac{2\pi}{\Omega}\ , \tag{6}$$

for

$$x(t) = \hat{x}\ sin(\Omega t + \varphi + \varphi). \tag{7}$$

In this way the operating point of the system is locked at $x = 0$, $\dot{x} = 0$ and equation (4) now holds for the fluctuating part of $F(t)$ only.

If we then replace (3) by (4), the coefficients c and d can be found from

$$c = \frac{1}{\pi\,\hat{x}}\int_0^{2\pi} g(\hat{x}sin\theta,\hat{x}\Omega cos\theta)\ sin\theta\ d\theta \tag{8}$$

$$d = \frac{1}{\pi\Omega\hat{x}}\int_0^{2\pi} g(\hat{x}sin\theta,\hat{x}\Omega cos\theta)\ cos\theta\ d\theta. \tag{9}$$

Of course also stochastic linearization can be applied /2/. This has been done in /3/. The results obtained so far are very similar, the only difference being that more test-signals can be used in the stochastic case.

4. Parameter identification

Applying harmonic linearization to the analytical model (1), we obtain

$$c = 0, \quad d = d_1 + \frac{8d_2}{3\pi}\hat{x}\Omega + \frac{4d_3}{\pi\hat{x}\Omega} \tag{10}$$

for the parameters of the linearized equation. These coefficients can easily be measured experimentally. Since d depends on the amplitude and on the frequency of the test signal one can identify d_1, d_2, d_3 by applying various test signals. Each measurement yields an equation of the form

$$d_1 + a_i\ d_2 + b_i\ d_3 = c_i\ . \tag{11}$$

If at least three linear independent equations are formulated the coefficients d_1, d_2, d_3 can be determined. Formulating more than three equations, the method of least squares can be applied.

5. Experimental results

Tests were performed in the laboratory of the Institut für Mechanik for a shock-absorber of the rear-axle suspension of a passenger car (Ford Sierra). Fig.2 shows the test facility with a damper mounted in the hydro-pulse machine. The damper end-point motion was controlled by the machine with the force being measured simultaneously. The parameter d was estimated experimentally using sinusoidal test-signals of different amplitudes and frequencies. Fig.3 shows the results obtained for a low temperature of the shock-absorber and test-signals of 2 Hz and 6 Hz respectively. Following the method described in the last chapter, the coefficients d_1, d_2 and d_3 were found to be

$$d_1 = 1.3866\ Ns/mm\ , \quad d_2 = 0\ , \quad d_3 = 1.5767\ N\ ,$$

when the 6 Hz curve is considered.

6. Conclusions

In a first step towards an accurate description of the shock-absorber dynamics a simple mathematical model was presented. The unknown coefficients were estimated using experimental data. The parameter identification technique used in the analysis is based on equivalent linearization and seems to be adequate for a large class of applications.

7. References

/1/ Bogoljubow, N. N., Mitropolski, J. A.: Asymptotische Methoden in der Theorie der nichtlinearen Schwingungen. Berlin: Akademie Verlag 1965.

/2/ Kozin, F.: Linearization techniques for non-linear stochastic vibrations. In Ziegler, F., Schueller, G. I. (eds.) Nonlinear stochastic dynamic engineering systems, IUTAM Symposium Innsbruck/Igls, Austria, June 21-26, 1987, Springer-Verlag, Berlin, Heidelberg, 1988.

/3/ Hagedorn, P., Wallaschek, J.: On equivalent harmonic and stochastic linearization for nonlinear shock-absorbers. In Ziegler, F., Schueller, G. I. (eds.) Nonlinear stochastic dynamic engineering systems, IUTAM Symposium Innsbruck/Igls, Austria, June 21-26, 1987, Springer-Verlag, Berlin, Heidelberg, 1988.

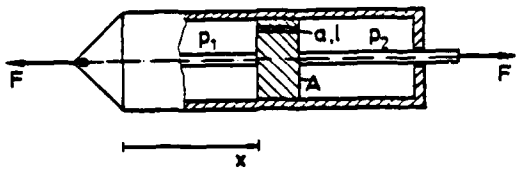

Fig.1 Basic model of a shock-absorber

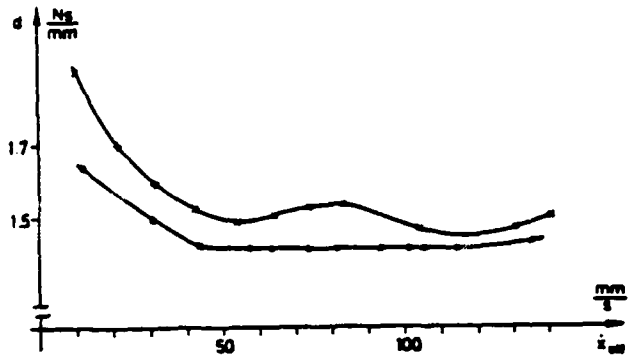

Fig.3 Equivalent damping rates for harmonic signals (f=2 Hz (x) and f=6 Hz (O)).

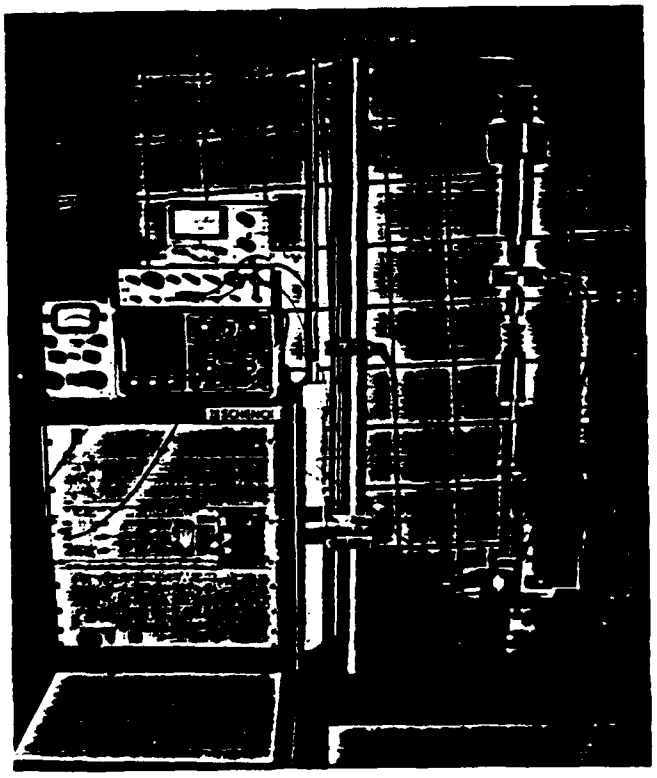

Fig.2 The test facility.

Prediction of Seismic Response Spectra for Bilinear Hysteretic Oscillators

S. R. Malushte and M. P. Singh

Department of Engineering Science & Mechanics, Virginia Tech, Blacksburg, VA 24061

A new approach for presenting the seismic response spectra of bilinear hysteretic oscillators in terms of "δ", the ratio of yield displacement to the maximum displacement of the corresponding elastic oscillator is proposed. Such spectra, which are defined in terms of the above mentioned reduction factor on spring forces provide a convinient and direct basis for comparison of response spectra for oscillators with different nonlinear characteristics. It is observed that the bilinear hysteretic oscillators with incorporation of low to moderate ductility levels cause a considerable reduction in acceleration in the medium and low frequency ranges. Also, for the same level of δ , it is seen that the bilinear hysteretic oscillators are more effective in controlling the permanent residual displacement than the corresponding elasto-plastic oscillators.

Estimation methods for predicting the required design ductility and maximum absolute acceleration are presented. It is seen that the proposed methods produce good a estimation of maximum acceleration in all frequency ranges. However, the prediction of ductility requirement is good, mainly for the case bilinear hysteretic oscillators with non-zero secondary stiffness and not so good for the case of elasto-plastic oscillators.